

# ARCHITECTURE & ENGINEERING

Volume 9 Issue 1 March, 2024



By Engineers. For Engineers

Architecture
Civil and Structural Engineering
Mechanics of Materials
Building and Construction
Urban Planning and Development
Transportation Issues in Construction
Geotechnical Engineering and Engineering Geology
Designing, Operation and Service
of Construction Site Engines

eISSN: 2500-0055 http://aej.spbgasu.ru/

# Architecture and Engineering

## Volume 9 Issue 1 (2024)

ISSN: 2500-0055

#### **Editorial Board:**

Prof. Askar Akaev (Kyrgyzstan)

Prof. Emeritus Demos Angelides (Greece)

Mohammad Arif Kamal (India)

Prof. Stefano Bertocci (Italy)

Prof. Tigran Dadayan (Armenia)

Prof. Milton Demosthenous (Cyprus)

Prof. Josef Eberhardsteiner (Austria)

Prof. Sergei Evtukov (Russia)

Prof. Georgiy Esaulov (Russia)

Prof. Andrew Gale (UK)

Prof. Theodoros Hatzigogos (Greece)

Prof. Santiago Huerta Fernandez (Spain)

Yoshinori Iwasaki (Japan)

Prof. Jilin Qi (China)

Prof. Nina Kazhar (Poland)

Prof. Gela Kipiani (Georgia)

Prof. Darja Kubečková (Czech Republic)

Prof. Hoe I. Ling (USA)

Prof. Evangelia Loukogeorgaki (Greece)

Prof. Jose Matos (Portugal)

Prof. Dietmar Mähner (Germany)

Prof. Saverio Mecca (Italy)

Prof. Menghong Wang (China)

Stergios Mitoulis (UK)

Prof. Valerii Morozov (Russia)

Prof. Aristotelis Naniopoulos (Greece)

Sandro Parrinello (Italy)

Prof. Paolo Puma (Italy)

Prof. Jaroslaw Rajczyk (Poland)

Prof. Marlena Rajczyk (Poland)

Prof. Sergey Sementsov (Russia)

Anastasios Sextos (Greece)

Eugene Shesterov (Russia)

Prof. Alexander Shkarovskiy (Poland)

Prof. Emeritus Tadatsugu Tanaka (Japan)

Prof. Sergo Tepnadze (Georgia)

Sargis Tovmasyan (Armenia)

Marios Theofanous (UK)

Georgia Thermou (UK)

Prof. Yeghiazar Vardanyan (Armenia)

Ikujiro Wakai (Japan)

Vardges Yedoyan (Armenia)

Prof. Askar Zhusupbekov (Kazakhstan)

Prof. Konstantin Sobolev (USA)

Michele Rocca (Italy)

Prof. Sergey Fedosov (Russia)

Francesco Di Paola (Italy)



**Editor in Chief:** 

Professor Evgeny Korolev (Russia)

#### **Executive Editor:**

Anastasia Sidorova (Russia)



#### **CONTENTS**

#### **Architecture**

#### 3 Ayman Assem, Doaa K. Hassan

Biophilia in the workplace: A pilot project for a living wall using an interactive parametric design approach

#### 17 Saumya Shrivastava,

Abir Bandyopadhyay, Vandana Agrawal

Regional Setting of Temples in Dakshina Kosala, India: Spatial Distribution and Connections

#### **Building Physics**

#### 29 Susan Susan, Safial Aqbar bin Zakaria, Sharifah Fairuz Syed Mohd Fadzil

Optimization of the building-integrated transparent photovoltaic configuration based on daylight and energy performance in school buildings in the tropics

#### Civil Engineering

#### 44 Boubakeur Fettar, Smail Boukeloua

Prediction of the performance of reinforced concrete elements under monotonic and cyclic lateral loading

### 61 Almaz Valiev, Irina Starovoitova, Alfred Suleymanov

Adhesive interaction in hybrid polymer composites. Energy characteristics of phases at the air interface

#### 71 Habte Yohannes Damir, Marina Rynkovskaya, Issaias Anday Sereke

Comparative buckling analysis of concrete and expanded polystyrene dome shells

#### **Urban Planning**

#### 79 Dhia Eddine Zakaria Lacheheb, Said Madani

Neighborhood renewal at stake: feedback on speculative redevelopment in Setif, Algeria

#### 91 Seyed Mohammad Mousavi, Shariyeh Hosseininasab, Waqas Ahmed Mahar

Buffer zone policy and its impact on the land value and the quality of the built environment in World Heritage sites: the case of Kampung Jawa, Melaka, Malaysia

#### **Architecture and Engineering**

peer-reviewed scientific journal Start date: 2016/03 4 issues per year

#### Founder, Publisher:

Saint Petersburg State University of Architecture and Civil Engineering

#### Indexina:

Scopus, Russian Science Citation Index, Directory of Open Access Journals (DOAJ), Google Scholar, Index Copernicus, Ulrich's Periodicals Directory, WorldCat, Bielefeld Academic Search Engine (BASE), Library of University of Cambridge and CyberLeninka

#### Corresponding address:

4 Vtoraya Krasnoarmejskaja Str., St. Petersburg, 190005, Russia

#### Website: http://aej.spbgasu.ru/

Phone: +7(812) 316 48 49 Email: aejeditorialoffice@gmail.com

Date of issue: March 29, 2024

The Journal was re-registered
by the Federal Service
for Supervision of Communications,
Information Technologies and Mass
Communications (Roskomnadzor)
on May 31, 2017;
registration certificate of media organization
El No. FS77–70026

#### Architecture

DOI: 10.23968/2500-0055-2024-9-1-3-16

## BIOPHILIA IN THE WORKPLACE: A PILOT PROJECT FOR A LIVING WALL USING AN INTERACTIVE PARAMETRIC DESIGN APPROACH

Ayman Assem\*, Doaa K. Hassan

Architectural Engineering Department, Faculty of Engineering, Ain Shams University, Egypt

\*Corresponding author's e-mail: ayman.assem@eng.asu.edu.eg

#### **Abstract**

Introduction: Workplace outcomes are significant not only for productivity and profitability but also for the value of the process and the experience elements involved in reaching these objectives. There is a continuous discussion between employers and employees regarding the concept of the workplace, concentrating on a thorough understanding of labor and its physical surroundings. This study focuses on the connection with the natural world, specifically how plants can improve aesthetics and support well-being in the built environment. The study explores the implementation of biophilic design to combat sick-building syndrome by integrating a living wall into workplace interiors. Methods: The study employs a parametric design approach to identify a design solution for incorporating a living wall into the workplace. This approach optimizes the correlation between multiple parameters influencing the design outcome. This approach operates on two levels: firstly, an analogical design process is employed to establish the form of green wall units and generate various iterations based on generation parameters derived from the natural concept source. Secondly, interactivity is incorporated to enhance users' perception of the green wall and its different states, ultimately leading to the creation of a unique ambiance suitable for diverse functions or activities within the space. Results: The results section would detail the specific outcomes of employing the parametric design approach, including the successful establishment of green wall units' forms, the generation of various iterations, and the enhancement of user perception through interactivity. The effectiveness of these design solutions in creating a unique ambiance and optimizing user engagement within the workplace is presented.

Keywords: biophilia, parametric design, green wall, interactive design.

#### Introduction

What makes a working experience good? Nowadays, thanks to modern organizations and their employees, it is not only about the end goal of productivity and profit, but also about the process and the experience itself in reaching the goal. By understanding the importance of the process, it will be easier to fix, enhance, and modify it for a better outcome. Then, the workplace is gaining meaning, while ensuring well-being and a sense of purpose. The definition of the workplace is still a matter of debate. Employers and employees are engaging in this debate about taking a more holistic view of work and the workplace, and the role they play in our daily lives. In this sense, a connection with nature becomes a significant part of such discussions (Browning and Cooper, 2015).

Natural settings have a crucial well-being and restorative impact (Gunawardena and Steemers, 2019). In this sense, the growing academic and organizational interest in biophilic design, regarding the positive outcomes for individuals and businesses, is driving more studies and applications in this area. The timing behind this growing interest lies in the broader socio-historical context of the movement of

populations from rural to urban environments. We are as disconnected from nature as we have ever been (Browning and Cooper, 2015). Biophilia is an innate urge of people to connect with nature and other forms of life and life-like processes. In fact, biophilia is an integral part of human development, both physically and mentally. Therefore, people are always looking for opportunities to experience nature outside of urban areas and even within them.

Then. integrating biophilic environments in workplaces can provide employees with psychologically restorative experiences by alleviating mental fatigue and reducing their levels of stress. In this respect, it is important to understand the components and characteristics of biophilic design. A number of studies in this area resulted in 14 patterns for biophilic design. The patterns were confirmed by intensive studies, the works of Christopher Alexander, Judith Heerwagen, Rachel and Stephen Kaplan, Stephen Kellert, Roger Ulrich, and many others, as well as considerable multidisciplinary study. These 14 patterns are intended to be flexible and adaptable, offering a wide range of possibilities for both indoor and outdoor spaces. These patterns are classified under three main categories: nature in

the space patterns, natural analogues patterns, and nature of the space patterns (Downton et al., 2017). The first category includes: (1) visual connection with nature; (2) non-visual connection with nature; (3) non-rhythmic sensory stimuli; (4) thermal and airflow variability; (5) presence of water; (6) dynamic and diffuse light; (7) connection with natural systems. The second category includes: (8) biomorphic forms and patterns; (9) material connection with nature; (10) complexity and order. The third category includes: (11) prospect; (12) refuge; (13) mystery; (14) risk/peril. The patterns of (10) complexity and order; (13) mystery; and (14) risk/peril have far less published material available on this topic (Peters and D'Penna, 2020).

In this sense, adopting plantation in terms of green surfaces is the most commonly used method to blend with nature. Including plant life has been identified to increase positive distractions and emotions, promote restoration from illness and stress, and enhance the socio-cultural climate. This impact is a result of the dynamic experience that plants add to spaces, creating a comprehensive sensory ambiance. The contribution of plants to the aesthetic and well-being enhancement is acknowledged in built environment discourse as biophilic design, in response to the need to alleviate symptoms of sick-building syndrome (Gunawardena and Steemers, 2019). In addition, surface greening has received much attention, particularly in cities with dense morphologies, as a response to the call for encouraging passive approaches such as green infrastructure (Assimakopoulos et al., 2020). Therefore, this research is examining the biophilic potential of living walls in terms of their ability to address the 14 patterns.

#### Literature review

Building exteriors, including their walls and roofs, have been greened for centuries. For the past 2,000 years, climbing plants have been positioned in traditional architecture at the base of building

facades or planter boxes to blend with the building elevations. The adoption of vertical greening, which integrates vegetation and buildings, has a significant impact on enhancing indoor and outdoor climates, aesthetics, insulation, reducing areenhouse gas emissions, and increasing ecological values (Sheweka and Magdy, 2011). In various climatic conditions, vertical greening can be used as an indoor or outdoor system (with the aid of natural or artificial lighting). Depending on the geography and environment, different plants and soils are selected. There are numerous vertical greening techniques available today that fall under the categories of green facade and living wall, which have similarities and important differences. Overall, forms of vertical greening can be defined as follows (Rakhshandehroo et al., 2015) (Fig. 1):

- Green facades (predominantly seen as exterior applications) are essentially vertical trellises or framework constructions that hold plant branch systems. These systems are positioned at the base of the building facades, in pots at the base of the framework, or in floating containers attached at regular intervals to the facade frame (Gunawardena and Steemers, 2019; Radić et al., 2019).
- Living walls (for exterior and interior applications) are structures with soil or another growing medium distributed over their surface or volume. Plants grow on them or have their root systems in them (Gunawardena and Steemers, 2019; Radić et al., 2019).

Whatever the approach, both green facades and living walls share many similar attributes and values (Lundegren, 2016; Sheweka and Magdy, 2011):

- Enhancement of aesthetic appearance and design.
  - Affective bonds and well-being.
  - Sound reduction and buffering.
- Climate regulation that generally occurs through insulation, which helps keep the cold out in winter and the interior cool in the summer. In other

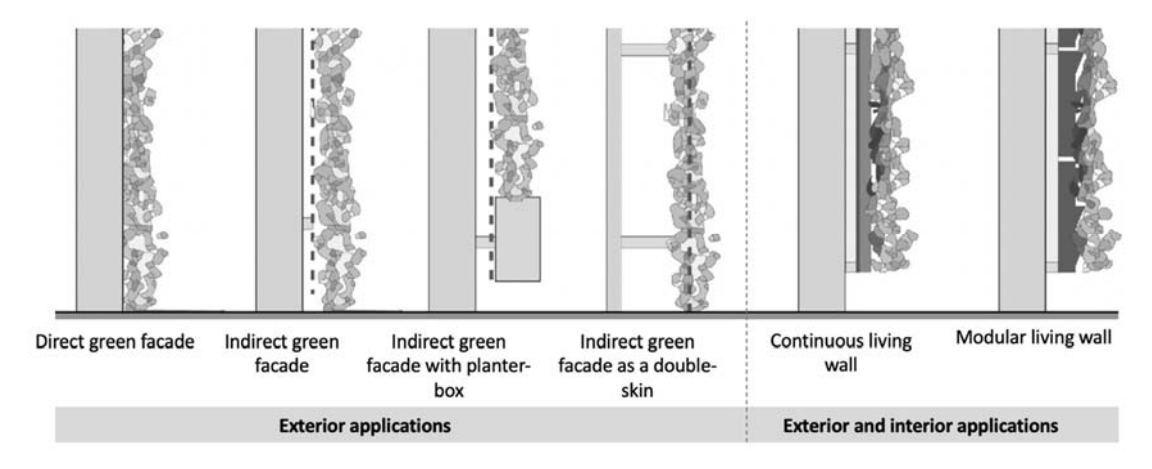


Fig. 1. Vertical greening categories (Gunawardena and Steemers, 2019)

words, summertime cooling involves less heat gain and evaporative cooling, while winter requires insulation and a wind barrier.

- Air filtration and better air quality (by reducing greenhouse gases such as carbon dioxide (CO<sub>2</sub>), carbon monoxide (CO), and nitrogen dioxide (NO<sub>2</sub>)).
- Possibilities for edible and medicinal plants and habitats for wildlife.

Our research focuses on the living wall system as a means of enhancing workplace interiors through the adoption of biophilic design patterns. Therefore, based on the patterns in the introduction section, nature in space and natural analogs will be the main focus in this regard. The phrase "nature in the space" addresses the immediate, tangible, and transient presence of nature. In addition to winds, noises, smells, and other natural elements, this also includes living things such as plants, water, and animals. Direct connections with these natural elements, particularly through diversity, mobility, and multi-sensory interactions, can lead to the most powerful spatial experiences. Natural analogs, on the other hand, deal with biological, non-living, and indirect evocations of nature. It is possible to use items, materials, colors, shapes, patterns, and arrangements found in nature to create artwork, decorations, furniture, and textiles for the built world. Contrary to the previous two methods, nature of space is concerned with the spatial configuration of spaces, which goes beyond the focus of adopting vertical greening as a single element. Therefore, the patterns related to the first two methods will be applied in this research (Downton et al., 2017).

Accordingly, it can be inferred that such designs incorporate many interrelated factors to optimize the solution. Then, a parametric design approach could be beneficial in this respect. A previous pilot study attempted to address the issue of separating parking garages from nature and urban connectivity by designing a combination facade and living and habitat wall systems. This design was created to measure and optimize aesthetics, temperature gradients, water supply, air quality, habitat, and cost. The final project demonstrated environmental benefits and costs associated with a combination of living wall and synthetic habitat technologies through the use of building information modeling (BIM) and other parametric design software (Briscoe, 2014). This pilot predicted the role of computation in understanding trends of migration and succession. Another pilot study emphasized that this parametric design makes it easier for designers to modify their work and create their own algorithms, resulting in a more effective way of designing and producing the final output. It was about designing interior panels using parametric modeling tools. This pilot study focused on reducing time consumption and eliminating unnecessary steps in the traditional process, while also taking into account the changeable and adaptive geometries (Kim et al., 2016). Accordingly, this research aims to parametrically design a responsive living wall in a workplace interior, adopting a biophilic design approach to maximize the efficiency of users' experience.

#### Methodology

This research is based on a pilot study that was completed as a primary requirement for a postgraduate course titled "Interactive and Responsive Architecture". Postgraduates were required to parametrically design an interior living wall in a workplace to enhance employees' performance through the physical settings of the interior environment, adopting biophilic design. The parametric design process will be adopted to optimize the interrelation values of the different parameters that affect the design product at two levels: analogical design and configuration, and interactivity.

Pilot description: design and configuration

The pilot description is presented in terms of the phases of the design process and the targeted attributes of the product as follows:

- Parametric analogical design;
- Technical installations;
- Interactivity with reference to both plants' and users' needs:
  - Fabrication and implementations.

To achieve the pilot goal, specific characteristics for the final product were designated to be analogical design-based, modular, and interactive to maximize the value of biophilic design. The patterns are applied as follows (Table 1):

#### Parametric analogical design process

In design, analogies are often used to solve problems. Since the design process is viewed as an exploratory activity based on visual thinking, the use of visual representation by analogy is considered a powerful creative problem-solving strategy. Accordingly, analogical thinking enables designers to find similarities between a target design space and an existing knowledge base and translate that existing knowledge into new design solutions (Kaumoodi, 2021).

The configuration of a living wall depends on specific parameters, such as using analogy as a source of idea generation, considering plantation aspects (including plant types, growth medium, irrigation, energy, and lighting), and utilizing new technology materials and fabrication.

In our concept, analogy as a source of idea generation was inspired by the following (Fig. 2):

- Form of specific fruits, such as pineapples, pine cones, and much more in a natural shape design.
  - Structure of plant leaves.

The modular living wall design was developed to produce two design proposals: one for the overall

|                 | lable 1. Proposal for the implementation of merging patterns in interior living wall systems |  |             |  |  |  |
|-----------------|--|--|-------------|--|--|--|
|                 | Patterns   | Definitions  | Application |  |  |  |
| Nature in Space | Visual connection with nature  | A view of the environment, including living things and natural processes.  | •           |  |  |  |
|                 | Non-visual<br>connection<br>with nature  | Stimuli that evoke a positive association with nature, living things, or natural processes through auditory, tactile, olfactory, or gustatory means.   | •           |  |  |  |
|                 | Non-rhythmic<br>sensory stimuli  | Connections with nature that are stochastic and transient and can be statistically examined but may not be precisely predicted.  (Movement and sensory effects are inherently brief — no more than 20 seconds every 20 minutes. For example, the flight of a butterfly or the journey of a cloud, or a simple shifting of light throughout the day.) |             |  |  |  |
|                 | Thermal<br>and airflow<br>variability  | Variations in the skin airflow, relative humidity, and temperature.  |             |  |  |  |
|                 | Presence of water  | Participation that enhances a location's experience through seeing, hearing, or touching water.  |             |  |  |  |
|                 | Dynamic and diffuse light  | Uses shifting light and shadow intensities that fluctuate over time to mimic natural conditions.   | •           |  |  |  |
|                 | Connection with natural systems  | Understanding of natural processes, particularly the seasonal and temporal fluctuations that characterize a thriving ecosystem.  |             |  |  |  |
| Analogs         | Biomorphic forms and patterns  | Figurative allusions to naturally occurring curved, patterned, textured, or numerical arrangements.  | •           |  |  |  |
|                 | Material<br>connection<br>with nature  | Minimally processed natural materials and components that represent the area's environment or geology and contribute to a strong sense of place.   |             |  |  |  |
| Natural         | Complexity and order   | understanding of natural processes, particularly the seasonal and temporal fluctuations that characterize a thriving ecosystem.  (A place with good complexity and order feels interesting and information-rich,   | •           |  |  |  |

striking an intriguing balance between being dull and overwhelming.)

Table 1 Proposal for the implementation of merging patterns in interior living wall systems

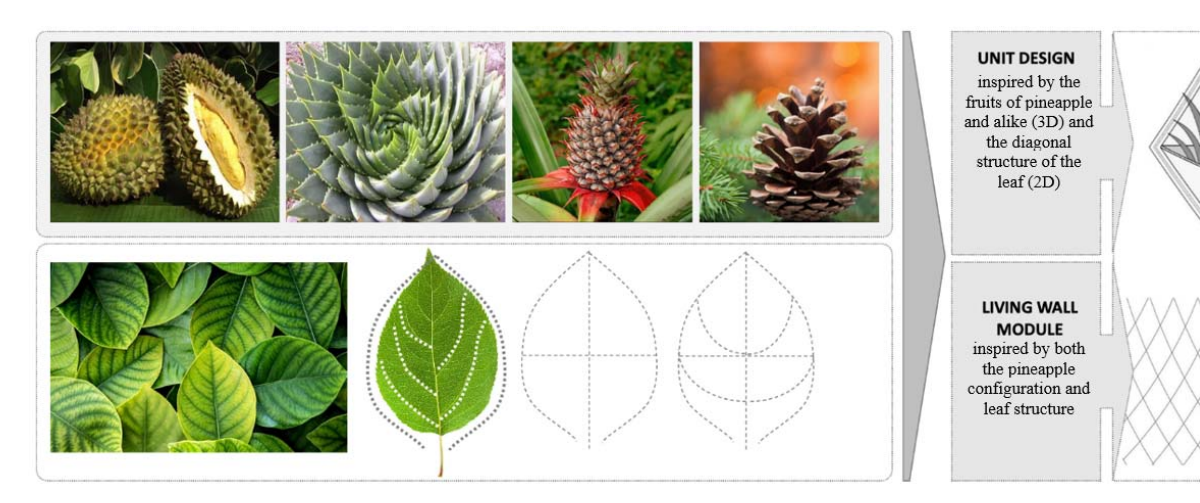


Fig. 2. Unit and living wall module: analogical design

wall to function as a unified whole, and another for the unit to function as an independent entity.

As previously mentioned, the parametric design approach was employed to enhance the interrelation of many parameters that impact the design result. This optimization occurred at two levels, namely analogical design and configuration, as well as interactivity, which are further elaborated upon in subsequent sections.

The applied parametric analogical design process (Fig. 3) consisted of five sequential processes.

It began by selecting a source of inspiration derived from natural elements. Subsequently, a visual analysis was conducted to emphasize the primary design features, visual principles, and rules for creating shapes. The next phase involved converting these constituent components into design parameters, which define the primary design elements, spatial arrangements, distances, forces, and other quantitative aspects. The fourth phase involved constructing the model algorithm using parametric design software. In our pilot study,

we used the Grasshopper plugin to develop the algorithm. This process resulted in the creation of many model iterations.

#### A.Living wall as a unified modular system

The living wall was constructed using a module system that was developed through a parametric design method, as previously mentioned. This modular system comprises multiple levels: 1. The base grid establishes the cellular modules of the planting pots and the structural framework system. 2. The steel structure mesh, which serves as the primary mounting system for the green wall. 3. The LED lighting lines. 4. The layer for the fixation of plant pots. 5. The empty fabricated pots. 6. Lastly, the soil and the planting process (Figs. 4 and 5).

#### B. Independent unit design (separate unit)

The concept of separate unit design involves the development of a unit that operates autonomously

with respect to all of its systems (Fig. 6). The aggregation of the cells has the potential to display various designs and encompass diverse wall areas. Furthermore, it can be installed as a unified cell unit. The adaptable nature of this design enables it to meet various requirements of both humans and plants, while also being suitable for any given spatial constraints.

#### Technical installations

This section covers the technical aspects related to plantation and water management systems, as outlined below:

#### A. Indoor plant types and requirements

Plants are the primary and fundamental elements of living walls. Particular types of plants are selected to fulfill the intended design objectives. Interior living walls typically incorporate a selection of tropical plant species, with a particular emphasis on vining,

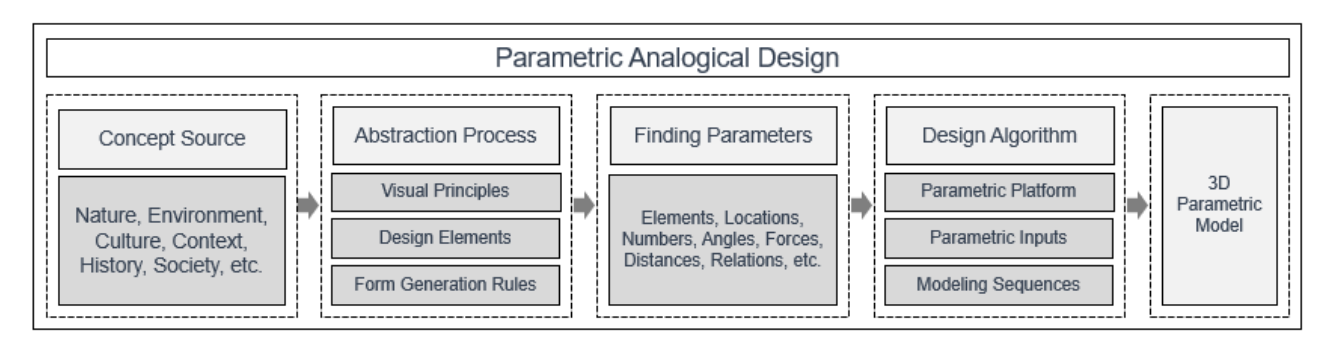


Fig. 3. Process of parametric analogical design

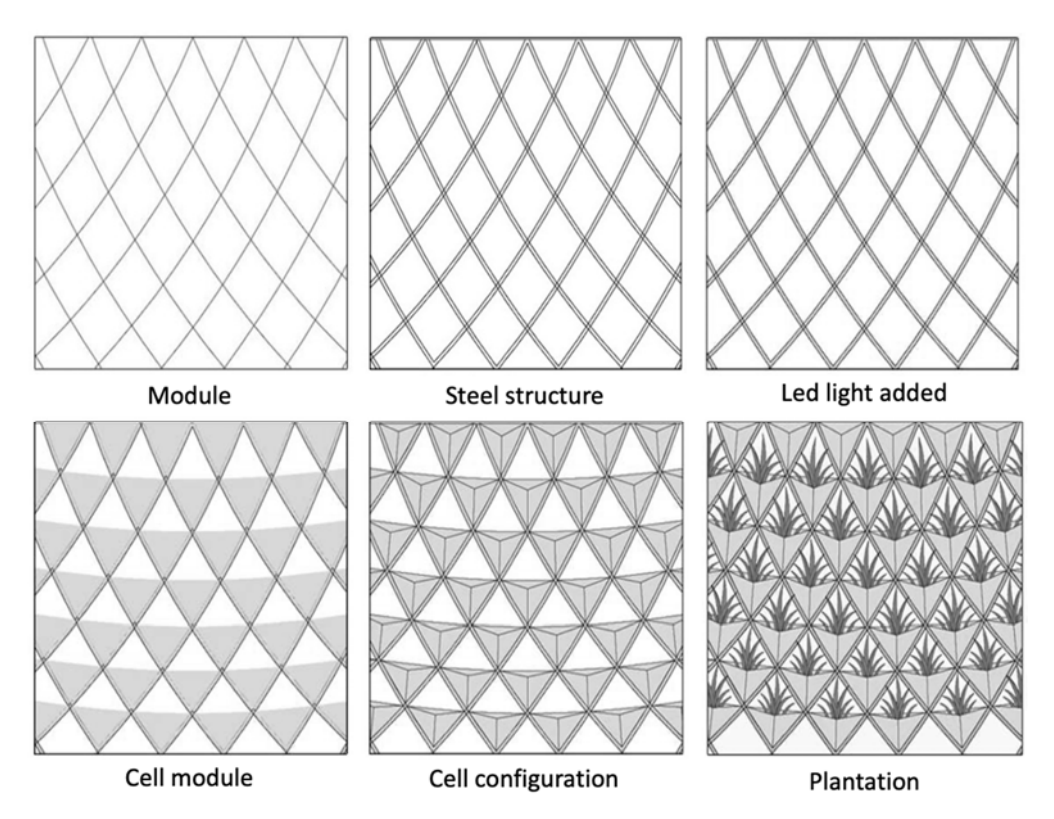


Fig. 4. Living wall design

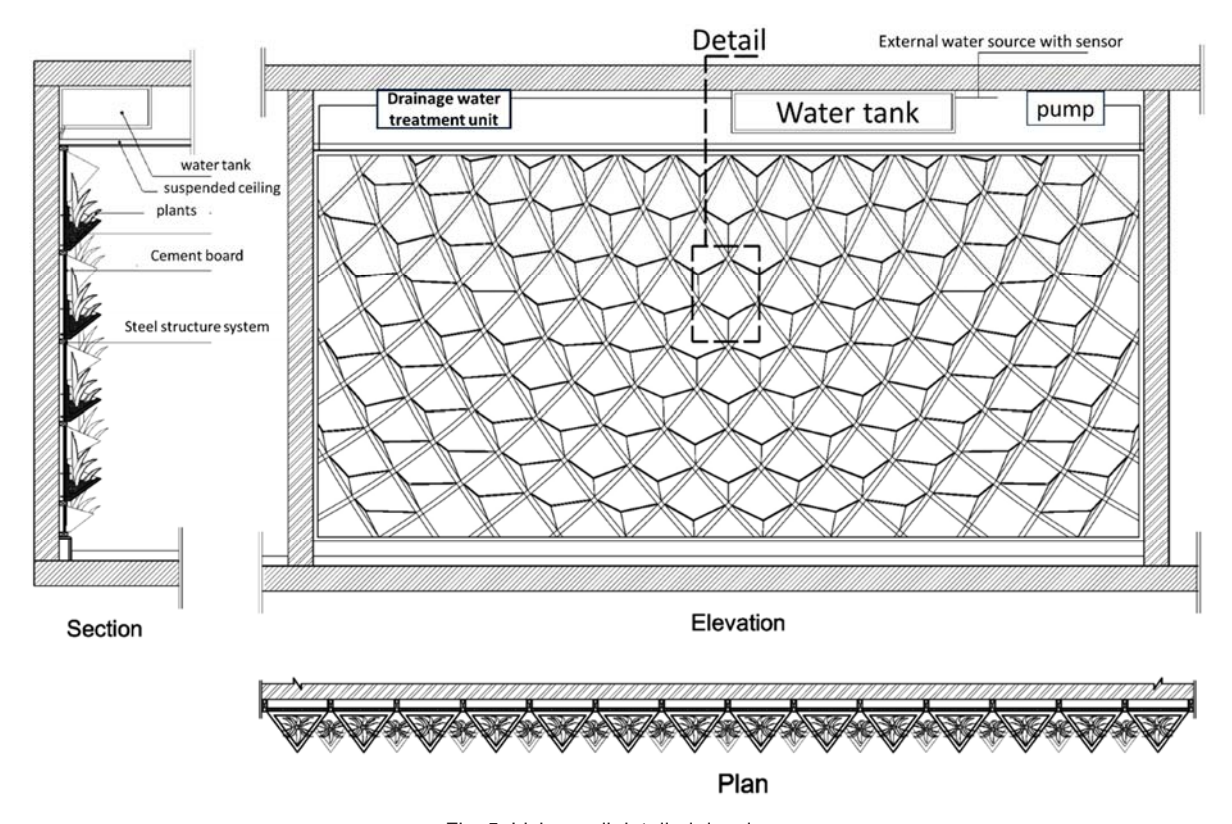


Fig. 5. Living wall detailed drawings

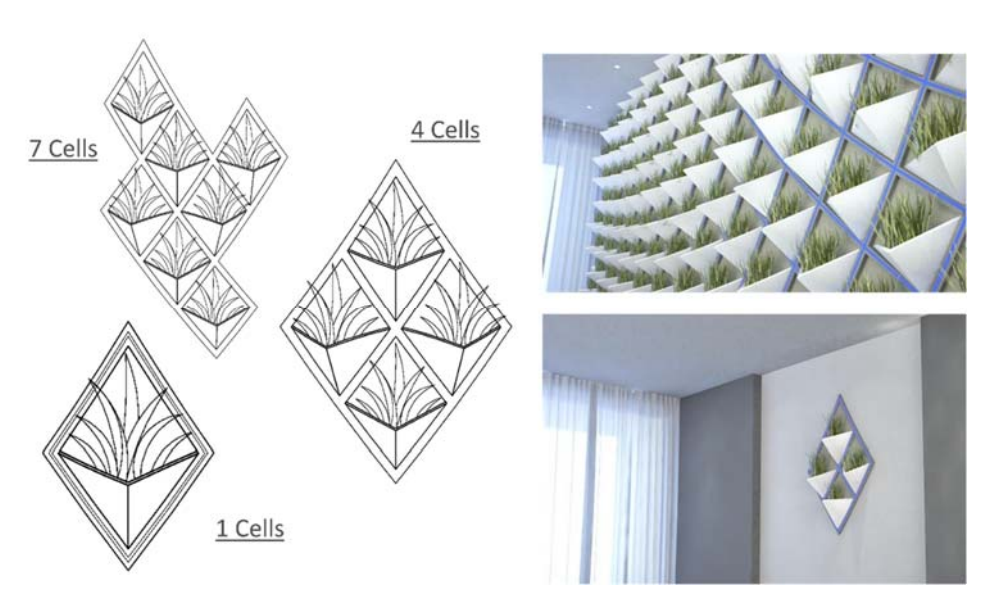


Fig. 6. Independent cell design and its various distributions

climbing, and fern varieties. Vertical gardens are a popular choice for cultivating a diverse array of attractive plant species. Specifically, a total of thirty-two species, including Asplenium thunbergii, Alocasia sanderiana, Anthurium crystallinum, Anthurium andraeanum, Aeschynanthus radicans, Chlorophytum bichetii, Cercestis mirabilis, Caladium lindenii, and Epipremnum aureum, are usually selected for this purpose (Sarkar, 2018). The Table 2 presents a comparison of different species of indoor plants that can be included in biophilic design settings.

Based on the comparison table above, the selection of Pothos (*Epipremnum aureum*) and Lipstick plant (*Aeschynanthus radicans*) for biophilic interior designs is justified because of their distinctive attributes that align with the concepts of enhancing indoor environmental quality and psychological well-being. The Pothos plant is highly efficient at enhancing indoor air quality and is capable of tolerating different lighting conditions and irregular watering. This makes it a suitable option for indoor plant care and air purification. The Lipstick

| lable 2. Comparison of indoor plant species for integration in biophilic design setting |                               |  |   |  |  |  |
|---|-------------------------------|--|---|--|--|--|
| Scientific Name   | Light<br>Requirements         | Watering &<br>Humidity                             | Growth & Appearance                           | Special Features   |  |  |
| Asplenium thunbergii<br>(Thunberg's<br>Spleenwort)                                      | Partial to full<br>shade      | Moist but well-<br>drained                         | Delicate fronds, prefers shaded environments  | Often used in terrariums, good for shaded gardens          |  |  |
| Alocasia sanderiana<br>(Kris plant)   | Bright, indirect<br>light     | High humidity, regular watering                    | Large, arrow-shaped leaves with white veins   | Striking foliage, prefers warm and humid environment       |  |  |
| Anthurium crystallinum (Crystal anthurium)  | Bright, indirect<br>light     | Regular watering,<br>high humidity                 | Heart-shaped leaves<br>with white veins       | Popular for decorative indoor use, needs warm environment  |  |  |
| Anthurium andraeanum (Flamingo flower)  | Bright, indirect<br>light     | Regular watering, enjoys humidity                  | Bright spathes<br>and contrasting<br>spadices | Often used in floral arrangements, ornamental              |  |  |
| Aeschynanthus radicans (Lipstick plant)   | Bright, indirect<br>light     | Consistent<br>moisture, prefers<br>humidity        | Trailing vines with tubular flowers           | Great for hanging baskets, attractive blooms               |  |  |
| Chlorophytum bichetii   | Bright, indirect<br>light     | Regular watering,<br>tolerates average<br>humidity | Arching leaves, grass-<br>like appearance     | Easy to care for, works well in various indoor settings    |  |  |
| Cercestis mirabilis   | Partial to full shade         | Moist, well-<br>drained soil                       | Large, heart-shaped leaves                    | Unique foliage, adaptable to indoor conditions             |  |  |
| Caladium lindenii<br>(Xanthosoma lindenii,<br>Angel's Wings)                            | Bright, indirect<br>light     | Consistent<br>moisture, high<br>humidity           | Arrow-shaped leaves<br>with white veins       | Eye-catching foliage,<br>sensitive to cold<br>temperatures |  |  |
| Epipremnum aureum (Pothos)  | Low to bright, indirect light | Can tolerate irregular watering,                   | Heart-shaped variegated leaves                | Air-purifying, extremely adaptable to indoor               |  |  |

average humidity

plant, characterized by its vivid, tubular flowers and preference for strong, indirect light, offers both visual appeal and psychological benefits, crucial for creating compelling and emotionally nurturing spaces. Incorporating these plants into indoor spaces enhances their visual appeal and promotes a healthier and more harmonious living environment. aligning with the core principles of biophilic design that emphasize the connection between nature, human well-being, and the built environment.

#### 1. Lipstick plant (Aeschynanthus radicans)

The Lipstick plant, known for its climbing nature, exhibits a visually captivating appearance, particularly when it is allowed to gracefully drape from suspended containers. The plant has aesthetically pleasing, succulent foliage that remains green throughout the year, accompanied by the production of visually striking, crimson tubular blossoms. The growth of Lipstick plants is a rather uncomplicated process. The plant can be cultivated in both indoor and outdoor environments. Additionally, due to its minimal soil requirements, it can be successfully grown on vertical surfaces. The optimal conditions for the growth of the Lipstick plant pertain to its chosen substrate, which includes consistently moist, nutrientrich, and well-drained soil. It is recommended to mix light, sandy soil with either humus or peat moss. The presence of peat moss in this mixture ensures that the humidity level is consistently optimized. During this period, the sand will provide sufficient drainage to prevent the occurrence of root rot. The ideal environmental conditions for the Lipstick plant involve exposure to bright, dappled light. Adequate illumination is necessary for its optimal growth and development. It is advisable to avoid exposing the plant to direct sunlight or complete darkness in its placement. The replication of a plant's natural environment can be achieved when it is kept indoors by using artificial lighting. Both fluorescent and LED lighting can be used without any issues. The objective is to select hues that lean towards the cooler end of the color spectrum, resembling the chromatic palette observed on a sunlit day with accompanying shadows. The daily requirement for exposure to light is limited to three hours (Johnstone, 2022) (Fig. 7a).

conditions

#### 2. Pothos (Epipremnum aureum)

The NASA/ALCA study on the use of common indoor plants for interior air purification designates Pothos as one of the top three plants with the commendable attribute of being an exceptional air-cleansing plant. Epipremnum aureum, also known as the golden pothos, exhibits aesthetically pleasing marbled leaves and possesses a resilient nature, requiring less maintenance. Consequently, it has gained significant popularity as a choice for indoor plants. One notable attribute of this plant is its ability to thrive in a hydroponic environment, such as a water-filled bottle or a soilless container. Even direct sunlight is not required. The plant has tolerance for bright light; however, optimal results are achieved when it is exposed to medium indirect light. Regular watering is necessary during the spring to fall seasons, while caution should be exercised to avoid excessive irrigation during the winter months. The optimal growth conditions for the plant are a combination of arid topsoil and warm, sunny temperatures. Sandy loam and clay soils are considered optimal for the growth of this particular species (Meshram and Srivastava, 2015) (Fig. 7b).

#### B. Growth medium

One of the primary concerns at hand pertains to the composition of the growing media, which plays a crucial role in facilitating the growth of plants and the formation of infrastructure. The growing medium should provide the essential needs of the plants, including water and air. When designing a living wall, it is important to take into account additional factors such as weight, durability, and stability. Based on the aforementioned rationales, it can be concluded that soilless culture is the optimal choice for implementing a living wall (Tamási and Dobszay, 2015).

Soilless culture refers to the practice of cultivating plants in the absence of traditional soil-based mediums. The use of traditional soil poses unique challenges, including the difficult and expensive management of soil-borne pests and diseases, salinity issues, insufficient fertility, and limited water availability. In contrast, soilless culture offers numerous advantages compared to conventional agricultural methods. These include the ability to obtain high-quality yields, exert control over root environments, optimize water utilization, cultivate crops regardless of unfavorable soil conditions, and mitigate the presence of weeds and soil-borne illnesses. Soilless cultures can be classified into two primary categories:

- 1. Substrate culture:
- Organic (peat moss, wood residues, rice hulls, etc.);
- Inorganic (perlite, sand, vermiculite, pumice, calcined clays, etc.) (Almusaed, 2011).
  - 2. Water culture.

Numerous studies indicate that inorganic materials are often favored as the primary material due to their superior stability and durability compared to organic growing media. Nevertheless, when evaluating the desirable attributes of plant growth media, it is evident that many physical and chemical aspects of inorganic growing media are comparatively inferior to those of organic growing media (Dede et al., 2019). Peat moss has been selected as the organic substrate culture in this pilot due to (Espiritu, 2022):

- Absorbency. Peat moss retains water much better than average soils.
- Compaction. It does not compact, unlike other organic materials. Soil compaction is damaging to gardens and reduces water absorption and plant growth. Peat moss remains springy when it is wet and rehydrates easily. Plus, one application of peat moss can last for years.
- Sterile planting medium. This means that it does not contain harmful pathogens or weed seeds. This, combined with its absorbency, makes it ideal for starting seedlings, which is why peat moss is an essential component in most seed starting mixes.
- Acidic pH. Acid-loving plants benefit greatly from peat moss applications.

#### C. Water management systems

In order for plants to undergo growth, they require the essential elements of water, light, and nutrients. Fulfilling these requirements is made easier with the implementation of an irrigation system. The effectiveness of irrigation systems depends on various factors, including spatial considerations, the type of crops being cultivated, and the associated expenses for both indoor and outdoor installations. When considering the cultivation of indoor plants, it is essential to address seven key components to establish an irrigation system that adequately caters to the plants' requirements. These components include selecting appropriate growing media, providing a sufficient water supply, establishing effective irrigation channels, implementing proper



Lipstick plant (Aeschynanthus radicans)
(Johnstone, 2022)



Pothos (*Epipremnum aureum*) (Wikimedia Commons, 2022)

Fig. 7. Used indoor plants

drainage mechanisms, providing essential nutrients, identifying suitable energy sources, and using appropriate light sources. This section provides an analysis of the requirements and their implementation within the pilot study (Figs. 8 and 9).

The quantity of water is one of the main factors affecting plant quality, and it depends on the type of plant, the season, the orientation of the vertical walls, and the temperature. The pilot irrigation system provides a watering timer to control the amount of water that plants need based on temperature and time. The water is provided using a water tank and pump (Wilkinson et al., 2021).

To distribute the water among the planting units, the irrigation channels are used as a main part of the system. They are usually poly tubing connected on one side to a water supply and on the other side to a vertical wall system, allowing water to drip slowly when placed on top of a vertical green wall. In our pilot, the irrigation channels are hidden, while in others they could be exposed and used as part of the decorative appearance of the system (Madani et al., 2013).

Drainage is an important factor in a green wall system. Effective drainage is necessary to prevent diseases, fungal or bacterial infections, and salt build-up in living wall planters. The drainage process usually occurs when the irrigation channels are sloped to end in a water basin.

In the pilot, an integrated piped system is used in the back of the entire wall, embedded into the steel structure system of the green wall. The water supply path starts from a ceiling-suspended water tank and moves to a water pump in order to control water pressure inside the pipes distributed along all plant cells.

#### D. Energy and lighting

Indoor vertical green walls require an energy source to facilitate the circulation of irrigation water

within the system, as well as to power LED lights. These lights serve a dual purpose by providing plants with the necessary light for photosynthesis and contributing to the aesthetic appeal of the installation.

#### Interactivity

The concept of interactive interior design pertains to the creation and integration of interactive components within a defined physical environment. Recent advancements in technology have facilitated the emergence of novel applications and engagement opportunities that can be seamlessly linked with the architectural aspects of places (Nabil and Kirk, 2019).

The concept of interactivity in the pilot study significantly influences users' perception of the green wall and its diverse states, ultimately resulting in the creation of distinct atmospheres suitable for various functions or activities within the space.

The design of interactive living walls is addressed through the utilization of various sensors, as outlined below:

- Plant: light and water/irrigation & drainage;
- Users: light mode (color and intensity) related to speech/sound level parameters.

This section examines three primary modes of interaction that are based on the use of three distinct types of sensors capable of detecting three specific categories of inputs: 1) detection of sound levels; 2) detection of soil moisture; 3) detection of light levels.

Fig. 10 illustrates the concept of interactivity related to the three distinct forms of detection. The system will then generate a response and implement the predetermined actions accordingly.

#### A. Sound detection sensor

The concept of interaction was derived from observing the impact that plants have on human beings. Research findings indicate that the presence of indoor plants has been associated with enhanced

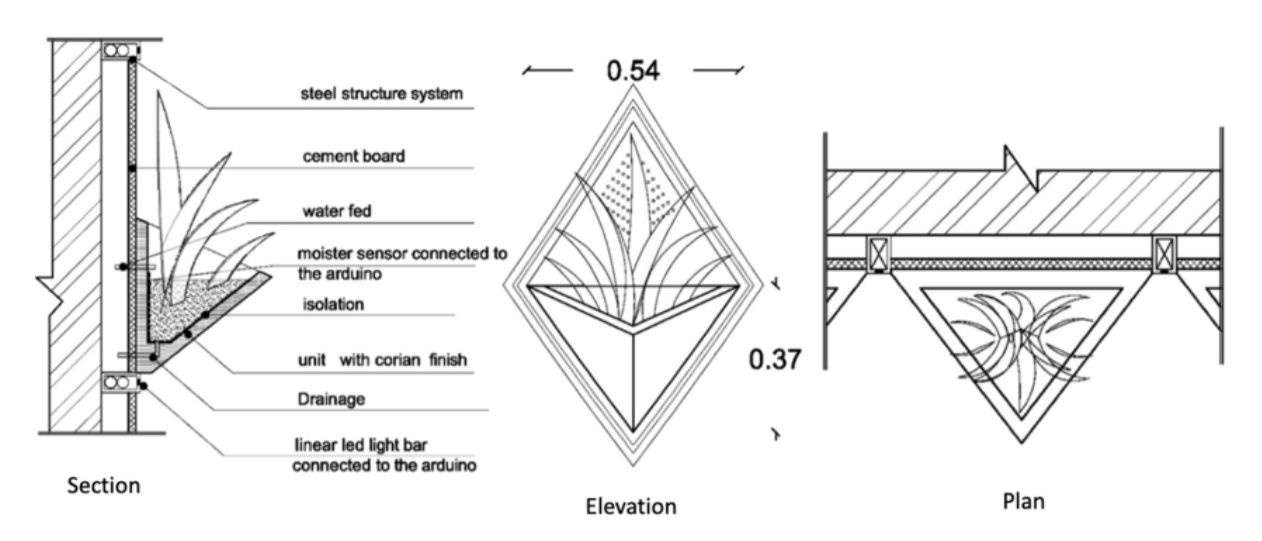


Fig. 8. Living wall details illustrating the components of the system

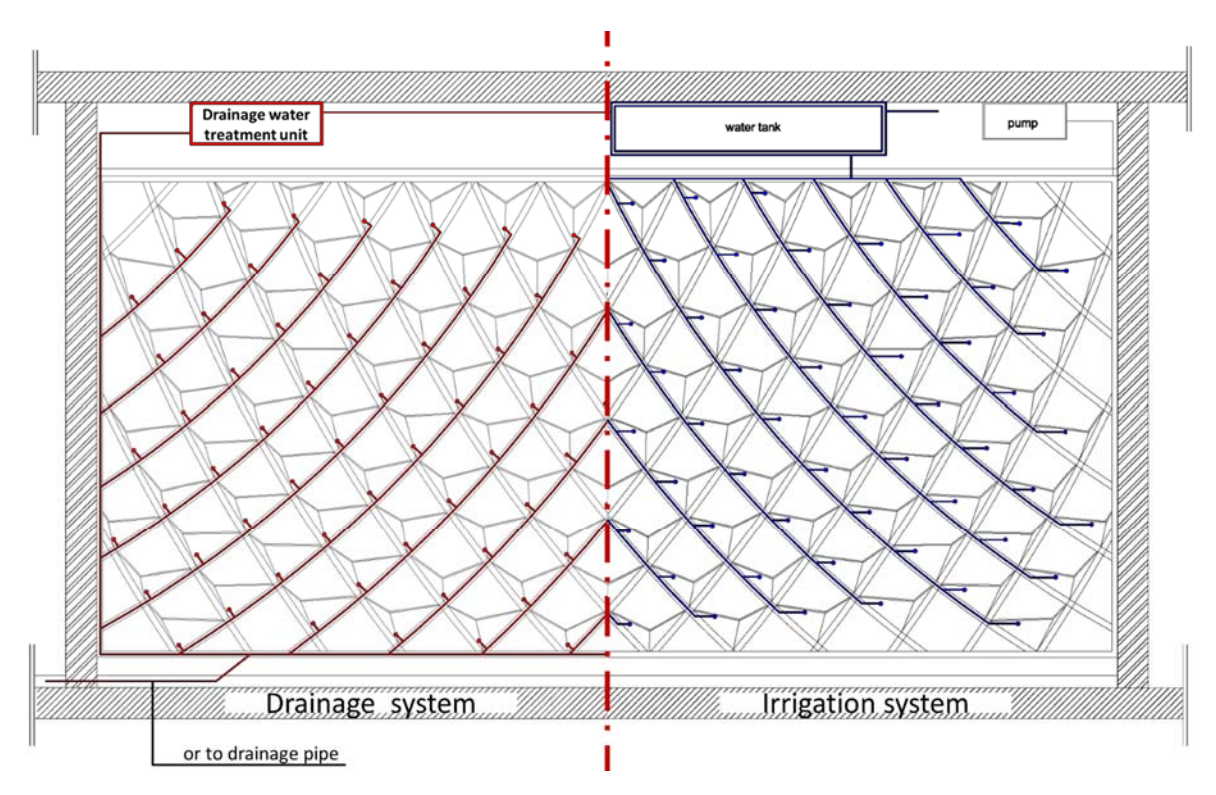


Fig. 9. Water management system for the pilot

concentration and productivity, alongside reduced stress levels and improved mood. This characteristic makes them well-suited for use not only in residential settings but also in commercial environments. Colors have the capacity to modify an individual's emotional state, transitioning it from a state of unhappiness or passivity to one characterized by cheerfulness or vitality.

Based on existing research on the impact of color on human emotions, a variety of hues were carefully

selected with the aim of enhancing individuals' moods and subsequently increasing productivity in the workplace. For example, the yellow color was specifically chosen to evoke feelings of happiness, while the blue color was deliberately chosen to cultivate a sense of tranquility (Fig. 11). The regulation of these various colors is achieved by detecting sound levels generated by individuals within an indoor environment, in accordance with

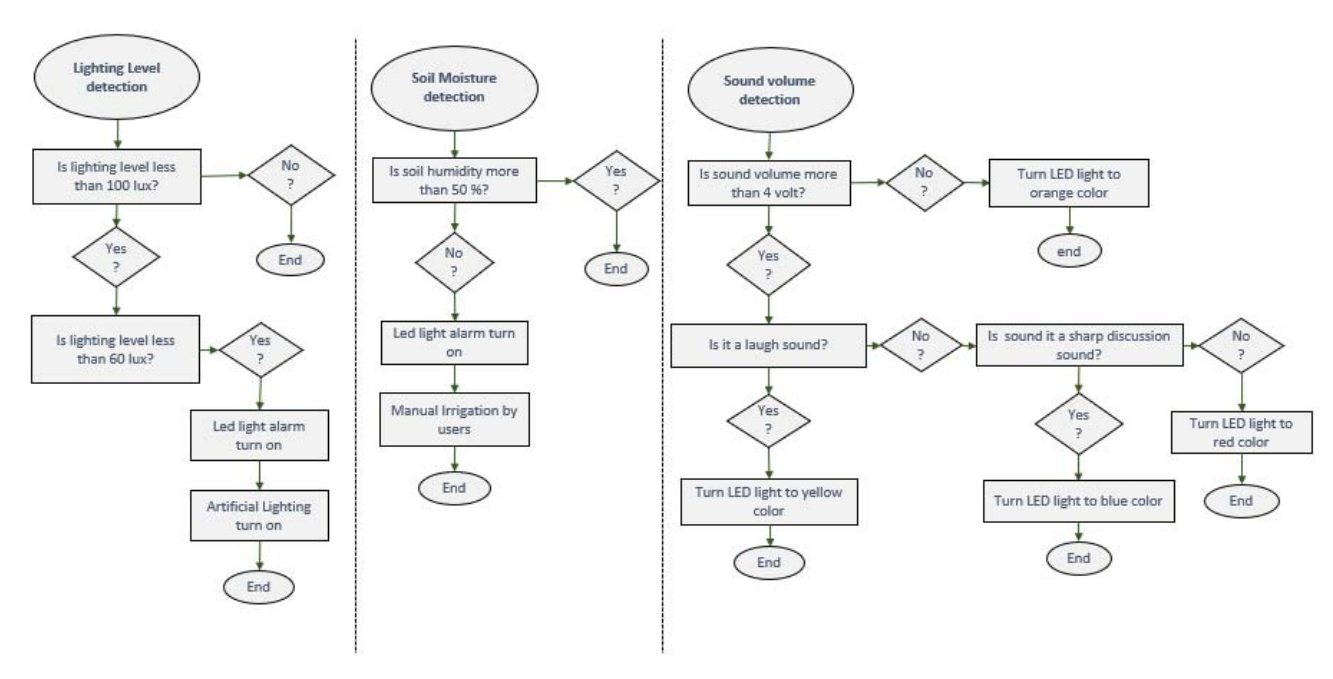


Fig. 10. Three different interactive status workflows for the three sensors in use

established guidelines for sound levels in such areas. The detection process involves identifying specific characteristics of sounds, including laughter, anger, and low conversational volumes.

Sound is quantified using the unit of measurement known as decibels (dB). A whisper typically registers at approximately 30 decibels (dB), whereas regular conversation often ranges around 60 dB. Prolonged exposure to noise levels exceeding 70 dB may potentially result in auditory impairment. Exposure to sound levels over 120 dB might result in rapid auditory damage.

The sound sensor module is equipped with both analog and digital output capabilities. The device operates across a range of supply voltages spanning from 3.3 to 5.3 V. This technology enables the detection of sound volume and the identification of distinct sound sources, facilitating the differentiation of the origin of the sound.

#### B. Soil moisture sensor

Anew interactive approach has been implemented to determine the water requirements of plants. This form of interactivity pertains to the mutual relationship and interactions between humans and plants. The soil moisture sensor is used to measure the moisture content in the soil, providing an indication of the soil humidity level. This information is valuable for determining whether the soil is experiencing drought conditions and requires irrigation. The concept revolves around examining the threshold of drought tolerance in the chosen plants, beyond which they are unable to sustain themselves. At this critical point, an illumination system will be activated to indicate the need for watering the plant (Rivas-Sánchez et al., 2019).

The resistive soil moisture sensor measures soil moisture levels by evaluating the relationship between water content and electrical resistance. The sensors are equipped with a pair of probes that

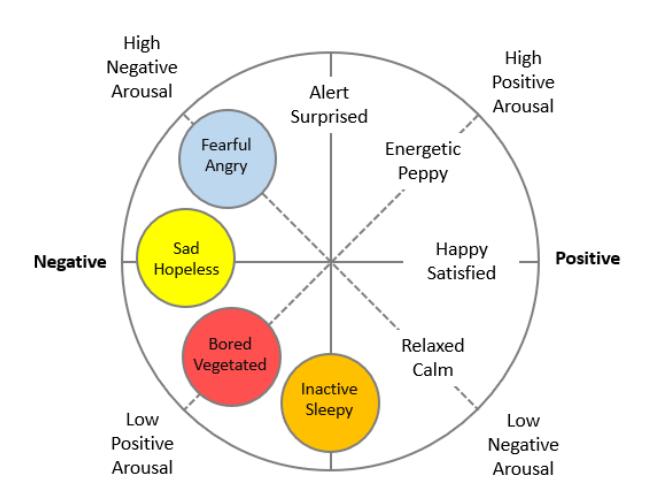


Fig. 11. Different color moods in response to negative or positive emotions

are fully inserted into the soil sample. There are two measurement scenarios based on the given information. In cases where the soil has high water content, there is a corresponding increase in its electrical conductivity. This increase in conductivity leads to a decrease in resistance levels, which serves as an indicator of elevated soil moisture levels. A decrease in the water content of soil leads to a reduction in its electrical conductivity, causing an increase in resistance, which serves as an indicator of low soil moisture.

#### C. Light sensors

The light sensor, commonly referred to as a photoelectric device, is capable of converting visible or infrared light energy, in the form of photons, into an electrical signal composed of electrons. Light sensors are commonly known as "photocensors" because they convert light energy, specifically photons, into electrical energy, specifically electrons (Rivas-Sánchez et al., 2019).

The green wall serves a primary function as a source of illumination due to two distinct factors. Primarily, it functions as the main source of ambient illumination for the occupants of the location. The ambient light of the green wall is activated in response to low levels of surrounding lighting. This light source serves to provide the plants with indirect illumination, which is crucial for their survival. In contrast to the sound sensor output, the response of this sensor is binary, activating when the ambient light level falls below a predetermined threshold based on the effectiveness of the lighting system, and deactivating when the room is adequately illuminated.

#### Fabrication and implementation

Three-dimensional printing stands as a notable example of additive manufacturing technologies that have had a substantial influence on the industrial sector. When it comes to developing prototypes for innovative concepts, it is widely acknowledged that 3D printing surpasses traditional methods by a significant margin. By utilizing virtual 3D models generated on a computer, it is possible to quickly fabricate three-dimensional objects using this approach. Throughout the duration of our pilot project, the green cell was fabricated into multiple components, which were subsequently joined together using adhesive materials before their installation on a steel framework system (Fig. 12).

The Arduino platform is an open-source system that includes user-friendly software and hardware components. The primary objective of this tool is to streamline the development process for diverse interactive projects across various scopes. Arduino is capable of perceiving its environment by receiving data from a diverse range of sensors. Additionally, it has the ability to exert an impact on its surroundings by manipulating various actuators, such as motors and lights, among others.



Fig. 12. Fabricated cell and its components

Arduino (Uno R3) was used in the pilot study to process data collected from three separate sensors and control the operation of the lighting system in order to display different color moods.

The completed design of the interactive green wall, along with its various components, is depicted in Fig. 13.

#### Conclusion

The purpose of this study is to improve the efficiency of the working atmosphere through the implementation of interior living walls. The present

study involves developing a proposal and product for the design of a living wall that incorporates the principles of biophilic design. This endeavor is undertaken through the use of parametric analogical design and interactivity as key design approaches.

The product effectively incorporates five distinct biophilic design patterns within the categories of "nature in space" and "natural analogs". The discussed patterns encompass both visual and nonvisual connections with nature, as well as dynamic and diffuse light, biomorphic forms and patterns, and complexity and order, as outlined in Table 3.

The adoption of this technique will not only enhance the performance efficiency of architectural spaces, but it will also imbue the components of interior design with a renewed purpose as a direct result of this transformation. Consequently, the green wall will engage individuals using the indoor space, helping them improve their effectiveness as participants in the activities conducted in that area.

#### **Acknowledgments**

This research is based on a pilot study that was completed as a primary requirement of a postgraduate course titled "ARC616 - Interactive and Responsive Architecture" in spring 2020. We are thankful to our postgraduate students (Ahmed Amin, Hamis Montaser, Hend Ehab, Mai Hassan, Mohamed Emad, Nada El-Moghazy, Shehab-Eldin Mohamed) who contributed greatly to the research efforts.

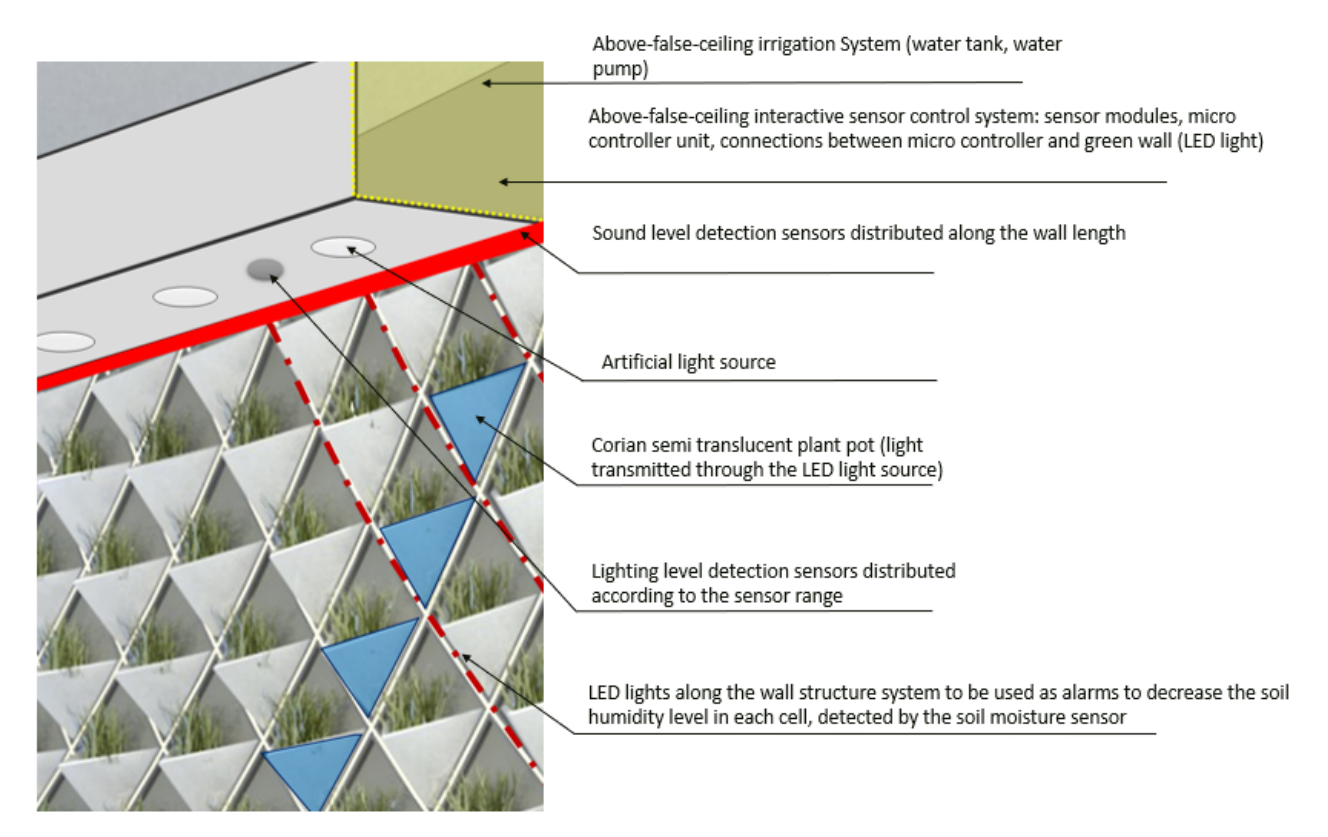


Fig. 13. Final design of the pilot and the Arduino controller

Table 3. Five biophilic design patterns utilized in the construction of the product

|                    | Patterns                          | Application  |  |
|--------------------|-----------------------------------|--|--|
|                    | Visual connection with nature     | Living wall in interior design                                       |  |
| ture               | Non-visual connection with nature | Living wall in interior design<br>Interactivity systems              |  |
| Nature<br>in Space | Dynamic and diffuse light         | Interactivity systems  |  |
| (0)                | Biomorphic forms and patterns     | Parametric analogical design   |  |
| Natural<br>Analogs | Complexity and order              | Living wall in interior design Technical installation considerations |  |

#### References

Almusaed, A. (2011). Introduction on growing media (soil). In: *Biophilic and Bioclimatic Architecture*. London: Springer, pp. 85–94. DOI: 10.1007/978-1-84996-534-7 6.

Assimakopoulos, M. N., de Masi, R. F., de Rossi, F., Papadaki, D., and Ruggiero, S. (2020). Green wall design approach towards energy performance and indoor comfort improvement: a case study in Athens. *Sustainability*, Vol. 12, Issue 9, 3772. DOI: 10.3390/SU12093772.

Briscoe, D. (2014). Parametric planting: green wall system research + design using BIM. In: *ACADIA 2014 - Design Agency: Proceedings of the 34<sup>th</sup> Annual Conference of the Association for Computer Aided Design in Architecture*, October 23–25, 2014, Los Angeles, USA, pp. 333–338. DOI: 10.52842/CONF.ACADIA.2014.333.

Browning, B. and Cooper, C. (2015). *Human spaces: the global impact of biophilic design in the workplace*. [online] Available at: https://greenplantsforgreenbuildings.org/wp-content/uploads/2015/08/Human-Spaces-Report-Biophilic-Global\_Impact\_Biophilic Design.pdf [Date accessed July 7, 2022].

Dede, G., Pekarchuk, O., Özer, H., and Dede, O. H. (2019). Alternative growing media components for green wall designs in terms of lightweight. In: 2<sup>nd</sup> International Congress on Engineering and Architecture, April 22–24, 2019, Marmaris, Turkey, pp, 374–383.

Downton, P., Jones, D., Zeunert, J., and Roös, P. (2017). Biophilic design applications: putting theory and patterns into built environment practice. In: *The International Conference on Design and Technology*, December 5–8, 2016, Geelong, Australia, pp. 59–65. DOI: 10.18502/KEG.V2I2.596.

Espiritu, K. (2022). *Peat moss: using sphagnum peat in the garden - epic gardening*. [online] Available at: https://www.epicgardening. com/peat-moss/ [Date accessed August 4, 2022].

Gunawardena, K. and Steemers, K. (2019). Living walls in indoor environments. *Building and Environment*, Vol. 148, pp. 478–487. DOI: 10.1016/J.BUILDENV.2018.11.014.

Johnstone, G. (2022). Lipstick plant: care & growing guide: a cascading and constantly flowering houseplant. [online] Available at: https://www.thespruce.com/lipstick-plant-care-5083734 [Date accessed August 4, 2022].

Kaumoodi (2021). Role of analogy in architecture design education. *International Journal of Engineering Research & Technology*, Vol. 10, Issue 9, pp. 164–172.

Kim, H., Huang, J., and Lee, J.-K. (2016). A case study: projecting images for designing interior panels using parametric modeling tool. In: 2016 Proceedings of the 33rd ISARC, July, 18–21, 2016, Auburn, USA, pp. 818–825. DOI: 10.22260/ISARC2016/0099.

Lundegren, M. (2016). *Green walls vs. green facades*. [online] Available at: https://archanatura.com/2016/02/01/green-walls-versus-green-facades/ [Date accessed February 2, 2016].

Madani, F., Mishra, A., Ibarra, M., Mansour, M., and Durairajan, S. (2013). *New product planning: case of indoor water plant system*. [online] Available at: https://papers.ssrn.com/sol3/papers.cfm?abstract\_id=3023593 [Date accessed July 9, 2022]. DOI: 10.2139/SSRN.3023593.

Meshram, A. and Srivastava, N. (2015). *Epipremnum aureum* (Jade pothos): a multipurpose plant with its medicinal and pharmacological properties. *Journal of Critical Reviews*, Vol. 2, Issue 2, pp. 21–25. DOI: 10.31838/jcr.02.01.04.

Nabil, S. and Kirk, D. (2019). Interactive interior design and personal data. In: Schnädelbach, H. and Kirk, D. (eds.). *People, Personal Data and the Built Environment. Springer Series in Adaptive Environments.* Cham: Springer, pp. 103–122. DOI: 10.1007/978-3-319-70875-1\_5.

Peters, T. and D'Penna, K. (2020). Biophilic design for restorative university learning environments: a critical review of literature and design recommendations. *Sustainability*, Vol. 12, Issue 17, 7064. DOI: 10.3390/SU12177064.

Radić, M., Dodig, M. B., and Auer, T. (2019). Green facades and living walls—a review establishing the classification of construction types and mapping the benefits. *Sustainability*, Vol. 11, Issue 17, 4579. DOI: 10.3390/SU11174579.

Rakhshandehroo, M., Mohd Yusof, M. J., and Arabi, R. (2015). Living wall (vertical greening): benefits and threats. *Applied Mechanics and Materials*, Vol. 747, pp. 16–19. DOI: 10.4028/WWW.SCIENTIFIC.NET/AMM.747.16.

Rivas-Sánchez, Y. A., Moreno-Pérez, M. F., and Roldán-Cañas, J. (2019). Environment control with low-cost microcontrollers and microprocessors: Application for green walls. *Sustainability*, Vol. 11, Issue 3, 782. DOI: 10.3390/SU11030782.

Sarkar, A. N. (2018). Selection of plants for vertical gardening and green roof farming. *International Research Journal of Plant and Crop Sciences*, Vol. 4, No. 3, pp. 132–153.

Sheweka, S. and Magdy, N. (2011). The living walls as an approach for a healthy urban environment. *Energy Procedia*, Vol. 6, pp. 592–599. DOI: 10.1016/J.EGYPRO.2011.05.068.

Tamási, A. and Dobszay, G. (2015). Requirements for designing living wall systems – analysing system studies on Hungarian projects. *Periodica Polytechnica Architecture*, Vol. 46, No. 2, pp. 78–87. DOI: 10.3311/PPar.8337.

Wikimedia Commons (2022). File:Money Plant (Epipremnum aureum 'N' Joy').jpg. [online] Available at: https://commons.wikimedia.org/wiki/File:Money\_Plant\_(Epipremnum\_aureum\_%27N%27\_Joy%27).jpg [Date accessed October 24, 2022].

Wilkinson, S., Carmichael, M., and Khonasty, R. (2021). Towards smart green wall maintenance and Wallbot technology. *Property Management*, Vol. 39, Issue 4, pp. 466–478. DOI: 10.1108/PM-09-2020-0062.

# БИОФИЛИЯ НА РАБОЧЕМ МЕСТЕ: ПИЛОТНЫЙ ПРОЕКТ ПО СОЗДАНИЮ ФИТОСТЕНЫ С ИСПОЛЬЗОВАНИЕМ ИНТЕРАКТИВНОГО ПАРАМЕТРИЧЕСКОГО ПРОЕКТИРОВАНИЯ

Айман Ассем\*, Доаа К. Хассан

Кафедра архитектурного проектирования, Инженерный факультет Университет Айн-Шамс, Египет

\*E-mail: ayman.assem@eng.asu.edu.eg

#### Аннотация

Введение: Результат работы определяется не только производительностью труда и прибылью. Сам процесс и практические аспекты, сопутствующие достижению целей, также имеют большое значение. Между работодателями и работниками ведется непрекращающаяся дискуссия относительно концепции того, каким должно быть рабочее место. Основное внимание уделяется формированию всеобъемлющего подхода к труду и той среде, в рамках которой выполняется работа. Это исследование рассматривает связь с миром природы, в частности то, каким образом растения могут улучшить эстетику и поддержать хорошее самочувствие. Рассматривается реализация биофильного дизайна для борьбы с синдромом «больного здания» путем интеграции живой стены в интерьер рабочего места. Методы: В исследовании используется параметрический подход к проектированию для определения дизайнерского решения по включению живой стены в рабочее место. Этот подход повышает корреляцию между несколькими параметрами, влияющими на результат проектирования. Данный подход действует на двух уровнях. Во-первых, для определения формы элементов фитостены и формирования различных вариантов на основе параметров генерирования, полученных из природных источников, используется аналоговое проектирование. Во-вторых, в целях улучшения восприятия фитостены и ее различных вариантов применяется интерактивность, что в конечном итоге приводит к созданию уникальной атмосферы, которая подходит для самых разных видов деятельности Результаты: Подробно описаны результаты использования параметрического проектирования, включая успешное создание различных вариантов и форм элементов зеленой стены и улучшение восприятия сотрудниками при помощи интерактивности. Представлена эффективность этих дизайнерских решений в создании уникальной атмосферы и оптимизации взаимодействия сотрудников на рабочем месте.

Ключевые слова: биофилия, параметрический дизайн, фитостена, интерактивный дизайн.

## REGIONAL SETTING OF TEMPLES IN DAKSHINA KOSALA, INDIA: SPATIAL DISTRIBUTION AND CONNECTIONS

Saumya Shrivastava\*, Abir Bandyopadhyay, Vandana Agrawal

National Institute of Technology, Raipur, Chhattisgarh, India

\*Corresponding author's e-mail: sshrivastava.phd2021.arch@nitrr.ac.in

#### Abstract

Introduction: The region of Dakshina Kosala (also known as South Kosala) is mentioned in various ancient Indian texts. The exact geographical boundary has continuously changed over time, and today, only a rough estimate can be made of the Dakshina Kosala region, which approximately covers the northern and central parts of the present-day state of Chhattisgarh, along with the western part of the state of Odisha, India. Excavations and writings show that this was a prosperous region near central India, without any seaport, but with large markets, trade centers, and educational institutions. To access this region, many trade routes were established from various parts of India. This led to the development of cities with markets along these trade routes. Many temples were also seen in this region, serving as examples of the intangible heritage of the place. Purpose of the study: This region made a significant contribution to the temple art and architecture of India. The present study aims to determine if there is a spatial and architectural link between the temples in this region. Methods: The methodology involved an initial phase of reading and analyzing pertinent literature to prepare detailed maps delineating the boundaries of Dakshina Kosala. Subsequently, employing rigorous analysis with Google Earth and GIS tools, ancient trade routes were traced, temples were located on the maps, and a comprehensive analysis was conducted to derive conclusive results. Results: This paper establishes a relationship between the geographical locations and construction materials of the temples within and outside the geographical boundary of Dakshina Kosala.

Keywords: boundaries of Dakshina Kosala, spatial links, connectivity, ancient trade routes, temple architecture.

#### Introduction

India has always been a place of attraction for foreign travellers (Lamb, 1958). It is evident from various pieces of literature that in ancient times India had a lot of foreign travelers who visited it in different periods, such as Megasthenes (302–298 BCE), Deimachus (320–273 BCE), Ptolemy (130 CE), Fa Hien (405–411 CE), Huen Tsang (630 CE), I Tsing (671–695 CE), Marco Polo (1292–1294 CE), and Ibn-E-Battuta (1333–1342 CE) (Bhattacharya, 2014; Chandra, 1977; Johnston, 1941; lasgyan.in, 2021; N.C.E.R.T., 2011; Thapar, 1992).

These travellers mentioned the conditions of India at that time in their travelogues. Fa-Hien described India as a rich and prosperous country (Chandra, 1977). Huen Tsang wrote that the Indian towns were very prosperous and unique, and also described Indians as lovers of education, literature, and fine arts (Pradhan and Yadav, 2013). Those travellers came through different trade routes in India, and descriptions of their journeys can be found in their travelogues and in the writings of various historians, archaeologists, and scholars (Chakrabarti and Rakshit, 1995; Nayak, 2004; Patnaik, 2013; Sahu & Chandra, 1983; Srivastava, 1968; Watters, 1904).

These trade routes connected inland cities of India with other countries. Many cities developed and flourished along these trade routes, exhibiting a conspicuous capacity to generate culture in the form of art, ideas, styles, and attitudes, as well as to induce high levels of economic innovation and growth, though not always simultaneously (Scott, 1997). Due to the existence of trade routes, cities became nodes of cultural dispersion. The culture of the cities would spread through these trade routes from one location to another.

#### Methods

For this study, existing literature about the geographical location, boundaries of Dakshina Kosala, and descriptions of the trade routes connecting Dakshina Kosala with other places in India, as well as with foreign countries, was examined. Also, literature related to the temples of the region and their architecture was reviewed. These texts were comprehensively analyzed, and the results related to the spatial relations among the temples in the region were identified. For a better understanding of the information pertaining to the location of temples and trade routes, maps were created using ArcGIS¹.

#### **Results and Discussion**

Boundaries of Dakshina Kosala

In ancient times, Dakshina Kosala was of great importance (Minj, 2015). It is evident from the writings of various scholars that the region of Dakshina Kosala used to be very rich and prosperous

<sup>&</sup>lt;sup>1</sup> Maps are generated through ArcGIS Online (GIS software). https://www.arcgis.com/home/index.html

(Majumdar, 2001). Many descriptions are available about the boundaries of Dakshina Kosala, but the earliest mention of it is found in the Ramayana, an ancient Indian text (Patnaik, 2016). According to the Ramayana, Lord Rama ruled over "Mahakosala", which means the larger Kosala, with boundaries extending from present-day Nepal in the north to the upper Mahanadi valley in the south (Patnaik, 2016). When Lord Rama divided his territory among his sons, he gave the upper part, Uttar Kosala (North Kosala), to his elder son Lav, and the lower part, Dakshina Kosala, to his younger son Kush (Patnaik, 2016) (Fig. 1). Uttar Kosala had its capital city, Ayodhya, in Uttar Pradesh, while Dakshina Kosala had its capital city at Kushavati (present-day Ranipur Jharial) in western Odisha (Mishra, 2013; Mishra, 1993). Later, various Puranic texts such as Matsya Purana, Brihat Samhita, Brahmanda Purana, and Ratnavali also mentioned the region of Kosala, but the descriptions only referred to the southern part of the region, i.e., Dakshina Kosala (Patnaik, 2016).

Later, Raychaudhuri (2006) described the boundaries of the Dakshina Kosala region based on the Vana Parva of the Mahabharata, an ancient Indian text. In the 7th century CE, the Chinese traveler Huen Tsang visited Dakshina Kosala and discussed its boundaries in his travelogue (Watters, 1904). Later, based on Huen Tsang's account, Cunningham in 1881–1882 and Watters in 1904 also discussed the boundaries of Dakshina Kosala (Nayak, 2004). Then, Sircar (1971) described the boundary of Dakshina Kosala, taking into account Cunningham's and Watter's boundaries for the region. For the present study, the boundaries of



Fig. 1. Kosala region as per Puranic texts. Source: Author, base map – Meena (2023)

Dakshina Kosala were identified by superimposing the boundaries identified in the above-mentioned studies, Patnaik (2016), and as per various district gazetteers<sup>2</sup>. As a result, the boundary of Dakshina Kosala consists of the undivided districts of Raipur, Bilaspur, and Raigarh in the state of Chhattisgarh, as well as Sambalpur, Nuapada, Bolangir, Kalahandi, Sundargarh, Boudh, and Subarnpur districts in the state of Odisha (Fig. 2).

#### Connectivity in the region

A great deal of trade and commerce made Dakshina Kosala a prosperous region (Patnaik, 2016). Dakshina Kosala had many important cities such as Juagarh, Sirpur, Sambalpur, Asurgarh, etc. (Nayak, 2004).

Kalinga (roughly the boundary of present-day Odisha), a neighboring region to Dakshina Kosala, was very famous for its textile industries (Dutt, 2009; Nayak, 2004). A lot of trade and commerce used to take place in Kalinga via Dakshina Kosala (Nayak, 2004). It is evident from the Roman coins found during excavations that diamonds and gemstones from the Dakshina Kosala region were popular among Romans (Das, 1978; Tripathy, 1996). The strong black elephants of Dakshina Kosala were in demand not only by Indian states, but also by foreign countries (Nayak, 2004). Dakshina Kosala had important educational centers and marketplaces like Sripura (present-day Sirpur in Mahasamund district, Chhattisgarh) (Sharma, 2012).

Various texts discuss the presence of highly significant trade routes in Dakshina Kosala (Nayak, 2004). For the present study, some of the major trade routes have been mapped. In India, the majority of ancient trade routes have been converted into state or national highways (Bhattacharyay and De, 2009).

<sup>2</sup> District Gazetteer of Raipur, Bilaspur, Korba, and Raigarh in the state of Chhattisgarh, as well as Sambalpur, Sundargarh, Boudh, Bargarh, Subarnapur, Bolangir, Kalahandi, and Nuapada in the state of Odisha.

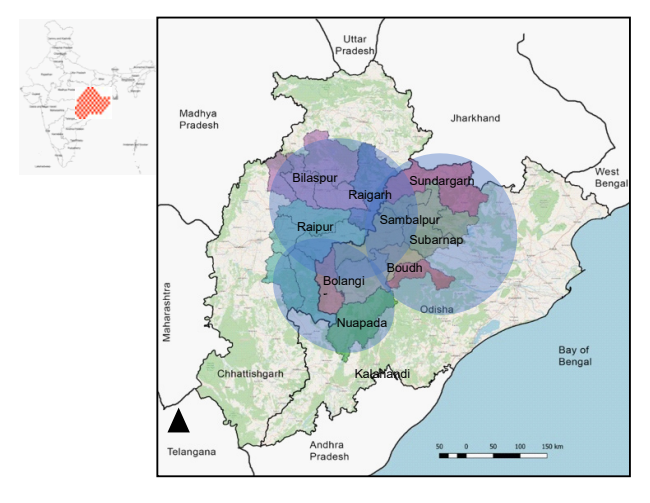


Fig. 2. Boundaries of Dakshina Kosala. Source: Author

|                            |            |              | with other parts of mula                         |  |  |
|----------------------------|------------|--------------|--|--|--|
| Route                      | Connec     | cting cities | Important cities in the route                    |  |  |
| Route 1 Tamralipti Toshali |            | Toshali      | Bhubaneswar, Jajpur                              |  |  |
| Route 2                    | Toshali    | Patliputra   | Tamralipti                                       |  |  |
| Route 3                    | Patliputra | Juagarh      | Bilaspur, Raipur, Asurgarh                       |  |  |
| Route 4                    | Mathura    | Sisupalgarh  | Via Vidisha, Bilaspur, Raipur, Asurgarh, Toshali |  |  |
| Route 5                    | Ahichhatra | Asurgarh     | Kanpur, Kaushambi, Bilaspur, Raipur, Sarguja     |  |  |
| Route 6                    | Kaushambi  | Ganjam       | Bilaspur, Raipur, Asurgarh, Juagarh              |  |  |
| Route 7                    | Ranchi     | Raipur       | Raigarh, Sambalpur                               |  |  |

Table 1. Ancient trade routes connecting Dakshina Kosala with other parts of India

Source: author.

For example, the ancient Grand Trunk route of India still exists as National Highway 3 (NH3), running from Attari to Jalandhar in Punjab, from Jalandhar in Punjab to Agra in Uttar Pradesh as NH44, and from Agra in in Uttar Pradesh to Kolkata in West Bengal as NH19 (Bhattacharyay and De, 2009). In order to map the ancient trade routes, various descriptions of these routes were studied and then matched with the closest present-day state or national highways connecting those old cities. These routes were traced and a map of the ancient trade routes of the Dakshina Kosala region was generated through geo-tagging in ArcGIS. Seven such routes were identified, as shown in Table 1.

The earliest account of trade routes shows the connectivity of the Dakshina Kosala region with the seaport (Bay of Bengal) in the 4th–2nd century BCE via Tamralipti (currently in the Midnapore district in West Bengal) and Toshali (currently a town near Bhubaneshwar) (Nayak, 2004), identified as route 1 in Table 1. During that period, the region had two major metropolises of the Mauryan kingdom named Juagarh and Sisupalgarh, which are currently locations near the city of Bhubaneswar in Odisha (Nayak, 2004). In ancient times, Tamralipti used to be a port city, and there are traces of foreign relations with south-east Asian countries from the port of Tamralipti (Patra and Patra, 1993; Srivastava, 1968).

Later, the region became very well connected to northern India by various land routes. One of those routes connected Patliputra (present-day Patna in Bihar) to Toshali (Acharya, 1955) in the 1<sup>st</sup> century BCE – the 2<sup>nd</sup> century CE (route 2 in Table 1) via Tamralipti.

There is a description of a trade route connecting Patliputra to Juagarh through Dakshina Kosala (Bilaspur, Raipur), and Asurgarh in the 2<sup>nd</sup> century CE (Acharya, 1955; Nayak, 2004), which can be identified as route 3 in Table 1. The route primarily connected Patna with Raipur via Sarguja, a district in the state of Chhattisgarh (Acharya, 1955). There were routes connecting Raipur to Juagarh and Ganjam via Asurgarh, also known as a "salt route" in ancient times (Acharya, 1955; Nayak, 2004).

Another trade route was established between the central part of India and the Kalinga region through Dakshina Kosala, which can be identified as route 4 in Table 1. The route connected present-day Mathura in Uttar Pradesh to Sisupalgarh (near present-day Bhubaneswar) in Odisha through land routes (Chandra, 1977) via Vidisha, Raipur, Bilaspur, Asurgarh, and Toshali. The route was originally established between Mathura and Vidisha, and later connectivity was extended to Dakshina Kosala and Kalinga.

One more trade route was developed during the Gupta rule ( $3^{rd}$  century CE  $-6^{th}$  century CE), known as the "brick trade route", connecting the present-day Ahichhatra near Kanpur in Uttar Pradesh to the present-day Asurgarh in Odisha (Nayak, 2004) (route 5 in Table 1).

A trade route connected Kaushambi with Ganjam, a port city in Odisha (Nayak, 2004). This route also connected with Dakshina Kosala and can be identified as route 6 in Table 1.

The main reason for the development of these routes was the Gupta ruling dynasty in both regions until the 5<sup>th</sup> century CE. After the 9<sup>th</sup> century CE, many land routes were developed in the region by the Kalchuri ruling dynasty. One of the major trade routes connecting present-day Ranchi in the state of Jharkhand with present-day Raipur can be identified as route 7 in Table 1 (Nayak, 2004) (Fig. 3).

Many cities were located along these trade routes, such as Raipur, Bilaspur, Sambalpur, Sirpur, Boudh, Asurgarh, Juagarh, etc. (Chandra, 1977; Nayak, 2004; Patnaik, 2016; Sharma, 2012). Besides, the region was also well connected with southern India. Geographically, the region acted as a bridge between southern and northern India.

In ancient times, in addition to land routes, riverine routes were also used. Of the two trade routes, one by water and the other by land, the former is better since it is less expensive but yields large profits (Shamasastry, 1929). The riverine routes were preferred over the land routes due to the lesser chance of getting attacked by other people and wild animals (Shamasastry, 1929). The famous rivers of Dakshina Kosala, which were used as trade routes in ancient times were Mahanadi, Tel, Vaitarani, Birupa and Brahmani (Nayak, 2004; Singh, 2020). After superimposing all the trade routes on a map, it is

clear that the entire region of Dakshina Kosala was well connected within itself and with other places in India through the trade routes (Fig. 3).

#### Temples of Dakshina Kosala

In Dakshina Kosala, a series of ancient temples can be found. The earliest temples belong to the 5th century CE, post-Gupta period (Greaves, 2015). Various research scholars have discussed and studied the temples of Dakshina Kosala. As Stadtner (1981) stated, Kosala was "an independent area in central India sponsoring a distinctive regional school of temple architecture and sculpture". Hardy (2020) said that "the history of Indian temple architecture would have been written differently if the Malhar (in Dakshina Kosala) temple had been discovered earlier". A list of the celebrated/famous temples in the region was compiled based on various studies conducted in the area (see Table 2). The coordinates of the temples are identified in GIS and mentioned in the list. The temples are sorted according to the approximate year of construction, as obtained from various available literature sources (Fig. 4).

To understand the regional setting of the temples, a map was created by identifying the location of the temples in Google Earth and then geo-tagging them in ArcGIS (Fig. 5). The numbering of the temples in Fig. 5 and Table 2 is the same.

Relation between the trade routes and the temples

When examining the locations of the temples as shown on Fig. 5, it can be seen that the temples

are clustered within a specific geographical zone, with three such clustered zones being apparent. To further analyze the spatial setting of these temples, the identified trade routes shown in Fig. 3 were superimposed over the temple locations. It was found that most of the temples either lie on the trade routes or in very close proximity to them. The number of temples identified along the trade routes is shown in Table 3 and Fig. 6.

Routes 1 and 2 have the Prachi group of temples and the Viraja temple near Jajpur. Route 3 connecting Patliputra to Juagarh has a total of 5 temples: the Shiva temple in Udaipur, the Shiva temple at Pali, the leaning Huma temple in Sambalpur, the Kosaleshwar temple at Boudh, and the brick temples of Asurgarh. There are a total of seven temples, as identified in Table 2, located on Route 4. These temples include the Bhoremdeo temple at Kawardha, the Devrani Jethani temple at Tala, the Dhobini temple at Damakheda, the Pataleshwar temple at Nuapada, the Somnath temple, the Indralath temple, and the 64 Yogini temples at Ranipur Jharial. On Route 5 (brick trade route), a total of 6 famous temples were identified. Three Vishnu temples in the Dakshina Kosala region are the Devrani Jethani temple, the Laxman temple at Sirpur, and the Vishnu temple of Asurgarh. Additionally, there are three temples outside the region: the temples at Ahichhatra, Bhitargaon, and Nibiya Khera, all located in Uttar Pradesh. The Paschima Somnath temple near Boudh district is located on Route 6. On Route 7, there are five

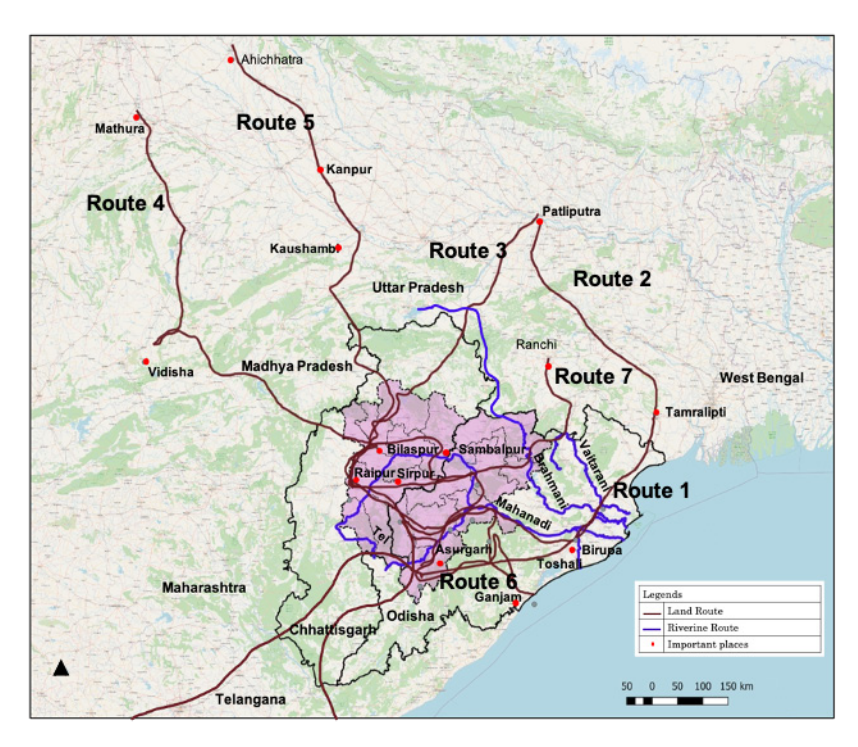


Fig. 3. Ancient trade routes of Dakshina Kosala. Source: Author

Table 2. List of Dakshina Kosala temples

| No. | Temple              | Location        | Year of construction (CE)                  | Coordinates<br>(latitude, longitude) |
|-----|---------------------|-----------------|--|--------------------------------------|
| 1   | Shiva               | Kalcha Bhadwahi | 10 <sup>th</sup> century                   | 23°1'4.59", 82°55'13.39"             |
| 2   | Bhoramdeo           | Kawardha        | 13 <sup>th</sup> century                   | 22°6'57.528", 81°8'54.1314"          |
| 3   | Vishnu              | Janjgir         | 11th century                               | 22°0'21.24", 82°34'19.9194"          |
| 4   | Pataleshwar         | Malhar          | 10th-12th century                          | 21°33', 82°12'                       |
| 5   | Devrani Jethani     | Tala            | 5 <sup>th</sup> –6 <sup>th</sup> century   | 21°54'25.9194", 82°1'33.5994"        |
| 6   | Citavari devi       | Dhobini         | 8 <sup>th</sup> century                    | 21°36'54.3234", 82°48'42.804"        |
| 7   | Andal deul          | Kharod          | 8 <sup>th</sup> century                    | 21°44'48.48", 82°34'46.5594"         |
| 8   | Shabari             | Kharod          | 8 <sup>th</sup> century                    | 21° 44' 24.4794", 82° 33' 51.1194"   |
| 9   | Keshavnarayan       | Shiverinarayan  | 9th-12th century                           | 21° 43' 18.48", 82° 35' 41.6394"     |
| 10  | Ram Janki           | Turturiya       | 9 <sup>th</sup> century                    | 21° 29' 32.6394", 82° 21' 46.0794"   |
| 11  | Siddheshwara        | Palari          | 9 <sup>th</sup> century                    | 21° 27' 12.8118", 82° 10' 39.5034"   |
| 12  | Sirpur Group        | Sirpur          | 6th-7th century                            | 21° 20' 39.12", 82° 11' 25.4394"     |
| 13  | Bhand Dewal         | Arang           | 9 <sup>th</sup> century                    | 19° 8' 59.6394", 72° 55' 51.96"      |
| 14  | Rajiv Lochan        | Rajim           | 8 <sup>th</sup> century                    | 20° 58' 23.4834", 81° 23' 21.8394"   |
| 15  | Bhongapal Group     | Kondagaon       | 5 <sup>th</sup> –6 <sup>th</sup> century   | 19° 48' 25.92", 81° 23' 21.8394"     |
| 16  | Group of temples    | Gadh Dhanora    | 9 <sup>th</sup> century                    | 19° 57' 53.28", 81° 45' 0.7914"      |
| 17  | Shiva Temple        | Pujaripali      | 9 <sup>th</sup> century                    | 21° 41′ 40.884″, 83° 21′ 5.112″      |
| 18  | Shiva Temple        | Pali            | 9th-10th century                           | 22° 22' 39", 82° 19' 31.8"           |
| 19  | Hatkeshwar          | Raipur          | 15 <sup>th</sup> –16 <sup>th</sup> century | 21° 12' 56.5194", 81° 35' 27.24"     |
| 20  | Mahamaya            | Bilaspur        | 12 <sup>th</sup> century                   | 22° 17' 29.3994", 82° 9' 53.64"      |
| 21  | Jagannath           | Jharsuguda      | 13 <sup>th</sup> century                   | 21° 51' 59.0034", 84° 0' 52.5234"    |
| 22  | Huma                | Sambalpur       | 9th-10th century                           | 21° 16' 53.3274", 83° 54' 44.604"    |
| 23  | Kapileshwar         | Binka           | 8 <sup>th</sup> century                    | 20° 59' 34.0794", 83° 47' 39.48"     |
| 24  | Pataleshwar         | Nuapada         | 9 <sup>th</sup> century                    | 20° 35' 1.896", 82° 40' 16.4634"     |
| 25  | 64 Yogini           | Ranipur Jharial | 9 <sup>th</sup> century                    | 20° 16' 58.8", 82° 57' 50.3994"      |
| 26  | Indralath           | Ranipur Jharial | 9 <sup>th</sup> century                    | 20° 17' 13.9194", 82° 58' 5.5194"    |
| 27  | Somnath             | Ranipur Jharial | 9 <sup>th</sup> century                    | 20° 16' 52.3194", 82° 57' 54"        |
| 28  | Asurgarh            | Kalahandi       | 5 <sup>th</sup> –6 <sup>th</sup> century   | 20° 5' 45.9594", 83° 20' 43.8"       |
| 29  | Kosaleswar          | Subarnapur      | 8 <sup>th</sup> century                    | 21° 12' 28.4394", 84° 25' 20.9994"   |
| 30  | Rameshwar           | Subarnapur      | 13 <sup>th</sup> century                   | 20° 50' 22.56", 83° 55' 17.7594"     |
| 31  | Manamunda           | Subarnapur      | 11th century                               | 20° 50' 4.1274", 83° 54' 52.344"     |
| 32  | Charisambhu         | Gandharadi      | 8 <sup>th</sup> century                    | 20° 52' 31.1514", 84° 12' 19.4034"   |
| 33  | Rameshwar           | Boudh           | 8 <sup>th</sup> century                    | 20° 50' 39.2634", 84° 18' 58.572"    |
| 34  | Paschima Somnath    | Boudh           | 8 <sup>th</sup> century                    | 20° 50' 38.76", 84° 18' 58.4634"     |
| 35  | Dhabaleshwar        | Boudh           | 8 <sup>th</sup> century                    | 20° 50' 38.688", 84° 18' 59.04"      |
| 36  | Nrushingnath        | Bargarh         | 14th century                               | 21° 47' 40.9554", 83° 56' 27.6714"   |
| 37  | Ashatshambhu        | Dhenkanal       | 10 <sup>th</sup> century                   | 20° 15' 38.1954", 85° 50' 3.6234"    |
| 38  | Viraja              | Jajpur          | 13 <sup>th</sup> century                   | 20° 21' 21.7794", 85° 49' 33.7794"   |
| 39  | Prachi Valley Group | Cuttack         | 7 <sup>th</sup> –16 <sup>th</sup> century  | 20° 16' 10.488", 85° 57' 17.8554"    |
| 40  | Samleshwari         | Sambalpur       | 15 <sup>th</sup> century                   | 21° 29' 40.992", 83° 57' 31.104"     |

Source: Greaves, 2015; Hardy, 2020; Kumar, 2003; Meister, 1988; Minj, 2015; Patnaik, 2016; Pradhan, 2008; Sarma & Sarma, 1941; Sharma, 2012; Singh, 2004; Stadtner, 1981; Tripathy, 1996.

temples including the leaning Huma temple at Sambalpur, the Pujaripali temple at Raigarh, the Vishnu Mandir at Janjgir, the Pataleshwar temple at Malhar, and the Devrani-Jethani temple at Tala (Table 2, Fig. 4). The temples are also located either on the riverine routes or in proximity to them. A total of 22 temples are found in the proximity of the riverine routes (Table 4).

The maximum number of temples i.e., 17 temples are found in the proximity of the Mahanadi River route which starts from the Sihawa mountain range

and ends at the Bay of Bengal (Table 4). All the listed temples (Table 1) are located either on a trade route (land route or river route) or in proximity to it (Fig. 6).

Similarities in temples of Dakshina Kosala

Given the proximity of the trade routes and the location of the temples in Dakshina Kosala, it is possible that they may share certain similarities or parallels. It has been observed that the temples bear similarities in architectural style, materials used in construction, etc. Other than this, the enshrined deity of the temples is also the same in the majority of

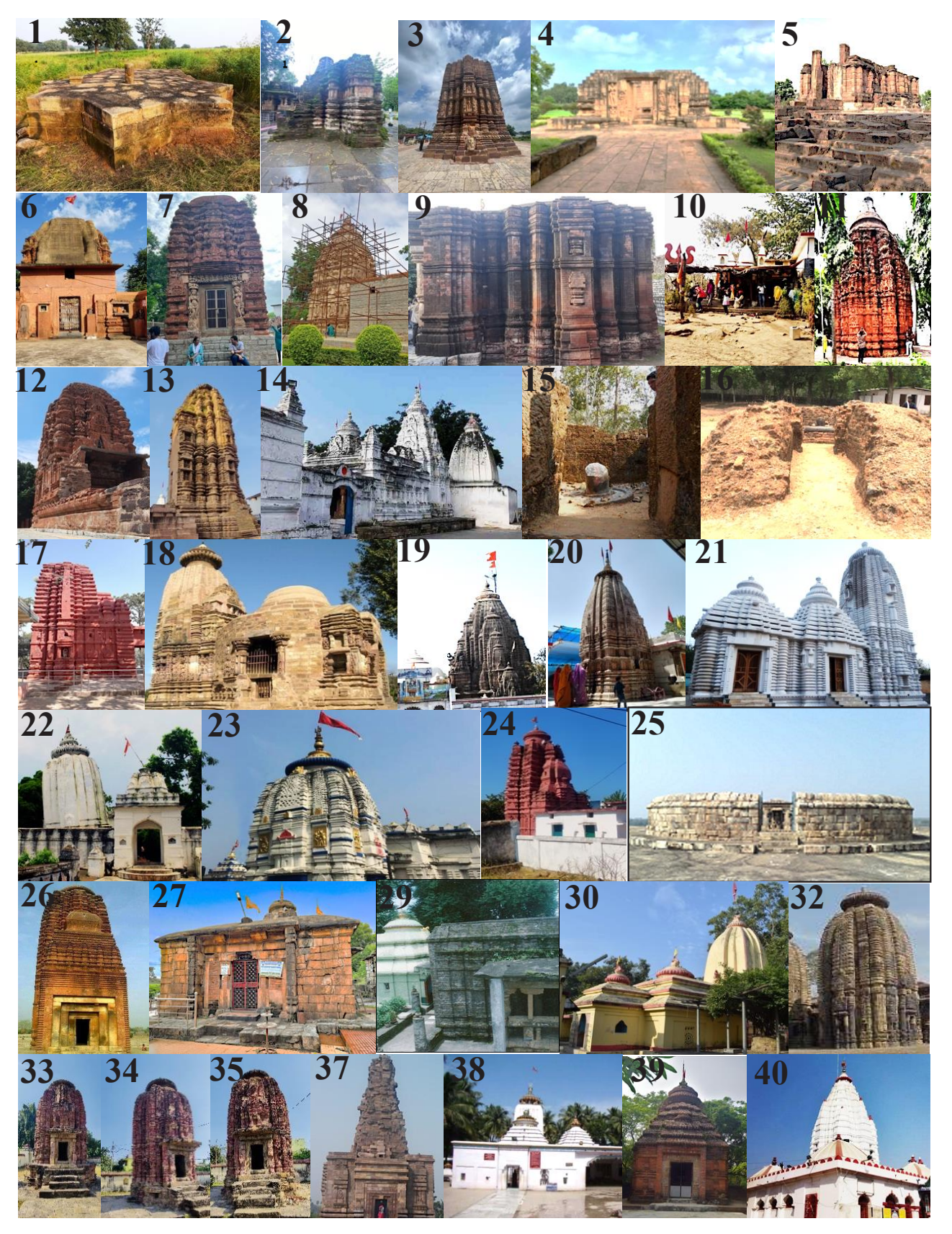


Fig. 4. Temples of Dakshina Kosala. Source: author

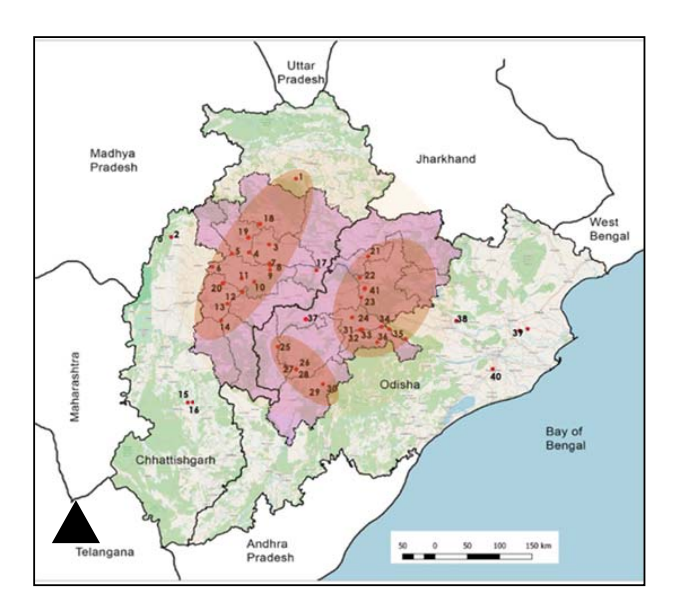


Fig. 5. Location of the listed temples. Source: author, locations of the listed temples. Raipur, Chhattisgarh: ArcGIS, 2023

Table 3. Temples in the proximity of the land trade routes

| Route          | No. of temples       | Material        |  |
|----------------|----------------------|-----------------|--|
| Routes 1 and 2 | 2 (group of temples) | Brick and stone |  |
| Route 4        | 7                    | Brick and stone |  |
| Route 6        | 1 Brick and          |                 |  |
| Route 3        | 5                    | Brick and stone |  |
| Route 5        | 6                    | Brick           |  |
| Route 6        | 2                    | Brick and stone |  |
| Route 7        | 5                    | Brick and stone |  |

Source: author.

temples. Most of the temples have been conserved and restored multiple times, and the people have changed the deities of the temples. However, the similarity in construction materials can still be easily seen in these temples. In ancient times (5th-14th century CE), the construction materials used for temple building in Dakshina Kosala were brick and

Table 4. Temples in the proximity of the riverine trade routes

| River     | From       | То            | No. of temples | Material        |
|-----------|------------|---------------|----------------|-----------------|
| Mahanadi  | Sihawa     | Bay of Bengal | 17             | Brick and stone |
| Tel       | Koraput    | Boudh         | 2              | Brick and stone |
| Vaitarani | Keonjhar   | Bay of Bengal | 1              | Stone           |
| Brahmani  | Sundergarh | Bay of Bengal | 2              | Brick and stone |

Source: author.

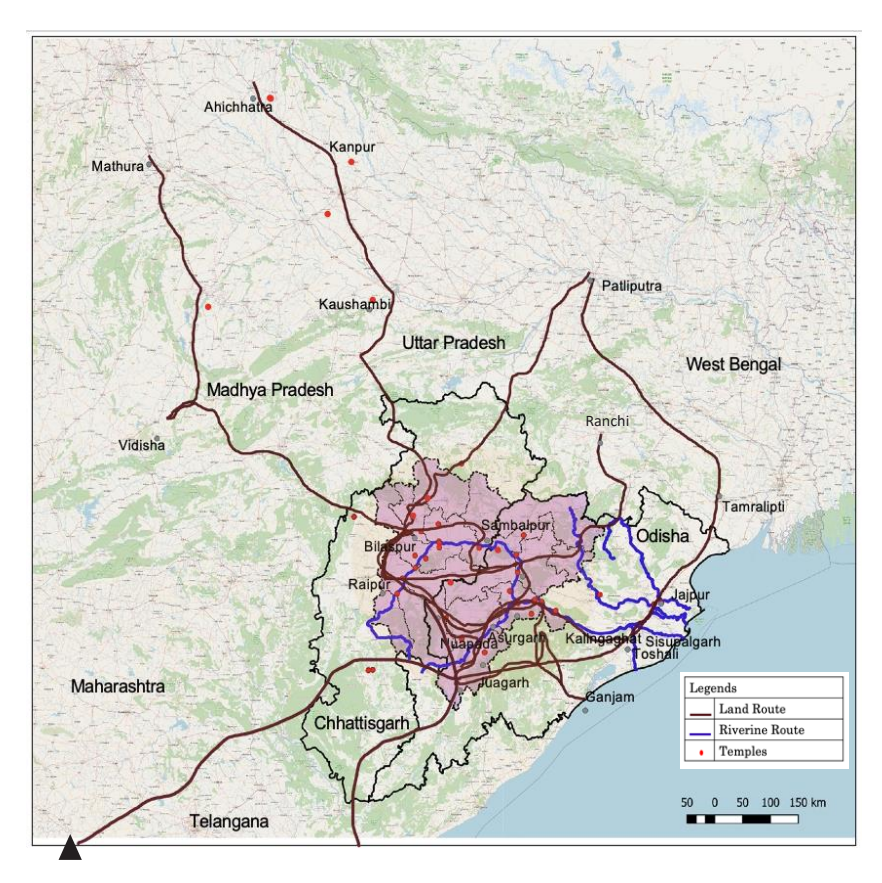


Fig. 6. Temples and trade routes of Dakshina Kosala Source: author, temples and trade routes of Dakshina Kosala. Raipur, Chhattisgarh: ArcGIS, 2023

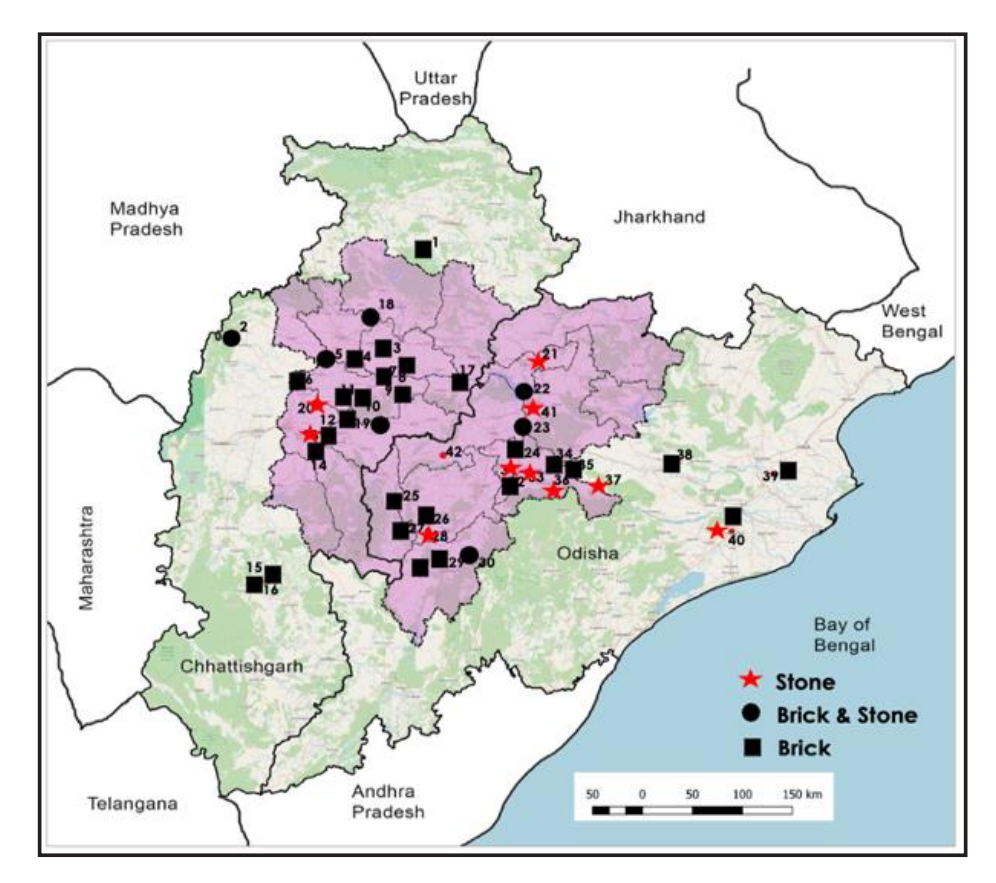


Fig. 7. Construction materials for temples. Source: author, construction materials for temples. Raipur, Chhattisgarh: ArcGIS, 2023

stone (Sharma, 2012). There were three types of temples, constructed completely with stone, with brick, and sometimes both materials were used (Fig. 7).

Brick was the primary construction material in Dakshina Kosala until the 12<sup>th</sup> century CE. As for the temples listed, 62 % of them are made of bricks (see Fig. 8). The earlier temples (5<sup>th</sup>–12<sup>th</sup> century CE) were mostly made of bricks, while in later times, stone became the main temple construction material. One of the influencing factors behind the use of bricks may be the trade routes. In North India, there are ancient brick temples along the trade routes, such as the Bhitargaon temple and the Nibiya Khera temple. It is possible that these structures and construction techniques were brought to the region through trade routes, resulting in the famous brick temples in Dakshina Kosala.

#### Conclusion

In ancient times, Dakshina Kosala had connectivity with other parts of the Indian subcontinent through trade routes. This study found that the renowned temples in the region are spatially linked because they are located either on a trade route or in close proximity to it. The construction of temples may have been a method to show power and influence in ancient times, as rulers built these magnificent structures along trade routes to showcase the prosperity and craftsmanship of the region.

Due to this connectivity, the temples of Dakshina Kosala share similarities that are reflected in the construction materials used for the temples. In ancient times, bricks used to be the main construction material in Dakshina Kosala, and the majority of the temples were made of bricks.

The connectivity of Dakshina Kosala with North India and the Kalinga region also influenced the

#### **CONSTRUCTION MATERIALS**

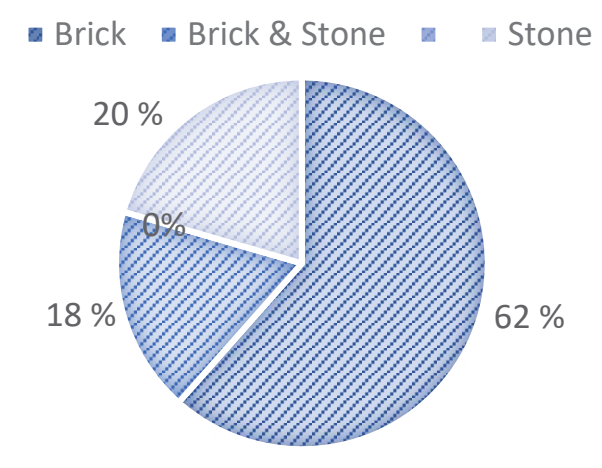


Fig. 8. Construction materials for temples. Source: author

temple architecture. In a hierarchy, the temples of North India, belonging to the Gupta period, come first based on timeline, followed by the temples of Dakshina Kosala, which belong to the post-Gupta period. There was a brick trade route, and it is possible that bricks were traded along this route. Through this connection, the techniques of brick manufacturing may have spread and led to a significant proliferation of brick temples in the region. The stone temples of the Kalinga region also influenced the temple architecture that can be seen in the later temples of the Dakshina Kosala.

It is possible that, in addition to these similarities, the temples also share resemblances in architectural style. Due to job opportunities, craftsmen and masons may have traveled along these trade routes, or kings may have employed workers from other regions. These masons could have carried architectural styles and intangible heritage from one region to another. This might have been reflected in the temples and created a link among the temples within and beyond the geographical boundaries of the region, which is a subject for further research.

#### References

Acharya, P. (1955). Ancient routes in Orissa. Proceedings of the Indian History Congress, Vol. 18, pp. 44–51.

Bhattacharya, R. (2014). Fa-hien's journey to the Land of Buddha. *Research Journal of Humanities and Social Sciences*, Vol. 5, Issue 3, pp. 310–319.

Bhattacharyay, B. N. and De, P. (2009). Restoring the Asian Silk Route: toward an integrated Asia. In: *ADBI Working Paper Series*, ADBI Working Paper 140. Tokyo: Asian Development Bank Institute.

Chakrabarti, D. K. and Rakshit, M. (1995). The archaeology of ancient Indian cities. Delhi: Oxford University Press, 296 p.

Chandra, M. (1977). Trade and trade routes in ancient India. Delhi: Abhinav Publications, 259 p.

Das, B. S. (1978). Studies in the economic history of Orissa from ancient times to 1833. Calcutta: Firma KLM, 300 p.

Dutt, B. B. (2009). Town planning in ancient India. Delhi: Gyan Publishing House, 379 p.

Greaves, L. R. (2015). Brick foundations: North Indian brick temple architecture and terracotta art of the fourth to sixth centuries. PhD Thesis. Cardiff: Cardiff University.

Hardy A. (2020). Vārāṭa temples: the lost tradition in-between. In: Greaves, L. R. and Hardy, A. (eds.). *Bridging Heaven and Earth: Art and Architecture in South Asia*. 3<sup>rd</sup> century BCE – 21<sup>st</sup> century CE. New Delhi: Dev Publishers & Distributors, pp. 57–80.

lasgyan.in (2021). List of foreign travellers to India. [online] Available at: https://www.iasgyan.in/blogs/list-of-foreign-travellers-to-india [Date accessed: February 21, 2023].

Johnston, E. H. (1941). Two notes on Ptolemy's geography of India. *Journal of the Royal Asiatic Society*, Vol. 73, Issue 3, pp. 208–222. DOI: 10.1017/s0035869x00097264.

Kumar, A. (2003). Passage to early medieval phase: emergence of temple centred society in early Bihar. *Proceedings of the Indian History Congress*, Vol. 64, pp. 247–253.

Lamb, H. B. (1958). The Indian merchant. Journal of American Folklore, Vol. 71, No. 281, pp. 231–240.

Majumdar, S. B. (2001). Core peripheral relationship in South Kosala — a regional study. *Proceedings of the Indian History Congress*, Vol. 62, pp. 98–103.

Meena, A. (2023). *Indian river map – PDF download physical map of India with rivers*. [online] Available at: https://schools.aglasem.com/river-map-india/ [Date accessed: November 02, 2023].

Meister, M. W. (1988). Prāsāda as palace: Kūṭina origins of the Nāgara temple. *Artibus Asiae*, Vol. 49, No. 3/4, pp. 254–280. DOI: 10.2307/3250039.

Minj, R. J. (2015). *Art and architecture of the brick temples of Chhattisgarh from 6<sup>th</sup> century to 14<sup>th</sup> century AD*. PhD Thesis. Raipur: Pt. Ravishankar Shukla University.

Mishra, M. K. (1993). Influence of the Ramayana tradition on the folklore of Central India. In: Singh, K. S. and Datta, B. (eds.). *Rama-Katha in tribal and folk traditions of India. Proceedings of a Seminar*. Calcutta: Seagull Books, pp. 15–30.

Mishra, N. K. (2013). Dakshin Kosala and Buddhist art. *International Journal of Advances in Social Sciences*, Vol. 1, Issue 2, pp. 66–69.

Nayak, C. (2004). Trade and urban centres in ancient and early medieval Orissa. PhD Thesis. Bhubaneswar: Utkal University.

N.C.E.R.T. (2011). Through the eyes of travellers perceptions of society (c. tenth to seventeenth century). In: *Themes in Indian History. Part II*. New Delhi: NCERT, pp. 115–137.

Patnaik, S. K. (2013). *Puri. The heritage city. A study of religion culture and tourism.* PhD Thesis. Bhubaneswar: Utkal University.

Patnaik, J. K. (2016). *Temples of South Kosala (6<sup>th</sup> century AD – 11<sup>th</sup> century AD). A case study of stellate temples*. Delhi: Agam Kala Prakashan, 254 p.

Patra, S. K. and Patra, B. (1993). Archaeology and the maritime history of ancient Orissa. *Orissa Historical Research Journal*, Vol. 47, No. 2, pp. 107–118.

Pradhan, A. K. (2008). New light on excavations at Pachrahi. *Proceedings of the Indian History Congress*, Vol. 69, pp. 1044–1055.

Pradhan, A. K. and Yadav, S. (2013). Sirpur — a unique township of early medieval India (fresh evidence from excavations). *Proceedings of the Indian History Congress*, Vol. 74, pp. 854–864.

Raychaudhuri, H. (2006). *Political history of ancient India: from the accession of Parikshit to the extinction of the Gupta dynasty*. New Delhi: Cosmo Publications, 571 p.

Sahu, J. K., & Chandra, J. B. (1983). Historical geography of Orissa From earliest time to 1110 A D [PhD Dissertation, Sambalpur University] pp. 35-41. https://shodhganga.inflibnet.ac.in:8443/jspui/handle/10603/187030

Sarma, L. P. P. and Sarma, L. P. P. (1941). Obscene carvings in the temples in Mahakosala. *Proceedings of the Indian History Congress*, Vol. 5, pp. 261–264.

Scott, A. J. (1997). The cultural economy of cities. *International Journal of Urban and Regional Research*, Vol. 21, Issue 2, pp. 323–339. DOI: 10.1111/1468-2427.00075.

Shamasastry, R. (1929). Kautilya's Arthasastra. 3rd edition. Mysore: Mysore Printing and Publishing House, 494 p.

Sharma, A. K. (2012). Ancient temples of Sirpur. New Delhi: BR Publishing Corporation, 202 p.

Singh, P. K. (2004). Asurgarh - An Early Urban Centre of Orissa. *Orissa Historical Research Journal*, Vol. 47, No. 3, pp. 49–54.

Singh, R. (2020). Political condition of the Tel Valley region during the early history period in Odisha. In: Hussain, S. and Mendaly, S. (eds.). *Recent Developments in Historical and Archaeological Researches in Odisha*, pp. 91–102.

Sircar, D. (1971). Studies in the religious life of ancient and medieval India. New Delhi: Motilal Banarsidass Publications, 292 p.

Srivastava, B. (1968). *Trade and commerce in ancient India (from the earliest times to c. A.D. 300)*. Varanasi: Chowkhamba Sanskrit Series Office, 346 p.

Stadtner, D. M. (1981). The Siddhesvara temple at Palāri and the art of Kosala during the seventh and eighth centuries. *Ars Orientalis*, Vol. 12, pp. 49–56.http://www.jstor.org/stable/4434249

Thapar, B. K. (1992). India's place on ancient trade routes. Senri Ethnological Studies, Vol. 32, pp. 117–125.

Tripathy, B. (1996). Archaeological exploration in Boudh District, Orissa: a preliminary report. *Bulletin of the Deccan College Research Institute*, Vol. 56/57, pp. 41–54.

Watters, T. (1904). On Yuan Chwang's travels in India (A.D. 629-645). London: Royal Asiatic Society 401 p.

# РЕГИОНАЛЬНОЕ РАСПОЛОЖЕНИЕ ХРАМОВ ДАКШИНА КОСАЛА В ИНДИИ: ПРОСТРАНСТВЕННОЕ РАСПРЕДЕЛЕНИЕ И СВЯЗИ

Саумья Шривастава\*, Абир Бандьопадхьяй, Вандана Агравал

Национальный технологический институт, Райпур, Чхаттисгарх, Индия

\*E-mail: sshrivastava.phd2021.arch@nitrr.ac.in

#### Аннотация

**Введение:** Регион Дакшина Косала (также известный как Южная Косала) упоминается в различных древнеиндийских текстах. Его географические границы постоянно менялись, и в настоящее время региону Дакшина Косала, который приблизительно охватывает северную и центральную части современного штата Чхаттисгарх наряду с западной частью штата Одиша, Индия, можно дать лишь приблизительную оценку.

Раскопки и письменные источники свидетельствуют о том, что это был процветающий регион недалеко от центральной Индии (без морского порта) с крупными рынками, торговыми и образовательными центрами. Для доступа в регион было проложено множество торговых путей из различных частей Индии. Это привело к развитию городов с рынками вдоль таких торговых путей. В регионе было построено множество храмов, которые стали примером его духовного наследия. **Цель исследования:** Регион внес значительный вклад в храмовое искусство и архитектуру Индии. Цель настоящего исследования — выяснить, существует ли какая-либо пространственная и архитектурная связь между храмами в данном регионе. **Методы исследования** заключались в анализе научной литературы для подготовки подробных карт, очерчивающих границы Дакшина Косала. Далее, используя тщательный анализ при помощи инструментов Google Earth и ГИС, были нанесены древние торговые пути и храмы. Был проведен всесторонний анализ для получения окончательных результатов. **Результаты:** В статье устанавливается взаимосвязь между храмами с точки зрения их географического расположения и использованных при их возведении строительных материалов в рамках географической границы Дакшина Косала и за ее пределами.

**Ключевые слова:** граница Дакшина Косала, пространственная связь, связность, древние торговые пути, храмовая архитектура.

#### **Building Physics**

DOI: 10.23968/2500-0055-2024-9-1-29-43

# OPTIMIZATION OF THE BUILDING-INTEGRATED TRANSPARENT PHOTOVOLTAIC CONFIGURATION BASED ON DAYLIGHT AND ENERGY PERFORMANCE IN SCHOOL BUILDINGS IN THE TROPICS

Susan Susan<sup>1,2\*</sup>, Safial Agbar bin Zakaria<sup>1</sup>, Sharifah Fairuz Syed Mohd Fadzil<sup>1</sup>

- <sup>1</sup> Universiti Sains Malaysia, Penang, Malaysia
- <sup>2</sup> Universitas Ciputra Surabaya, Surabaya, East Java, Indonesia
- \*Corresponding author's e-mail: susan@student.usm.my / susan@ciputra.ac.id

#### **Abstract**

Introduction: Numerous previous studies addressed the use of vertical facades for side lighting. They were found to be an effective daylighting aperture that helps to establish a pleasant environment, improve academic performance in schools, and promote better health. Recent studies also identified the potential for using vertical facades on high-rise buildings as building-integrated photovoltaic (BIPV) systems thanks to the large available area. In the tropics, this potential use is also supported by the availability of abundant solar energy. The technology of transparent PV (TPV) offers the opportunity to meet both needs. It serves as a side lighting aperture and building-integrated transparent photovoltaic (BITPV) depending on several factors, such as the visible transmittance (VT) value and the number of cells. For side lighting, a higher VT value is required to allow for optimal daylight penetration. However, more cell numbers and lower VT are preferable for BITPV. Previous studies found that BITPV is suggested for buildings with a window-to-wall ratio (WWR) of 45 % or more, which seems too high for tropical buildings where the suggested WWR is typically in the range of 30-40 %. Purpose of the study: This study aims to find the optimum configuration and present a systematic method for optimizing BITPV for tropical school building facades. Methods: An experimental approach using simulation as a tool was employed to achieve the objective. A site with a typical school layout in the tropics was selected as the research context. Treatment based on VT and cell numbers was applied to create several post-test models. Results and discussion: In the tropics, when using low-transparency TPV, BITPV with 31.25 % WWR and 30 % cell coverage ratio is found to provide the optimum visual health and comfort, as well as energy performance. Meanwhile, BITPV with 31.25 % WWR and 50 % cell coverage ratio is found to be the optimum configuration when using high-transparency TPV. Furthermore, this study presents a systematic method for designing BITPV for a multi-story school building in the tropics.

**Keywords:** BITPV, energy substitution, illuminance, school building, tropics.

#### Introduction

One of the major challenges in a building's life cycle is energy consumption. Buildings account for 32 % of total global final energy use, 51 % of global energy consumption, and 19 % of greenhouse gas emissions (Berardi, 2017). According to the Energy Information Administration (2022), 20 % of a building's energy consumption is allocated to artificial lighting. This number accounts for a significant portion of the overall building energy consumption. Choosing energy-saving equipment and implementing energysaving management for lighting can be adopted as a strategy to reduce lighting energy consumption (Shankar et al., 2021). Meanwhile, switching to renewable energy resources is an advantageous strategy to generate clean electrical energy (Gholami and Røstvik, 2020). The Indonesian government has shown concern for energy use by issuing a Mixed-Energy Use Program. This program aims to replace non-renewable energy with renewable For citations: Susan, S., Zakaria, S. A., Syed Fadzil, S. F. (2024).

energy by up to 25 % by 2025 and 31 % by 2050 (ENERGI INDONESIA 2019 SEKRETARIAT JENDERAL DEWAN ENERGI NASIONAL, 2019). In Indonesia, solar energy is the largest renewable energy resource, with a capacity of 207.8 GWp. The application of BIPV on vertical facades is considered potential and advantageous for optimizing the use of solar energy in the rapid development of urban high-rise buildings in Indonesia. The solar irradiance received might not be as high as that received by the horizontal facade; however, the larger area of the vertical facade is likely to satisfy the building's energy demand.

The vertical facade has the potential to be integrated with photovoltaic (PV) systems and generate clean electrical energy to meet the demand for lighting. The intensive use of energy in school buildings is mostly related to their high occupancy density, lighting power density, and receptacle power density (ASHRAE, 2016; Badan Standarisasi

Optimization of the building-integrated transparent photovoltaic configuration based on daylight and energy performance in school buildings in the tropics. Architecture and Engineering, No 1 (9), pp. 29–43. DOI: 10.23968/2500-0055-2024-9-1-29-43.

Nasional, 2000). Hence, the function of the vertical facade ensuring side daylighting cannot be neglected. Side lighting is the most widely used natural lighting system in buildings (Milaningrum, 2015). It is mostly found in the form of a window and has several other functions, such as providing access to outdoor views, natural ventilation, and sound dampening. Daylighting itself is an important element in building design. A well-designed daylighting system can enhance the performance of both buildings and their occupants. In terms of the building's performance, daylighting contributes to reducing the demand for lighting energy. As for the occupants, daylighting will enhance their health, social interaction, psychological well-being, emotions, and visual comfort. In particular, previous studies already found a significant relationship between daylighting and the educational process, especially in school buildings. It was found that students at schools with daylighting performed better and achieved better results than students at schools with artificial illumination. Good daylighting was found to contribute to creating a pleasant environment, enhancing academic performance, and promoting better health (Tsikra and Andreou, 2017).

The technology of transparent PV (TPV) offers the opportunity to meet both needs. For buildings, the extensive development of this technology offers advantages primarily because of its ability to provide clean energy and maintain the function of the building envelope as a daylighting aperture. Previous studies found that the application of PV windows can result in significant energy performance improvements if a high window-to-wall ratio (i.e., ≥45 %) is provided (Sun et al., 2019). However, windows account for a significant amount of heat gain and heat loss (Abbaas et al., 2023). Enlarging windows to install TPV and increase energy production is not a good option in the tropics, where 30-40 % window-towall ratio (WWR) is considered the optimum ratio to achieve a balance between energy and lighting. Therefore, it is necessary to find another strategy to optimize the implementation of building-integrated transparent photovoltaic (BITPV) in the tropics. The study proposes an optimization strategy using TPV with different visible transmittance (VT) values based on the spacing between TPV cells on a transparent substrate region. The optimum configuration here is defined as the one that provides an adequate amount of energy production as well as promotes sufficient indoor illumination.

Several previous studies on the use of PV windows or TPV were conducted in mid to high latitude areas, for example in Italy, the US, the UK, and China (Do et al., 2017; Hu et al., 2024; Musameh et al., 2022; Polo López and Sangiorgi, 2014). A study in the UK found the advantages of PV windows in terms of a lower heat transfer

coefficient and lower solar heat gain compared to those of transparent single glazing (Alrashidi et al., 2020a). Furthermore, it was found that PV windows can achieve higher net energy savings compared to single-glazed windows (Alrashidi et al., 2020b). An experimental investigation was conducted on PV windows in China, which found that human comfort in a room with a PV window can be achieved when the working surface illuminance ranges between 500-2200 lx (Hu et al., 2024). Other investigation in China found that building shadows have a greater impact on the decrease in power generation and efficiency than the amount of solar radiation received (Xiong et al., 2022). Xuan et al. (2021) proposed the use of concentrator PV to enhance the energy performance of PV windows. The results showed that concentrator PV could enhance the active illumination area by up to 6.69 times. Meanwhile, Fan et al. (2021) attempted to find optimal area ratio-based design strategies for skylight-integrated photovoltaic based on indoor light performance. They considered vertical facadeintegrated transparent photovoltaic based on visible transmittance and cell coverage ratio (percentage of PV cells arranged with a certain spacing on a transparent substrate region). The consideration of these two indicators is proposed as a strategy for optimizing tropical BITPV. It is important to conduct measurements not only for daylight performance but also for energy performance. Therefore, two software programs for lighting and energy simulation were used as the tools in the experimental method. The configuration found in this study could be used for the selected building and others that are relevant to the indicated building typologies. Furthermore, the systematic method used in this study can be generalized to design building-integrated transparent photovoltaic in a multi-story school building in the tropics.

Building-Integrated Transparent Photovoltaic (BITPV)

The operation of BITPV depends on several groups of factors: external factors, PV-related factors, and building-related factors. The external factors refer to the amount of solar irradiance. It is known that the intensity of solar radiation is getting less as the latitude of the area is getting higher (McMullan, 2018). Areas with lower latitudes, particularly those in the tropics, receive relatively higher solar irradiance. However, the amount of solar irradiance fluctuates based on several reasons. The average solar irradiance fluctuates around 1353 W/m<sup>2</sup>. The amount of solar radiation emitted is different from the amount of solar radiation received. The amount of solar irradiance received represents a combination of direct, diffuse, and reflected solar radiation. The amount received on a vertical plane is also different from the one received on a horizontal plane.

When it comes to PV-related factors, performance will depend on the PV temperature, types of silicon, efficiency, and the number of cells in a module (Lee et al., 2020). The condition in which PV can operate optimally is called Standard Test Condition (STC), which refers to a condition at 25 °C and 1000 W/m2. However, when PV receives solar radiation, its temperature will increase, and the actual energy output will decrease. The measured difference between the expected energy output and the actual energy output (discrepancy factor) is about 6 %. The PV technology has moved towards transparent photovoltaic, which is industrially known as PV glass, PV window, or transparent PV. This technology allows a certain amount of visible light to transmit into indoor areas. There are several types of technology for creating TPV. One frequently used technology is called selective light transmission. The use of lighttransmissive TPV modules on a vertical facade will contribute to generating clean on-site electrical energy for lighting energy demand. Their use will also influence the daylighting performance within the building in terms of providing suitable conditions for visual health and comfort. Fig. 1a shows the light-transmissive PV module application. Here, PV cells are arranged with a certain spacing on a transparent substrate region (Lee et al., 2020). Basically, there are three types of silicon: monocrystalline, polycrystalline, and amorphous silicon. The types of silicon used in TPV influence its efficiency. As is generally known, the crystalline type has higher efficiency compared to the amorphous type. The PV cell here also has a certain VT value. It is developed using c-Si micro-sized PV cells arranged at various densities, ranging from 5.1 to 15.4 cells/cm<sup>2</sup>, to adjust the transmittance from 35 to 70 % (as shown in Fig. 1b).

Recently, manufacturers have developed two types of TPV cells: high solar cell density with 15 % VT and low solar cell density with 38 % VT. Higher light transmittance leads to lower TPV efficiency.

The efficiency of a PV system can be calculated using the equation below:

Efficiency = output/input  
= 
$$(V_{mpp} \times I_{mpp}) / (GxA)$$
. (1)

Based on the equation above, the electrical energy output of a PV system can be calculated if the PV efficiency and the input are known. It can be measured by the following equation.

Ouput = efficiency x input  
= efficiency x (GxA), 
$$(2)$$

where:

 $V_{mpp}$  = maximum power point voltage (V);  $I_{mpp}$  = maximum power point current (A); G = solar radiation intensity (W/m²); A = PV area (m²).

The spacing arrangement between TPV cells impacts the number of PV cells. The greater the spacing, the fewer the number of TPV cells, which means less electrical energy generation as well.

When it comes to building-related factors, the form of the building, shading conditions, tilt and orientation angles, and the available area for PV modules are factors that influence the performance of BITPV. The buildings in the tropics are typically designed to minimize the amount of solar radiation they receive. The shape and layout are usually elongated and shallow in response to this climate (Markus and Morris, 1980). To optimize the performance of BITPV, the building should have relatively low obstruction, so it has less shading from the surroundings and more access to daylight and solar radiation (Al Mamun et al., 2017; Ubisse and Sebitosi, 2009). As a rule of thumb, the tilt of PV panels in building-integrated photovoltaic (BIPV) applications is usually set at the same angle as the geographical latitude. Meanwhile, the south orientation is determined to be the optimal position in terms of visual comfort and energy yield (Mangkuto et al., 2024). The availability of the PV



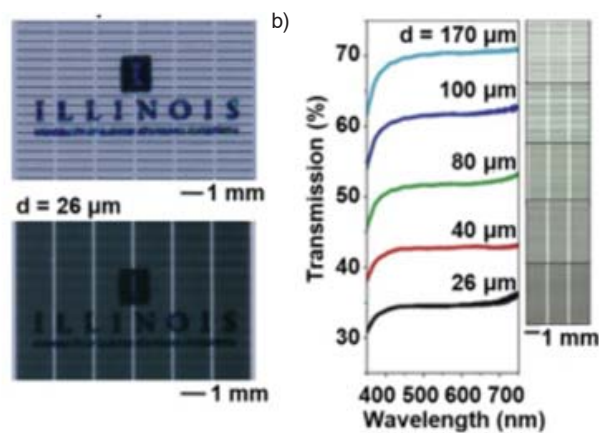


Fig. 1. Light-transmissive TPV modules (Lee et al., 2020; Peng et al., 2011)

area will directly impact the amount of solar radiation received. The larger area means the higher amount of solar radiation received and greater electrical energy generated (Roberts and Guariento, 2009). The available area on a vertical facade depends on the proportion of transparent and opaque materials. Previous studies addressed various ratios of transparent to opaque materials. Nowadays, there is an opportunity for PV to be integrated as a transparent material. Therefore, there is a need to address the ratio of TPV to transparent material (opening). This study addresses BITPV configurations based on VT and the number of TPV cells. VT is influenced by the density of micro-sized PV cells applied, which can be found in the market as low-transparency TPV type and high-transparency TPV type. The number of cells depends on the various spacing ratios of the TPV cells on a transparent substrate region (opening). The studied spacing ratio ranged from 20 to 80 %.

Lighting

Lighting is widely discussed both in terms of daylighting and artificial lighting. Daylight can be introduced into a room through top lighting, side lighting, or combination of both (Lechner, 2014). Since buildings in the tropics receive high solar irradiance, therefore, side lighting seems to be the most preferable strategy to provide natural light without excessive heat. The strategy of daylighting can be divided into four main considerations: site development, external elements, internal elements, and roof and in-wall systems (Ander, 2003; Heerwagen, 2003). When it comes to in-wall systems, the glazing properties, particularly VT, are critical parameters that need to be considered in order to enhance adequate daylight within the building. It represents a fraction of visible light that is transmitted through the glazing system. Higher VT means a greater opportunity for daylight penetration. Light-transmissive TPV modules have opaque PV arranged with specific spacing on a transparent substrate region. The transparent substrate region is usually made of low-E glass, which has a transmittance value of up to 79 %. Meanwhile, the PV cells commonly found in the market have transmittance values of 15 and 38 %. The strategies chosen will influence the quality of daylight within the building. Furthermore, daylight is considered to be of good quality if there is enough natural light between 8:00 am and 4:00 pm (Badan Standarisasi Nasional, 2000). The quality of daylight can be measured by several indicators, including illuminance level (E), useful daylight illuminance (UDI), daylight factor (DF), daylight autonomy (DA), and spatial daylight autonomy (sDA). Regarding these indicators, there are many international standards. However, some countries already have their own national standards (Vardanyan, 2021). In Indonesia, according to Green Building Council Indonesia (GBCI), 300 lux for

illuminance level is considered as a good indicator of conditions that provide visual health and comfort for a classroom (Green Building Council Indonesia, 2014; McMullan, 2018).

Since daylighting is very dynamic, artificial lighting is needed as a supplement to daylighting. It is the second biggest building energy consumer after the air conditioning (Kwong and Ali, 2011). To optimize the lighting energy performance, buildings are suggested to use artificial lighting energy-saving equipment (Gandah et al., 2022), while still maintaining the illuminance level standard. As mentioned before, lighting contributes to 20 % of building energy consumption, and the average energy consumption index for buildings in Indonesia is measured at around 240 kWh/m<sup>2</sup> per year (Biantoro and Permana, 2017). Lighting power density (LPD) can be used as a parameter for energy-saving equipment. LPD indicates the amount of lighting power consumption (in watts) per unit area (m²). This parameter can be used to ensure that the artificial lighting system does not exceed the maximum power density. According to GBCI, the standard for LPD in classrooms is 15 W/m<sup>2</sup>. To achieve better lighting energy performance, GBCI determined that LPD should be 20 % less than the standard.

#### Methods

This study used an experimental method with simulation as its tool. The experiment aimed to find the optimum configuration of BITPV. Optimization is the act of obtaining the best result under given circumstances (Rao, 2009). This means that optimization is the process of finding the conditions that yield the maximum or minimum value of a function. A gradient method is a general optimization strategy that iteratively changes the parameters to increase (or decrease in the case of minimization) the gradient (Sugiyama, 2016). This study aims to analyze the data on illuminance and the percentage of lighting electrical energy substitution for a school building in the tropics. The analysis is based on experimental results obtained from the glazing system, which involved TPV application. The application varied in terms of the spacing between TPV cells and VT of the TPV cells. The constraint is an illuminance level of 300 lux and a substitution percentage of 25-31 % of renewable to non-renewable energy. In this study, lighting energy consumption is measured based on 20 % of the energy consumption index, which is around 240 kWh/m² per year. The optimal configuration is defined as the configuration that can reach the constraint optimally.

#### Research context

The research context is chosen based on several rules of thumb, including the organization of school layout and the typology of buildings in the tropics. Based on previous studies, there are several general organizational layouts for schools.

The central corridor layout with classrooms on its perimeter gives an advantage in terms of optimizing daylight penetration. Commonly, classrooms have several types of proportions, such as 3:2, 2:3, or 1:1 (Montenegro et al., 2012). Meanwhile, due to climate-responsive strategies, buildings in the tropics are usually characterized by (1) an elongated shape and shallow layout, aiming to optimize cross ventilation (Markus and Morris, 1980), as well as (2) the placement of main functional rooms on the building perimeter, aiming to optimize the use of daylight (Heerwagen, 2003). The selected room should be one that is relatively placed on a high floor, has fewer obstructions (Ubisse and Sebitosi, 2009), and has openings on its south orientation (Mangkuto et al., 2024). Furthermore, the selected building should be a multi-story building with the potential for a vertical facade to be integrated with TPV (Xiang and Matusiak, 2022).

Following these general rules of thumb, a school building, namely Universitas Ciputra Surabaya (UCS), was selected as the research context. Fig. 2 shows the site plan and the perspective of UCS. UCS is located at 7°29' S 112°63' E. This location itself indicates the potential for solar radiation. This area has a hot and humid climate, with maximum and minimum temperatures ranging around 31.3-35.9 °C and 20.4–23.9 °C, respectively. Meanwhile, the average relative humidity ranges around 65 to 84 %. The highest precipitation mostly occurs from December to February, while September and October appear to be the driest months of the year. The duration of sunshine hours is quite high, reaching 72.27 %. The room being studied is a classroom / drawing studio used by the School of Creative Industry (Fig. 3). The area of the classroom is 192 m<sup>2</sup> with a width of 12 m and a length of 16 m. The floor-to-floor height is 4 m, while the clear height (finished floor to exposed beam) is 3.5 m. The total clear opening width is 17.5 m, and the clear opening height is 2 m. This room has a 112 m² exterior wall, with 35 m² being the opening. The building's response to the surrounding climate is demonstrated by its 31.25 % window-to-wall ratio (WWR), which falls within the preferred range for buildings in tropical regions. Fig. 3 shows the layout of the room selected.

#### Experimental setting

The experimental method is chosen to discover the impact of the VT value, as well as cell numbers, as a result of the TPV ratio arrangement on a transparent substrate region (opening). The experimental method requires three stages: a pretest condition, treatment, and a post-test condition. Table 1 shows the experimental method settings, while Table 2 shows the TPV ratio settings for the opening of the building's vertical facade.

Following the experimental method, simulations were chosen as a tool to generate data on illuminance levels and solar radiation received in each configuration. Velux was used to generate data on illuminance levels, and the simulation was run for several time periods (09:00, 12:00, 16:00) to validate the feasibility of the experimental method and procedure. As for the data on solar radiation received, Archipak was used, followed by mathematical calculations to measure the electrical energy generation. A gradient diagram was used to determine the optimum configuration of BITPV, which is defined as the one that has the optimum illuminance level and substitutes a minimum of 25-31 % of conventional lighting energy with the electrical energy generated from PV. The optimization workflow is shown in Fig. 4.



Location of the room selected

Fig. 2. Site plan and perspective of Universitas Ciputra Surabaya

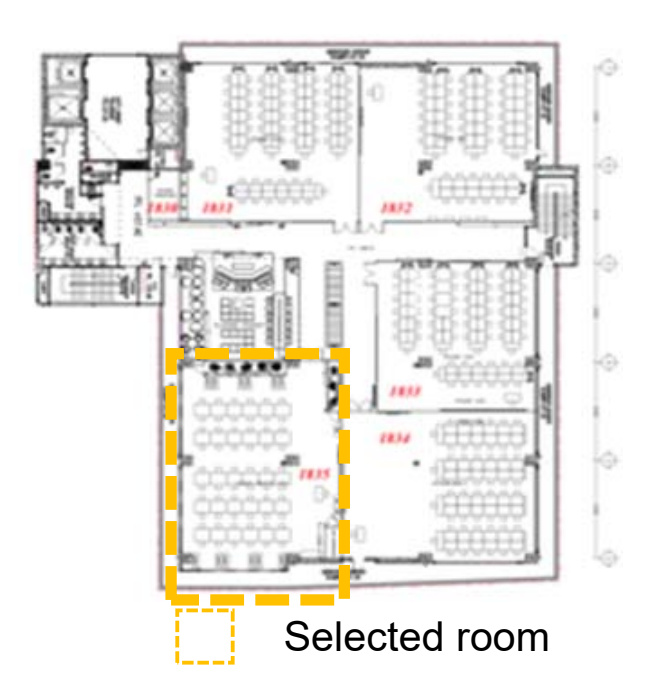


Fig. 3. Layout of the room selected

#### VELUX simulation: validation and setting

A previous study showed that simulation results matched well with the results obtained from field measurements (Kousalyadevi and Lavanya, 2019). The reliability of Velux results was also confirmed by another previous study conducted by Xiang and Matusiak (2022). In that study, Velux was employed to find a balance of daylight on a colored facade-

integrated photovoltaic design for a high-rise building with balconies. It mentioned the following advantages of Velux software: the most architectfriendly software, a satisfying general interface and graphic treatment of results, accurate prediction of daylight levels and the appearance of a daylit area. Furthermore, Velux was chosen because it is known as software that has the ability to generate automated reports with user-defined daylight measurement zones (work planes). It is validated in accordance with the CIE 171:2006 test cases to assess the accuracy of lighting computer programs (Labayrade et al., 2009). However, to increase accuracy and reliability, it is suggested that simulated results be validated by measured results (Wong, 2017). The illuminance value and illuminance distribution pattern can be used to determine whether the model is able to generate realistic data (Lakhdari et al., 2021). It is assumed that the simulation result matches well with the measurement result if the difference is less than 4 % (Sun et al., 2019). Therefore, measurements and simulations under base case conditions are conducted to generate data on illuminance values and their distribution patterns. The measurements were conducted in grids of 1.20 ×1.20 m, resulting in 134 measured points. An example of a measurement result, particularly in April at 12:00, is shown in Table 2. Meanwhile, the simulation resulted in 42 simulated points, as shown in Table 3. The distribution patterns for the measured and simulated results are illustrated

Table 1. Experimental method

|  |  | Table 1. Laperiniental inethou                |
|--|--|---|
| Pre-test   | Treatment  | Post-test                                     |
| A model classroom in a tropical, multi-story school building | BITPV configuration based on PV with different VT: | Various configuration of glass cladding-BIPV: |
| with an active system that has                               | PV1 = low transparency (15 % VT,                   | 1. 20 % - PV1                                 |
| optimal solar access   | 38 Wp/m <sup>2</sup> , 16 % efficiency)            | 2. 20 % - PV2                                 |
| ·  | PV2 = high transparency (38 % VT,                  | 3. 30 % - PV1                                 |
|  | 22 Wp/m <sup>2</sup> , 9.3 % efficiency)           | 4. 30 % - PV2                                 |
|  | 3,   | 5. 40 % - PV1                                 |
|  | BITPV configuration based on PV                    | 6. 40 % - PV2                                 |
|  | with different cell numbers, as a                  | 7   |
|  | result of the ratio arrangement                    | 8   |
|  | of transparent PV to transparent                   | 9   |
|  | substrate (20 % 30 % 80 %)                         |   |

Table 2. Setting of the TPV to Opening Ratio

|                 |            | - · · · · · · · · · · · · · · · · · · · |    |               | 5      |
|-----------------|------------|---|----|---------------|--------|
| Tractme         | nt code    | Window area (m²)                        |    | TPV area (m²) |        |
| Treatme         | ent code   | S                                       | W  | S             | W      |
| 0 % (base case) |            | 11                                      | 24 | 0             | 0      |
| 20 % - PV1      | 20 % - PV2 | 11                                      | 24 | 2.244         | 5.000  |
| 30 % - PV1      | 30 % - PV2 | 11                                      | 24 | 3.366         | 7.272  |
| 40 % - PV1      | 40 % - PV2 | 11                                      | 24 | 4.555         | 9.792  |
| 50 % - PV1      | 50 % - PV2 | 11                                      | 24 | 5.466         | 12.600 |
| 60 % - PV1      | 60 % - PV2 | 11                                      | 24 | 6.722         | 14.712 |
| 70 % - PV1      | 70 % - PV2 | 11                                      | 24 | 7.844         | 16.656 |
| 80% - PV1       | 80% - PV2  | 11                                      | 24 | 8.822         | 19.032 |

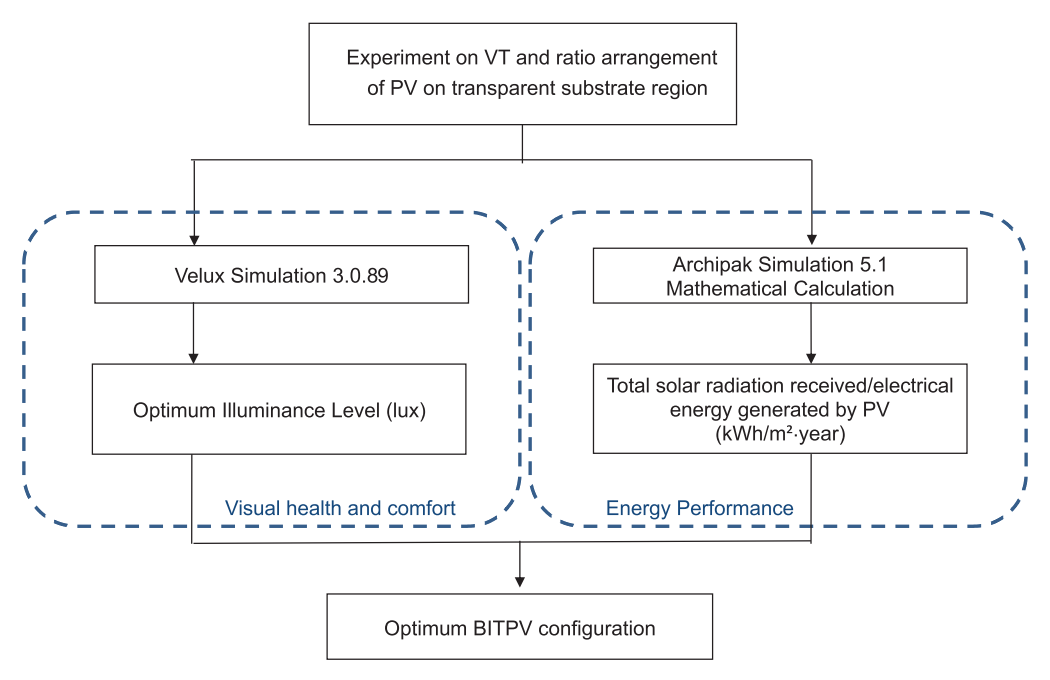


Fig. 4. Optimization workflow

in Fig. 5. The difference in average illuminance, which ranges from 0.58 to 3.72 %, and the similarity in distribution patterns indicate the reliability of the simulation.

The materials and finishes for each room element are shown in Table 4. PV is set as another customized material, with a glass surface and two options for transmittance: 15 % (PV1) and 38 % (PV2). The location is customized based on the building's longitude (112°63' E) and latitude (7°29' S). Other settings include the camera, which is set to perspective for still images; the render type, which is set to illuminance; overcast sky conditions; a year-long time frame; and several times of the day, including 09:00, 12:00, and 16:00. The Velux simulation was run 540 times (15 models  $\times$  12 months  $\times$  3 times).

#### ARCHIPAK simulation setting

Archipak is a software developed by Szokolay and validated through comparison with other software, namely TEMPER, CHEETAH, and QUICK, as well as through comparison of simulation results and measured data (Ahmad and Szokolay, 1993; Szokolay, 1986). It is an integrated program for thermal and solar radiation that was used in several previous studies. In some recent studies, Archipak was described as a digital architecture tool that specifically helps users in simulating physical building needs (Andadari et al., 2021). It is used to determine comfort zones and control potential zones (Rabah and Tamakan, 2002), as well as to calculate solar radiation, annual cooling, and overheating energy (Noerwasito and Nirwansyah, 2019; Noerwasito, 2022; Susan and Wardhani, 2020a, 2020b). In this study, Archipak was used to generate data on the

solar radiation received at a determined orientation and tilt angle. The simulation settings on Archipak consist of location and climatic data input, retrieving climatic data for simulating solar radiation received, and setting data output for an average day of 12 months. This is for an area with a 90° tilt angle from the horizon (vertical facade), oriented at 180° and 270°. Previous studies showed that the predicted data of PV energy output matches well with the measured data when the measured solar radiation data is used as input to the simulation software (Wu et al., 2015; Andadari et al., 2021). Therefore, climatic data for Surabaya derived from Badan Meteorologi and Geofisika Juanda was used as the input for climatic data. The climatic data is listed in Table 5. To enhance reliability, a 10–30 % reduction in every shading condition (Feng et al., 2023; Ubisse and Sebitosi, 2009; Zomer and Rüther, 2017), as well as a 1-6 % discrepancy factor (Trinuruk et al., 2009; Wu et al., 2015), were taken into account in the power output calculation.

#### Results and discussion

As shown in the workflow in Fig. 4, simulations using Velux were applied after setting up the experiment on VT and the ratio arrangement of PV on the transparent substrate region (Table 2). Every model was simulated in Velux for 12 months, three times a day. The simulation output in the form of images displays data from 42 points measuring illuminance. This data will include information about the location, time, orientation, sky conditions, and external illumination. For every simulation output, the levels of illuminance are observed in terms of minimum ( $E_{min}$ ), maximum ( $E_{max}$ ), and average ( $E_{avo}$ ) values. For example, in the base case model,

| Table 2 | Measured      | results  | (lux |
|---------|---------------|----------|------|
| Iable 2 | . IVICASUI CU | 1 Courto | (IUX |

| Grid<br>No. | 1    | 2    | 3    | 4   | 5   | 6   | 7    | 8   | 9   | 10  | Total | Average illuminance |
|-------------|------|------|------|-----|-----|-----|------|-----|-----|-----|-------|---------------------|
| 1           | 281  | 882  |      |     |     |     |      | 52  | 14  |     | 1229  |                     |
| 2           | 310  | 765  | 64   | 49  | 37  | 27  | 20   | 9   | 14  |     | 1295  |                     |
| 3           | 572  | 882  | 173  | 82  | 49  | 37  | 27   | 14  | 14  |     | 1850  |                     |
| 4           | 572  | 281  | 173  | 107 | 49  | 49  | 27   | 20  | 27  |     | 1305  |                     |
| 5           | 572  | 445  | 173  | 136 | 49  | 37  | 37   | 49  | 82  | 354 | 1934  |                     |
| 6           | 572  | 281  | 173  | 128 | 49  | 49  | 37   | 49  | 64  | 445 | 1847  |                     |
| 7           | 572  | 281  | 136  | 107 | 49  | 49  | 281  | 173 | 27  | 445 | 2120  |                     |
| 8           | 572  | 173  | 136  | 107 | 64  | 64  | 56   | 82  | 27  | 572 | 1853  |                     |
| 9           | 959  | 218  | 218  | 107 | 64  | 64  | 54   | 54  | 82  | 354 | 2174  |                     |
| 10          | 959  | 281  | 281  | 281 | 82  | 82  | 37   | 107 | 107 | 354 | 2571  |                     |
| 11          | 959  | 281  | 281  | 173 | 107 | 107 | 82   | 59  | 82  | 354 | 2485  |                     |
| 12          | 3398 | 445  | 354  | 281 | 173 | 173 | 107  | 49  | 49  | 445 | 5474  |                     |
| 13          | 2256 | 218  | 218  | 136 | 107 | 107 | 218  | 107 |     |     | 3367  |                     |
| 14          | 2121 | 354  | 173  | 173 | 107 | 107 | 173  | 281 |     |     | 3489  |                     |
| 15          | 354  | 1559 | 1114 | 882 | 572 | 572 | 1211 |     |     |     | 6264  |                     |
|             |      |      |      |     |     |     |      |     |     |     | 39257 | 292.96              |

Table 3. Simulated results (lux)

| Grid<br>No. | 1     | 2     | 3     | 4     | 5     | 6     | 7     | Total    | Average illuminance |
|-------------|-------|-------|-------|-------|-------|-------|-------|----------|---------------------|
| 1           | 159.1 | 176.3 | 180.1 | 190.5 | 138.4 | 49.2  | 237.3 | 1130.9   |                     |
| 2           | 185.2 | 132.4 | 62.7  | 81.7  | 331.1 | 290.1 | 76.1  | 1159.3   |                     |
| 3           | 192.9 | 188.7 | 252.2 | 254.8 | 219.1 | 0     | 148.9 | 1256.6   |                     |
| 4           | 337.4 | 260.5 | 418.6 | 595.6 | 303.8 | 0     | 181.8 | 2097.7   |                     |
| 5           | 489.8 | 499.2 | 585.5 | 619.5 | 725.0 | 723.2 | 151.4 | 3793.6   |                     |
| 6           | 332.5 | 348.6 | 337.5 | 423.0 | 429.7 | 510.0 | 557.1 | 2938.4   |                     |
|             |       |       |       |       |       |       |       | 12.376.5 | 294.68              |

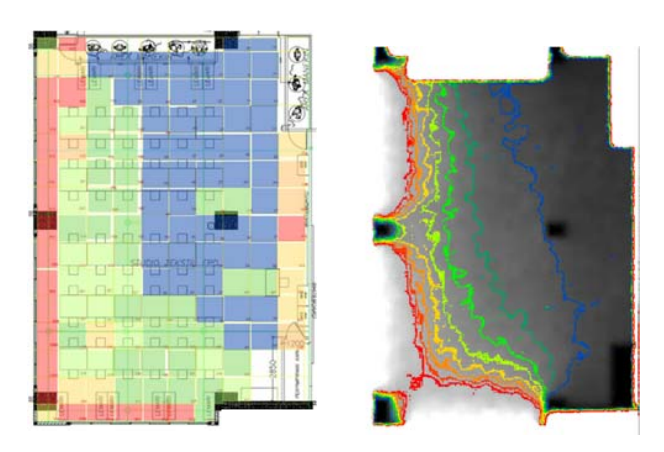


Fig. 5. Distribution patterns of (a) measured results and (b) simulated results

simulations in March, June, September, and December at 12:00 resulted in illuminance value ranges of 51.4–771.6 lux, 44.1–650 lux, 49.8–855.8 lux, and 49.6–727.9 lux, respectively. In this case, the average illuminance value calculated from every 42 points of measuring illuminance is 303.8 lux, 262.5 lux, 303.8 lux, and 290.6 lux, respectively for March, June, September, and December. Another example is for the model of 30 % - PV1. The illuminance value ranges are 34.5–826 lux, 27.6–736.6 lux, 38.1–751.6 lux, 39.4–813.4 lux. The average illuminance values for the four consecutive months mentioned before are 213.1 lux, 184.5 lux, 179.9 lux, and 210.7 lux, respectively. The annual average illuminance results are shown in Table 5.

Table 4. Room material and finishing settings

| Element | Material    | Thickness | Color       | Transmittance | Reflectance | Specularity | Roughness |
|---------|-------------|-----------|-------------|---------------|-------------|-------------|-----------|
| Ceiling | Concrete    | -         | White matte | -             | 0.94        | 0.05        | 0.01      |
| Wall    | Hebel       | -         | Light gray  | -             | 0.71        | 0.05        | 0.01      |
| Opening | Low-E glass | 12 mm     | Clear       | 0.71          | 0.043       | -           | -         |
| Framing | Aluminum    | -         | Black matte | -             | -           | 0           | 0.1       |
| Floor   | Ceramic     | -         | Gray-glossy | -             | 0.58        | 0.05        | 0.3       |

The monthly maximum average illuminance, particularly for September (equinox), is shown in Table 6. The annual and monthly average illuminance will be used for optimization considerations.

The Archipak simulation was run to generate data on solar radiation received. For vertical facade facing 180° and 270° orientations, the amount of solar radiation received is 1777 kWh/m² per year and 2213 kWh/m² per year, respectively. As mentioned earlier, the selected classroom has an area of 192 m² and an energy consumption index of 240 kWh/m² per year. With 20 % of the energy consumption allocated to lighting, the total energy demand for the selected class is 9216 kWh per year. Based on this energy demand, mathematical equations were used to calculate the percentage of renewable energy substitution as a parameter for lighting energy performance. The calculation is shown in Table 7.

The data on the illuminance level and energy performance is then plotted on the gradient diagram. It was found that the annual average illuminance dropped below the standard. Based on this result, the optimum configuration is determined as a configuration with an annual illuminance level that is closest to the standard and has energy substitution within 25–31 %. The monthly maximum average illuminance is also analyzed and used to support the determination of the optimum configuration, which is defined as the configuration with monthly maximum average illuminance ranging within 300 lux and having energy substitution within 25–31 %. Figs. 6 and 7 show the gradient diagram for the optimization process.

#### Conclusion

This study aimed to find the optimum configuration of BITPV for a school building in the tropics. A site was selected based on its typology

Table 5. Overall average illuminance value

| Treatment  |       |        | Overall a | verage i | lluminar | ce value | in ever | y month | · (lux) |       |       |
|------------|-------|--------|-----------|----------|----------|----------|---------|---------|---------|-------|-------|
| code       | Jan   | Feb    | Mar       | Apr      | May      | Jun      | Jul     | Oct     | Nov     | Dec   | Avg   |
| Base case  | 220.0 | 223.85 | 225.3     | 216.8    | 202.4    | 190.9    | 191.6   | 218.2   | 227.8   | 238.9 | 224.6 |
| 20 % - PV1 | 169.3 | 171.5  | 161.8     | 159.9    | 148.7    | 140.7    | 146.9   | 149.9   | 155.0   | 166.8 | 166.6 |
| 30 % - PV1 | 156.1 | 158.9  | 157.6     | 152.2    | 141.6    | 134.0    | 134.1   | 143.0   | 133.2   | 157.7 | 156.6 |
| 40 % - PV1 | 146.7 | 145.3  | 145.7     | 140.1    | 133.5    | 124.2    | 123.5   | 130.7   | 122.5   | 145.2 | 145.2 |
| 50 % - PV1 | 123.9 | 129.7  | 123.1     | 116.2    | 109.1    | 118.9    | 119.4   | 124.7   | 111.3   | 140.3 | 141.5 |
| 60 % - PV1 | 109.4 | 112.1  | 113.2     | 107.6    | 100.4    | 98.8     | 99.1    | 101.7   | 100.8   | 111.2 | 111.3 |
| 70 % - PV1 | 100.8 | 102.1  | 101.6     | 103.9    | 99.6     | 95.0     | 95.0    | 102.1   | 94.0    | 107.2 | 101.3 |
| 80 % - PV1 | 80.5  | 86.3   | 90.0      | 93.8     | 91.7     | 85.4     | 86.6    | 93.5    | 84.0    | 89.9  | 84.2  |
| 20 % - PV2 | 193.1 | 195.7  | 195.6     | 188.5    | 175.7    | 169.8    | 166.8   | 176.4   | 163.2   | 194.8 | 196.0 |
| 30 % - PV2 | 163.9 | 159.8  | 159.6     | 154.9    | 155.6    | 135.9    | 135.7   | 143.9   | 147.9   | 160.3 | 158.6 |
| 40 % - PV2 | 153.0 | 149.1  | 149.9     | 143.4    | 143.1    | 126.2    | 129.6   | 136.8   | 145.3   | 151.5 | 150.1 |
| 50 % - PV2 | 137.9 | 140.5  | 140.3     | 135.1    | 130.0    | 103.0    | 127.5   | 134.8   | 136.2   | 149.6 | 148.8 |
| 60 % - PV2 | 113.2 | 116.0  | 116.8     | 111.7    | 104.6    | 99.2     | 100.0   | 105.4   | 108.5   | 116.2 | 115.9 |
| 70 % - PV2 | 109.4 | 111.5  | 112.7     | 109.3    | 100.7    | 95.4     | 97.6    | 105.4   | 101.5   | 112.6 | 111.5 |
| 80 % - PV2 | 86.7  | 92.7   | 99.9      | 102.4    | 93.6     | 92.6     | 95.2    | 95.0    | 92.9    | 97.4  | 91.5  |

Table 6. Average maximum illuminance in September

| Treatment code | E <sub>max</sub> at 09:00 (lux) | E <sub>max</sub> at 12:00<br>(lux) | E <sub>max</sub> at 16:00<br>(lux) | Avg of E <sub>max</sub> (lux) |
|----------------|---------------------------------|------------------------------------|------------------------------------|-------------------------------|
| Base case      | 693.7                           | 855.8                              | 492.0                              | 680.5                         |
| 20 % - PV1     | 575.3                           | 805.6                              | 405.2                              | 595.4                         |
| 30 % - PV1     | 523.6                           | 751.6                              | 370.6                              | 548.6                         |
| 40 % - PV1     | 397.8                           | 594.0                              | 304.6                              | 432.1                         |
| 50 % - PV1     | 340.3                           | 502.0                              | 249.0                              | 363.8                         |
| 60 % - PV1     | 280.3                           | 406.4                              | 207.1                              | 297.9                         |
| 70 % - PV1     | 261.1                           | 384.4                              | 200.5                              | 282.0                         |
| 80 % - PV1     | 225.2                           | 331.4                              | 186.8                              | 247.8                         |
| 20 % - PV2     | 603.5                           | 727.3                              | 425.5                              | 603.5                         |
| 30 % - PV2     | 600.8                           | 719.8                              | 427.9                              | 600.8                         |
| 40 % - PV2     | 490.0                           | 629.9                              | 306.8                              | 490.0                         |
| 50 % - PV2     | 462.0                           | 550.5                              | 302.1                              | 462.0                         |
| 60 % - PV2     | 374.4                           | 511.2                              | 247.4                              | 374.4                         |
| 70 % - PV2     | 332.1                           | 469.0                              | 241.6                              | 332.1                         |
| 80 % - PV2     | 223.4                           | 304.4                              | 152.3                              | 223.4                         |

Table 7. Lighting energy performance

|                              | Disc. Electrical energy Percentage | factor generated (kWh per of substitution | (%) year)     |   | (m) $(h) = (k) \times (l) - (m)$ $(k) = (h)/9216 \times 100\%$ | 0 0 9      |      | 6 1685.83 18 | 6 2472.26 27 | 6 3333.50 36 | 6 4210.79 46 | 6 4984.24 54 | 6 5689.37 62 | 6 6472.93 70 | 6 979.86 11 | 6 1436.98 16 | 6   1937.57   21 | 6 2447.50 27 | 6 2897.06 31 | 6 3306.92 36 | 6 2767.26 |
|------------------------------|------------------------------------|---|---------------|---|--|------------|------|--------------|--------------|--------------|--------------|--------------|--------------|--------------|-------------|--------------|------------------|--------------|--------------|--------------|-----------|
|                              | δ                                  | eff.                                      | (%)           |   | €  | 16         |      | 16           | 16           | 16           | 16           | 16           | 16           | 16           | 9.3         | 9.3          | 9.3              | 9.3          | 9.3          | 9.3          | C         |
|                              | Total annual rad                   | rec. (kWh per                             | year)         |   | (k) = (cxi)+(dxj)  | 0          |      | 10536.81     | 15452.02     | 20834.75     | 26317.82     | 31151.86     | 35558.96     | 40456.16     | 10536.81    | 15452.02     | 20834.75         | 26317.82     | 31151.86     | 35558.96     | 70456 46  |
| Electrical energy generation | Annual rad rec.                    | kWh/m² per year)                          | after shading | 8 | (j)  | 1549.1     |      | 1549.1       | 1549.1       | 1549.1       | 1549.1       | 1549.1       | 1549.1       | 1549.1       | 1549.1      | 1549.1       | 1549.1           | 1549.1       | 1549.1       | 1549.1       | 7 0 7 1   |
| l energy g                   | Annua                              | (kWh/m <sup>2</sup>                       | after s       | S | ( <u>i</u> )   | 1243.9     |      | 1243.9       | 1243.9       | 1243.9       | 1243.9       | 1243.9       | 1243.9       | 1243.9       | 1243.9      | 1243.9       | 1243.9           | 1243.9       | 1243.9       | 1243.9       | 10100     |
| Electrica                    | ual rad rec.                       | m² per year)                              | re shading    | * | (h)  | 2213       |      | 2213         | 2213         | 2213         | 2213         | 2213         | 2213         | 2213         | 2213        | 2213         | 2213             | 2213         | 2213         | 2213         | 0770      |
|                              | Annua                              | (kWh/m                                    | before        | တ | (g)  | 1777       |      | 1777         | 1777         | 1777         | 1777         | 1777         | 1777         | 1777         | 1777        | 1777         | 1777             | 1777         | 1777         | 1777         | 4777      |
|                              |                                    | PV area (%)                               |               | 8 | (£)  | 0          |      | 20.8         | 30.3         | 40.8         | 52.5         | 61.3         | 69.4         | 79.3         | 20.8        | 30.3         | 40.8             | 52.5         | 61.3         | 69.4         | 70.2      |
|                              |                                    | PV ar                                     |               | ഗ | (e)  | 0          |      | 20.4         | 30.5         | 41.4         | 49.6         | 61.1         | 71.3         | 80.2         | 20.4        | 30.5         | 41.4             | 49.6         | 61.1         | 71.3         | 000       |
|                              |                                    | PV area (m²)                              |               | ≯ | (p)  | 0          |      | 5.000        | 7.272        | 9.792        | 12.600       | 14.712       | 16.656       | 19.032       | 5.000       | 7.272        | 9.792            | 12.600       | 14.712       | 16.656       | 40.000    |
|                              |                                    | PV ar                                     |               | တ | (၁)  | 0          |      | 2.244        | 3.366        | 4.555        | 5.466        | 6.722        | 7.844        | 8.822        | 2.244       | 3.366        | 4.555            | 5.466        | 6.722        | 7.844        | 0 000     |
|                              | 1000                               | window                                    | 3a (III )     | > | (q)  | 24         |      | 24           | 24           | 24           | 24           | 24           | 24           | 24           | 24          | 24           | 24               | 24           | 24           | 24           | 70        |
|                              | 747                                | > 6                                       | ā             | ഗ | (a)  | 7          |      | 7            | 7            | 7            | 1            | 1            | 7            | 1            | 7           | 1            | 11               | 7            | 1            | 1            | 7         |
|                              | 0                                  | anoo                                      |               |   |  | 0 % - base | case | 20 % - PV1   | 30 % - PV1   | 40 % - PV1   | 50 % - PV1   | 60 % - PV1   | 70 % - PV1   | 80 % - PV1   | 20 % - PV2  | 30 % - PV2   | 40 % - PV2       | 50 % - PV2   | 60 % - PV2   | 70 % - PV2   | 0/10 % 00 |

that conforms to general school organization, is responsive to tropical climate, and has the potential to be integrated with BITPV. Treatments based on different VT and cell numbers were applied to the selected site, which functioned as the base case or pre-test model. The variation in VT is a result of the micro-sized PV density arrangement, while the number of cells is a result of the various spacing between PV cells in a module. Data generated from the simulation shows the levels of illuminance and energy generation for several post-test models. It was found that the annual average illuminance for both the pre-test and post-test models falls below the standard. The annual average illuminance for the pre-test model, which has 31.25 % WWR, is 224.6 lux. The level of illuminance drops within a range of 27–59 % for BITPV with low-transparency PV, and 15–56 % for BITPV with high-transparency PV. However, considering energy substitution as a parameter for optimization, configurations of 30 % PV1 and 50 % PV2 can be proposed as the optimum BITPV. These configurations result in an annual average illuminance that is closest to the standard while still maintaining an energy substitution percentage of 27 %.

However, if we consider the maximum illuminance value, the average ranges from 223.4 lux to 680.5 lux. Based on the maximum illuminance value and energy substitution, there are three configurations that can comply with the optimization standard. These are 30 % PV1, 50 % PV2, and 60 % PV2. These configurations can provide a monthly maximum average illuminance above the standard (548.6 lux, 438.2 lux, and 377.7 lux, respectively), while still maintaining percentages of energy substitution within the range of 25-31 %. Furthermore, this study presented a systematic method to design buildingintegrated transparent photovoltaic in a multi-story school building in the tropics (as shown in Fig. 8). It started with site selection, building and room geometry, daylight simulation for several selections of TPV cell coverage ratio and visual transmittance, and continued with solar radiation simulation, which was then used to determine the optimal BITPV configuration. Using this approach, indoor daylighting and energy performance can be well optimized.

Daylighting and energy performance in this study are based on simulated data. Actual daylighting and energy performance can be monitored in future research using full-scale physical samples, following the development of TPV technology as well.

#### Acknowledgments

The research was conducted with Dr. Safial Aqbar bin Zakaria and Dr. Sharifah Fairuz Syed Mohd Fadzil from the School of Housing, Building, and Planning at Universiti Sains Malaysia. This research was funded by Universitas Ciputra Surabaya.

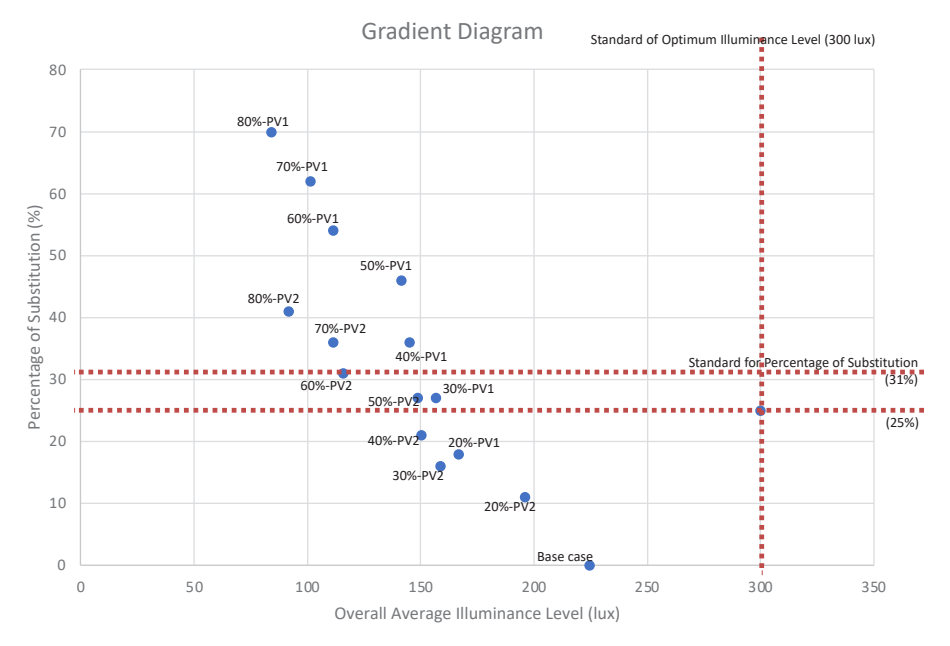


Fig. 6. Optimization diagram based on annual average illuminance and annual energy substitution

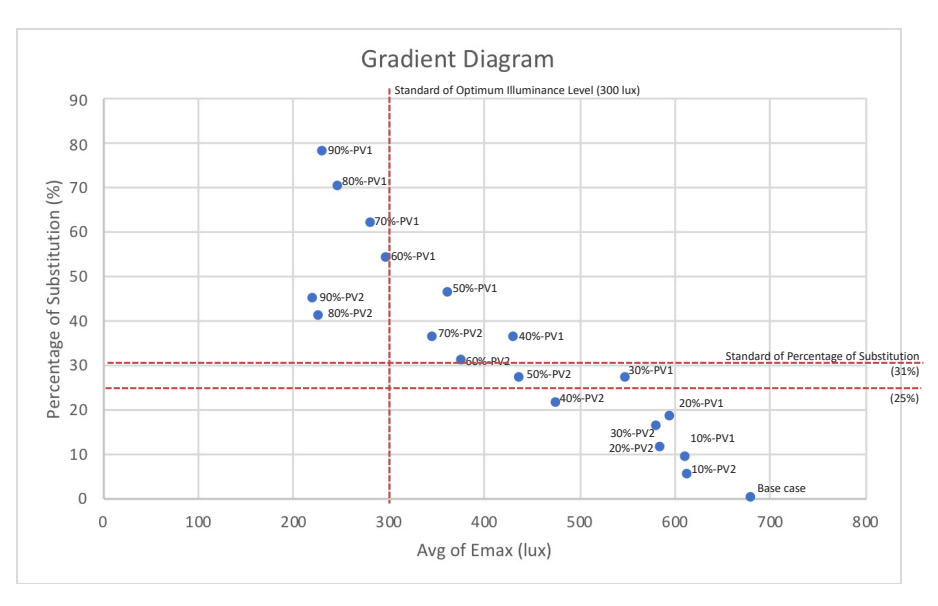


Fig. 7. Gradient diagram based on monthly maximum average illuminance and annual energy substitution

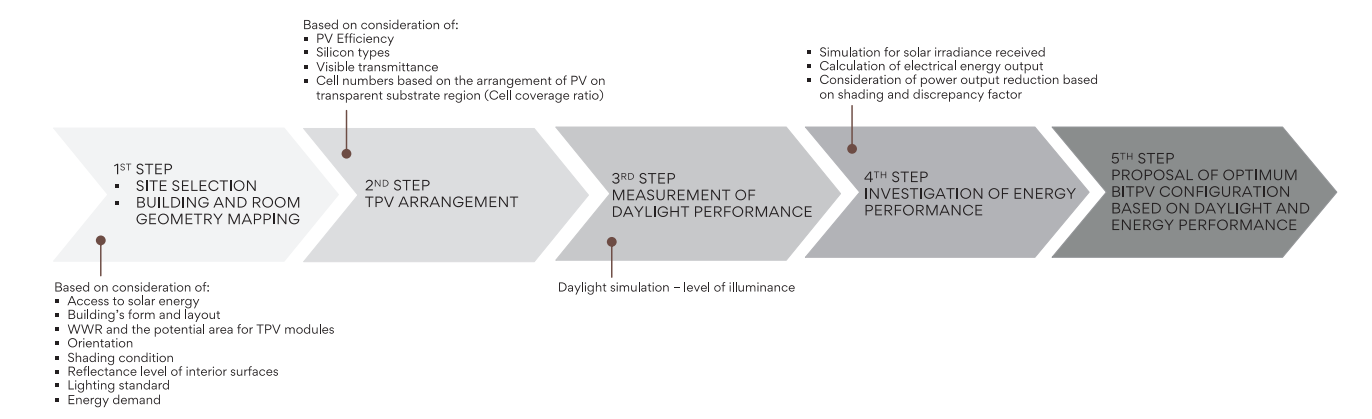


Fig. 8. Systematic method to design BITPV

#### References

Abbaas, E. S., Ismail, M., Saif, A. A., and Ghazali, M. A. (2023). Impact of window shading on the thermal performance of residential buildings of different forms in Jordan. *Architecture and Engineering*, Vol. 8, No. 1, pp. 25–36. DOI: 10.23968/2500-0055-2023-8-1-25-36.

Ahmad, Q. T. and Szokolay, S. V (1993). Thermal design tools in Australia: A comparative study of TEMPER, CHEETAH, ARCHIPAK and QUICK. In: *Proceedings of the IBPSA Building Simulation Conference*, August 16–18, 1993, Adelaide, SA, Australia. Vol. 93, pp. 351–357.

Al Mamun, M. A., Hasanuzzaman, M., and Selvaraj, J. (2017). Experimental investigation of the effect of partial shading on photovoltaic performance. *IET Renewable Power Generation*, Vol. 11, Issue 7, pp. 912–921. DOI: 10.1049/iet-rpg.2016.0902.

Alrashidi, H., Ghosh, A., Issa, W., Sellami, N., Mallick, T. K., and Sundaram, S. (2020a). Thermal performance of semitransparent CdTe BIPV window at temperate climate. *Solar Energy*, Vol. 195, pp. 536–543. DOI: 10.1016/j. solener.2019.11.084.

Alrashidi, H., Issa, W., Sellami, N., Ghosh, A., Mallick, T. K., and Sundaram, S. (2020b). Performance assessment of cadmium telluride-based semi-transparent glazing for power saving in façade buildings. *Energy and Buildings*, Vol. 215, 109585. DOI: 10.1016/j.enbuild.2019.109585.

Andadari, T. S., Purwanto, L. M. F., Satwiko, P., and Sanjaya, R. (2021). Study of digital architecture technology: theory and development. *Journal of Architectural Research and Education*, Vol. 3, No. 1, pp. 14–21. DOI: 10.17509/jare.v3i1.30500.

Ander, G. D. (2003). Daylighting performance and design. 2nd edition. Hoboken: John Wiley & Sons, 336 p.

ASHRAE (2016). Standard 90.1. User's manual. ASHRAE, Atlanta, GA 30329, USA, 478 p.

Badan Standarisasi Nasional (2000). *Prosedur audit energi pada bangunan gedung. SNI 03-6196-2000*. Badan Standarisasi Nasional, Jakarta, 13 p.

Berardi, U. (2017). A cross-country comparison of the building energy consumptions and their trends. *Resources, Conservation and Recycling*, Vol. 123, pp. 230–241. DOI: 10.1016/j.resconrec.2016.03.014.

Biantoro, A. W. and Permana, D. S. (2017). Analisis Audit Energi untuk Pencapaian Efisiensi Energi di Gedung AB, Kabupaten Tangerang, Banten. *Jurnal Teknik Mesin*, Vol. 6, No. 2, pp. 85–93. DOI: 10.22441/jtm.v6i2.1186.

Do, S. L., Shin, M., Baltazar, J.-C., and Kim, J. (2017). Energy benefits from semi-transparent BIPV window and daylight-dimming systems for IECC code-compliance residential buildings in hot and humid climates. *Solar Energy*, Vol. 155, pp. 291–303. DOI: 10.1016/j.solener.2017.06.039.

ENERGI INDONESIA 2019 SEKRETARIAT JENDERAL DEWAN ENERGI NASIONAL (2019). Available at: https://www.esdm.go.id/assets/media/content/content-indonesia-energy-outlook-2019-english-version.pdf (Date accessed: 1 December 2022).

Energy Information Administration (2022). *Annual Energy Outlook 2022. Electricity*. [online] Available at: https://www.eia.gov/outlooks/archive/aeo22/narrative/electricity/sub-topic-01.php [Date accessed 20 December 2022].

Fan, Z., Yang, Z., and Yang, L. (2021). Daylight performance assessment of atrium skylight with integrated semi-transparent photovoltaic for different climate zones in China. *Building and Environment*, Vol. 190, 107299. DOI: 10.1016/j. buildenv.2020.107299.

Feng, X., Ma, T., Yamaguchi, Y., Peng, J., Dai, Y., and Ji, D. (2023). Potential of residential building integrated photovoltaic systems in different regions of China. *Energy for Sustainable Development*, Vol. 72, pp. 19–32. DOI: 10.1016/j. esd.2022.11.006.

Gandah, F., Al-Adayleh, M., and Al-Ruwaishedi, M. R. (2022). Adopting smart building concept in historical building: case of Abu Jaber museum, Jordan. *Architecture and Engineering*, Vol. 7, No. 3, pp. 3–12. DOI: 10.23968/2500-0055-2022-7-3-03-12.

Gholami, H. and Røstvik, H. N. (2020). Economic analysis of BIPV systems as a building envelope material for building skins in Europe. *Energy*, Vol. 204, 117931. DOI: 10.1016/j.energy.2020.117931.

Green Building Council Indonesia (2014). *GREENSHIP rating tools. GREENSHIP existing building. Version 1.1.* [online] Available at: https://gbcindonesia.org/files/resource/093ec9dc-9f1d-47e3-805a-07887b8c4d81/Summary%20 GREENSHIP%20Existing%20Building%20V1.1.pdf [Date accessed 24 October 2022].

Heerwagen, D. (2003). Passive and active environmental controls: informing the schematic designing of buildings. New York: McGraw-Hill Science/Engineering/Math, 940 p.

Hu, Y., Xue, Q., Wang, H., Zou, P., Yang, J., Chen, S., and Cheng, Y. (2024). Experimental investigation on indoor daylight environment of building with Cadmium Telluride photovoltaic window. *Energy and Built Environment*, Vol. 5, Issue 3, pp. 404–413. DOI: 10.1016/j.enbenv.2023.01.001.

Kousalyadevi, G. and Lavanya, G. (2019). Optimal investigation of daylighting and energy efficiency in industrial building using energy-efficient velux daylighting simulation. *Journal of Asian Architecture and Building Engineering*, Vol. 18, Issue 4, pp. 271–284. DOI: 10.1080/13467581.2019.1618860.

Kwong, Q. J. and Ali, Y. (2011). A review of energy efficiency potentials in tropical buildings – Perspective of enclosed common areas. *Renewable and Sustainable Energy Reviews*, Vol. 15, Issue 9, pp. 4548–4553. DOI: 10.1016/j.rser.2011.07.097.

Labayrade, R., Jensen, H. W., and Jensen, C. (2009). Validation of Velux Daylight Visualizer 2 against CIE 171:2006 test cases. In: *Building Simulation 2009. Eleventh International IBPSA Conference*, July 27–30, 2009. Glasgow, Scotland, pp. 1506–1513.

Lakhdari, K., Sriti, L., and Painter, B. (2021). Parametric optimization of daylight, thermal and energy performance of middle school classrooms, case of hot and dry regions. *Building and Environment*, Vol. 204, 108173. DOI: 10.1016/j. buildenv.2021.108173.

Lechner, N. M. (2014). Heating, cooling, lighting: Sustainable design methods for architects. 4th edition. Hoboken: John Wiley & Sons, 720 p.

Lee, K., Um, H.-D., Choi, D., Park, J., Kim, N., Kim, H., and Seo, K. (2020). The development of transparent photovoltaics. *Cell Reports Physical Science*, Vol. 1, Issue 8, 100143. DOI: 10.1016/j.xcrp.2020.100143.

Mangkuto, R. A., Tresna, D. N. A. T., Hermawan, I. M., Pradipta, J., Jamala, N., Paramita, B., and Atthaillah (2024). Experiment and simulation to determine the optimum orientation of building-integrated photovoltaic on tropical building façades considering annual daylight performance and energy yield. *Energy and Built Environment*, Vol. 5, Issue 3, pp. 414–425. DOI: 10.1016/j.enbenv.2023.01.002.

Markus, T. A. and Morris, E. N. (1980). *Buildings, climate, and energy*. 2<sup>nd</sup> edition. London: Pitman Publishing Limited, 540 p.

McMullan, R. (2018). Environmental science in building. 8th edition. London: Palgrave, 399 p.

Milaningrum, T. H. (2015). Optimalisasi Pencahayaan Alami dalam Efisiensi Energi di Perpustakaan UGM. In: *Prosiding Seminar Topik Khusus/ Juli 2015*.

Montenegro, E., Potvin, A., and Demers, C. (2012). Impact of school building typologies on visual, thermal and energy performances. In: *PLEA2012 - 28<sup>th</sup> Conference, Opportunities, Limits & Needs Towards an Environmentally Responsible Architecture*, November 7–9, 2012, Lima, Peru. DOI: 10.13140/2.1.3557.5363.

Musameh, H., Alrashidi, H., Al-Neami, F., and Issa, W. (2022). Energy performance analytical review of semi-transparent photovoltaics glazing in the United Kingdom. *Journal of Building Engineering*, Vol. 54, 104686. DOI: 10.1016/j. jobe.2022.104686.

Noerwasito, V. T. (2022). Sawdust and soil block as wall in simple buildings to gain the optimum heat and embodied energy in humid tropical area. *IOP Conference Series: Earth and Environmental Science*, Vol. 1007, 012002. DOI: 10.1088/1755-1315/1007/1/012002.

Noerwasito, V. T. and Nirwansyah, R. (2019). Simple energy-efficient house wall material selection in a humid tropical area — case study in Surabaya. *Advances in Engineering Research*, Vol. 156, pp. 52–55.

Peng, C., Huang, Y., and Wu, Z. (2011). Building-integrated photovoltaics (BIPV) in architectural design in China. *Energy and Buildings*, Vol. 43, Issue 12, pp. 3592–3598. DOI: 10.1016/j.enbuild.2011.09.032.

Polo López, C. S. and Sangiorgi, M. (2014). Comparison assessment of BIPV façade semi-transparent modules: Further insights on human comfort conditions. *Energy Procedia*, Vol. 48, pp. 1419–1428. DOI: 10.1016/j.egypro.2014.02.160.

Rabah, K. and Tamakan, Z. (2002). Application of ARCHIPAK for development of passive solar energy-efficient building in North Cyprus. *Architectural Science Review*, Vol. 45, Issue 3, pp. 219–229. DOI: 10.1080/00038628.2002.9697513.

Rao, S. S. (2009). Engineering optimization: theory and practice. 4th edition. Hoboken: John Wiley & Sons, 813 p.

Roberts, S. and Guariento, N. (2009) Building integrated photovoltaics: a handbook. Basel: Walter de Gruyter, 192 p.

Shankar, A., Vijayakumar, K., and Babu, B. C. (2021). Energy saving potential through artificial lighting system in PV integrated smart buildings. *Journal of Building Engineering*, Vol. 43, 103080. DOI: 10.1016/j.jobe.2021.103080.

Sugiyama, M. (2016). *Introduction to statistical machine learning*. Waltham, MA 02451 USA: Elsevier, 534 p. DOI: 10.1016/C2014-0-01992-2.

Sun, Y., Shanks, K., Baig, H., Zhang, W., Hao, X., Li, Y., He, B., Wilson, R., Liu, H., Sundaram, S., Zhang, J., Xie, L., Mallic, T., and Wu, Y. (2019). Integrated CdTe PV glazing into windows: energy and daylight performance for different window-to-wall ratio. *Energy Procedia*, Vol. 158, pp. 3014–3019. DOI: 10.1016/j.egypro.2019.01.976.

Susan, S. and Wardhani, D. (2020a). Building integrated photovoltaic as GREENSHIP'S on site renewable energy tool. *Results in Engineering*, Vol. 7, 100153. DOI: 10.1016/j.rineng.2020.100153.

Susan, S. and Wardhani, D. K. (2020b). Photovoltaic and wind turbine: a comparison as building integrated renewable energy in Indonesia. *Humaniora*, Vol. 11, No. 1, pp. 51–57. DOI: 10.21512/humaniora.v11i1.6294.

Szokolay, S. V. (1986). ARCHIPAK an integrated design tool for small solar buildings. *Intersol Eighty Five. Proceedings of the Ninth Biennial Congress of the International Solar Energy Society*, pp. 379–383. DOI: 10.1016/B978-0-08-033177-5.50080-6.

Trinuruk, P., Sorapipatana, C., and Chenvidhya, D. (2009). Estimating operating cell temperature of BIPV modules in Thailand. *Renewable Energy*, Vol. 34, Issue 11, pp. 2515–2523. DOI: 10.1016/j.renene.2009.02.027.

Tsikra, P. and Andreou, E. (2017). Investigation of the energy saving potential in existing school buildings in Greece. The role of shading and daylight strategies in visual comfort and energy saving. *Procedia Environmental Sciences*, Vol. 38, pp. 204–211. DOI: 10.1016/j.proenv.2017.03.107.

Ubisse, A. and Sebitosi, A. (2009). A new topology to mitigate the effect of shading for small photovoltaic installations in rural sub-Saharan Africa. *Energy Conversion and Management*, Vol. 50, Issue 7, pp. 1797–1801. DOI: 10.1016/j. enconman.2009.03.016.

Vardanyan, E. (2021). Sustainability in the process of development permit acquisition (Armenia). *Architecture and Engineering*, Vol. 6, No. 3, pp. 62–69. DOI: 10.23968/2500-0055-2021-6-3-62-69.

Wong, I. L. (2017). A review of daylighting design and implementation in buildings. *Renewable and Sustainable Energy Reviews*, Vol. 74, pp. 959–968. DOI: 10.1016/j.rser.2017.03.061.

Wu, X., Liu, Y., Xu, J., Lei, W., Si, X., Du, W., Zhao, C., Zhong, Y., Peng, L., and Lin, J. (2015). Monitoring the performance of the building attached photovoltaic (BAPV) system in Shanghai. *Energy and Buildings*, Vol. 88, pp. 174–182. DOI: 10.1016/j. enbuild.2014.11.073.

Xiang, C. and Matusiak, B. S. (2022). Façade Integrated Photovoltaics design for high-rise buildings with balconies, balancing daylight, aesthetic and energy productivity performance. *Journal of Building Engineering*, Vol. 57, 104950. DOI: 10.1016/i.jobe.2022.104950.

Xiong, W., Liu, Z., Wu, Z., Wu, J., Su, F., and Zhang, L. (2022). Investigation of the effect of Inter-Building Effect on the performance of semi-transparent PV glazing system. *Energy*, Vol. 245, 123160. DOI: 10.1016/j.energy.2022.123160.

Xuan, Q., Li, G., Lu, Y., Zhao, B., Wang, F., and Pei, G. (2021). Daylighting utilization and uniformity comparison for a concentrator-photovoltaic window in energy saving application on the building. *Energy*, Vol. 214, 118932. DOI: 10.1016/j. energy.2020.118932.

Zomer, C. and Rüther, R. (2017). Simplified method for shading-loss analysis in BIPV systems. Part 2: Application in case studies. *Energy and Buildings*, Vol. 141, pp. 83–95. DOI: 10.1016/j.enbuild.2017.02.043.

# ОПТИМИЗАЦИЯ КОНФИГУРАЦИИ ИНТЕГРИРОВАННЫХ В ЗДАНИЕ ПРОЗРАЧНЫХ ФОТОЭЛЕКТРИЧЕСКИХ СИСТЕМ С УЧЕТОМ ДНЕВНОГО СВЕТА И ЭНЕРГОЭФФЕКТИВНОСТИ В ШКОЛЬНЫХ ЗДАНИЯХ В ТРОПИКАХ

Сьюзан Сьюзан<sup>1,2\*</sup>, Сафиал Акбар бин Закария<sup>1</sup>, Шарифа Файруз Сайед Мохд Фадзил<sup>1</sup>

- 1 Университет Сайнс Малайзия, Пенанг, Малайзия
- <sup>2</sup> Университет Чипутра Сурабая, Сурабая, Восточная Ява, Индонезия
- \*E-mail: susan@student.usm.my / susan@ciputra.ac.id

#### Аннотация

Введение: Использование вертикальных фасадов для бокового освещения рассматривается в многочисленных исследованиях. Установлено, что вертикальные фасады представляют собой эффективное средство обеспечения доступа дневного света, которое помогает создать приятную атмосферу, повысить успеваемость в школах и улучшить здоровье обучающихся. Недавние исследования также выявили потенциал использования вертикальных фасадов в высотных зданиях в качестве интегрированных в здание фотоэлектрических систем (BIPV) благодаря большой доступной площади. В тропиках такое потенциальное применение также обусловлено большим количеством солнечного света. Технология прозрачных фотоэлектрических систем (TPV) дает возможность удовлетворить обе потребности. В зависимости от ряда факторов, таких как коэффициент пропускания видимого света (VT) и количество ячеек, она обеспечивает боковое освещение и применяется в интегрированных в здание прозрачных фотоэлектрических системах (BITPV). Для бокового освещения требуется более высокий коэффициент пропускания видимого света (VT), который позволит обеспечить оптимальное проникновение дневного света. При этом для интегрированных в здание прозрачных фотоэлектрических систем (BITPV) предпочтительно большее количество ячеек и более низкий коэффициент пропускания видимого света (VT). Предыдущие исследования показали. что интегрированные в здание прозрачные фотоэлектрические системы (BITPV) предлагаются для зданий с соотношением площади окна к площади стены (WWR) в 45 % и более, которое кажется довольно высоким для зданий, располагающихся в тропиках, где соотношение WWR обычно предлагается в диапазоне 30-40 %. Цель исследования: Данное исследование направлено на поиск оптимальной конфигурации и представление систематического метода оптимизации интегрированных в здание прозрачных фотоэлектрических систем (ВІТРV) фасадов школ в тропиках. Методы: Для достижения поставленной цели использован экспериментальный подход с применением моделирования. В качестве объекта исследования был выбран участок с планировкой, типичной для школ, располагающихся в тропиках. Для формирования пост-экспериментальных моделей был учтен коэффициент пропускания видимого света (VT) и количество ячеек. Результаты и обсуждение: В тропиках при использовании фотоэлектрических систем с низкой прозрачностью, интегрированные в здание прозрачные фотоэлектрические системы (BITPV) с соотношением площади окна к площади стены (WWR) 31,25 % и 30 % коэффициентом покрытия ячейками обеспечивают оптимальный визуальный комфорт и энергоэффективность. При этом интегрированные в здание прозрачные фотоэлектрические системы (BITPV) с соотношением площади окна к площади стены (WWR) 31.25 % и 50 % коэффициентом покрытия ячейками представляют собой оптимальную конфигурацию при использовании фотоэлектрических систем с высокой прозрачностью. В данном исследовании также представлен систематический метод проектирования интегрированных в здание прозрачных фотоэлектрических систем (ВІТРУ) для многоэтажных школьных зданий в тропиках.

**Ключевые слова:** интегрированные в здание прозрачные фотоэлектрические системы (BITPV), энергозамещение, освещенность, школьное здание, тропики.

#### **Civil Engineering**

DOI: 10.23968/2500-0055-2024-9-1-44-60

## PREDICTION OF THE PERFORMANCE OF REINFORCED CONCRETE ELEMENTS UNDER MONOTONIC AND CYCLIC LATERAL LOADING

Boubakeur Fettar\*, Smail Boukeloua

Department of Civil Engineering, Faculty of Sciences of Technology, Mentouri Brothers University (Constantine 1), Constantine, Algeria

Laboratory of Mechanics of Soils and Structures (LMSS), Mentouri Brothers University (Constantine 1), Constantine, Algeria

\*Corresponding author's e-mail: boubakeur.fettar@doc.umc.edu.dz

#### Abstract

Introduction: The nonlinear behavior of reinforced concrete elements under monotonic and cyclic loading is one of the most important research topics in seismic regions. Over the past 30 years, several experimental investigations have been conducted with the aim of better understanding the behavior of reinforced concrete elements and determining the various parameters influencing this behavior. Purpose of the study: The present research investigates this behavior and aims to develop an interactive computer program designed for use within the Windows environment. Methods: Several material models (confined/unconfined concrete and reinforcing steel), as well as hysteresis laws, are employed in an analytical approach using the fiber element. For each specimen, geometric characteristics, material models, plastic hinge locations, axial loads, and the history of corresponding horizontal displacements were input into the program. Numerical predictions are validated against experimental results from diverse studies. Results: Convergence analysis using experimental data demonstrated good agreement between numerical and experimental results, particularly in hysteresis behavior, force-displacement envelope curves, maximum strength, initial stiffness, stiffness degradation, and cumulative energy dissipation. The findings underscore the efficacy of the developed program in accurately predicting the nonlinear behavior of reinforced concrete elements. The developed program provides a reliable tool for predicting the nonlinear behavior of reinforced concrete elements under cyclic loading, validated through convergence analysis with experimental data.

**Keywords:** computer program, fiber element, hysteresis, materials models, moment-curvature.

#### Introduction

Performance-based design is a methodology aimed at achieving predictable behavior of a structure and its elements during an earthquake (Djebbar, 2006; Esmaeily and Peterman, 2007). This prediction of damage evolution requires a realistic assessment of the performance and behavior of different structural elements (Chadwell and Imbsen, 2004; Sato et al., 2002). The failure of these elements in a precise chronological order and at targeted locations (fuse element) will cause progressive structural failure.

The behavior of reinforced concrete columns is considered to be a very important research topic in seismic-prone areas (Nawy, 1996; Rodrigues et al., 2013b). The nonlinear behavior of reinforced concrete columns has been the subject of several experimental studies (Rodrigues et al., 2013b; Shirmohammadi and Esmaeily, 2015). The behavior depends on the level of the applied axial load, the history of lateral loading, geometric characteristics of the cross section, properties of the materials (concrete and reinforcing steel), density, and the configuration of longitudinal

and transverse reinforcement (Abd El Fattah, 2012; Furtado et al., 2015; Rodrigues et al., 2013a, 2014; Shirmohammadi, 2015; Shirmohammadi and Esmaeily, 2015). Evaluating one or more of these parameters is costly. Therefore, numerical simulation becomes an unavoidable alternative for conducting possible parametric studies on the behavior of reinforced concrete columns under cyclic loading (Shirmohammadi and Esmaeily, 2015).

Most available analysis tools are limited to analysis under monotonic loading and are difficult for engineers to use. Engineers prefer easy analytical approaches with satisfactory accuracy (Esmaeily and Peterman, 2007).

The main objective of the present study is to develop an interactive computer program that is easy to use in the Windows environment and capable of predicting the behavior of reinforced concrete elements under both monotonic and cyclic loading with acceptable precision. The second part of the study is dedicated to validating the program by comparing the numerical results with those of tests conducted by various authors.

Development of the computer program for analysis

Basis of analysis

The analysis is based on the fiber element, which is widely used by several researchers and software (Esmaeily and Peterman, 2007). In this analysis, the concrete cross section is divided into a number of rectangular finite elements called fibers (Fig. 1). The reinforcing steel bars are not meshed due to their small surface areas. Each fiber of the cross section is associated with a set of data: coordinates (Y, Z), surface area, and material type identifier (confined/unconfined concrete and reinforcing steel) (Sato et al., 2002).

The geometry of the cross section, the mesh size, the quantity, and the configuration of reinforcing steel (Fig. 2), as well as the models and material hysteresis laws (Fig. 3), can be defined or selected by the user through the graphical user interface (GUI).

The axial load, the plastic length model (Fig. 4), and the monotonic or cyclic displacement (Fig. 5) serve as input data for controlled displacement analysis. This approach captures the state of strain, stress, force, and moment of each fiber section. The history of each fiber is archived, traced, and updated at each step of the analysis (Chadwell and Imbsen, 2004; Esmaeily and Peterman, 2007; Sato et al., 2002).

Material models (concrete and steel) Interface presentation

For the stress-strain material relationship, multiple material models and hysteresis laws are provided (Fig. 3), which can be selected and customized depending on the user's choice and analysis needs. Tensile strength is not considered in any of the concrete models (confined and unconfined). In the case of reinforced concrete, three material models

and hysteresis laws must be defined (reinforcing steel, confined concrete, and unconfined concrete).

Monotonic unconfined concrete models

Seven unconfined concrete models (Fig. 3) can be selected and configured based on user preferences. These models include Popovics 1973 (Lee, 2017; Popovics, 1973), Mander 1988 (Mander, 1983, Mander et al., 1988), Kent & Park 1971 (Kent, 1969; Kent and Park, 1971; Lee, 2017; Park and Paulay, 1991; Park et al., 1982; Scott, 1980), Hognestad 1951 (Hognestad, 1951; Lee, 2017; Scott, 1980), Carreira & Chu 1985 (Carreira and Chu, 1985), Tsai 1988 (Tsai, 1988), Desayi & Krisnan 1964 (Desayi and Krishnan, 1964). These models can be adjusted according to specific requirements (modulus of elasticity, yield stress, yield strain, ultimate strain), offering a wide variety for unconfined concrete.

Monotonic confined concrete models

The user has four choices (Fig. 3): three confined concrete models Mander 1988 (Mander, 1983, Mander et al., 1988), Kent & Park 1971 (Kent, 1969; Kent and Park, 1971; Lee, 2017; Park and Paulay, 1991; Park et al., 1982; Scott, 1980), Cusson & Paultre 1994 (Cusson and Paultre, 1994, 1995) and a fourth option obtained by selecting the fourth checkbox, indicating the exclusion of the confinement effect.

Confined and unconfined concrete hysteresis law A single linear elastic hysteresis law is employed for all concrete models, whether confined or unconfined, because of its simplicity to program.

Monotonic and cyclic models of reinforcing steels
To simulate the behavior of longitudinal steel
bars, three models were incorporated (Fig. 3):
the elasto-plastic model (Li, 2004), the GiuffrèMenegotto-Pinto model (Bosco et al., 2016;
Carreño et al., 2020; Menegotto and Pinto, 1973;
opensees.berkeley.edu, 2023), and the Esmaeily

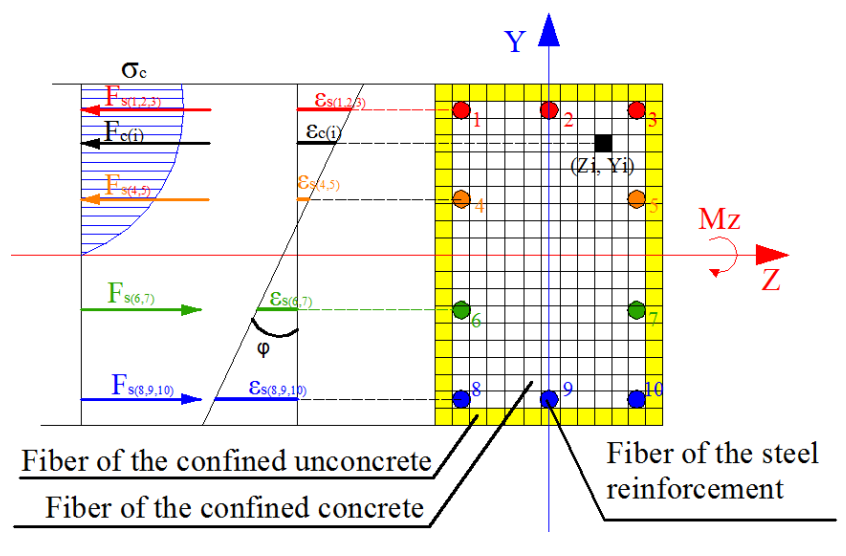


Fig. 1. Discretization of reinforced-concrete sections

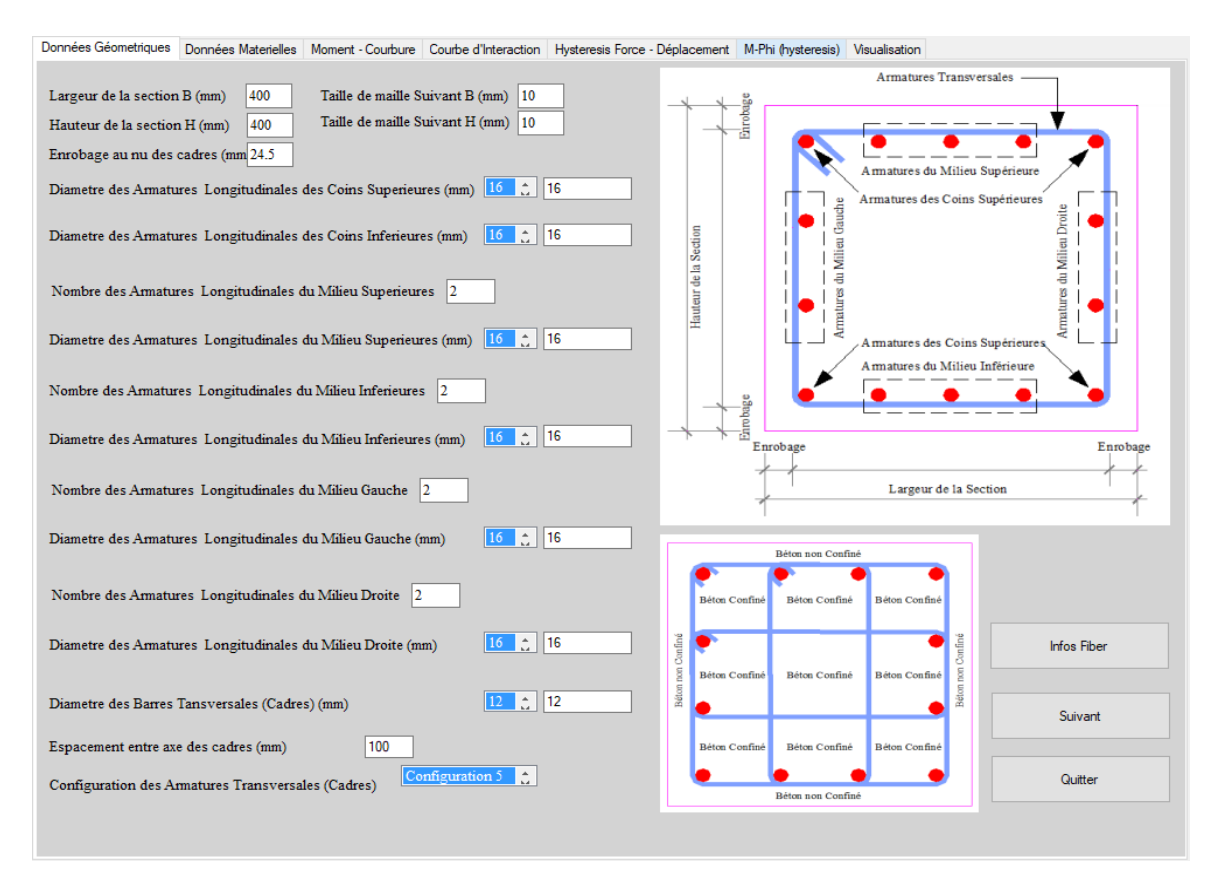


Fig. 2. Main window: definition of geometric characteristics of the cross section

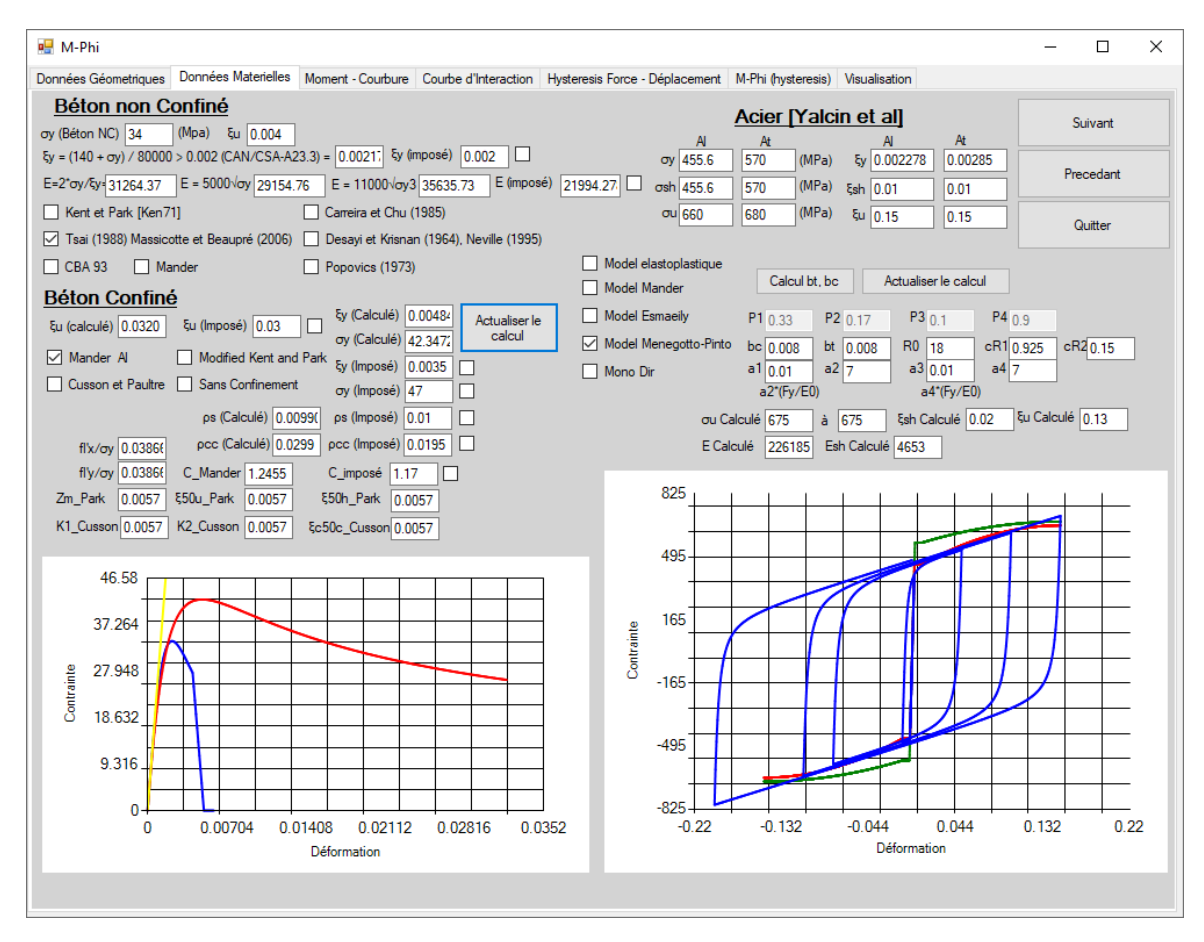


Fig. 3. Window for configuring the selected material models

model (Esmaeily and Peterman, 2007; Esmaeily and Shirmohammadi, 2014; Esmaeily-Ghasemabadi and Xiao, 2002; Shirmohammadi, 2015). Those models were selected for their ease of programming, extensive usage, and numerical stability.

#### Hinge plastic length calculation models

The user can select one of the four programmed methods (Fig. 4): Esmaeily & Xiao 2002 (Esmaeily and Shirmohammadi, 2014; Esmaeily-Ghasemabadi and Xiao, 2002; Shirmohammadi, 2015), Sheikh & Khoury 1993 (Mortezaei and Ronagh, 2013; Shirmohammadi, 2015; Zhao et al., 2011), Paulay & Priestley 1992 (Esmaeily and Shirmohammadi, 2014; Esmaeily-Ghasemabadi and Xiao, 2002; Mortezaei and Ronagh, 2013; Shirmohammadi, 2015; Zhao et al., 2011) and Priestly & Park 1987 (Esmaeily and Shirmohammadi, 2014; Esmaeily-Ghasemabadi and Xiao, 2002; Mortezaei and Ronagh, 2013; Priestley and Park 1987; Shirmohammadi, 2015; Zhao et al., 2011), and also manually define the plastic length.

#### Analysis process

#### Moment-curvature relation

The concrete in the analyzed section is divided into a number of fibers, and each steel reinforcement considered as a fiber (Fig. 6). Each fiber is associated with a series of data, including the type of material, area, and coordinates (Chadwell and Imbsen, 2004; Sato et al., 2002).

The strain at each fiber and the curvature are determined by the variation of the neutral axis and the strains from the most compressed to the most tensile fiber (Fig. 7) using the following relationships:

$$\varphi = \frac{\varepsilon_{mc}}{Y_{mc}} = \frac{\varepsilon_{mt}}{Y_{mt}}; \qquad (1)$$

$$\varepsilon_i = \varphi \times (Y_i - Y_N), \tag{2}$$

where:  $\phi$  — curvature,  $\epsilon_{mc}$  — strains in the most compressed fiber,  $\epsilon_{mt}$  — strains in the most tensile fiber,  $\epsilon_i$  — strains in the fiber (i),  $Y_{mc}$  — coordinate of the most compressed fiber,  $Y_{mt}$  — coordinate of the most tensile fiber,  $Y_i$  — coordinate of the fiber (i),  $Y_N$  — coordinate of the neutral axis.

The stress in each fiber can be estimated using the calculated strain and the material model (stressstrain) adopted by the user (Fig. 3).

The position of the neutral axis, the curvature of the cross section, and the stress and strain state of each fiber will be determined, and the bending moment of the section can be evaluated using relationship (4), only if the equilibrium of relationship (3) between internal and external forces is satisfied.

$$P = FandF = \sum_{i=1}^{n} \sigma_{ci} * A_{ci} + \sum_{j=1}^{m} \sigma_{sj} * A_{sj};$$
 (3)

$$M = \sum_{i=1}^{n} \sigma_{ci} * A_{ci} * d_i + \sum_{j=1}^{m} \sigma_{sj} * A_{sj} * d_j,$$
 (4)

where: P — external axial force, F — internal force in the section, M — moment in the section,  $\sigma_{ci}$  — stress in the fiber (i) of concrete,  $\sigma_{sj}$  — stress in the fiber (j) of a reinforcement bar,  $A_{ci}$  — area of

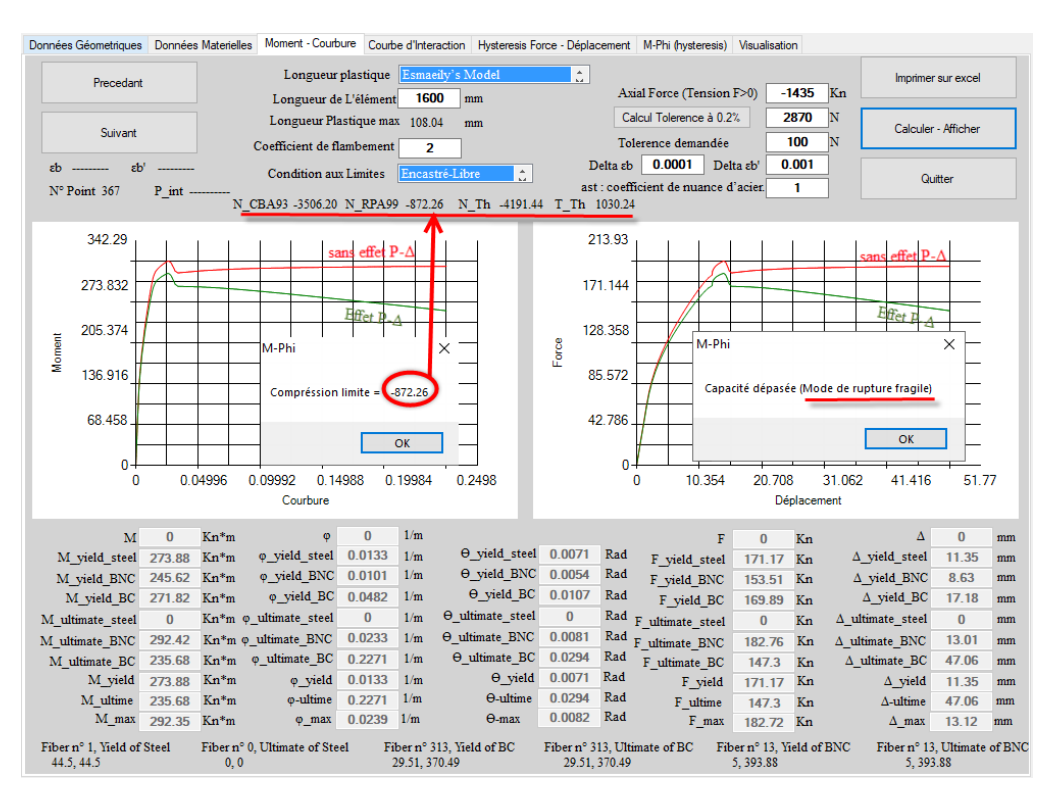


Fig. 4. Window for the analysis of a section under monotonic loading

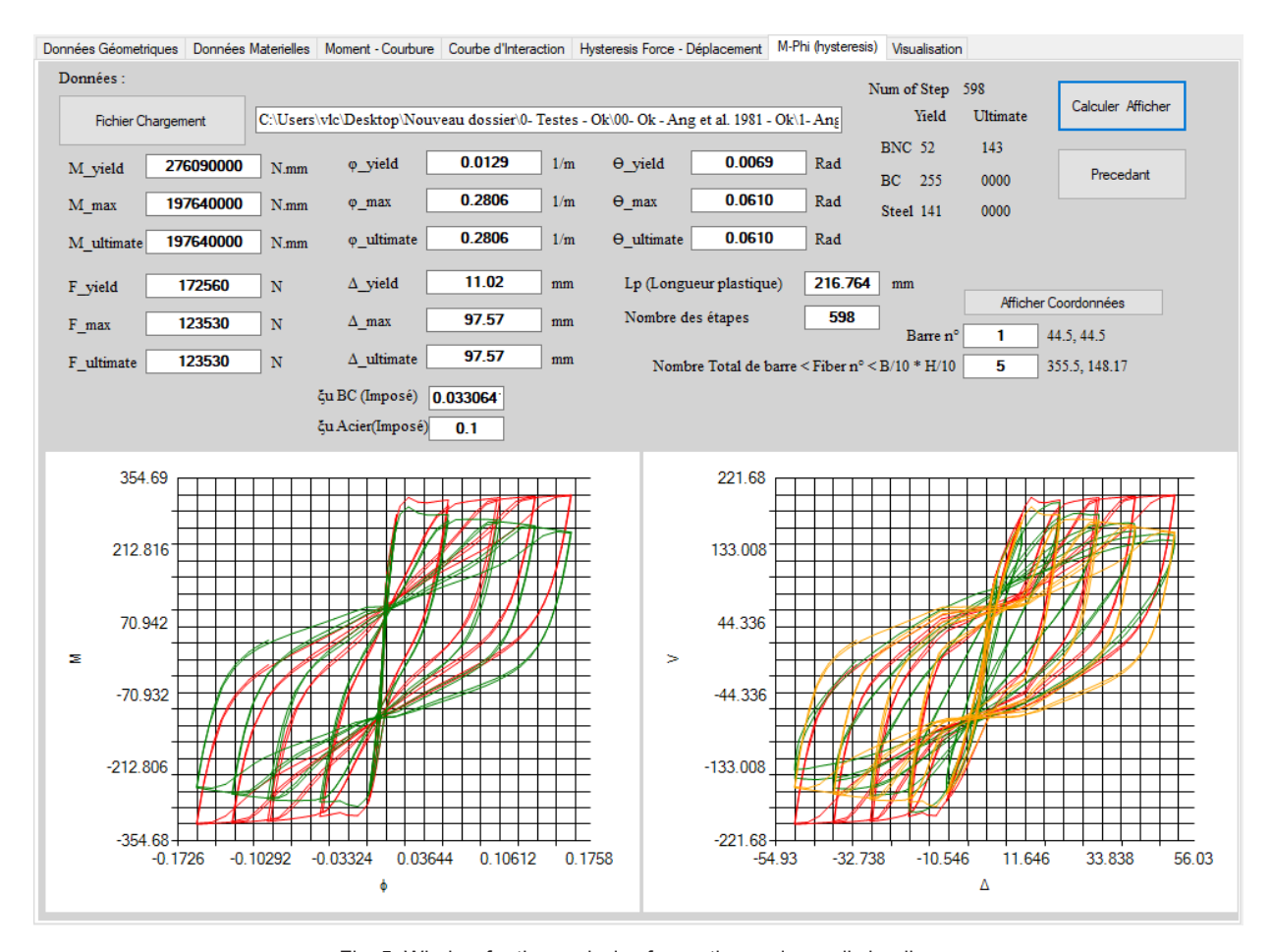


Fig. 5. Window for the analysis of a section under cyclic loading

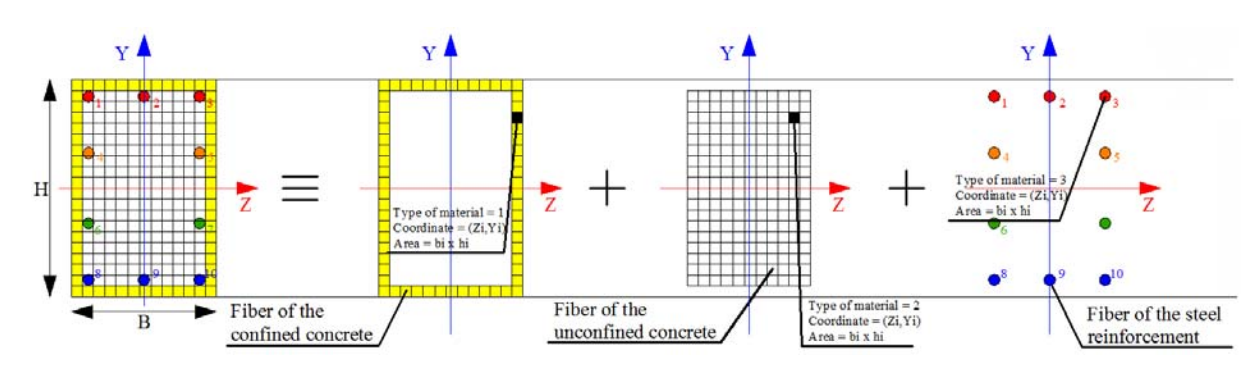


Fig. 6. Details of reinforced concrete section discretization

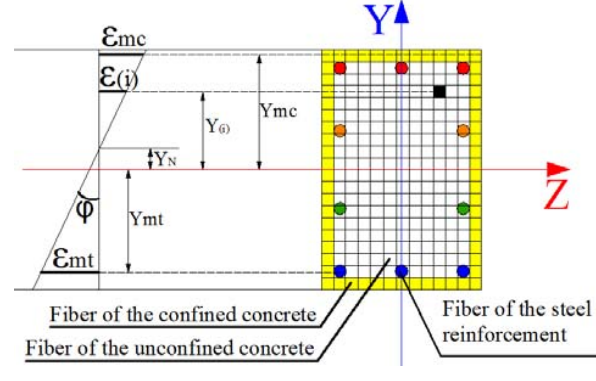


Fig. 7. Estimation of the strain in each fiber

the fiber (i) of concrete,  $A_{sj}$  — area of the fiber (j) of a reinforcement bar,  $d_i$  — coordinate of the fiber (i) of concrete,  $d_j$  — coordinate of the fiber (j) of a reinforcement bar.

Fig. 8 illustrates the numerical moment-curvature analysis algorithm for sections under monotonic loading.

#### Force-displacement relationship

The force-displacement analysis of the element is based on the moment-curvature analysis. Before conducting the monotonic or cyclic analysis, the user must determine the loading history, member length, and plastic hinge method (Figs. 4 and 5). The force-

displacement curve will be determined using the following relationships:

$$\Delta = \begin{cases} \phi_{calc} \leq \phi_{y} \phi_{calc} \times L^{2} / 3; \\ \phi_{y} \leq \phi_{calc} \leq \phi_{u} \left[ \phi_{y} \times L^{2} / 3 \right] + \\ + \left[ L_{p} \times \left( \phi_{calc} - \phi_{y} \right) \times \left( L - 0.5 L_{p} \right) \right]; \end{cases}$$
 (6)

Fig. 9 illustrates the numerical force-displacement analysis algorithm for sections under monotonic and cyclic loading.

#### Convergence analysis of the program

The convergence analysis serves as a comprehensive validation of the program reliability and accuracy in predicting the behavior of reinforced concrete elements under both monotonic and cyclic loading. To evaluate the performance and efficiency of the computer program developed, the data from several experimental tests were input into the program (Table 1).

The Mander model (Mander, 1983; Mander et al., 1988) is used to simulate the uniaxial stress-strain

relationship of confined and unconfined concrete fibers with an elastoplastic hysteresis law, while the Giuffrè-Menegotto-Pinto model (Bosco et al., 2016; Carreño et al., 2020; Menegotto and Pinto, 1973; opensees.berkeley.edu, 2023) is used for modeling the stress-strain relationship of the longitudinal reinforcing bars. The numerical results obtained from the simulation are then compared with the corresponding experimental results.

#### Presentation and discussion of the results

In this section, several results are presented and discussed, including hysteresis loops, force-displacement envelope curves, maximum resistance, initial stiffness, stiffness degradation, and cumulative energy dissipation.

#### Hysteresis loops

The hysteresis behavior, the shear force history at each analysis step, and the shear force at the peak of the first cycle of each imposed displacement resulting from the simulation are presented in Fig. 10 and compared with the results of the experimental tests.

The ratio between the simulated shear force and the experimental shear force, calculated at the peak of the first cycle of each imposed

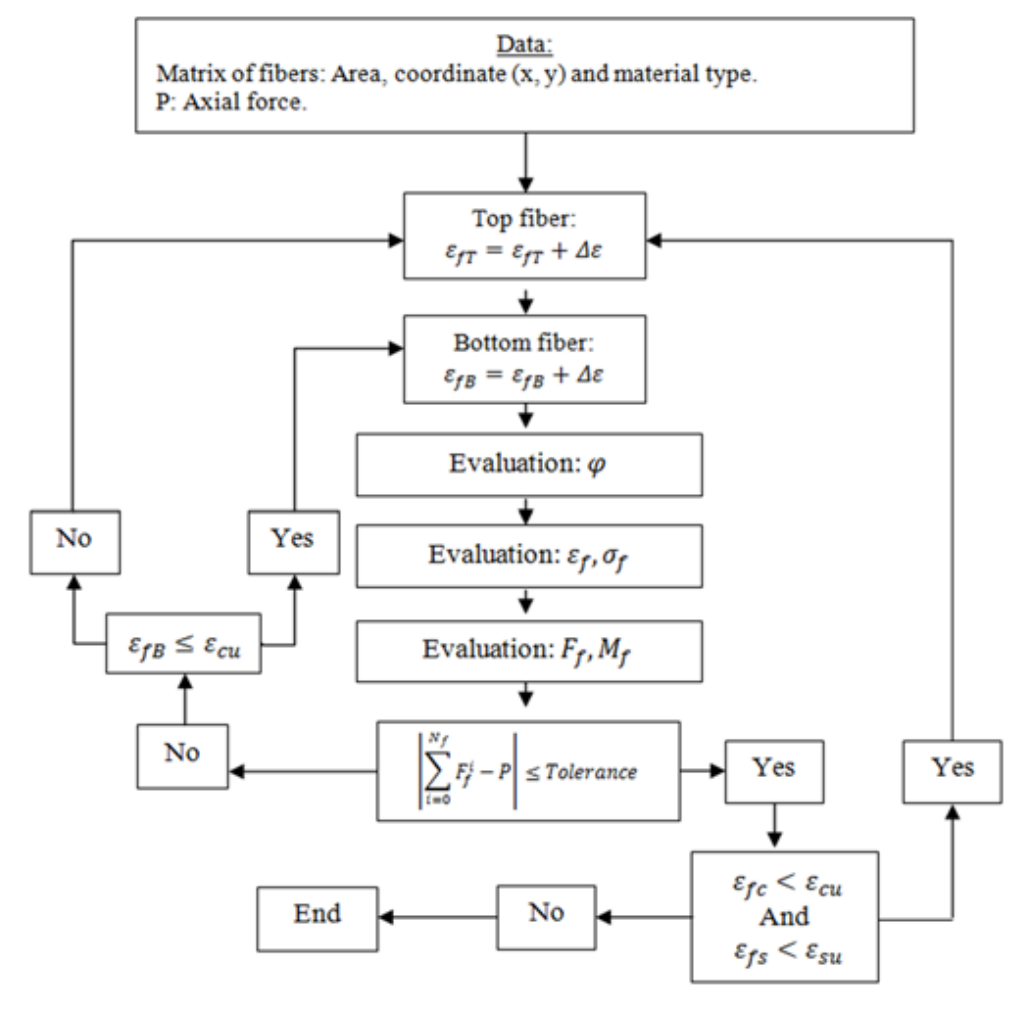


Fig. 8. Numerical moment-curvature analysis algorithm for sections under monotonic loading

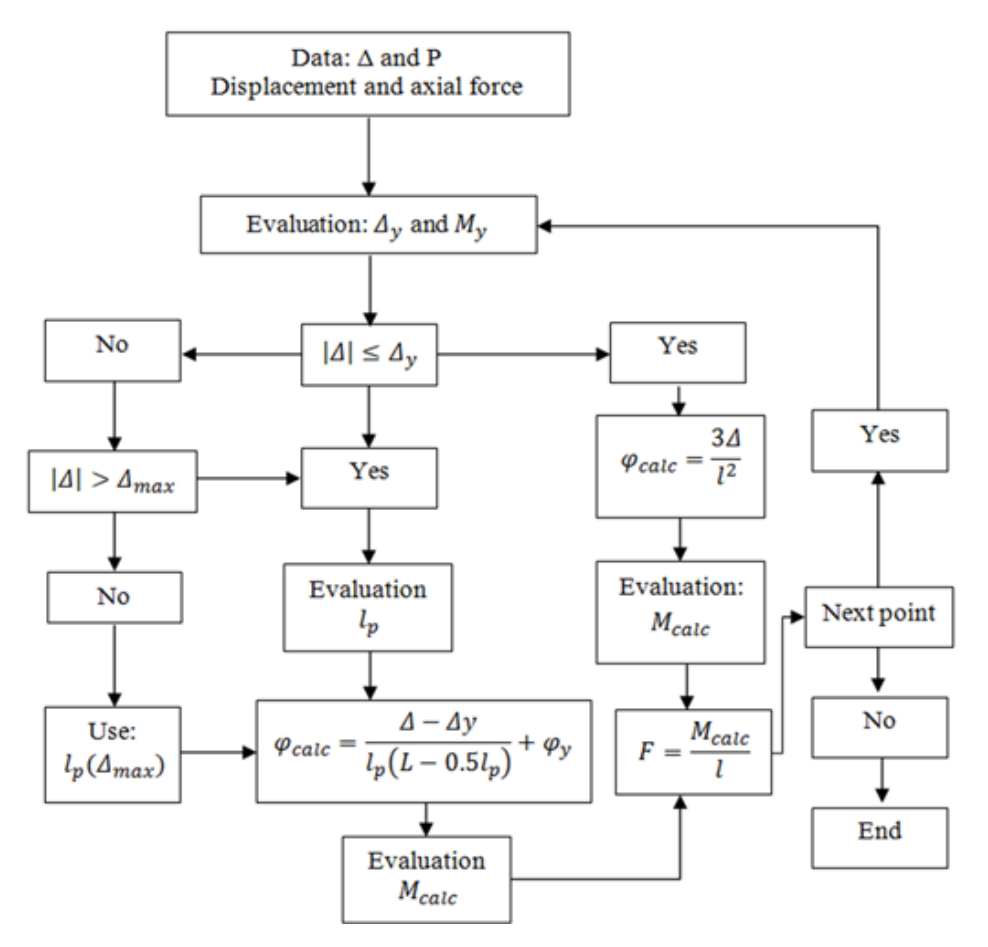


Fig. 9. Numerical force-displacement and moment-curvature analysis algorithm for sections under cyclic loading:  $\Delta$  — displacement,  $\Delta_y$  — yield displacement,  $\Delta_{\max}$  — maximum displacement,  $\phi_y$  — yield curvature,  $\phi_{calc}$  — calculated curvature, l — element length,  $l_p$  — plastic hinge length,  $l_p$  ( $\Delta_{\max}$ ) — plastic hinge length at maximum displacement,  $M_y$  — yield moment,  $M_{calc}$  — calculated moment, and F — internal force

displacement, shows (Fig. 10c) a good correlation between the numerical model and the experimental results for most tests (0.02 to 13.75 %) and a variation of the order of 19.14 to 33.07 % for the two tests: test h (Alfarah, 2017; Maranhão et al., 2021; nisee.berkeley.edu, 2003; Tanaka, 1990) and test i (nisee.berkeley.edu, 2003; Park and Paulay, 1990), probably associated with a linear elastic numerical response.

In general, a good representation of the global response of the elements is obtained. In the majority of cases, it was also observed that the cyclic unloading response phase of the columns obtained with the numerical models does not capture the pinching effect observed experimentally.

#### Envelope capacity curves

A good agreement was found between the experimental test capacity curves and those of the computer program. The envelope curves obtained based on the cyclic responses are shown in Fig. 11.

#### Initial stiffness

The ratio between the experimentally determined initial stiffness and the values obtained

numerically was calculated and illustrated in Fig. 12 to evaluate the program accuracy in terms of initial stiffness.

The initial stiffness  $K_i$  is the ratio between the shear force and the displacement corresponding to the yield point. Based on the results obtained, it can be concluded that:

- For the following tests: test a (Atalay and Penzien, 1975; nisee.berkeley.edu, 2003), test b (Ang, 1981; nisee.berkeley.edu, 2003), test c (Ang, 1981; nisee.berkeley.edu, 2003), test d (nisee. berkeley.edu, 2003; Ohno and Nishioka, 1984), test e (nisee.berkeley.edu, 2003; Ohno and Nishioka, 1984), test f (nisee.berkeley.edu, 2003; Tanaka, 1990), test g (nisee.berkeley.edu, 2003; Tanaka, 1990), and test h (Alfarah, 2017; Maranhão et al., 2021; nisee.berkeley.edu, 2003; Tanaka, 1990), the computer program provides a good estimate of the initial stiffness with a variation of 0–19 %.
- There is a significant variation in the initial stiffness between the experimental test (nisee. berkeley.edu, 2003; Park and Paulay, 1990) and the program, with an overestimation of the initial stiffness

**B**×H **Symbol Test** Specimen N(KN)  $\sigma_{a}$  (MPa)  $\sigma_{a}$  (MPa) σ, (MPa) ρ (%) ρ, (%) (mm<sup>2</sup>) Atalay and Penzien 75 3S1 305 x 305 1676 267 29.2 367 1.63 363 1.5 а (Atalay and Penzien 1975; nisee.berkeley.edu, Ang 81 (Ang, 1981; nisee. S3 400x400 1600 1435 23.6 b berkeley.edu, 2003) С Ang 81 (Ang, 1981; nisee. S4 400x400 1600 840 25.0 427 1.51 280 2.2 berkeley.edu, 2003) 127 d Ohno and Nishioka 84 L1 400x400 1600 24.8 362 1.42 325 0.3 (nisee.berkeley.edu, 2003; Ohno and Nishioka, 1984) е Ohno and Nishioka 84 L2 400x400 1600 127 24.8 362 1.42 325 0.3 (nisee.berkeley.edu, 2003; Ohno and Nishioka, 1984) 333 f Tanaka & Park 90 (nisee. No. 1 400x400 1600 819 25.6 474 1.57 2.5 berkeley.edu, 2003; Tanaka, 1990) Tanaka & Park 90 (nisee. No. 4 400x400 1600 819 25.6 474 1.57 333 2.5 g berkeley.edu, 2003; Tanaka, 1990) h Tanaka & Park 90 No. 6 550x550 1650 968 32.0 511 1.25 325 1.7 (Alfarah, 2017; Maranhão et al., 2021; nisee. berkeley.edu, 2003; Tanaka, 1990) i Park and Paulay 90 1784 646 432 305 2.2 No. 9 400x600 26.9 1.88 (nisee.berkelev.edu. 2003; Park and Paulay, 1990)

Table 1. Geometric and material characteristics of the specimens used in the simulation

Where: B — element width, H — element depth, L — element length, N — axial load,  $\sigma_c$  — concrete strength,  $\sigma_s$  — yield strength of longitudinal reinforcement,  $\rho_s$  — longitudinal reinforcement ratio,  $\sigma_t$  — yield strength of transverse reinforcement, ρ, — transverse reinforcement ratio.

by 33 %. This overestimation could be explained by an underestimation of the yield displacement obtained from the program.

#### Maximum strength

The maximum strength ratio between program simulations and experimental tests is calculated at the maximum imposed displacement of each hysteresis curve.

The maximum strength ratio clearly demonstrates the effectiveness of the program in predicting the maximum strength of reinforced concrete elements (Fig. 13) with satisfactory accuracy (0.07-11.80 %).

#### Stiffness degradation

The evolution of stiffness degradation as a function of relative imposed displacement is shown in Fig. 14. The relative stiffness is the ratio of the stiffness at the peak of the first cycle of each imposed displacement and the initial stiffness.

Based on the results obtained, it can be noticed that the program provides a good estimate of the stiffness degradation for the various specimens. It can be said that the program accuracy is excellent in representing the stiffness degradation of reinforced concrete elements.

#### Cumulative energy dissipation

The evolution of the dissipated energy (Fig. 15) and the cumulative energy dissipation (Fig. 16) for each specimen was determined and compared with the results obtained by the computer program. Based on the results obtained, it can be concluded that:

· In general, the results for all tested elements show a very good correlation between the experimental dissipated energy and the program's dissipated energy. Nevertheless, an underestimation of the cumulative energy dissipation for relative imposed displacement of the order of 0 to 1 %, associated with a quasi-linear numerical response, and a slight overestimation for relative imposed displacement greater than 1 % was observed. This slight overestimation of the cumulative energy dissipation could be justified by the inadequacy of the numerical models in representing the pinching effect in experimentally observed hysteresis loops.

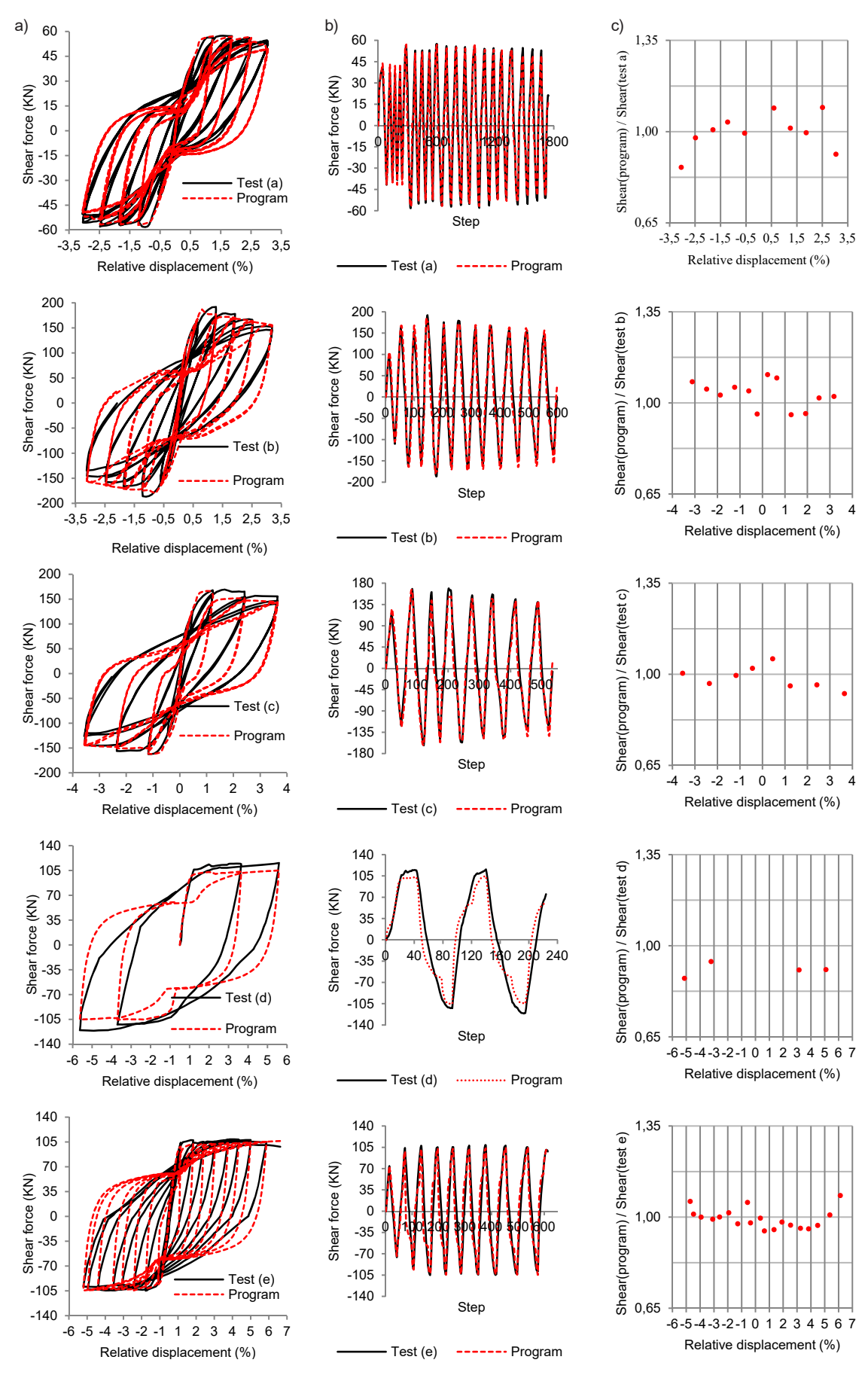


Fig. 10. (a) hysteresis shear force – relative displacement, (b) shear force history at each analysis step, (c) ratio of the simulated shear force to the test shear force (beginning)

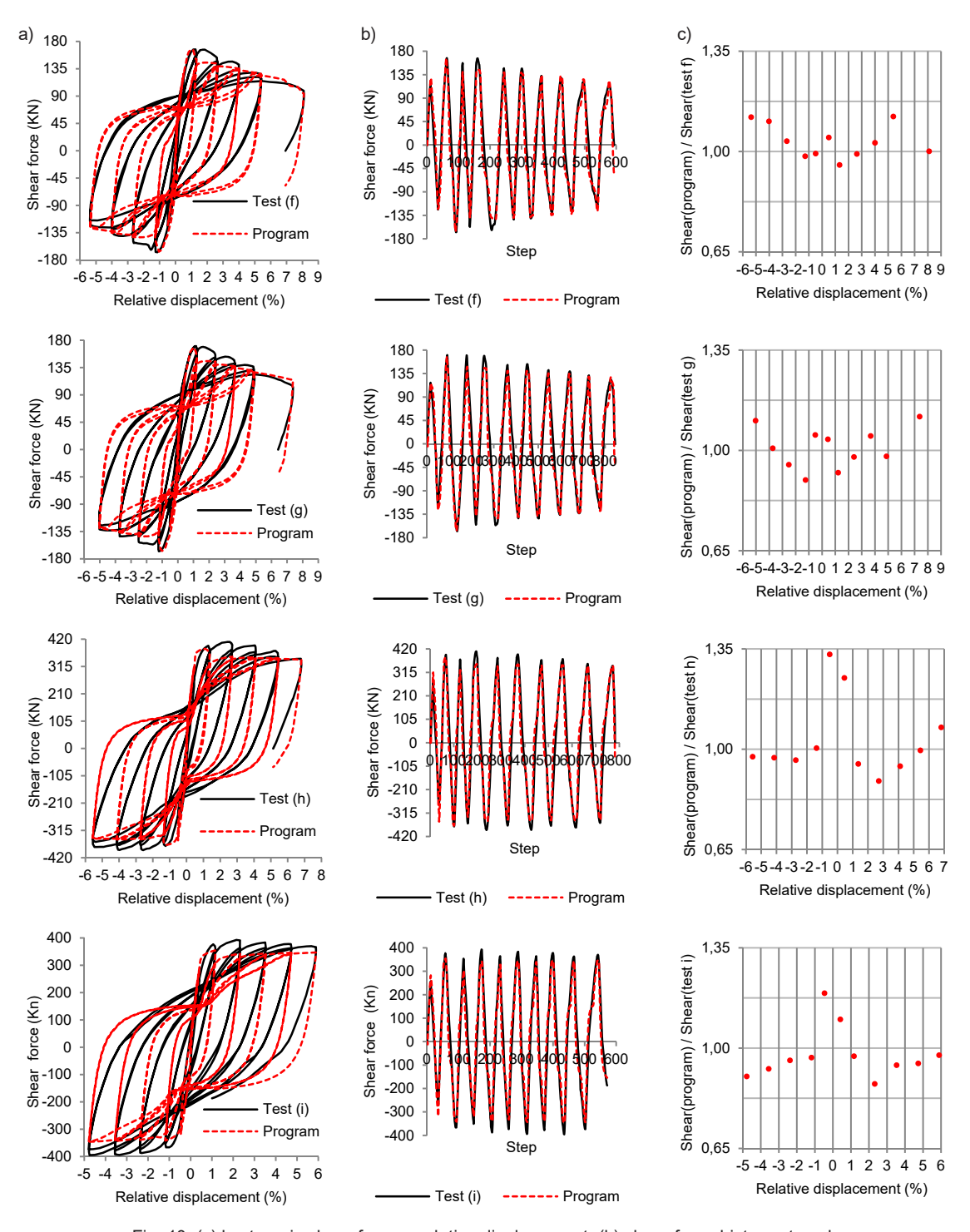


Fig. 10. (a) hysteresis shear force – relative displacement, (b) shear force history at each analysis step, (c) ratio of the simulated shear force to the test shear force (ending)

The convergence analysis in this paper assesses the predictive accuracy of the developed interactive computer program for the nonlinear behavior of reinforced concrete elements under monotonic and cyclic lateral loading. The program utilizes a fiber element approach with various material models and hysteresis laws. Hysteresis loops are examined, revealing a strong correlation between numerically simulated and experimental shear forces. Force-displacement envelope curves demonstrate the

program's ability to accurately predict the overall response of reinforced concrete elements, affirming its efficacy in estimating maximum resistance. The initial stiffness estimation generally aligns with the experimental values, but a notable discrepancy in one test suggests potential areas for improvement. The maximum strength ratio analysis confirms the program's effectiveness in predicting maximum strength. The assessment of stiffness degradation indicates that the program provides a good

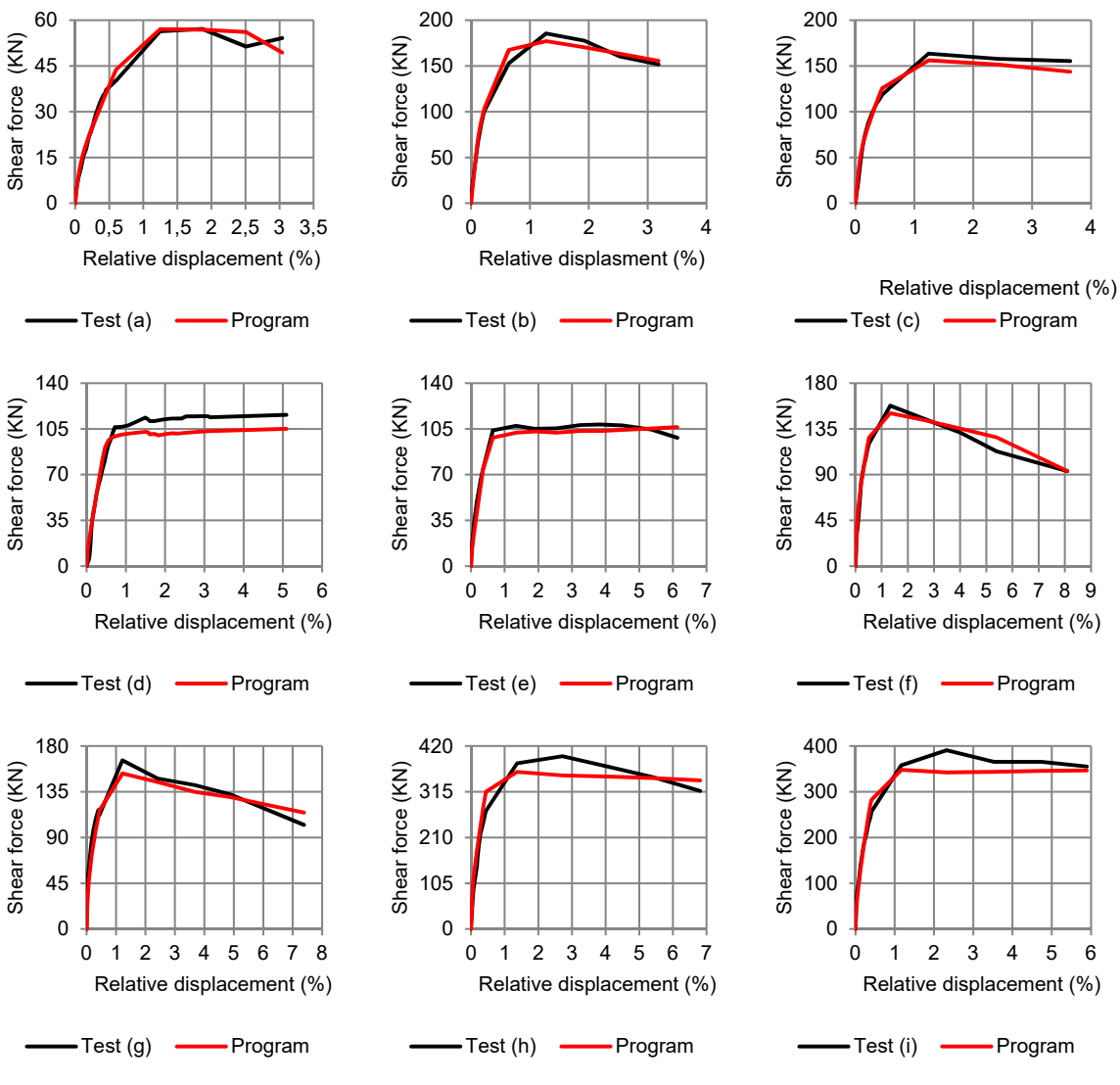


Fig. 11. Envelope capacity curves

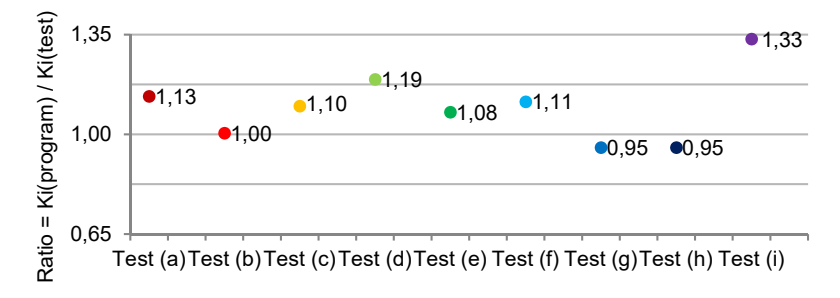


Fig. 12. Initial stiffness ratio

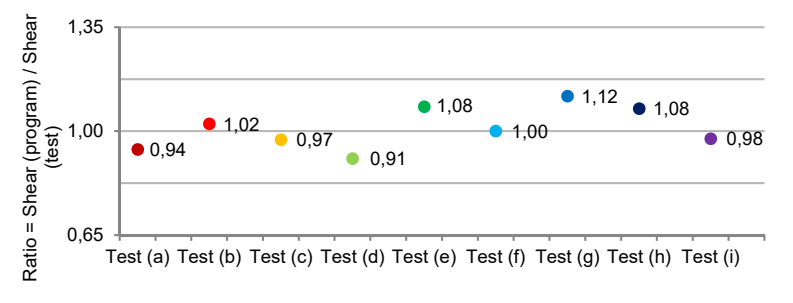


Fig. 13. Maximum strength ratio

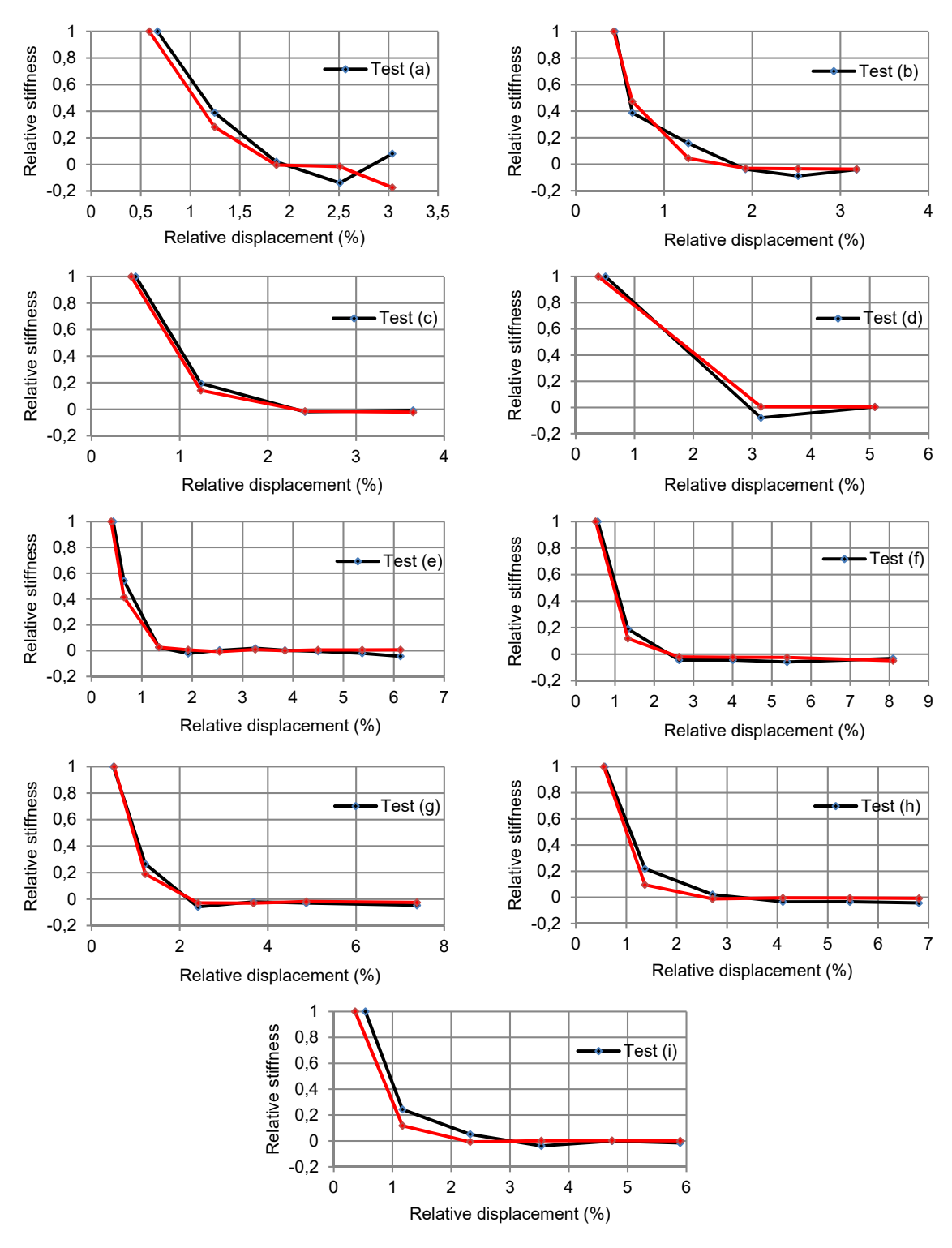


Fig. 14. Stiffness degradation as a function of relative displacement demand

estimation of degradation across various specimens. Cumulative energy dissipation analysis reveals a strong correlation between experimental and program-predicted dissipated energy, with minor differences attributed to numerical model limitations. Overall, the convergence analysis validates the program's reliability and accuracy in predicting reinforced concrete element behavior under both

monotonic and cyclic loading, substantiating its suitability for engineering applications.

#### Conclusion

In conclusion, this study has successfully developed and validated a computer interactive program designed to predict the nonlinear behavior of reinforced concrete columns under both monotonic and cyclic loading conditions, utilizing established

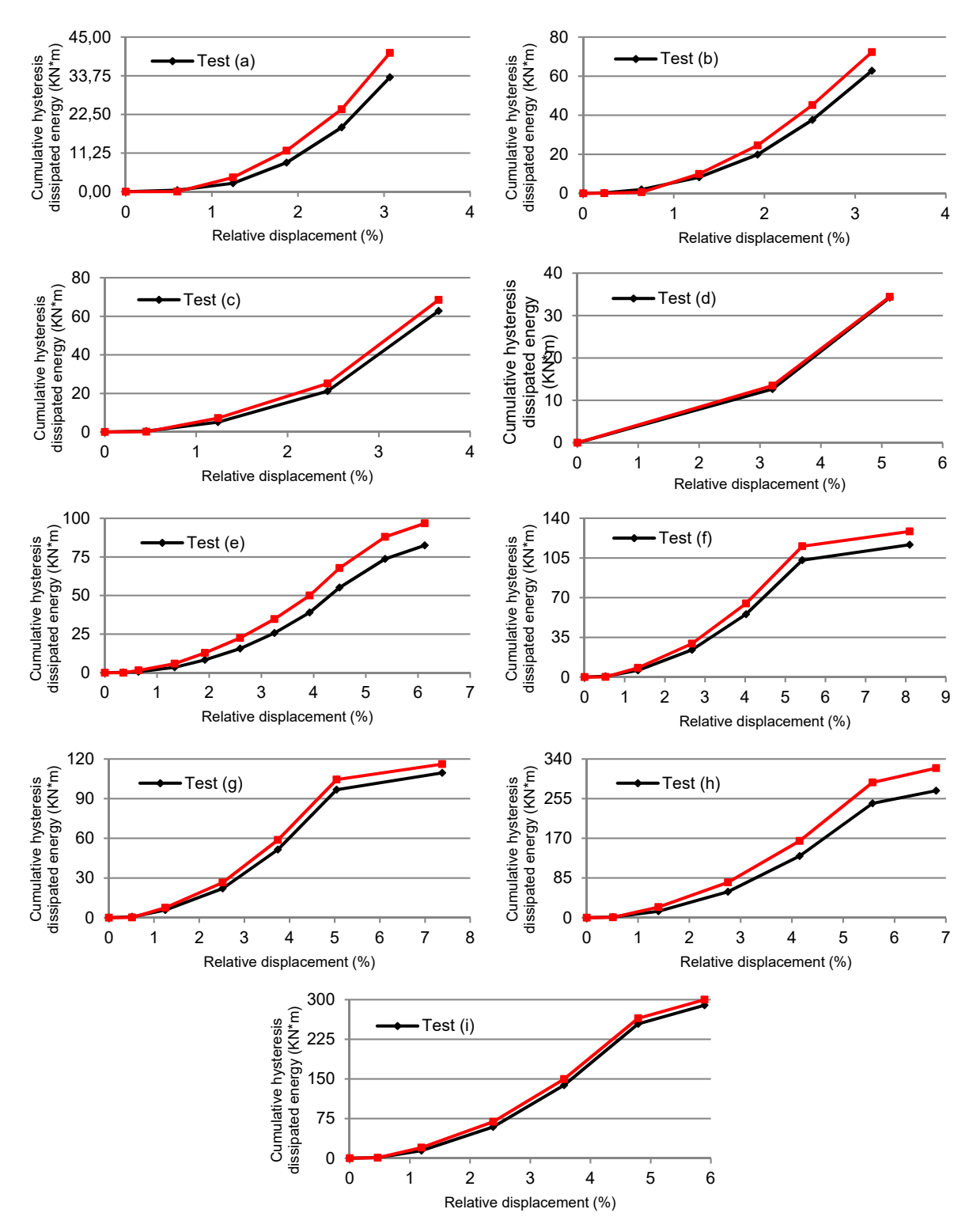


Fig. 15. Cumulative energy dissipation in relation to relative displacement demand

models for concrete stress-strain relationships and reinforcing steel behavior.

The results of the convergence analysis show a strong correlation with the experimental data, further enhancing the reliability and accuracy of the program. This showcases the program's efficiency in simulating the behavior of reinforced concrete elements, particularly in terms of

maximum resistance and initial stiffness. Despite limitations in representing the pinching effect during unloading-reloading phases and some differences in energy dissipation, the program proves to be very efficient and sufficiently accurate.

Furthermore, the program's capability to perform realistic nonlinear analysis of reinforced concrete

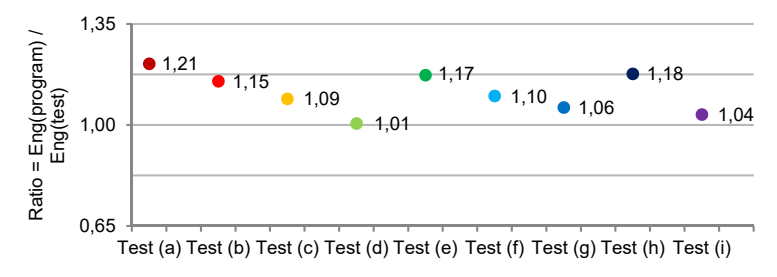


Fig. 16. Ratio between the simulated cumulative energy dissipation and the actual cumulative energy dissipation in the tests

element behavior can prove to be very useful for various parametric studies. It is a valuable tool for examining the effectiveness of certain material models against experimental tests and serves as a good learning aid in graduate university classes and continuing education. The program's user-friendly interface and graphical representations make it a valuable tool for concrete research within

earthquake engineering and a practical asset for design offices.

In summary, the developed program, with its robust numerical tools and innovative applications, stands as a promising tool for researchers, engineers, and educators involved in the analysis and design of concrete structures, particularly in the context of seismic considerations.

#### References

Abd El Fattah, A. M. (2012). Behavior of concrete columns under various confinement effects. PhD Thesis. Kansas State University.

Alfarah, B. (2017). Advanced computationally efficient modeling of RC structures nonlinear cyclic behavior. Doctoral Thesis. Universitat Politècnica de Catalunya.

Ang, B. G. (1981). *Ductility of reinforced concrete bridge piers under seismic loading*. [online] Available at: https://ir.canterbury.ac.nz/server/api/core/bitstreams/4f53f5d2-1374-4a1c-834e-c7f0678cccba/content [Date accessed: November 28, 2021].

Atalay, M. B. and Penzien, J. (1975). The seismic behavior of critical regions of reinforced concrete components as influenced by moment, shear and axial force. Berkeley: University of California, Earthquake Engineering Research Center, 235 p.

Bosco, M., Ferrara, E., Ghersi, A., Marino, E. M., and Rossi, P. P. (2016). Improvement of the model proposed by Menegotto and Pinto for steel. *Engineering Structures*, Vol. 124, pp. 442–456. DOI: 10.1016/j.engstruct.2016.06.037.

Carreira, D. J. and Chu, K.-H. (1985). Stress-strain relationship for plain concrete in compression. *ACI Journal Proceedings*, Vol. 82, Issue 6, pp. 797–804. DOI: 10.14359/10390.

Carreño, R., Lotfizadeh, K. H., Conte, J. P., and Restrepo, J. I. (2020). Material model parameters for the Giuffrè-Menegotto-Pinto uniaxial steel stress-strain model. *Journal of Structural Engineering*, Vol. 146, Issue 2, 04019205. DOI: 10.1061/(ASCE)ST.1943-541X.0002505.

Chadwell, C. B. and Imbsen, R. A. (2004). XTRACT: A tool for axial force - ultimate curvature interactions. In: Blandford, G. E. (ed.). *Structures 2004: Building on the Past, Securing the Future*. Reston: ASCE, pp. 1–9. DOI: 10.1061/40700(2004)17.

Cusson, D. and Paultre, P. (1994). High-strength concrete columns confined by rectangular ties. *Journal of Structural Engineering*, Vol. 120, Issue 3: pp. 783–804. DOI: 10.1061/(ASCE)0733-9445(1994)120:3(783).

Cusson, D. and Paultre, P. (1995). Stress-strain model for confined high-strength concrete. *Journal of Structural Engineering*, Vol. 121, Issue 3, pp. 468–477. DOI: 10.1061/(ASCE)0733-9445(1995)121:3(468).

Desayi, P. and Krishnan, S. (1964). Equation for the stress-strain curve of concrete. *ACI Journal Proceedings*, Vol. 61, Issue 3, pp. 345–350. DOI: 10.14359/7785.

Djebbar, N. (2006). Contribution à l'étude de la performance parasismique des éléments linéaires en béton. Doctoral Thesis. Université Mentouri.

Esmaeily, A. and Peterman, R. J. (2007). Performance analysis tool for reinforced concrete members. *Computers and Concrete*, Vol. 4, No. 5, pp. 331–346. DOI: 10.12989/cac.2007.4.5.331.

Esmaeily, A. and Shirmohammadi, F. (2014). *Performance and capacity assessment of reinforced concrete bridge piers considering the current load and resistance factor design provisions and plastic hinge length in Kansas*. Topeka: Kansas Department of Transportation, 180 p.

Esmaeily-Ghasemabadi, A. and Xiao, Y. (2002). Seismic behavior of bridge columns subjected to various loading patterns. Berkeley:Pacific Earthquake Engineering Research Center, 321 p.

Furtado, A., Rodrigues, H., and Arêde, A. (2015). Numerical modelling of RC columns subjected to biaxial horizontal loading and variable axial load. *American Journal of Civil Engineering and Architecture*, Vol. 3, Issue 1, pp. 28–38. DOI: 10.12691/ajcea-3-1-5.

Hognestad, E. (1951). Study of combined bending and axial load in reinforced concrete members. [online] Available at: https://core.ac.uk/download/pdf/4814295.pdf [Date accessed: July 17, 2022].

Kent, D. C. (1969). *Inelastic behaviour of reinforced concrete members with cyclic loading*. PhD Thesis. University of Canterbury.

Kent, D. C. and Park, R. (1971). Flexural members with confined concrete. *Journal of the Structural Division*, Vol. 97, Issue 7, pp. 1969–1990. DOI: 10.1061/JSDEAG.0002957.

Lee, J. H. (2017). Development of sectional analysis platform for reinforced and prestressed concrete elements. MSc Thesis. College of Engineering, Seoul National University.

Li, K.-N. (2004). CANNY: 3-Dimentional Nonlinear Static and Dynamic Structural Analysis, Computer Program, User's Manual. CANNY Structural Analysis, Vancouver, BC, Canada.

Mander, J. B. (1983). Seismic design of bridge piers. PhD Thesis. University of Canterbury.

Mander, J. B., Priestley, M. J. N., and Park, R. (1988). Theoretical stress-strain model for confined concrete. *Journal of Structural Engineering*, Vol. 114, Issue 8, pp. 1804–1826. DOI: 10.1061/(ASCE)0733-9445(1988)114:8(1804).

Maranhão, H., Varum, H., and Pimentel, M. (2021). Nonlinear finite element model calibration of a reinforced concrete column with distributed plasticity. *U. Porto Journal of Engineering*, Vol. 7, No. 3, pp. 114–125. DOI: 10.24840/2183-6493\_007.003\_0010.

Menegotto, M. and Pinto, P. E. (1973). Method of analysis for cyclically loaded R.C. plane frames including changes in geometry and non-elastic behaviour of elements under combined normal force and bending. In: *Proceedings of IABSE Symposium on Resistance and Ultimate Deformability of Structures Acted on by Well Defined Repeated Loads*, Vol. 11, pp. 15–22. DOI: 10.5169/seals-13741.

Mortezaei, A. and Ronagh, H. R. (2013). Plastic hinge length of reinforced concrete columns subjected to both far-fault and near-fault ground motions having forward directivity. *The Structural Design of Tall and Special Buildings*, Vol. 22, Issue 12, pp. 903–926. DOI: 10.1002/tal.729.

Nawy, E. G. (1996). Reinforced concrete: a fundamental approach. New York: Prentice Hall, 832 p.

nisee.berkeley.edu (2003). PEER Structural Performance Database. [online] Available at: https://nisee.berkeley.edu/spd/index.html [Date accessed: December 31, 2020].

Ohno, T. and Nishioka, T. (1984). An experimental study on energy absorption capacity of columns in reinforced concrete structures. *Doboku Gakkai Ronbunshu*, Vol. 1984, No. 350, pp. 23–33. DOI: 10.2208/jscej.1984.350 23.

opensees.berkeley.edu (2023).*OpenSees, Steel02 Class Reference*. [online] Available at: https://opensees.berkeley.edu/OpenSees/api/doxygen2/html/classSteel02.html#89419d80cb36795e222642834cc88c96 [Date accessed: December 31, 2020].

Park, R. and Paulay, T. (1990). Use of interlocking spirals for transverse reinforcement in bridge columns. *Strength and Ductility of Concrete Substructures of Bridges, RRU (Road Research Unit) Bulletin 84*, Vol. 1, pp. 77–92.

Park, R. and Paulay, T. (1991). Reinforced concrete structures. New York: John Wiley & Sons, 800 p.

Park, R., Priestley, M. J. N., and Gill, W. D. (1982). Ductility of square-confined concrete columns. *Journal of the Structural Division*, Vol. 108, Issue 4, pp. 929–950. DOI: 10.1061/JSDEAG.0005933.

Popovics, S. (1973). A numerical approach to the complete stress-strain curve of concrete. *Cement and Concrete Research*, Vol. 3, Issue 5, pp. 583–599. DOI: 10.1016/0008-8846(73)90096-3.

Priestley, M. J. N. and Park, R. (1987). Strength and ductility of concrete bridge columns under seismic loading. *ACI Structural Journal*, Vol. 84, Issue 1, pp. 61–76.

Rodrigues, H., Arêde, A., Silva, J. P., Rocha, P., and Furtado, A. (2014). Behaviour of RC columns under variable load and bidirectional horizontal loading. In: *Proceedings of the Second European Conference on Earthquake Engineering and Seismology*, August 25–29, 2014, Istanbul, Turkey. DOI: 10.13140/2.1.3788.9921.

Rodrigues, H., Arêde, A., Varum, H., and Costa, A. G. (2013a). Experimental evaluation of rectangular reinforced concrete column behaviour under biaxial cyclic loading. *Earthquake Engineering & Structural Dynamics*, Vol. 42, Issue 2, pp. 239–259 DOI: 10.1002/eqe.2205.

Rodrigues, H., Varum, H., Arêde, A., and Costa, A. G. (2013b). Behaviour of reinforced concrete column under biaxial cyclic loading—state of the art. *International Journal of Advanced Structural Engineering*, Vol. 5, Issue 1, 4. DOI: 10.1186/2008-6695-5-4.

Sato, T., Shimada, I., and Kobayashi, H. (2002). A simple numerical method for biaxial bending moment-curvature relations of reinforced concrete column sections. *Memoirs of the Faculty of Engineering, Osaka City University*, Vol. 43, pp. 59–67.

Scott, B. D. (1980). Stress-strain relationships for confined concrete: rectangular sections. [online] Available at: https://ir.canterbury.ac.nz/items/ce2efa4e-4c5c-4ad2-81b2-148a54a0af49 [Date accessed July 25, 2021].

Shirmohammadi, F. (2015). *Effect of load pattern and history on performance of reinforced concrete columns*. PhD Thesis. Kansas State University.

Shirmohammadi, F. and Esmaeily, A. (2015). Performance of reinforced concrete columns under bi-axial lateral force/displacement and axial load. *Engineering Structures*, Vol. 99, pp. 63–77. DOI: 10.1016/j.engstruct.2015.04.042.

Tanaka, H. (1990). Effect of lateral confining reinforcement on the ductile behaviour of reinforced concrete columns. PhD Thesis. University of Canterbury.

Tsai, W. T. (1988). Uniaxial compressional stress-strain relation of concrete. *Journal of Structural Engineering*, Vol. 114, Issue 9, pp. 2133–2136. DOI: 10.1061/(ASCE)0733-9445(1988)114:9(2133).

Zhao, X., Wu, Y.-F., Leung, A. Yt., and Lam, H. F. (2011). Plastic hinge length in reinforced concrete flexural members. *ProcediaEngineering*, Vol. 14, pp. 1266–1274. DOI: 10.1016/j.proeng.2011.07.159.

## ПРОГНОЗИРОВАНИЕ ЭКСПЛУАТАЦИОННЫХ ХАРАКТЕРИСТИК ЖЕЛЕЗОБЕТОННЫХ ЭЛЕМЕНТОВ ПРИ МОНОТОННОМ И ЦИКЛИЧЕСКОМ БОКОВОМ НАГРУЖЕНИИ

Бубакер Феттар\*, Смаил Букелуа

Кафедра гражданского строительства, факультет технологических наук, Университет братьев Ментури (Константина 1), Константина, Алжир

Лаборатория механики грунтов и сооружений (LMSS), Университет братьев Ментури (Константина 1), Константина, Алжир

\*E-mail: boubakeur.fettar@doc.umc.edu.dz

#### Аннотация

Введение: Основной целью данной работы является изучение нелинейного поведения железобетонных элементов при монотонном и циклическом нагружении. За последние 30 лет было проведено несколько экспериментальных исследований с целью получения более полного представления о нелинейном поведении железобетонных элементов и определения различных параметров, влияющих на это поведение. Цель исследования: Данное исследование изучает это поведение и направлено на разработку интерактивной компьютерной программы. предназначенной для использования в среде Windows. Методы: В аналитическом подходе с применением волокнистого элемента используются несколько моделей материалов (железобетон с поперечным армированием / железобетон без поперечного армирования и арматурная сталь), а также законы гистерезиса Для каждого образца в программу введены геометрические характеристики, модели материалов, варианты расположения пластических шарниров, осевые нагрузки и история соответствующих горизонтальных перемещений. Численные прогнозы проверены и подтверждены результатами экспериментальных испытаний, проведенных различными авторами. Результаты: Результаты моделирования оказались очень близки к экспериментальным, особенно для петель гистерезиса, огибающих кривых силы-перемещения, начальной жесткости, снижения жесткости, максимальной прочности и кумулятивной диссипации энергии. Программа способна прогнозировать нелинейное поведение железобетонных элементов. Разработанная программа представляет собой надежный инструмент для прогнозирования нелинейного поведения железобетонных элементов при циклическом нагружении. Точность подтверждена анализом сходимости с экспериментальными данными.

**Ключевые слова:** компьютерная программа, волокнистый элемент, гистерезис, модели материалов, моменткривизна.

### ADHESIVE INTERACTION IN HYBRID POLYMER COMPOSITES. ENERGY CHARACTERISTICS OF PHASES AT THE AIR INTERFACE

Almaz Valiev1\*, Irina Starovoitova2, Alfred Suleymanov1

- <sup>1</sup> Kazan University of Architecture and Civil Engineering, Kazan, Russia
- <sup>2</sup>LLC "Research and Production Company "Rekon", Kazan, Russia

#### **Abstract**

Introduction: The study of the adhesive strength formation mechanisms in polymer composites involves the deliberate selection of components to facilitate their joint action in transferring stresses from the fibers to the binder through the phase interface. The strength of the adhesive interaction between components can be expressed through their energy characteristics, provided technological and other factors are ensured. Purpose of the study: The study aims to investigate the energy characteristics of hybrid polymer composite phases at the air interface. Methods: The optical method was used to capture micrographs of wetting fibers of different nature by liquids, based on which contact angles were determined. Tensile tests of fibers were conducted, and thermal analysis of fibers was performed using a synchronous thermal analyzer. The surface tension of epoxy resin and the epoxy resin / hardener system was determined using a tensiometer. Results: The method for determining surface energies of solids was upgraded. The upgraded method makes it possible to determine the free surface energy of fibers of different nature and the surface tension of the binder. The effect of oiling compositions (finishing agents) was quantitatively evaluated.

Keywords: composite, hybrid, adhesion, wetting, adhesion action, free surface energy.

#### Introduction

Polymer composite is a system with a complex hierarchical structure, the components of which differ significantly in their elastic-mechanical and thermophysical characteristics (Kayumov and Shakirzyanov, 2021; Mercier et al., 2021; Zheng and Guo, 2021).

Hybrid composites are composites that contain more than one type of reinforcing component in the matrix. An additional reinforcing component is included to improve the elastic-mechanical characteristics of the material (in particular, to reduce strains) and makes it possible to obtain structures with optimal balanced properties (Gunyaev, 1977; Skudra and Bulavs, 1978). In construction, these materials are used in pedestrian bridge structures, etc. As a rule, such products are manufactured using the vacuum infusion technology in accordance with GOST 27751–2014.

The fiber/matrix interfacial region contributes significantly to the elastic-mechanical properties of the finished composite. At maximum effect, it allows for using the filler strength to a large extent (Hughes, 1991; Kim and Mai, 1998). During binder curing, due to chemical reactions between the resin and the hardener as well as spatial reorientation of molecules, parameters of the free surface energy of the binder change with time and reach maximum values only after complete curing.

The interaction between two condensed phases results in a physical or chemical bond, which can

be evaluated by its strength. As known, there are several adhesion theories: mechanical, electrical (electronic), adsorption (molecular), relaxation, and weak layer theories. Each of the theories was developed to explain the basic mechanisms of adhesion contact formation. Regulation of interfacial interaction properties makes it possible to reduce residual stresses in the finished product and obtain the required physical and mechanical properties.

In case of fiber composites, the fracture strength is determined by the adhesive strength of the fiber/ binder bond  $(\tau_0)$ , and wetting is the most important process in the occurrence of bonding between the reinforcing filler and binder at the phase interface (Kramarev et al., 2017; Shakhmurzova et al., 2022). The adhesive strength of the fiber/ binder bond can be determined by both micro- and macromechanical tests (pull-out method, pushout method, fragmentation method, methods of finished composite product failure under shear, bending, etc.) (Gulyaev et al., 2019; Zhang, 2012). Despite the variety of methods, adhesive interaction is considered a statistical value, which is mainly determined by the random distribution of defects at the phase interface, hence it can be observed that the results of adhesive strength determination are sensitive to the specimen size.

Adhesive interaction at the phase interface in the matrix-filler bond depends on a wide range of factors. The strength of adhesive interaction between components can be expressed through the energy

<sup>\*</sup>Corresponding author's e-mail: tatcomposite@mail.ru

characteristics of the surface: thermodynamic work of adhesion  $(W_a)$ , free surface energy and its dispersion and acid/base components  $(\gamma^d, \gamma^{ab})$ (Karzov et al., 2010). Various wetting methods (sessile drop method (Danilov et al., 2019), sitting drop method, method of determining the contact angle of an elementary fiber using a cuvette with liquid, mounted on a horizontal microscope, Washburn method, Adam-Schütte method, etc.) using test liquids with known free surface energy parameters (Starostina and Stoyanov, 2010) are prioritized in this respect since the experimental determination of free surface energy parameters is quite effort-consuming in practice.

The surface tension of liquids is also measured by various methods (Wilhelmy plate method (Wilhelmy, 1863), Du Nouy rings (Lecomte du Nouy, 1925), etc.). These measurements determine surface tension by measuring the force acting on the object immersed in a liquid (plates, rings, etc.) and the length of the wetted surface.

Estimating the parameters of the free surface energy of phases in a hybrid composite with a combination of fibers of different nature is a key task in predicting elastic-mechanical properties and optimizing the selection of components.

The energy of wetting solid surfaces to determine the chemical nature when determining the contact angle is also related to numerous factors (wetting hysteresis, surface roughness, test temperature and

The thermodynamic work of adhesion and parameters of free surface energy between liquid and solid phases can be determined by experimental measurements of the contact angle of wetting of a solid surface by liquids with known free surface energy parameters using various equations (Young-Dupre (Dupre, 1869), Owens-Wendt (Owens and Wendt, 1969), Vann Oss-Chaudhury-Good (Vann Oss et al., 1989), etc.). Among them the Vann Oss-Chaudhury-Good theory has the priority. According to this theory, three test fluids with known free surface energy parameters should be used to determine the free surface energy of a solid surface by solving a system of equations with three unknowns.

According to the Vann Oss-Chaudhury-Good theory, the thermodynamic work of adhesion and free surface energy parameters are determined by equation (1) (Vann Oss et al., 1989):

$$W_{a} = \gamma_{l} \left( 1 + \cos \theta \right) =$$

$$= 2 \left( \gamma_{l}^{d} \gamma_{s}^{d} \right)^{1/2} + 2 \left( \gamma_{l}^{+} \gamma_{s}^{-} \right)^{1/2} + 2 \left( \gamma_{s}^{+} \gamma_{l}^{-} \right)^{1/2}, \quad (1)$$
where:

 $\gamma^+$  — acid parameter;  $\gamma^-$  — base parameter;  $\gamma^d$  — dispersion parameter;

l — liquid phase;

s — solid phase;

 $\theta$  — contact angle.

For a bipolar substance, the acid/base component  $(\gamma^{ab})$  is determined by equation (2):

$$\gamma^{ab} = 2\sqrt{\gamma^+} \sqrt{\gamma^-}.$$
 (2)

It should be noted that test fluids also include monopolar fluids. For example, neutral hydrocarbons (n-hexane) have zero acid/base components of free surface energy, while the full value is 18.43 mJ/m<sup>2</sup>  $(\gamma_I = \gamma_I^d)$ . This type of test fluid is used in selective wetting.

The parameters of the free surface energy of solid surfaces are usually determined by linear approximation, where the resulting solution of the system depends on the choice of test fluids and is unstable (Starostina and Stoyanov, 2010).

The problem of obtaining a general solution for the parameters of the free surface energy of solid surfaces was solved by Starostina et al. (2013) by transforming equation (1) to the equation of plane z = Ax + By + C:

$$\frac{\gamma_{l}\left(1+\cos\theta\right)}{2\sqrt{\gamma_{l}^{-}}} = \frac{\sqrt{\gamma_{l}^{d}}}{\sqrt{\gamma_{l}^{-}}}\sqrt{\gamma_{s}^{d}} + \frac{\sqrt{\gamma_{l}^{+}}}{\sqrt{\gamma_{l}^{-}}}\sqrt{\gamma_{s}^{-}} + \sqrt{\gamma_{s}^{+}}.$$
 (3)

A more accurate way to find the unique values of the parameters of the free surface of solid surfaces is by the spatial three-dimensional method rather than by linear approximation, as was previously done by researchers (Starostina et al., 2011; McCafferty, 2002). Based on the spatial method, the free surface energy parameters of a large number of solid surfaces (polymers, polymer composites, glass, metals) were estimated. The spatial threedimensional method has not been used to determine the free surface energy parameters of elementary fibers of different nature.

This study aims to investigate the energy characteristics of hybrid polymer composite phases at the air interface. The objectives of the study are as follows: (1) determining the variation in the free surface energy parameters of elementary fibers of different nature to investigate the contribution of oiling compositions and finishing agents, using the spatial method and the Vann Oss-Chaudhury-Good theory, (2) determining the surface tension of low-viscosity epoxy resin and binder (Du Nouy rings method), (3) estimating the contact angle of elementary fibers with binder for vacuum infusion.

#### Subject, tasks, and methods

To determine the variation in the free surface energy parameters of hybrid polymer composite components, estimated by the contact angle, and analyze their wetting, the following materials were

- 1. Fiber reinforcing fillers:
- a) Unidirectional carbon fabric FibArm Tape 230 manufactured by JSC Umatex, Rosatom State

Corporation (Technical Specifications 1916-018-61664530–2013).

- b) Unidirectional glass fabric (tape) Ortex 400 O 250 manufactured by BauTex (Technical Specifications 13.20.46.000-006-52788109–2019).
- c) Basalt woven fabric BNPP-B-10-610-KV-41 (Technical Specifications 5952-007-13307094-12) manufactured by LLC Kamenny Vek.
  - 2. Modified epoxy resin L for vacuum infusion.
- 3. Hardener GL2 manufactured by R&G Faserverbundwerkstoffe GmbH, Germany (ratio resin L / hardener GL2 100:30, viscosity at  $25~^{\circ}\text{C}$   $248 \pm 100~\text{mPa}\cdot\text{s}$ ).

Fiber calcination with the aim to remove the initial oiling composition (finishing agent) was carried out in a muffle furnace preheated to a temperature of +420 °C for carbon fiber and +560 °C for glass fiber based on the evaluation of thermal characteristics of fabrics with the use of an STA 6000 synchronous thermal analyzer. Heating rate: 10±1 °C/min.

The fibers with initial oiling compositions (finishing agents) and after annealing were tensile tested using cardboard overlays and cyanoacrylate adhesive to prevent the specimens from slipping out. In case of glass fiber, the linear density according to the technical data is 1200 tex, in case of carbon fiber — 800 tex, the length of the working area — 100 mm. The calculations used only data on testing the specimens in which failure occurred between the clamps in the working area.

With the use of the optical method with horizontal positioning of an MPSU-1 simplified stereoscopic microscope (with 4.8x optical head magnification) and attachment of an AmScope SLR/DSLR adapter (with 2 magnification) compatible with Nikon D3100 camera (14.2 megapixels) (total magnification — 9.6), micrographs of wetting glass, carbon and basalt elementary fibers were obtained for different test fluids with known free surface energy parameters:

- a) distilled water according to GOST R 58144– 2018;
  - b) aniline according to GOST 5819-78;
  - c) ethylene glycol according to GOST 10164-75.

Table 1 shows the free surface energy parameters of the test fluids,  $mJ/m^2$ , at T = 20 °C.

The contact angle was determined based on video and micrographs of the meniscus during the elementary fiber movement, with the use of the AutoCad graphic environment, by drawing a

Table 1. Surface energy and its components for test fluids

| Test fluid      | $\gamma_l$ | $\gamma_l^d$ | $\gamma_l^+$ | $\gamma_l^-$ | $\gamma_l^{ab}$ |
|-----------------|------------|--------------|--------------|--------------|-----------------|
| Distilled water | 72         | 22           | 28.34        | 22.23        | 50              |
| Aniline         | 43.2       | 41.2         | 0.18         | 5.71         | 2               |
| Ethylene glycol | 48.3       | 29.3         | 12.08        | 7.47         | 19              |

tangent line. The air temperature during the test was +(20±2) °C, air humidity was ~55 %. Fig. 1 shows a scheme for determining the contact angle.

The free surface energy parameters of the epoxy binder for vacuum infusion directly depend on the epoxy and hydroxyl groups (in general, their amount is determined according to GOST 17555-72) of the resin and on the type and characteristics of the hardener. According to the technical data, resin L is an epoxy resin based on bisphenol (A+F), diluted with a bifunctional compound, and is characterized by low viscosity (at 25 °C — 710 ± 70 mPa·s), lack of solvents, fillers, nonylphenol and benzil alcohol in the composition; the epoxy value is 0.56 (100/eq), and the epoxy equivalent is 179 (g/eq). Due to the high reactivity of epoxy groups and the presence of hydroxyl groups, different methods of epoxy resin curing can be selected. Hardener GL2 is a composition based on a mixture of aliphatic and cycloaliphatic amines. The curing of resin L with hardener GL2 is almost shrinkage-free.

The surface tension of low-viscosity epoxy resin L and the resin L + hardener GL2 system (component ratio 100:30) was determined based on the Du Nouy rings method on a TD 3 Lauda tensiometer.

#### Results and discussion

Inorganic (glass and basalt) and carbon fibers undergo oiling or finishing stages (with oiling compositions or finishing agents where aqueous dispersions of organic resins are the film-forming component). This process step ensures the manufacturability of fiber processing, in particular, protecting fibers against mechanical damage as well as improving adhesion between the fibers (reinforcing filler) and the binder (matrix) when obtaining polymer composite materials. To investigate the contribution of oiling compositions and finishing agents, it is necessary to study the issue of their removal as well.

In research literature, the following is distinguished regarding the removal of the oiling compositions (finishing agents) of fibers: washing with organic solvents or pyrolysis in a muffle furnace at high temperatures. It should be noted that even with repeated washing of fibers in organic solvent solutions, a part of the oiling composition (finishing agent) remains in the preforms, while pyrolysis ensures almost complete removal (this method is more environmentally friendly compared to washing with organic solvent solutions) (Petrova and Beider, 2016).

A thermal decomposition method was selected for the removal of the oiling composition (finishing agent). Temperature ranges of thermal decomposition of the initial oiling compositions (finishing agent) of fabrics were determined by thermogravimetric analysis. Figs. 2–4 show the results in the form of TG-DTG, DTA thermal analytical curves for glass, carbon, and basalt fabrics, respectively, weight variation in the range of 30–850 °C (% wt.) is presented in Table 2.

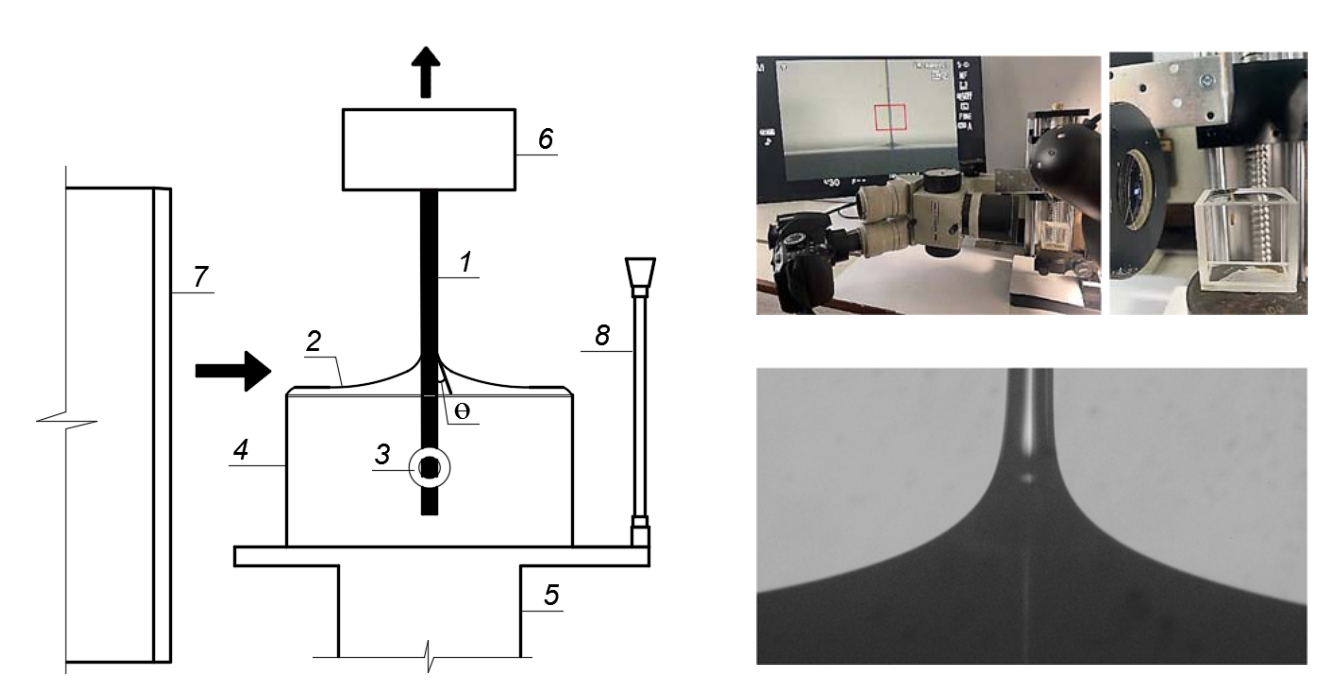


Fig. 1. Scheme for determining the contact angle (θ): (1 — elementary fiber, 2 — test fluid, 3 — weight, 4 — cuvette, 5 — mechanical platform, 6 — holder of elementary fiber, 7 — horizontal microscope, 8 — moving mirror (with a light source))

Based on the results of thermogravimetric analysis (TG curve), it can be inferred that the weight loss in case of glass fabric occurs at 200–560°C (-0.64 % wt.) in case of carbon fabric — at 130–420°C (-1.47 % wt.), in case of basalt fabric — at 170–600°C (-1.11 % wt.), and it is obvious that this is largely due to the removal of the oiling composition (finishing agent). It can be assumed that further weight loss is due to thermal degradation of the material. GOST 6943.1–2015 regulates the conditions of oiling composition (finishing agent) removal from the surfaces of glass and carbon fibers, and it is recommended to perform calcination of

fibers in a muffle furnace preheated to a temperature of (625±20)°C during 20–30 minutes for glass fibers, and to a temperature of (450±5)°C during 15–25 minutes for carbon fibers. The TG results and the GOST 6943.1–2015 recommendations are close in values, therefore, all subsequent studies were conducted on materials pre-annealed at 560°C for 30 minutes in case of glass fabric, at 420°C for 25 minutes in case of carbon fabric, and at 600°C for 30 minutes in case of basalt fabric.

Fig. 5 shows the histograms of residual tensile strength for glass and carbon fibers after annealing at different temperatures.

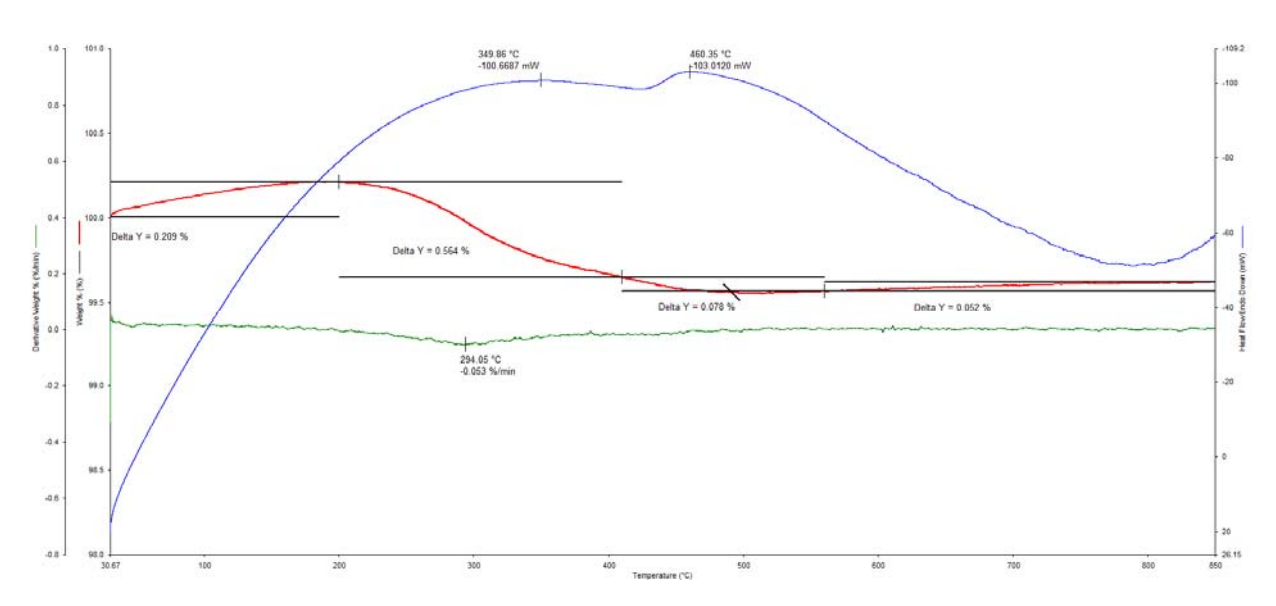


Fig. 2. TG-DTG, DTA thermal analytical curves for glass fabric (red — TG curve, green — DTG curve, blue — DTA curve)

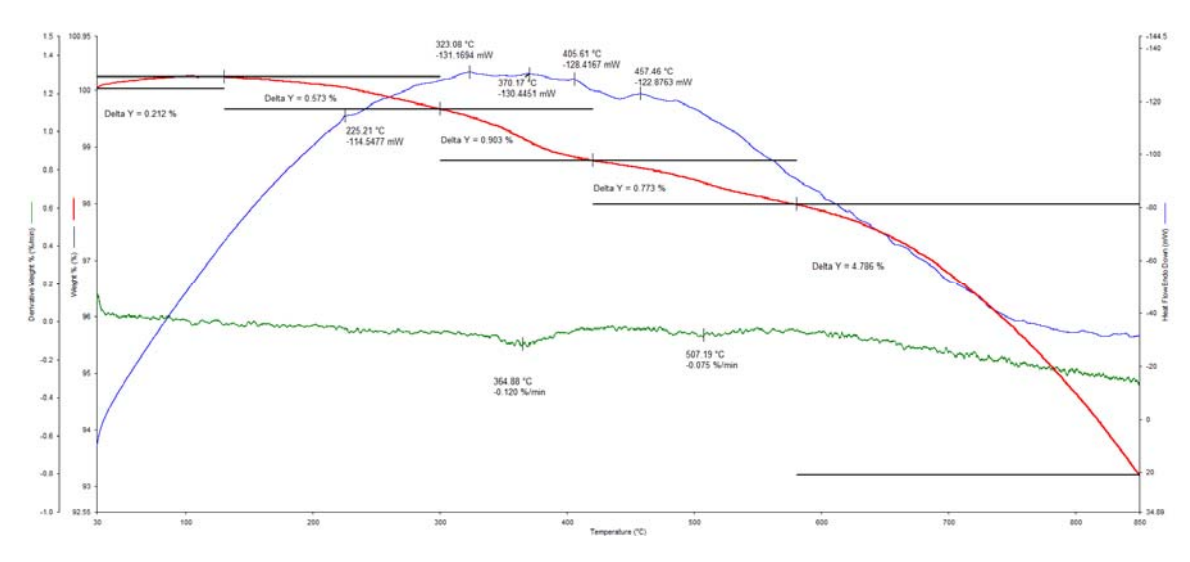


Fig. 3. TG-DTG, DTA thermal analytical curves for carbon fabric (red — TG curve, green — DTG curve, blue — DTA curve)

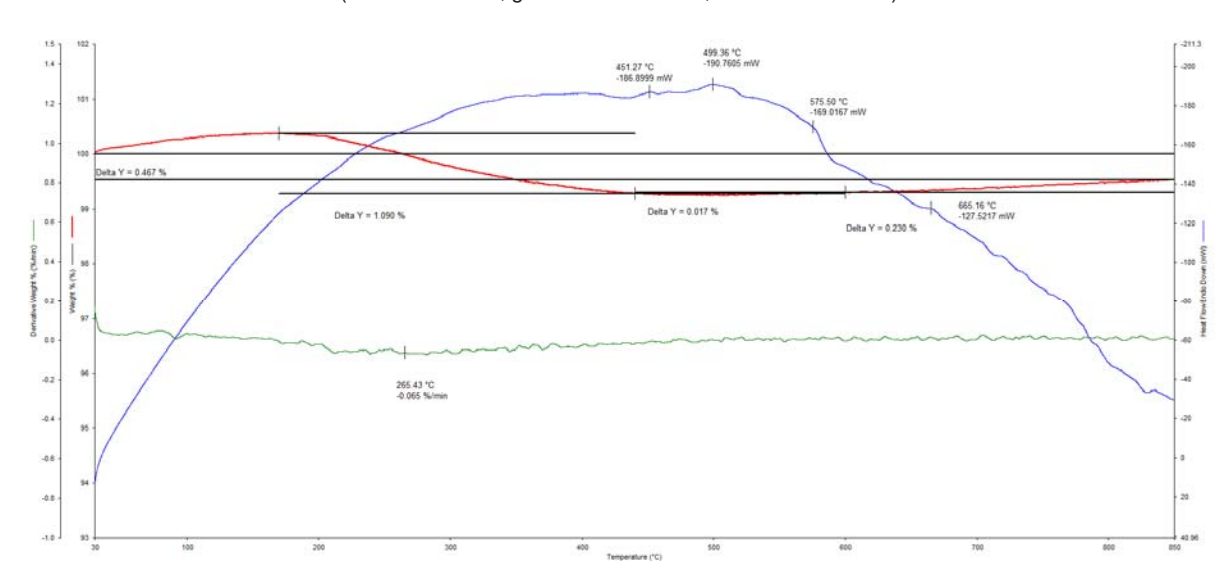


Fig. 4. TG-DTG, DTA thermal analytical curves for basalt fabric (red — TG curve, green — DTG curve, blue — DTA curve)

Table 2. Temperature ranges of anomalies and fiber weight changes

| No. | Fabric type      |                     | <u>Temperatur</u><br>w      | Weight change<br>in the range<br>of 30–850°C, % wt. |                             |       |       |
|-----|------------------|---------------------|-----------------------------|---|-----------------------------|-------|-------|
| 1   | Glass fabric     | 30-200 (-)<br>+0.21 | 200-410 (294)<br>-0.56      | <u>410–560 (–)</u><br>–0.08                         | <u>560–850 (–)</u><br>+0.05 |       | -0.38 |
| 2   | Carbon<br>fabric | 30–130 (–)<br>+0.21 | <u>130–300 (–)</u><br>–0.57 |   |                             | -6.82 |       |
| 3   | Basalt<br>fabric | 30-170 (-)<br>+0.47 |                             |   |                             |       | -0.37 |

The relative breaking load for carbon fiber after annealing at 300°C increased slightly by 0.9 %, at 400°C — by 2 %, and at 420°C it decreased by 13.4 % (pyrolysis can also lead to the activation of its surface (increase in the specific surface area, sorption capacity (Khaskov et al., 2019; Nacharkina et al. 2021)); for glass fiber at 350°C, it decreased by 12.1 %, at 400°C — by 34.4 %,

at  $560^{\circ}\text{C}$  — by 98.5~%; the similar was true for basalt fabric as well.

Patterns of wetting glass, carbon, and basalt elementary fibers with test fluids were obtained by the optical method and then analyzed. Table 3 shows the results of determining the contact angles of fibers of different nature with test fluids, resin L, and binder. Measurement error — up to 10–15 %

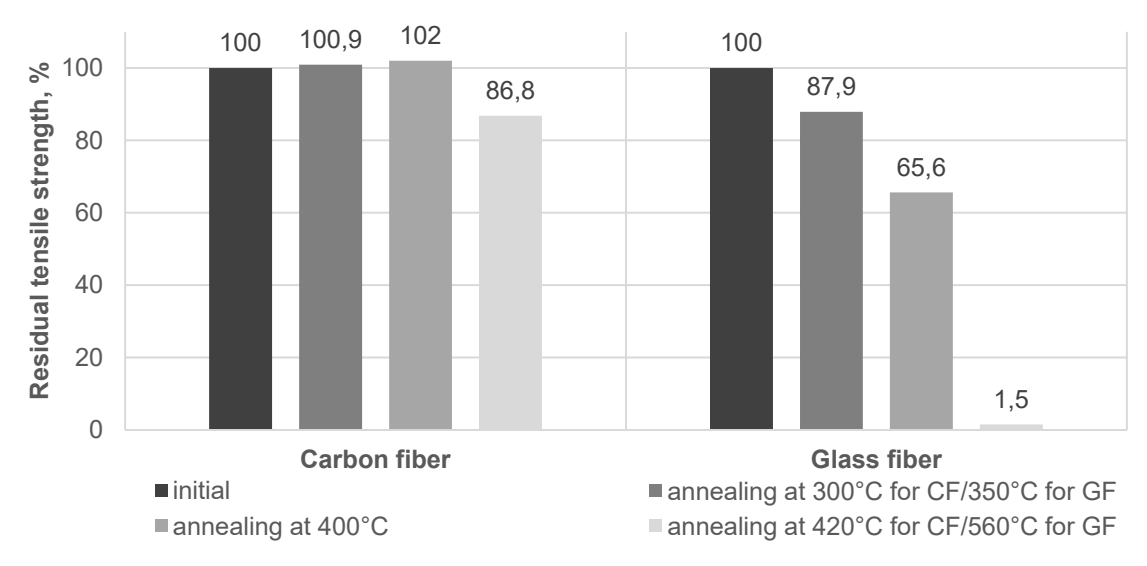


Fig. 5. Histograms of residual tensile strength for glass and carbon fibers after annealing at different temperatures

Table 3. Contact angles in wetting of fibers with test fluids

|           |                 | with test halas |  |  |  |  |  |
|-----------|-----------------|-----------------|--|--|--|--|--|
| Curfoss   | Contact a       | angle, θ, °     |  |  |  |  |  |
| Surface   | initial         | annealed        |  |  |  |  |  |
| Glass     | Distilled       | d water         |  |  |  |  |  |
| monofiber | 19±2            | 10±1            |  |  |  |  |  |
|           | Ethylen         | e glycol        |  |  |  |  |  |
|           | 14±1            | 9±1             |  |  |  |  |  |
|           | Ani             | line            |  |  |  |  |  |
|           | 22±3            | 12±1            |  |  |  |  |  |
| Carbon    | Distilled       | d water         |  |  |  |  |  |
| monofiber | 18±2            | 14±1            |  |  |  |  |  |
|           | Ethylene glycol |                 |  |  |  |  |  |
|           | 22±2            | 29±3            |  |  |  |  |  |
|           | Ani             | line            |  |  |  |  |  |
|           | 13±1            | 27±3            |  |  |  |  |  |
| Basalt    | Distille        | d water         |  |  |  |  |  |
| monofiber | 8±1             | _               |  |  |  |  |  |
|           | Ethylen         | e glycol        |  |  |  |  |  |
|           | 7±1             | _               |  |  |  |  |  |
|           | Ani             | Aniline         |  |  |  |  |  |
|           | 13±1            | _               |  |  |  |  |  |

(e.g., for angles  $\sim 10^\circ$ , the error is  $\pm 1^\circ$ , for angles ~18–30°, the error is  $\pm (2 \div 3)$ °).

In Eq. 3, all the characteristics of the test fluids, as well as the contact angles presented in Table 3, are known. Three values are unknown: the dispersion component as well as the acid and base parameters of the same characteristic. With the use of multivariate approximation, planes in coordinates y, z) were built, which are known values ;  $\frac{\sqrt{\gamma_l^+}}{\sqrt{\gamma_l^-}}$ ;  $\frac{\gamma_l\left(1+\cos\theta\right)}{2\sqrt{\gamma_l^-}}$ ). Unknown are the values

of the coefficients: A =  $\sqrt{\gamma_s^d}$ ; B =  $\sqrt{\gamma_s^-}$ ; C =  $\sqrt{\gamma_s^+}$ .

The coefficients were calculated automatically in the STATISTICA software. Three-dimensional planes demonstrating the obtained solution were also built there. For better accuracy, it is recommended to use as much data as possible on wetting fibers by fluids with known free surface energy parameters.

Fig. 6 shows the diagrams and equations of the approximated planes for glass and carbon elementary fibers; the same principle is used for basalt elementary fiber calculations.

Table 4 presents the free surface energy parameters of glass, carbon, and basalt elementary fibers with and without oiling compositions (finishing agents).

It should be noted that in the initial state (with oiling or finishing agent), carbon fibers have the lowest surface energy (18.72 mJ/m<sup>2</sup>) and the contribution of the polar component is ~77 %, glass and basalt fibers are characterized by high surface energy (38.31 and 33.98 mJ/m<sup>2</sup>, respectively), and the contribution of the polar component is ~85 %.

Based on the results of determining changes in the parameters of the free surface energy of fibers after removal of the oiling composition / finishing agent by pyrolysis, a decrease in their free surface energy is observed: by 15.3 % for glass fibers, by 22.3 % for carbon fibers; a decrease in the dispersion component  $(\gamma_s^d)$  by 7.7 % for glass fibers and by 49.2 % for carbon fibers; a decrease in the polar component  $(\gamma_s^{ab})$  by 16.6 % for glass fibers and by 14.3 % for carbon fibers; an increase in electronaccepting (acid) interactions ( $\gamma_s^+$ ) by 12.9 % for glass and carbon fibers (wetting by polar fluids (water, etc.) improves, wetting by nonpolar fluids (aniline, etc.) deteriorates); a decrease in electron-donating (base) interactions  $(\gamma_s^-)$  by 39.6 % for glass fibers and by 37.1 % for carbon fibers.

Table 5 presents the results of determining the surface tension of low-viscosity epoxy resin L and

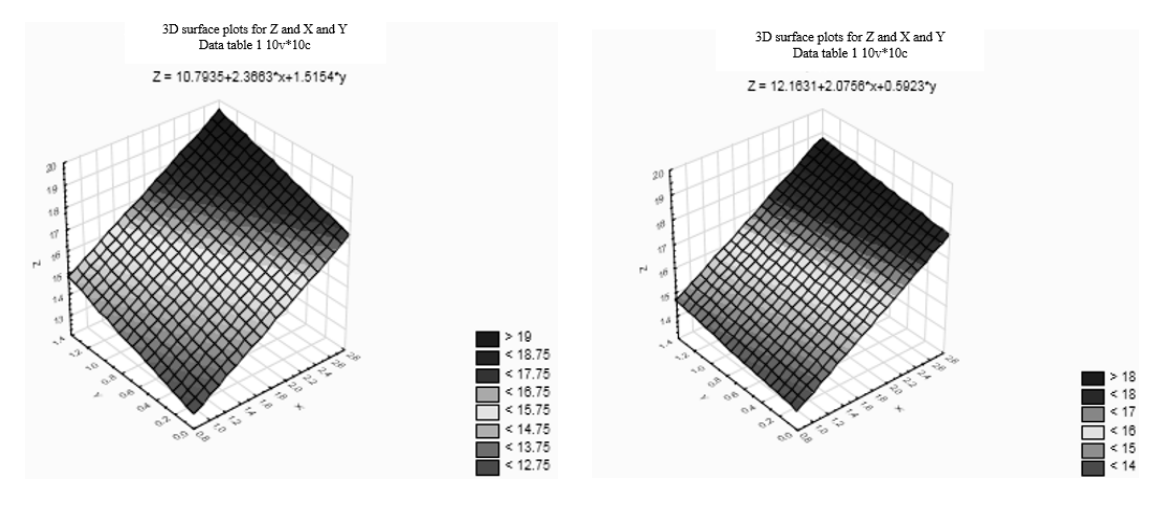


Fig. 6. Diagrams and equations of the approximated planes for: a) glass monofiber; b) carbon monofiber

 $\gamma_s^{ab} = 2\sqrt{\gamma_s^+} \sqrt{\gamma_s^-}$  $\gamma_s^d$  $\gamma_{\it s}$ , mJ/m<sup>2</sup> **Surface**  $\gamma_S^+$  $\gamma_s^-$ 32.71 2.3 Glass monofiber initial 38.31 5.6 116.5 annealed 32.45 5.17 27.28 133.68 1.39 Difference, mJ/m<sup>2</sup> -5.86-0.43-5.43+17.18 -0.91 Carbon monofiber 18.72 4.31 14.41 147.94 0.35 initial 14.54 2.19 12.35 169.92 0.22 annealed Difference, mJ/m<sup>2</sup> -4.18 -2.12-2.06+21.98 -0.13Basalt monofiber initial 33.98 5.15 28.83 132.81 1.56

Table 4. Free surface energy and its components for different fibers

Table 5. Surface tension and viscosity of epoxy resin and resin/hardener system

|  |            | •                        |
|--|------------|--------------------------|
| Fluid  | σ, mN/m    | Viscosity at 25°C, mPa·s |
| Resin L  | 44.54±0.05 | 710±70                   |
| Resin L + hardener GL2 after 5 minutes of stirring | 37.36±0.47 | 248±100                  |

the resin L + hardener GL2 system (component ratio 100:30)» after 5 minutes of stirring (with the platinum ring already catalyzing the polymerization process) using the Du Nouy rings method.

Due to the introduction of hardener, having lower viscosity and representing a mixture of aliphatic and cycloaliphatic amines, into the modified epoxy resin, structural plasticization is observed, which is manifested in a sharp decrease in viscosity (more than 2 times), surface tension of the system — by 15.6 % after five minutes of stirring (due to the spatial reorientation of molecules). Therefore, it is reasonable to study wetting of elementary fibers of different nature both with epoxy resin and with the epoxy resin / hardener system.

Based on the results of determining wetting (Table 6) of elementary fibers of different nature in defect-free areas (without various inclusions) by low-viscosity resin L, it can be concluded that optimal

Table 6. Contact angles of epoxy compositions

| Contact a                    | angle, θ, °   |  |  |  |
|------------------------------|---|--|--|--|
| initial                      | annealed  |  |  |  |
| Ероху                        | resin L   |  |  |  |
| 9±1                          | 10±1  |  |  |  |
| Epoxy resin L +              | hardener GL2  |  |  |  |
| 4±1                          | 5±1   |  |  |  |
| Epoxy resin L                |   |  |  |  |
| 16±2 19±3                    |   |  |  |  |
| Epoxy resin L + hardener GL2 |   |  |  |  |
| 3±1                          | 4±1   |  |  |  |
| Ероху                        | resin L   |  |  |  |
| 13±1 –                       |   |  |  |  |
| Epoxy resin L + hardener G   |   |  |  |  |
| 4±1                          | _   |  |  |  |
|                              | initial Epoxy 9±1 Epoxy resin L + 4±1 Epoxy 16±2 Epoxy resin L + 3±1 Epoxy 13±1 Epoxy resin L + |  |  |  |

wetting occurs in case of glass fiber, then — basalt fiber, and the worst — in case of carbon fiber, which is due to higher surface tension of low-viscosity resin L and a smaller difference in the polarities of the contacting phases. Measurement error — up to 10-15% (e.g., for angles  $\sim 10^\circ$ , the error is  $\pm 1^\circ$ , for angles  $\sim 16-20^\circ$ , the error is  $\pm (2 \div 3)^\circ$ ).

When a mixture of epoxy resin and hardener (L + GL2) is used for wetting, the wettability of all

types of fibers significantly increases, which is manifested in a multiple reduction of the contact angle — up to  $3-5^{\circ}$ , and can be attributed to a decrease in viscosity and surface tension in the system (L + GL2 compared to epoxy resin L).

Application of oiling compositions on the surface of glass and basalt fibers as well as finishing agents on the surface of carbon fibers ensures bonding of individual filaments providing comprehensive protection against mechanical damage, and positively affects fiber wetting (up to 3°) by increasing the polarity of the fiber surface by creating active areas that promote the formation of hydrogen bonds with the implementation of the van der Waals interaction between the surface of fibers of different nature and binder molecules, improving the interfacial adhesion.

#### **Conclusions**

This paper presents the results of evaluating the energy characteristics of phases at the air interface, affecting the adhesion interaction in hybrid polymer composites:

1. The method for determining surface energies of solids was upgraded. The upgraded method makes it

possible to determine the free surface energy of fibers of different nature and the surface tension of the binder.

- 2. Pyrolysis in air slightly deteriorates the elastic-mechanical properties of carbon fibers (by 13.4 % at 420°C), decreases free surface energy (by 22.3 %), significantly decreases the dispersion component (by 49.2 %), decreases the polar component (by 14.3 %); an increase in acid interactions was 12.9 %, a decrease in base interactions was 37.1 %. Pyrolysis in air of glass fabrics results in substantial losses of glass fiber strength (by 98.5 % at 560°C), decreases free surface energy (by 15.3 %), the dispersion component (by 7.7 %), and the polar component (by 16.6 %); an increase in acid interactions was 12.9 %, a decrease in base interactions was 39.6 %.
- 3. Quantitative evaluation (by changes in elasticmechanical properties, free surface energy and its components) of the effect of oiling compositions (finishing agents) was performed. It is reasonable to select these compositions with account for the free surface energy parameters of fibers of different nature to increase the interfacial adhesion in polymer composites.

#### References

Danilov, V. E., Korolev, E. V., Ayzenshtadt, A. M., and Strokova, V. V. (2019). Features of the calculation of free energy of the surface based on the model for interfacial interaction of Owens–Wendt–Rabel–Kaelble. *Stroitel'nye Materialy [Construction Materials]*, No. 11, pp. 66–72. DOI: 10.31659/0585-430X-2019-776-11-66-72.

Dupre, M. A. (1869). Théorie mécanique de la chaleur. Paris: Gauthier-Villars, 484 p.

Gulyaev, A. I., Medvedev, P. N., Sbitneva, S. V., and Petrov, A. A. (2019). Experimental research of "fiber-matrix" adhesion strength in carbon fiber epoxy/polysulphone composite. *Aviation Materials and Technologies*, No. 4 (57), pp. 80–86. DOI: 10.18577/2071-9140-2019-0-4-80-86.

Gunyaev, G. M. (1977). Polycomponent high-modulus composites. *Polymer Mechanics*, Issue 5, pp. 685–692. DOI: 10.1007/BF00860318.

Hughes, J. D. H. (1991). The carbon fibre/epoxy interface—a review. *Composites Science and Technology*, Vol. 41, Issue 1, pp. 13–45. DOI: 10.1016/0266-3538(91)90050-Y.

Karzov, I. M., Alent'ev, A. Yu. Bogdanova, Yu. G., Kostina, Yu. V., and Shapagin, A. V. (2010). Influence of energy characteristics of the fiber-binder interface on polymer composite strength. *Moscow University Chemistry Bulletin*, Vol. 65, Issue 6, pp. 384–391. DOI: 10.3103/S0027131410060106.

Kayumov, R. A. and Shakirzyanov, F. R. (2021). Large deflections and stability of low-angle arches and panels during creep flow. In: Altenbach, H., Eremeyev, V. A., and Igumnov, L. A. (eds.). *Multiscale Solid Mechanics. Advanced Structured Materials*, Vol. 141. Cham: Springer, pp. 237–248. DOI: 10.1007/978-3-030-54928-2 18.

Khaskov, M. A., Zelenina, I. V., Sorokin, O. Yu., and Gulyaev, A. I. (2019). Ceramic interfacial coating on carbon fibers based on polycarbosilane and oligovinylsilazane. *Glass Physics and Chemistry*, Vol. 44, Issue 6, pp. 601–606. DOI: 10.1134/S108765961806010X.

Kim, J.-K. and Mai, Y.-W. (1998). Engineered interfaces in fiber reinforced composites. Oxford: Elsevier, 416 p.

Kramarev, D. V., Osipchik, V. S., Chalaya, N. M., Berezina, A. B., and Kolesnikov, A. V. (2017). Study of interfacial phenomena at the fiber–binder interface in imido-organoplastics. *Plasticheskie Massy*, No. 7–8, pp. 3–6. DOI: 10.35164/0554-2901-2017-7-8.

Lecomte du Nouy, P. (1925). An interfacial tensiometer for universal use. *Journal of General Physiology*, Vol. 7, Issue 5, pp. 625–633. DOI: 10.1085/jgp.7.5.625.

McCafferty, E. (2002). Acid-base effects in polymer adhesion at metal surfaces. *Journal of Adhesion Science and Technology*, Vol. 16, Issue 3, pp. 239–255. DOI: 10.1163/156856102317295478.

Mercier, C., Khelil, A., Al Mahmoud, F., Blin-Lacroix, J.-L., and Pamies, A. (2021). Experimental investigations of buckling behaviour of steel scaffolds. *Structures*, Vol. 33, pp. 433–450. DOI: 10.1016/J.ISTRUC.2021.04.045.

Nacharkina, A. V., Zelenina, I. V., Valueva, M. I., and Voronina, O. G. (2021). Influence of additional sizing of carbon fiber in producing volume-reinforced preforms on the properties of high-temperature carbon fiber. *Scientific and Technical Journal "Proceedings of VIAM"*, No. 1 (95), pp. 54–65. DOI: 10.18577/2307-6046-2021-0-1-54-65.

Owens, D. K. and Wendt, R. C. (1969). Estimation of the surface free energy of polymers. *Journal of Applied Polymer Science*, Vol. 13, Issue 8, pp. 1741–1747. DOI: 10.1002/app.1969.070130815.

Petrova, G. N. and Beider, E. Ya. (2016). Development and research of finishing compositions for thermoplastic carbon plastics. *Scientific and Technical Journal "Proceedings of VIAM"*, No. 12 (48), pp. 65–73. DOI: 10.18577/2307-6046-2016-0-12-9-9.

Shakhmurzova, K. T., Kurdanova, Zh. I., Kalmykova, G. Z., Slonov, A. L., Beev, A. A., and Khashirova, S. Yu. (2022). Surface modification of fiberglass with high temperature sizing agents. *Proceedings of the Kabardino-Balkarian State University*, Vol. XII, No. 2, pp. 67–74.

Skudra, A. M. and Bulavs, F. Ya. (1978). Structural theory of reinforced plastics. Riga: Zinatne, 192 p.

Starostina, I. A. and Stoyanov, O. V. (2010). Development of methods for the evaluation of the surface acid-base properties of polymeric materials. *Bulletin of Kazan Technological University*, No. 4, pp. 58–68.

Starostina, I. A., Stoyanov, O. V., Makhrova, N. V., and Deberdeev, R. Ya. (2011). Application of test polymer surfaces for the determination of free surface energy parameters. *Doklady Akademii Nauk*, Vol. 440, No. 1, pp. 64–66.

Starostina, I. A., Stoyanov, O. V., and Sokorova, N. V. (2013). Determination of free surface-energy parameters using a spatial method. *Polymer Science Series D*, Vol. 6, pp. 157–159. DOI: 10.1134/S1995421213020135.

Vann Oss, C. J., Chaudhury, M. K., and Good, R. J. (1989). The mechanism of phase separation of polymers in organic media—apolar and polar systems. *Separation Science and Technology*, Vol. 24, Issue 1–2, pp. 15–30. DOI: 10.1080/01496398908049748.

Wilhelmy, L. (1863). Ueber die Abhängigkeit der Capillaritäts-Constanten des Alkohols von Substanz und Gestalt des benetzten festen Körpers. *Annalen der Physik und Chemie*, Vol. 195, Issue 6, pp. 177–217. DOI: 10.1002/andp.18631950602.

Zhang, J. (2012). Different surface treatments of carbon fibers and their influence on the interfacial properties of carbon fiber/epoxy composites. [online] Available at: https://tel.archives-ouvertes.fr/tel-01146459 [Date accessed: September 10, 2023].

Zheng, Y. and Guo, Z. (2021). Investigation of joint behavior of disk-lock and cuplok steel tubular scaffold. *Journal of Constructional Steel Research*, Vol. 177, 106415. DOI: 10.1016/J.JCSR.2020.106415.

## АДГЕЗИОННОЕ ВЗАИМОДЕЙСТВИЕ В ГИБРИДНОМ ПОЛИМЕРНОМ КОМПОЗИТЕ. ЭНЕРГЕТИЧЕСКИЕ ХАРАКТЕРИСТИКИ ФАЗ НА ГРАНИЦЕ С ВОЗДУХОМ

Валиев Алмаз Илсурович\*1, Старовойтова Ирина Анатольевна2, Сулейманов Альфред Мидхатович1

<sup>1</sup>Казанский архитектурно-строительный университет, г. Казань, Россия

<sup>2</sup>ООО «Научно-производственная фирма «Рекон», г. Казань, Россия

\*E-mail: tatcomposite@mail.ru

#### Аннотация

Введение. Исследование механизмов формирования адгезионной прочности полимерных композитов заключается в целенаправленном выборе компонентов, обеспечивающих их совместную работу с эффективной передачей напряжений от волокон к связующему через границу раздела фаз. Прочность адгезионного взаимодействия компонентов при этом может быть выражена через их энергетические характеристики при обеспечении технологических и других факторов. Цель исследования: изучение энергетических характеристик фаз гибридного полимерного композита на границе с воздухом. Методы: оптическим методом получены микрофотографии смачивания волокон различной природы жидкостями, по которым определены краевые углы смачивания, проведены испытания волокон на растяжение, с использованием синхронного термоанализатора выполнен термический анализ волокон, с использованием тензиометра определены поверхностные натяжения эпоксидной смолы, системы «эпоксидная смола — отвердитель». Результаты: Проведена модернизация метода определения поверхностных энергий твердых тел. Модернизированный метод позволяет проводить определение свободной поверхностной энергии волокон различной природы и поверхностного натяжения связующего. Проведена количественная оценка эффекта от замасливающих композиций (аппретов).

Ключевые слова: композит, гибрид, адгезия, смачивание, работа адгезии, свободная поверхностная энергия.

### COMPARATIVE BUCKLING ANALYSIS OF CONCRETE AND EXPANDED POLYSTYRENE DOME SHELLS

Habte Yohannes Damir<sup>1,2\*</sup>, Marina Rynkovskaya<sup>1</sup>, Issaias Anday Sereke<sup>1,2</sup>

<sup>1</sup> Peoples' Friendship University of Russia named after Patrice Lumumba (RUDN University), Moscow, Russia

#### Abstract

**Introduction:** Various studies have been conducted to analyze the buckling behavior of concrete spherical shells. Nonetheless, no research is available that would investigate the buckling behavior of EPS (expanded polystyrene) shells. EPS has a very low self-weight compared to concrete. **The purpose of the study** is to investigate the comparative buckling characteristics of concrete and EPS shells. The respective self-weight and live load of 1.5 kN/m² were considered. **The methods** used are Linear buckling analysis (LBA) and geometrically nonlinear buckling analysis (GNA) of sample domes with and without imperfections performed using Abaqus software. **The results** of the comparative analyses show that the critical buckling pressure of EPS and concrete spherical shells of the same geometry was found to be 122,634 N/m² and 5560 N/m², respectively. The ratio of the critical buckling pressure to the practical ultimate (dead load + live load) loading of concrete is 23.2, while for EPS, it is 2.22. Moreover, increasing the thickness of EPS from 100 to 200 mm increased the critical buckling pressure factor by 15.4 times. The maximum loading displacement of EPS (15.6 mm) was times less than the displacement caused by the buckling pressure. This finding demonstrates the feasibility of constructing EPS shells, with further research on the optimum geometry and construction mechanism.

Keywords: shells, buckling, dome, concrete, EPS.

#### Introduction

Shell structures

In general, shell structures are defined as spatially curved surface structures that support externally applied loads (Farshad, 1992). Accordingly, shells can be described as structures with a small thickness compared to their other dimensions, which can be used to cover large spans by developing in-plane stresses under the actions of membrane forces (Ter Maten et al., 2013). Adriaenssens et al. (2014) defined shell structures as "constructed systems described by three-dimensional curved surfaces, in which one dimension is significantly smaller compared to the other two. They are form-passive and resist external loads predominantly through membrane stresses". Shells are structures with the most efficient structural elements, found in both nature and technological designs. The generation of shell surfaces, from a theoretical perspective, could be considered the most effective construction method (Huijben et al., 2011). The use of new materials in thin pavilions, experimental structures, and shells promotes the development of future architecture (Jovanovic et al., 2017).

To achieve effective design of shell structures, it is important to optimize the geometric shape as well as the material usage to make the structure as light as possible. In the context of optimizing material use, the practical utilization of various materials such as concrete, steel, masonry blocks, EPS, and others

can be considered for optimum alternative selection. When it comes to concrete structures, their selfweight is the main component of the overall structural load. Concrete shell structures have been widely used since the 1930s (Huijben et al., 2011). Concrete is a widely used structural construction material, and EPS is also well known for its implementation in various structural sectors as a filler and insulation. often used to cover slabs and stairs. It is known as a light-weight material due to its relatively low density. Ibrahim et al. (2013) advocate that their study confirms that the compressive strength of EPS with an appropriate thickness was found to be adequate to support dead and live loads. Furthermore, the study by Khalaj et al. (2020) demonstrates that the elastic modulus of EPS increases with an increase in EPS density. For a better comparative display, the structural properties of concrete and EPS are summarized below in Table 1.

In any structural analysis, the stability of shell structures is of primary importance. The behavior of the material structure should be determined from the ultimate buckling loads and load-displacement relations (Ellobody et al., 2014). The design of a thin shell is generally more governed by buckling stability requirements, rather than just by the material strength and characteristics.

This paper examines the critical buckling loads that can be induced in concrete and EPS shells in comparison to their characteristic strength, which

<sup>&</sup>lt;sup>2</sup> Mai Nefhi College of Engineering and Technology, Asmara, Eritrea

<sup>\*</sup>Corresponding author's e-mail: habte88eng@gmail.com

determines the maximum deformation of a given geometry.

Buckling analysis of spherical shells

The critical buckling load pressure for the stability analysis of shells of revolution can be computed using the governing equations given below (Mekjavić, 2011). These equations are derived from the equation for computing the buckling load of a full sphere, which is used to approximate the buckling load for a dome shell.

$$q_{cr} = \frac{2E}{\sqrt{3(1-v^2)}} \left(\frac{t}{r}\right)^2,\tag{1}$$

where:  $q_{cr}$  (in MPa) is critical buckling pressure, with E, v, t, and r being the modulus of elasticity (GPa), Poisson's ratio, shell thickness (m), and shell radius (m), respectively.

The corresponding critical stress ( $\sigma_{cr}$ ) can be determined as follows:

$$\sigma_{cr} = \frac{q_{cr}r}{2t} = \frac{Et}{r\sqrt{3(1-v^2)}}.$$
 (2)

In this study, a comparative analysis was performed using nonlinear finite element analysis with Abaqus software. All structural responses, such as deformations, stresses, and buckling, were analyzed. To investigate the displacement of the load against the maximum magnitudes, a manual computation was performed using Eqs. 1 and 3 (see details in *Results of Loading Displacements*). The applied load pressure includes the self-weight and an area live load of 1.5 kN/m² normal to the surface.

#### Materials and methods

Concrete in general is made from mixtures of cement, sand, aggregates, and water in a designed proportion (Gagg, 2014). Normal concrete has a unit weight of 22–25 kN/m³. The high density of concrete is the main factor contributing to the self-weight loading in load combination cases. As can be noted from Table 1, concrete has a compressive strength that is about 10 times higher than its tensile strength.

This demonstrates that concrete is fundamentally brittle and becomes stronger when compressed. In contrast, due to its low tensile strength, it is prone to failure from shearing and/or tensile forces. In this study, the randomly selected concrete has the following properties:

 $\gamma_c$  = 24 kN/m³ E<sub>c</sub> = 30 GPa Poison's ratio: 0.2 where:  $\gamma_c$  and E<sub>c</sub> are the unit weight and modulus of elasticity of the concrete used for the analyses.

EPS is a light-weight cellular polymeric material used in various areas of civil engineering (Khalaj et al., 2017, 2020; Ni et al., 2020; Ramli Sulong et al., 2019; Vilau and Dudescu, 2020). The individual granular components of EPS can be found in varying fine sizes and shapes, including circular, hexagonal, octagonal, and others. EPS is used in various construction applications to withstand different loading stresses. According to Table 1, it has a relatively low unit weight ranging from 0.12 to 0.35 kN/m<sup>3</sup>, which is approximately 100 times lower than that of concrete. Similarly, EPS has very low compressive strength characteristics of 0.04-10.9 MPa. Nonetheless, its tensile strength is about 10 times higher than that of concrete. Another important factor is the modulus of elasticity of EPS, which is on average 1.32 GPa, almost 30 times less than that of concrete. With all these different values, it is important to investigate the feasibility of using EPS material in shell structures. Furthermore, concrete and EPS materials can be mixed to achieve the desired characteristics. The experimental study by Saheed et al. (2020) demonstrates that a composite EPS-concrete slab structure has the potential to be a construction material with combined density and strenath benefits.

For this reason, the authors of this paper searched for research articles related to the analysis of EPS shell structures in Google Scholar, ResearchGate, and Google search engines. Surprisingly, no single article was found that would provide detailed structural analysis regarding the material strength and stability requirements of EPS shells. The only paper related to EPS shell structures found from

Table 1. Varying material properties of concrete and EPS

| No. | Symbol         | Description                      | Unit  | Concrete          | EPS         |
|-----|----------------|----------------------------------|-------|-------------------|-------------|
| 1.  | Υ              | Unit weight                      | kN/m³ | 22–25             | 0.12–0.35   |
| 2.  | f <sub>c</sub> | Compressive strength             | MPa   | 20–40             | 0.04–10.9   |
| 3   | f <sub>t</sub> | Tensile strength                 | MPa   | 2–5               | 47–51       |
| 4.  | f <sub>b</sub> | Flexural strength                | MPa   | 0.864 -1.207      | 0.075–3     |
| 5.  | V              | Shear strength                   | MPa   | 6–17              | 0.124-0.3   |
| 6.  | Е              | Modulus of elasticity            | MPa   | 14,000–41,000     | 6.5–2650    |
| 7.  | μ              | Permeability                     | cm/s  | 10 <sup>-10</sup> | 0.5–3.5     |
| 8.  | α              | Coefficient of thermal expansion | C1    | 10 <sup>-5</sup>  | 63–80       |
| 9.  | V              | Poisson's ratio                  | -     | 0.2-0.21          | 0.05-0.5    |
| 10  | k              | Thermal conductivity             | W/m·k |                   | 0.027-0.045 |

a Google search was the paper by Jovanovic et al. (2017). In that paper, the experimental model (Fig. 1) illustrates the tessellation and robotic form generation of a parabolic shell revolution, but does not include the structural analysis.

This paper is aimed at investigating the structural and kinematic responses of EPS shell forms in comparison to concrete shells of similar geometry. Spherical dome shapes were developed and analyzed for EPS and concrete materials. The two models were analyzed for the same geometric shape dimensions and thickness. The EPS parameters of unit weight  $(\gamma_{\rm eps})$ , modulus of elasticity  $(E_{\rm eps})$ , and Poisson's ratio (v) used in the calculations are as mentioned below:

$$\begin{split} \gamma_{\rm eps} &= 0.24 \text{ kN/m}^3 \quad \text{E}_{\rm eps} = 1.32 \text{ GPA} \\ \text{Poison's ratio, v} &= 0.275 \end{split}$$

The availability of advanced computer programming tools made it possible to analyze the nonlinear behavior of shells (Eisenbach, 2017). To optimize the structural behavior, several models were developed by making geometric and size modifications. The ideal numerical models of the two materials were analyzed. Moreover, it is important to develop a template model that can be consistently used throughout the process of form generation and structural analysis, to evaluate stability and deformations using general finite element analysis. The evaluation of kinematic indeterminacy and the analysis of large deformations in concrete and EPS shells were eventually investigated.

#### Linear buckling analysis

Eigenvalue linear buckling analysis is commonly used to determine the critical buckling load of a structure (Novoselac et al., 2012). Eigenvalue buckling analysis is described as an analysis of linear buckling, where the structures are considered to be elastic and without imperfections. Nevertheless, no structure is purely elastic in every situation and it cannot be free of any imperfections due to discrepancies in geometries, material properties, and workmanship (Imran et al., 2020). Performing nonlinear buckling analysis along with linear analysis is important for creating more accurate models (LUSAS, 2017).

#### Geometrically nonlinear buckling analysis

Geometrically nonlinear analysis is also referred to as load-displacement nonlinear geometry analysis (Ellobody et al., 2014). When geometric nonlinearity is considered, a significant deviation of deflection from the linear effect of loading exists (Semenov, 2016). As discussed in the previous section, GNA follows the initial conditions of stress analysis or linear eigenvalue buckling. Moreover, spherical shells are extremely susceptible to nonlinear buckling conditions when subjected to external pressure loads (Hutchinson and Thompson, 2017). In this paper, the effects of geometric nonlinearity and imperfections on the behavior of the selected material properties of concrete and EPS spherical shells are examined. Nonlinear buckling analyses were carried out in Abagus software. As a result, the conditions for the ultimate load pressure and load displacement were determined for the given shell geometries and material properties. For both materials under consideration, an ideal spherical dome shell with the same geometric details for both materials and a thickness of 0.1 m is shown in Fig. 2.

#### Results and discussion

Linear buckling analysis models of the two materials were run in Abaqus software. The maximum buckling pressure was determined based on the respective moduli of elasticity of concrete (30 GPa) and EPS (1.32 GPa). Accordingly, the eigenvalues of the concrete and EPS domes generated from the LBA were found to be 0.39 MPa and 0.018 MPa, respectively. Furthermore, the maximum buckling pressure determined by the GNA was found to be 0.122 MPa (concrete) and 0.005560 MPa (EPS).

#### LBA results

According to the LBA, the maximum displacements in the concrete and EPS models under the first eigenvalue pressure were found to be 1 m and 1.364 m, respectively. These values exist for plain, unreinforced concrete and EPS shells with a thickness of 0.1 m and a span of 48 m, under the eigenvalue pressure of 0.395 MPa and 0.018 MPa, respectively. These LBA loadings are approximately 70 and 7.4 times the ultimate imposed loadings listed in Table 2. These displacements are significantly



Fig. 1. Experimental EPS shell structure (Jovanovic et al., 2017)

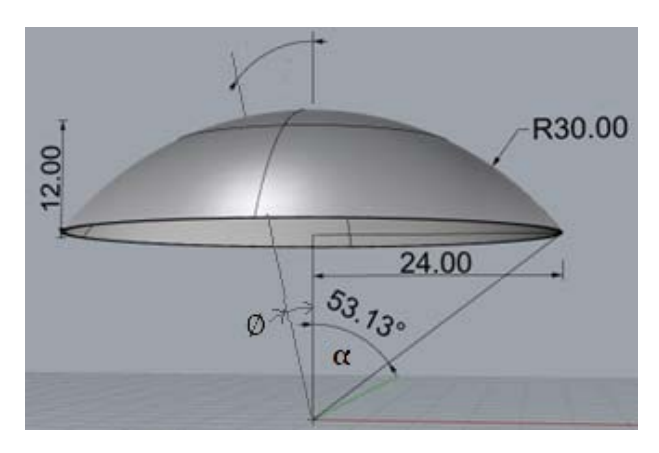


Fig. 2. Geometric details of the domeshaped shell under analysis

reduced when the models are analyzed in GNA, as discussed in the following sections. Moreover, in real-world construction, using appropriate thicknesses and actual loads (which are much smaller than LBA loads) and considering reinforcement can result in feasible deformations. The linear buckling analysis is computed taking into account the respective values of modulus of elasticity and Poisson's ratio. The maximum deflection in EPS demonstrates a 36% higher value compared to concrete, as the deflection computation is not linearly proportional to the values of E and eigenvalue taken.

#### GNA results

The geometric nonlinear analyses were performed without and with imperfection considerations, as shown in Figs. 3-5, respectively. Shell structures are known to be very sensitive to loading and geometric imperfections. Generally, spherical domes are classified as either shallow, deep, or complete based on the central vertical angle (Wagner et al., 2020). In this study, a half central angle of 53° was considered. Furthermore, the behavior of spherical domes towards imperfections is governed by the angles taken from the edges (Tomas et al., 2009). It is stated that for spherical shells loaded by uniform pressure, critical loads are highly sensitive to initial geometric imperfections (Bushnell, 1981). Furthermore, the paper argues that open cap spherical (dome) shells are likely to exhibit non-symmetric buckling modes depending on their shallowness. Considering the effects of imperfection sensitivity in concrete domes, it is recommended to apply a reduction factor ranging from 0.05 to 0.1 to the theoretical buckling load (Farshad, 1992). Tomas et al. (2009) argue that imperfections in concrete domes are unavoidable, as material homogeneity is affected by creep, plasticity, and cracking. They emphasize that for homogeneous elastic materials, a value of 1 is taken if the shell is sensitive to imperfections; otherwise, a value less than 1 is used. Considering

an average value from this range, such as 0.075, an imperfection amplitude is applied in ABAQUS.

The results of the GNA performed without imperfections are displayed, showing maximum displacement magnitudes of 0.090 m for concrete and 0.289 m for EPS, as depicted in Figs. 3 and 4, respectively. Similarly, simulations with imperfections exhibit maximum displacements of 0.456 m for concrete and 0.643 m for EPS, as shown in Fig. 5. The displacement deviation induced by imperfections appears to be 4.5 times greater in concrete and 2.22 times greater in EPS. This result aligns with the logic that EPS has a larger Poisson's ratio and elasticity.

Despite the loading being symmetrical, applying the first eigen mode as an imperfection test with an imperfection amplitude of 0.075 causes the dome to exhibit non-symmetrical behavior.

#### Results of loading displacements

The displacement resulting from each imposed ultimate load was calculated using both the analytical formula shown in Eq. (3) and numerical analysis conducted with Abaqus software.

The comprehensive formula (w) is used to determine the deformation field in a spherical shell as follows:

$$W_{\varnothing} = \frac{R^{2}q}{Et} \times \begin{bmatrix} \left(\cos\varnothing - \frac{1}{1 + \cos\varnothing}\right) + \\ \left(1 + v\right)\cos\varnothing \left[\ln\left(1 + \cos\varnothing\right) - \\ -\ln\left(1 + \cos\alpha\right) + \frac{1}{1 + \cos\alpha} - \frac{1}{1 + \cos\varnothing} \right] \end{bmatrix}, \quad (3)$$

where:  $\Phi$  is the meridian angle from the central axis to the points of consideration and  $\alpha$  is the overall meridional angle of the dome. In this study, the dome radius and meridian angles are taken as R = 30 m;  $\Phi$  = 0;  $\alpha$  = 53.130. As shown in Fig. 2, the value of  $\alpha$  is the half central angle of the dome shell and  $\Phi$  = 0 represents the location of the top crest of the dome.

The displacement resulting from the loading (self-weight dead load + 1.5 KN/m² live load) was calculated using Eq. (3) for both the concrete and EPS shells of the same geometry, as shown in Table 2. The loads are factored into the ultimate load combination using the American Concrete Institute (ACI) loading code [1.2x Dead Load (DL) + 1.6x Live Load (LL)].

The results in Table 2 show that for a thickness of 100 mm in concrete and EPS domes, the maximum displacements are 1.45 mm and 15.6 mm, respectively, under their respective self-weight and 1.5 KN/m² live load. These results are more accurate and stable compared to the magnitude of maximum displacements computed for buckling analysis. Furthermore, in Tables 3 and 4, the

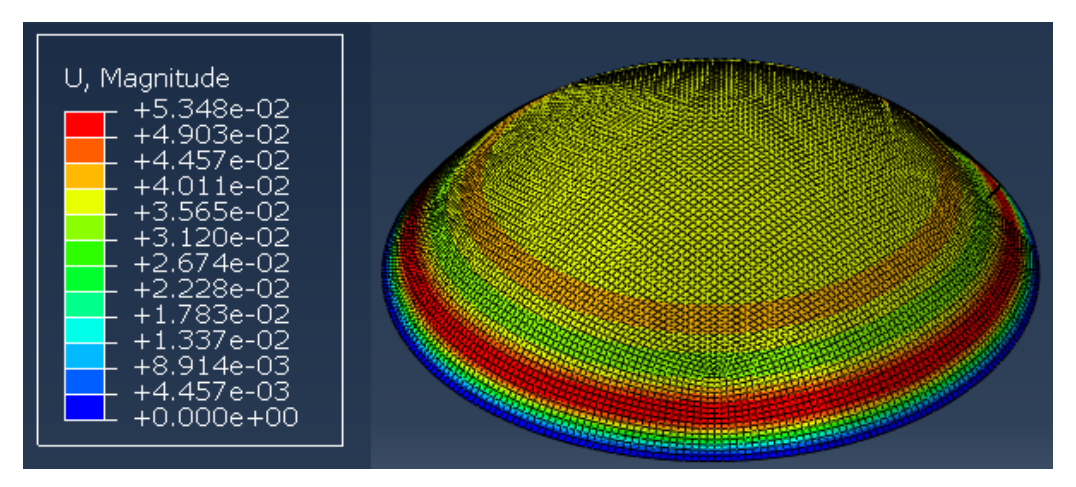


Fig. 3. Deformed shape of concrete with maximum displacement after GNA analysis without imperfections

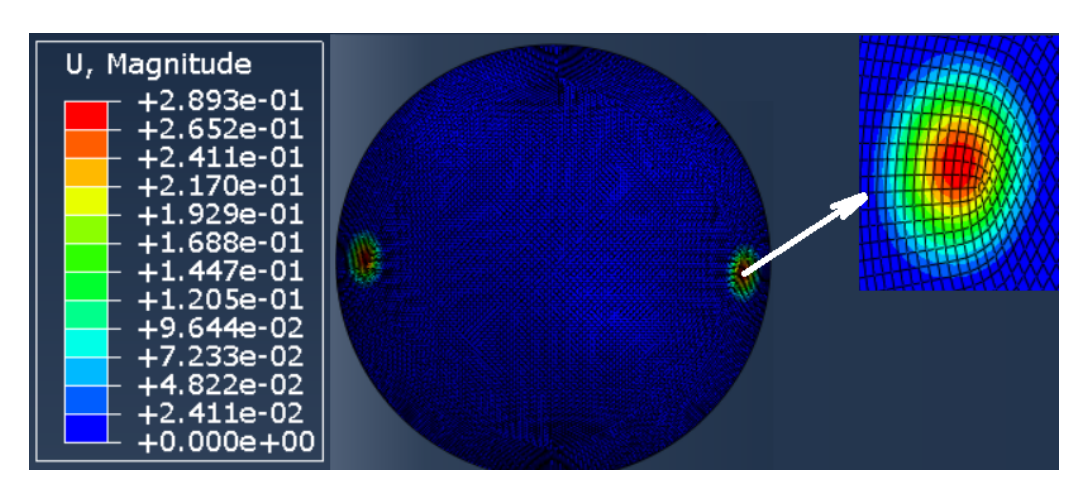


Fig. 4. Deformed shape of EPS with maximum displacements after GNA analysis without imperfection

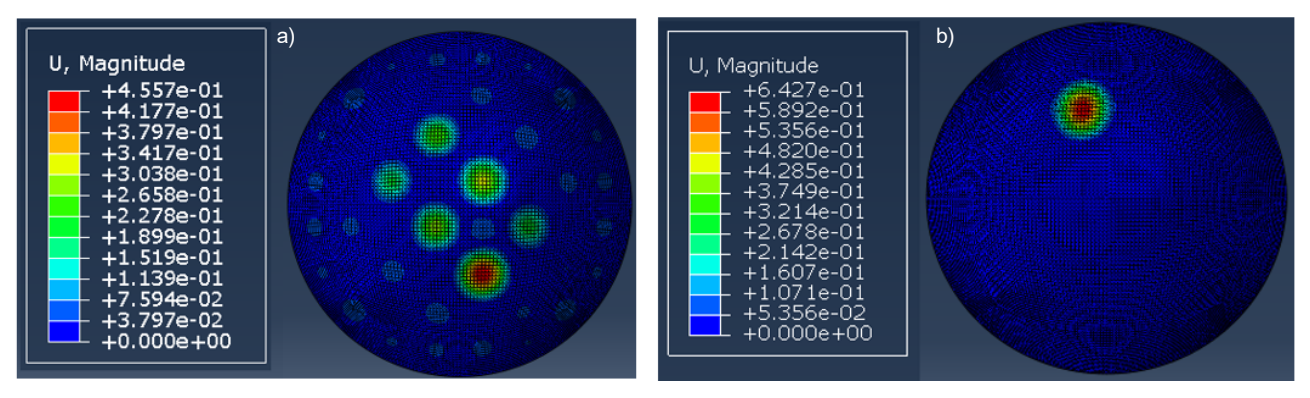


Fig. 5. Deformed shape with maximum displacements after GNA analysis with imperfection: a) concrete b) EPS

comparative displacement results demonstrate that the values are lower when computed numerically using software. This can be justified by the fact that numerical software analyses consider nonlinearity and plasticity effects, resulting in deflections that continue to decrease.

#### Conclusion

The results of the comparative analyses show that the maximum displacements from the LBA

analyses are slightly higher than those from the GNA. It is known that in a spherical shell buckling case, snap-through buckling controls the behavior, and the difference in the results of these two analyses identifies an elastic imperfection reduction value derived from this snap-through buckling. The real buckling strength of a perfect shell is detected more accurately by GNA than by LBA. This is due to the fact that GNA follows a progressive alteration of

| Concrete ( $E_c = 30 \text{ GPA}$ ; $v = 0.2$ ; $\gamma_c = 24 \text{ kN/m}^3$ ) |                        |                    |                   | EPS ( $E_{eps} = 1.32 \text{ GPA}; v = 0.27; \gamma_c = 0.24 \text{ kN/m}^3$ ) |  |                    |                   |
|--|------------------------|--------------------|-------------------|--|--|--------------------|-------------------|
| t, thickness<br>(m)  | q (self-weight) (N/m²) | q (DL + LL) (N/m²) | Displacement (mm) | t, thickness<br>(m)  | q <sub>(self-weight)</sub> (N/m <sup>2</sup> ) | q (DL + LL) (N/m²) | Displacement (mm) |
| 0.1  | 2880                   | 5280               | 1.45              | 0.1  | 28.8   | 2428.8             | 15.64             |
| 0.15   | 4320                   | 6720               | 1.23              | 0.15   | 43.2   | 2443.2             | 10.49             |
| 0.2  | 5760                   | 8160               | 1.12              | 0.2  | 57.6   | 2457.6             | 7.91              |
| 0.25   | 7200                   | 9600               | 1.06              | 0.25   | 72   | 2472               | 6.37              |
| 0.3  | 8640                   | 11,040             | 1.01              | 0.3  | 86.4   | 2486.4             | 5.34              |

Table 3. Loading displacements of concrete using analytical and numerical computation

| Concrete ( $E_c = 30 \text{ GPA}$ ; $v = 0.2$ ; $\gamma_c = 24 \text{ kN/m}^3$ ) |                        |                      | Analytical (manual) | Numerical (Abaqus) |
|--|------------------------|----------------------|---------------------|--------------------|
| t, thickness (m)   | q (self-weight) (N/m²) | $q_{(DL+LL)}(N/m^2)$ | Displacement (mm)   | Displacement (mm)  |
| 0.1  | 2880                   | 5280                 | 1.45                | 1.78               |
| 0.15   | 4320                   | 6720                 | 1.23                | 1.08               |
| 0.2  | 5760                   | 8160                 | 1.12                | 0.82               |
| 0.25   | 7200                   | 9600                 | 1.06                | 0.69               |
| 0.3  | 8640                   | 11,040               | 1.01                | 0.62               |

Table 4. Loading displacements of EPS using analytical and numerical computation

| EPS (E <sub>eps</sub> = 1.32 GPA; $v = 0.27$ ; $\gamma_c = 0.24 \text{ kN/m}^3$ ) |                        |                      | Analytical (manual) | Numerical (Abaqus) |
|---|------------------------|----------------------|---------------------|--------------------|
| t, thickness (m)  | q (self-weight) (N/m²) | $q_{(DL+LL)}(N/m^2)$ | Displacement (mm)   | Displacement (mm)  |
| 0.1   | 28.8                   | 2428.8               | 15.64               | 21.3               |
| 0.15  | 43.2                   | 2443.2               | 10.49               | 8.76               |
| 0.2   | 57.6                   | 2457.6               | 7.91                | 5.35               |
| 0.25  | 72                     | 2472                 | 6.37                | 3.82               |
| 0.3   | 86.4                   | 2486.4               | 5.34                | 2.97               |

geometry under the applied loads resulting from the snap-through analysis. Moreover, the magnitudes of the maximum displacements from the nonlinear buckling analyses are significantly affected by the imperfections considered. The maximum displacement without imperfections, which was 90 mm for the concrete dome and 289 mm for the EPS dome, increased to 456 mm and 643 mm, respectively, when an imperfection factor of 0.055 was induced. This 4.5 times change in concrete and 2.22 times change in EPS corresponds to the fact that EPS has higher elasticity and Poisson's ratio compared to concrete.

Furthermore, to investigate the possibility of constructing domes using light-weight EPS material, the same geometric model was subjected to a factored ultimate load comprising self-weight and a live load of 1.5 kN/m². The total load imposed was 2428.8 N/m², which is 2.3 times less than the maximum buckling pressure of 5560 N/m². This total loading was found to produce a maximum displacement of 15.64 mm for the spherical shell with a thickness of 100 mm and a radius of 30 m. Although the displacement values are found to be very small

and feasible for real-world construction, the actual ultimate loading, which is close to its buckling pressure, can be questioned, especially compared to that of concrete. In the case of concrete, the ultimate loading is 5280 N/m², which is 23 times less than the maximum buckling pressure of 122,364 N/m². To achieve more reliable buckling factors, the geometry of the EPS model was modified to a thickness of 200 mm. With an LBA eigenvalue of 71,190 N/m², the GNA (with imperfection) yields a maximum buckling pressure of 37,322 N/m², indicating a more accurate assessment. This thickness, loaded with a factored ultimate load of 2429 N/m², exhibits a maximum deflection of 15.4 mm.

Finally, the paper recommends conducting a practical large-scale experiment on EPS domes. Further research should investigate methods for constructing curved surface EPS domes using innovations such as cast in-situ techniques and/or robotic arm technologies.

#### **Acknowledgements**

This publication has been supported by the RUDN University Scientific Projects Grant System, project No. 202247-2-000.

#### References

Adriaenssens, S., Block, P., Veenendaal, D., and Williams, C. (2014). Shell structures for architecture: form finding and optimization. London and New York: Routledge Taylor & Francis Group, 323 p.

Bushnell, D. (1981). Buckling of shells—pitfall for designers. *AIAA Journal*, Vol. 19, No. 9, pp. 1183–1226. DOI: 10.2514/3.60058.

Eisenbach, P. (2017). *Processing of slender concrete shells*—fabrication and installation. [online] Available at: http://www.uni-kassel.de/upress/online/OpenAccess/978-3-7376-0258-7.OpenAccess.pdf [Date accessed April 18, 2021].

Ellobody, E., Feng, R., and Young, B. (2014). Chapter 4 - Linear and non-linear finite element analyses. In: Ellobody, E., Feng, R., and Young, B. (eds.). *Finite Element Analysis and Design of Metal Structures*. Waltham: Butterworth-Heinemann, pp. 56–71. DOI: 10.1016/B978-0-12-416561-8.00004-4.

Farshad, M. (1992). Design and analysis of shell structures. Dordrecht: Springer-Science+Business Media, 424 p. DOI: 10.1007/978-94-017-1227-9.

Gagg, C. R. (2014). Cement and concrete as an engineering material: An historic appraisal and case study analysis. *Engineering Failure Analysis*, Vol. 40, pp. 114–140. DOI: 10.1016/j.engfailanal.2014.02.004.

Huijben, F., van Herwijnen, F., and Nijsse, R. (2011). Concrete shell structures revisited: introducing a new and 'low-tech' construction method using vacuumatics formwork. [online] Available at: http://resolver.tudelft.nl/uuid:18354f6f-2187-467f-ad98-bc815caa285b [Date accessed January 10, 2023].

Hutchinson, J. W. and Thompson, J. M. T. (2017). Nonlinear buckling behaviour of spherical shells: barriers and symmetry-breaking dimples. *Philosophical Transactions of the Royal Society A*, Vol. 375, Issue 2093, 20160154. DOI: 10.1098/rsta.2016.0154.

Ibrahim, D., Bankole, O. C., Ma'aji, S. A., Ohize, E. J., and Abdul, B. K. (2013). Assessment of the strength properties of polystyrene material used in building construction in Mbora district of Abuja, Nigeria. *International Journal of Engineering Research and Development*, Vol. 6, Issue 12, pp. 80–84.

Imran, M., Shi, D., Tong, L., Waqas, H. M., Muhammad, R., Uddin, M., and Khan, A. (2020). Design optimization and non-linear buckling analysis of spherical composite submersible pressure hull. *Materials*, Vol. 13, Issue 11, 2439. DOI: 10.3390/ma13112439.

Jovanovic, M., Vucic, M., Mitov, D., Tepavčević, B., Stojakovic, V., and Bajsanski, I. (2017). Case specific robotic fabrication of foam shell structures. *Fabrication - Robotics*, Vol. 2, pp. 135–142.

Khalaj, O., Azizian, M., Tafreshi, S. N. M., and Mašek, B. (2017). Laboratory investigation of buried pipes using geogrid and EPS geofoam block. *IOP Conference Series: Earth and Environmental Science*, Vol. 95, Issue 2, 022002. DOI: 10.1088/1755-1315/95/2/022002.

Khalaj, O., Siabil, S. M. A. G., Tafreshi, S. N. M., Kepka, M., Kavalir, T., Křížek, M., and Jeníček, S. (2020). The experimental investigation of behaviour of expanded polystyrene (EPS). *IOP Conference Series: Materials Science and Engineering*, Vol. 723, 012014. DOI: 10.1088/1757-899X/723/1/012014.

LUSAS (2017). CSN/LUSAS/1014. *Non-linear buckling analysis with initial imperfection. Customer support note*. [online] Available at: https://www.lusas.com/user\_area/documentation/1014\_Nonlinear%20Buckling%20Analysis%20with%20 Initial%20Imperfection.pdf [Date accessed January 10, 2023].

Mekjavić, I. (2011). Buckling analysis of concrete spherical shells. *Tehnički vjesnik*, Vol. 18, No. 4, pp. 633–639. DOI: 10.17265/1934-7359/2012.07.013.

Ni, X., Wu, Z., Zhang, W., Lu, K., Ding, Y., and Mao, S. (2020). Energy utilization of building insulation waste expanded polystyrene: pyrolysis kinetic estimation by a new comprehensive method. *Polymers*, Vol. 12, Issue 8, 1744. DOI: 10.3390/polym12081744.

Novoselac, S., Ergić, T., and Baličević, P. (2012). Linear and nonlinear buckling and post buckling analysis of a bar with the influence of imperfections. *Tehnički vjesnik*, Vol. 19, No. 3, pp. 695–701.

Ramli Sulong, N. H., Mustapa, S. A. S., and Abdul Rashid, M. K. (2019). Application of expanded polystyrene (EPS) in buildings and constructions: A review. *Journal of Applied Polymer Science*, Vol. 136, Issue 20, 47529. DOI: 10.1002/app.47529.

Saheed, S., Aziz, F. N. A. A., Amran, M., Vatin, N., Fediuk, R., Ozbakkaloglu, T., Murali, G., and Mosaberpanah, M. A. (2020). Structural performance of shear loaded precast EPS-foam concrete half-shaped slabs. *Sustainability*, Vol. 12, Issue 22, 9679. DOI: 10.3390/su12229679.

Semenov, A. A. (2016). Strength and stability of geometrically nonlinear orthotropic shell structures. *Thin-Walled Structures*, Vol. 106, pp. 428–436. DOI: 10.1016/j.tws.2016.05.018.

Ter Maten, R. N., Grunewald, S., and Walraven, J.C. (2013). UHPFRC in large span shell structures. In: *Proceedings of the RILEM-fib-AFGC international symposium on ultra-high performance fibre-reinforced concrete*, October 1–3, 2013, Marseille, France, pp. 327–334.

Tomas, A., Marti, P., and Tovar, J. P. (2009). Imperfection sensitivity in the buckling of single curvature concrete shells. In: *Proceedings of the International Association for Shell and Spatial Structures (IASS) Symposium 2009*, 28 September – 2 October, 2009, Valencia, Spain, pp. 1713–1721.

Vilau, C. and Dudescu, M. C. (2020). Investigation of mechanical behaviour of expanded polystyrene under compressive and bending loadings. *Materiale Plastice*, Vol. 57, Issue 2, pp. 199–207. DOI: 10.37358/MP.20.2.5366.

Wagner, H. N. R., Hühne, C., Zhang, J., and Tang, W. (2020). On the imperfection sensitivity and design of spherical domes under external pressure. *International Journal of Pressure Vessels and Piping*, Vol. 179, 104015. DOI: 10.1016/j. ijpvp.2019.104015.

## СРАВНИТЕЛЬНЫЙ АНАЛИЗ ПОТЕРИ УСТОЙЧИВОСТИ БЕТОННЫХ И ПЕНОПОЛИСТИРОЛЬНЫХ КУПОЛЬНЫХ ОБОЛОЧЕК

Хабте Йоханнес Дамир<sup>1,2\*</sup>, Марина Рынковская<sup>1</sup>, Иссайас Андей Сереке<sup>1,2</sup>

- ¹ Российский университет дружбы народов имени Патриса Лумумбы (РУДН), Москва, Россия
- <sup>2</sup> Инженерно-технологический колледж Майнефхи, Асмэра, Эритрея

#### Аннотация:

Введение: Известны исследования анализа поведения бетонных сферических оболочек при потере устойчивости. Тем не менее, отсутствуют исследования, изучающие поведение оболочек из пенополистирола при потере устойчивости. Пенополистирол характеризуется довольно низким собственным весом по сравнению с бетоном. Цель данной работы — исследование сравнительных характеристик потери устойчивости бетонных оболочек и оболочек из пенополистирола. Были приняты во внимание собственный вес и временная нагрузка 1,5 кН/м². Методы: С помощью программного обеспечения Abaqus выполнены линейный расчет устойчивости (LBA) и геометрически нелинейный расчет устойчивости (GNA) образцов куполов с учетом несовершенств формы и без их учета. Сравнительный анализ показал, что критическое давление потери устойчивости сферических оболочек из пенополистирола и бетона одинаковой геометрии составило 122 634 H/м² и 5560 H/м² соответственно. Отношение критического давления потери устойчивости к практической предельной нагрузке (постоянная нагрузка + временная нагрузка) составило 23,2 для бетона и 2,22 для пенополистирола. Более того, увеличение толщины пенополистирола со 100 до 200 мм увеличило коэффициент критической нагрузки при потере устойчивости в 15,4 раза. Максимальное смещение пенополистирола при нагрузке (15,6 мм) было в разы меньше смещения при потере устойчивости. Этот результат демонстрирует возможность изготовления оболочек из пенополистирола, при этом необходимо провести дальнейшие исследования по выбору оптимальной геометрии и механизма изготовления.

Ключевые слова: оболочки, потеря устойчивости, купол, бетон, пенополистирол.

<sup>\*</sup>E-mail: habte88eng@gmail.com

#### **Urban Planning**

DOI: 10.23968/2500-0055-2024-9-1-79-90

### NEIGHBORHOOD RENEWAL AT STAKE: FEEDBACK ON SPECULATIVE REDEVELOPMENT IN SETIF, ALGERIA

Dhia Eddine Zakaria Lacheheb<sup>1,2\*</sup>, Said Madani<sup>2,3</sup>

- <sup>1</sup> Institute of Architecture and Urbanism, University of Batna 1, Batna, Algeria
- <sup>2</sup> Lab PUViT, Ferhat Abbas University Setif 1, Setif, Algeria
- <sup>3</sup> Institute of Architecture and Earth Sciences, Ferhat Abbas University Setif 1, Setif, Algeria
- \*Corresponding author's e-mail: zakaria.lacheheb@univ.batna.dz

#### Abstract

Introduction: This paper examines a type of real estate speculation that plays a key role in urban redevelopment, characterized by densification and unaffordability. Purpose of the study: The study aims to analyze how pericentral housing in the form of a garden city is being subjected to incremental renewal in the historic core of Setif, Algeria. It reflects on UN Sustainable Development Goal #11, Sustainable Cities and Communities, in terms of relationships between housing densification, loss of green spaces, and socio-economic implications. Methods: We used a survey strategy based on observation and a sustainability indicator questionnaire as quantitative sources as well as semi-structured interviews and focus groups as qualitative sources. Results: Our study revealed that the typological shift from single-family houses to multi-family apartment buildings is not driven by changing housing preferences, but rather by a profit-oriented land-use strategy. This shift has led to affordability issues and gentrification, which in turn challenge socioeconomic cohesion. The process of densification and apartmentization causes the erosion of the architectural character of buildings and the physical characteristics of the neighborhood. The study emphasizes the importance of proactive, participatory, and inclusive methods in urban planning and management for a bottom-up approach to counteract speculative neighborhood renewal driven by liberal policies. It proposes a densification toolkit to promote the principles expressed in the sustainable development goals (SDGs).

**Keywords:** neighborhood renewal, real estate speculation, densification, social capital, gentrification.

#### Introduction

Strategic planning and local urban management are particularly crucial in developing countries that are embracing profitability and liberalization (Bennedjai and Bencherif, 2022). The National Report on Housing (National report, 2014) stated that urban areas were already crowded and that urbanization at an unprecedented rate had made the development of new suburban areas critical. Some intermediate interior cities in Algeria's fast-growing regions have doubled in size over the past 30 years (Diafat, 2016). In parallel, there are challenges with population distribution, land use, wealth, and growth of the local and national economies (Bounoua et al., 2023). This is addressed through urban consolidation and structuring public projects (Boudjabi et al., 2018) to boost housing capacity, attractiveness, and competitiveness. However, while undergoing restructuring, cities concurrently accumulate deficiencies and issues (Bibri et al., 2020). The primary focus on building the city over the city is the urban reorganization and reuse of the existing urban fabric, along with social redeployment to reduce social inequalities and curb urban sprawl and segregation (Armstrong. 2023; Neuman, 2005). The redefinition of the urban physical structure is crucial for sustainability and inclusion in redevelopment (Sharifi and Yamagata, 2016). Urban renewal continues to advocate for the enhancement of the physical environment to attract more investment opportunities, while neighborhood renewal aims to upgrade existing homes (Pinnegar et al., 2015). Various stakeholders with competing needs and interests attempt to redress housing stock quality and correct market obsolescence through redevelopment (Harris et al., 2014). Indeed, valorization and prioritization enable various forms of urban densification and occupation (Giddings and Rogers, 2021). The slow and steady adjustment and commodification have affected both the collective and individual types of inherited vacant housing stock. However, when adaptation is insufficient to meet changing socioeconomic conditions, family structures and needs, the transformation and replacement of the obsolete built form become inevitable (Amer et al., 2017; Mouaziz-Bouchentouf, 2022). Developers' speculative renewal is capital (re)investment that anticipates future demand, taking into account laws of attraction and identifying the most appropriate locations for housing or mixed-use development, commodification of space, and displacement (Cavicchia, 2023; Lees et al., 2008). It can involve the conversion, transformation, or redevelopment of single-family housing in a sequence of institutive, repletive, climax, and recessive phases, measurable in terms of building coverage, followed by urban fallow (Conzen, 1969). By doing so, it increases housing prices and, consequently, encourages overbuilding in a privately redeveloped neighborhood (Dessouky et al., 2023).

This could be the first paper to examine pericentral neighborhood renewal, building from scratch, and the correlation between the housing market and social capital in Algeria. Furthermore, this study proposes two interrelated hypotheses. First, knock down rebuild (KDR) can increase density and lead to real estate speculation. Second, speculative neighborhood renewal (SNR) may be the main reason for the shifts in demographics and typology.

There is very little monitoring and evaluation at the neighborhood level to harness available resources, stimulate central areas, and overcome the loss of welfare. Therefore, this research supports the idea that adopting a densification toolkit, morphological regulation, and an approach involving residents and stakeholders in decision-making can help mitigate the negative effects of SNR on the urban landscape and housing affordability to meet the predetermined neighborhood renewal SDGs.

Multifaceted mutations have resulted from rapid territorial and urban changes in the city of Setif (Belmahdi, 2022). The capital of the Algerian highlands now plays a more significant role in the national land development plan (SNAT 2030). We deliberately chose a former pericentral neighborhood in this mostly residential, intermediate, and monocentric city, which is experiencing visible symptoms of a brewing crisis due to the pressure of a speculative market with uncontrolled and uncoordinated redevelopment. Large-scale transformations and housing densification support our choice. While neighborhood renewal is questionable in terms of effectiveness, adequacy, and appropriateness, social capital is often overlooked.

#### **Methods**

This research primarily relies on sociological survey methodology and map analysis to study the incremental growth and site structure of a case study community. It aims to comprehend the development from housing estates to neighborhoods with changing character but lasting fame and attractiveness.

A survey was conducted over a three-month period with a randomized sample of 120 long-term neighborhood households, focusing on the KDR process, physical features, perceptions, and interactions.

An 86 % response rate based on 103 questionnaires was achieved. Semi-structured interviews were conducted with diverse stakeholders with various interests and priorities, including developers, architects, scholars, and researchers, to understand the design of patterns, construction methods, redevelopment dynamics, drivers, and governance, and determine the extent to which redevelopment affects building and block land use, typology, morphological elements, and social capital. Furthermore, we used general rules of urbanism, such as overlooking (vis-à-vis), building coverage ratio (BCR), and floor area ratio (FAR), to assess the built character.

This study aims to identify redevelopment priorities and capture the perspectives of the local community. Qualitative sources, such as field observations and informal discussions, were used alongside quantitative data sources (Table 1 and 2), most notably, survey questionnaires based on the components of urban environments, attractiveness, and a set of sustainability principles and indicators (Table 3).

We also explored alternatives for more affordable and sustainable housing supply for existing communities facing gentrification. We found that implementing certain regulations is recommended to mitigate the impact of densification and apartmentization on social sustainability.

Questionnaire framework and targeted respondents

The questionnaire was designed in two languages, Arabic and French, with the aim of reaching the highest number of respondents. Afterwards, it was administered in two different formats: online (Google form), which was sent to a previously collected mailing list and via social media, and printed (distributed and collected). The electronic form was more time-saving because the surveyor and respondent did not need a second contact. However, both methods were used to ensure a comprehensive response from case study residents, developers, scholars, and researchers.

The questionnaire was divided into eight sections. The first section, based on the filter questions, aimed to gather basic information about the respondents. The definitions of the criteria were attached to the questionnaire to provide guidance and clarification whenever needed by the respondent. Dichotomous (closed) questions used to guide the discussion were typically followed by conditional questions. Multiple-choice questions (MCQs) were used to obtain further details. The Likert scale (evaluation grid) was used for experience-based aspects and open-ended response questions for explanations of pros and cons.

#### Case study presentation

The city under consideration is one of Algeria's major cities, located 300 km northeast of the capital,

Algiers. It sits at an elevation of 1000 m above sea level and is 80 km from the coastline of the Mediterranean Sea.

Known as the capital of the High Plateaux, Setif is an example of radiocentric urban expansion, created ex nihilo. Due to its strategic location, it has become an economic magnet at the crossroads between the east-west and north-south Algerian cities, as well as the commercial hub of the region.

According to the 2018 population census, the main town has a total area of 127.30 km² and a population of 287,574 people, with a density of 3,419 persons per square kilometer and a land area of 11,641 km².

According to Prenant (1953), Setif witnessed two main waves of real estate speculation. The first one started in 1887 through the conversion of agricultural areas into housing estates, beyond the military servitude zone (Cité Levy named after the developer also called Bon marché, now Tlidjene neighborhood) between the Negro village and the Arab market, beyond the southern city gate Bab Biskra. After 1914 World War I, came the "budget" housing estate fever to relocate and reconcile, so the upper and middle class established themselves around the main retail avenues and thoroughfares. As a result, the upper and lower train station suburbs were affected by a sudden increase in value (Fig. 1).

On July 13, 1928, with Loucheur's law (French Minister of Labor), public authorities became involved in managing the housing crisis, including housing supply, slum clearance, and the renovation of substandard housing. Land prices rose sharply after the HLM and HBM housing programs, as well as real estate development, between the Constantine and Sillegue roads.

The second, "higher", suburb of the train station, established in 1930, was a garden city-style housing neighborhood designed by the architect Berardi. The district aimed to connect the planned "lower" suburb with the large, spontaneous autochthonous ("indigenous") settlement called Tandja in the north (Fig. 1). The area under consideration is located in the eastern part of the First Ring suburb on a flat site in the pericentral area of Setif, with a regular urban fabric that has almost a century of urban history. The decumanus, tramway, and railway in the south, the double track in the east, and the former city center in the west define its boundaries.

Indigenous vernacular multi-family rental houses were introverted and organized around a patio (hara), while the veranda houses surrounding the railway workers' neighborhood (RWN) were conceived as extraverted single-family houses with front gardens and low fences open to public spaces for ostentatious and supremacy reasons (Lacheheb, 2017).

A 24,000 m² area consisting of eight former regular blocks and 300 m² rectangular plots stretched along the frontage of the roads. For assertion and domination, one of the 40 x 60 m blocks was initially set up as a square, garden, and playground, but now serves as an open space for social networking empowerment. Four semi-blocks were placed to the north before the extension (Fig. 2). The neighborhood extends to 1st of November Avenue and Boulevard Port Said (Fig. 3), as the former city center expands and reorganizes its functional spaces. The case under consideration is an integral part of this expansion. The area is called both "Bled", which means "city center" in the local language, and "Cheminots", which literally means "railway workers'

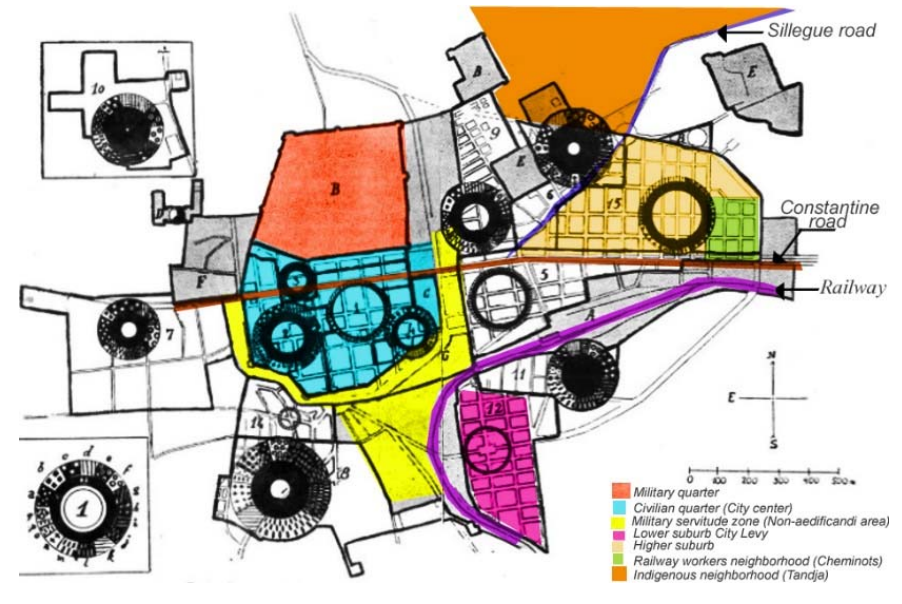


Fig. 1. Density and housing estate fever after railway passage. Source: Prenant (1953). Adapted by the authors

neighborhood". RWN stands for "railway workers' neighborhood" for the rest of the paper.

From the French occupation to postindependence, cultural and ideological changes in the area were resisted. However, the transition from a socialist to a liberal economy has led to undesirable phenomena affecting spatial justice and the balance of social structure (Colonna, 1988), particularly impacting central and pericentral neighborhoods. Their strategic location near the city center, within a 10-minute walkable radius (Fig. 3), with multiple exits, health centers, medical care, markets, shopping centers, public transport, green open spaces, playgrounds, kindergartens, primary schools, and mosques, makes this self-sufficient neighborhood attractive.

#### Data collection and analysis

Our data collection was conducted using a comprehensive approach that integrated insitu observations and a concise framework encompassing attributes specifically related to the research concepts, dimensions, and criteria listed in the previous literature review. The information was then enhanced by spatial analysis and the administration of a structured questionnaire.

First, sociodemographic data concerning the RWN users was collected to determine whether the neighborhood fostered diversity or homogeneity. Excel was used to analyze the survey findings and generate data in the form of percentages.

The housing characteristics, transformation clusters, and drivers were analyzed to examine possible causal connections.

Then the evaluation criteria were outlined as follows:

- a) Users' interaction with the features and mechanisms of the physical environment
  - b) Comfort level and quality of public facilities
- c) Aesthetic and landscape perceptions based on attractiveness and physical maintenance
- d) Users' interactions with each other to assess sociability, vibrancy, and the public realm

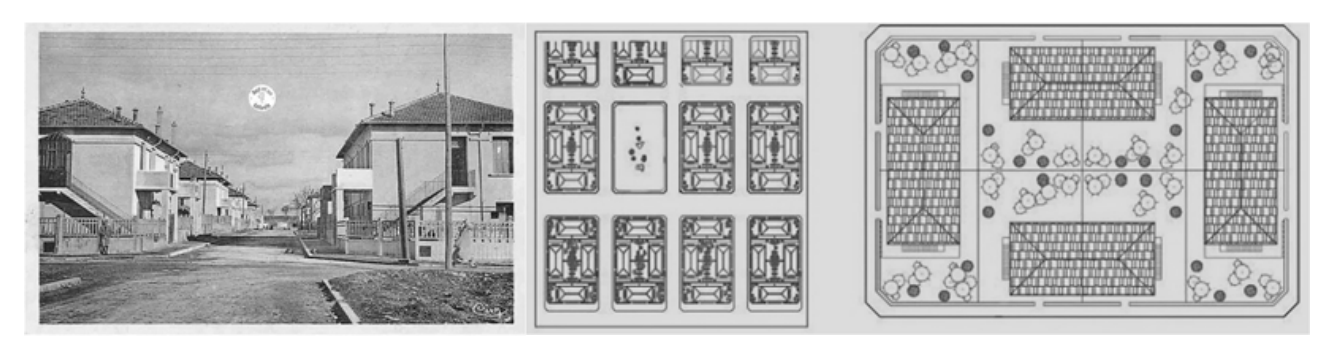


Fig. 2. Semi-detached houses with side gardens in the RWN around 1931. Source: archive, adapted by the authors

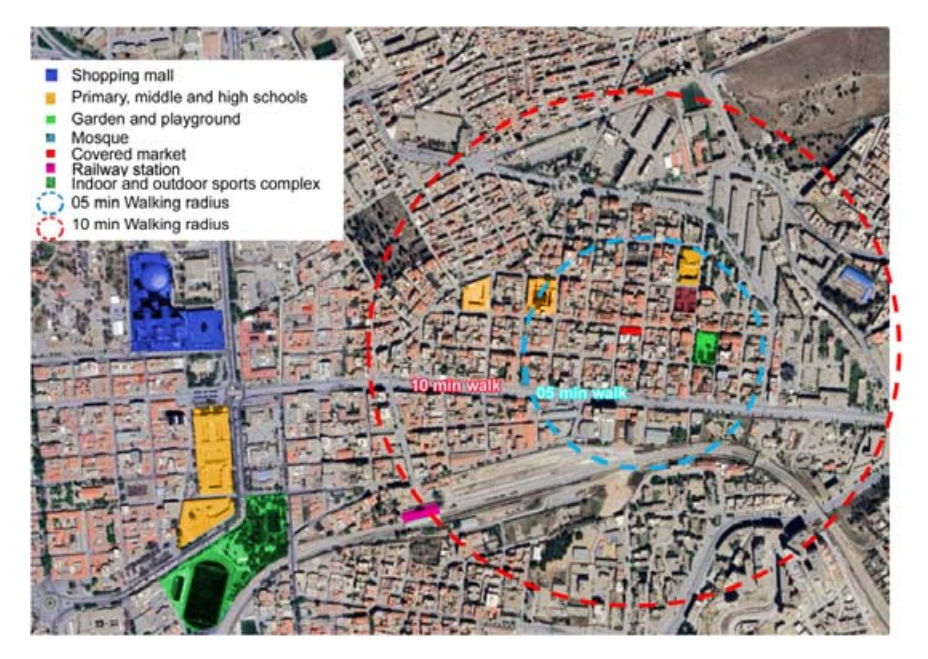


Fig. 3. Location, facilities, and walking radius. Source: Google Earth 2023, adapted by the authors

The components of the rebuilt urban environment after alterations and renewal in the neighborhood were also assessed using attractiveness indicators related to physical features, social practices, and perceptions (Table 3). The "effective" and "not effective" qualifiers assess the usability, practicality, and durability of urban environmental components and layouts. They indicate whether the built environment meets residents' expectations, with "effective" indicating a positive evaluation and "not effective" indicating a negative evaluation (Guedoudj et al., 2020). The number of responses is next to the qualifier, for example, 94 out of the total questionnaire number (103), equivalent to the percentage (91.27 %) of the total questionnaires (100 %).

#### Results

The accumulated histories of colonization, trial and error in constantly changing urban policies, and mismanagement by post-colonial regimes are believed to be key factors in deficiencies and shortages.

Table 1. Household profiles

| Users' characteristics and categorizations                    |   |                            |   |  |  |
|---|---|----------------------------|---|--|--|
|   | (N = 103)                                       | (%)                        |   |  |  |
| Gender  | Female  | 12                         | 11.65                                     |  |  |
|   | Male  | 91                         | 88.34                                     |  |  |
| Age   | 10–15   | 01                         | 0.97                                      |  |  |
|   | 15–20   | 03                         | 2.91                                      |  |  |
|   | 20–30   | 26                         | 25.24                                     |  |  |
|   | 30–50   | 69                         | 66.99                                     |  |  |
|   | 50+   | 04                         | 3.88                                      |  |  |
| Number of years<br>lived in the<br>neighborhood<br>(duration) | 0–5<br>5–10<br>10–15<br>15–30<br>30+            | 24<br>23<br>17<br>25<br>11 | 23.30<br>22.33<br>16.50<br>24.27<br>10.67 |  |  |
| Previous housing  | Apartment                                       | 64                         | 62.13                                     |  |  |
| (reference)   | Villa   | 36                         | 34.95                                     |  |  |
| Commuting   | Close   | 71                         | 68.93                                     |  |  |
| distance  | Distant   | 26                         | 25.24                                     |  |  |
| Means of transport  | Walk<br>Car<br>ownership<br>Public<br>transport | 45<br>19<br>33             | <b>43.68</b><br>18.44<br>32.03            |  |  |
| Academic level  | Uneducated Primary Secondary Higher             | 10<br>24<br>31<br>32       | 9.70<br>23.30<br>30.09<br><b>31.06</b>    |  |  |
| Income * Minimum income = 20,000 DA/month 1 DA = 0.0073 USD)  | Low<br>Moderate<br>High                         | 26<br>39<br>32             | 25.24<br><b>37.86</b><br>31.06            |  |  |
| Employment  | Student   | 22                         | 21.35                                     |  |  |
| status  | (Self)<br>employed                              | 31                         | 30.09                                     |  |  |
|   | Unemployed                                      | 27                         | 26.21                                     |  |  |
|   | Retired   | 17                         | 16.50                                     |  |  |

The process of reinvesting in the existing urban territory has only recently begun, with its pros and cons. First, the shift in the land value from the patrimonial value to the market value per square meter after the 1981 vacant housing law provided impetus for transformation. Second, the economic and political crises of 1986 sparked liberalization and increased the value of land in the aftermath of the transition from a socialist to a market economy system.

Sustainable neighborhood renewal on a house-by-house basis, without improving the transparency and fairness of decision-making and setting clear economic boundaries, is challenging. Likewise, KDR, lacking mature planning tools and local urban management, is far from being entirely positive. Even though it is still feasible and practical for rundown, old, and inefficient properties, it can generate substantial unexpected and adverse effects.

Accordingly, we divided the multifaceted findings into five sections, starting with the environmental, urban design, economic, social, and governance perspectives.

#### From an environmental perspective

In the case study, the apartment-based KDR process intensified property ownership, increased building co-ops, and improved the housing landscape.

The population density rate formula calculates the total number of residents by multiplying the number of occupied housing units by the occupancy rate per house (6.7 from the 2008 census). Originally, 72 houses had a density of 482 residents. After speculation-driven renewal, 46 houses were preserved, and 26 properties were redeveloped into an average of three-unit

Table 2. Housing characteristics

| Housing characteristics and categorizations |                                |    |       |  |  |  |
|---|--------------------------------|----|-------|--|--|--|
| of transformation                           |                                |    |       |  |  |  |
| <u>Housing</u>                              | Preserved                      | 50 | 48.54 |  |  |  |
| characteristics                             | Refurbished                    | 24 | 23.30 |  |  |  |
|   | Built from scratch             | 29 | 28.15 |  |  |  |
| <u>Type</u>                                 | Single-family house (SFH)      | 26 | 25.24 |  |  |  |
|   | Multi-family 18<br>house (MFH) |    | 17.47 |  |  |  |
|   | Apartment building (AB)        | 32 | 31.06 |  |  |  |
| <u>Use</u>                                  | Residential                    | 83 | 80.58 |  |  |  |
|   | Mixed use                      | 16 | 15.53 |  |  |  |
|   | Non-residential                | 01 | 0.97  |  |  |  |
| <u>Transformation</u>                       | Surface                        | 16 | 15.53 |  |  |  |
| driver(s)                                   | Functional                     | 14 | 13.59 |  |  |  |
|   | Reconstruction                 | 14 | 13.59 |  |  |  |
|   | Income                         | 04 | 3.88  |  |  |  |
|   | generation                     | 44 | 42.71 |  |  |  |
|   | Embellishment                  |    |       |  |  |  |

Neighborhood urban Neighborhood observations and questionnaire results environment Attractiveness Railway workers' neighborhood (RWN) **RWN** (%) indicators (N = 103)Accessibility - Safe, with some narrow sidewalks Effective 9 8.73 % - Layout, conditions, and - Footpaths with rough pavement and uneven corners comfort of streets and - Pedestrian ways easily accessible from all directions 94 91.27 % Not effective sidewalks (not suitable for mobility-impaired users) Poor maintenance of the cycling path - Rush hour congestion hindering accessibility - Limited parking availability Improved street lighting - Integration of CCTVs (security systems) - Traffic calming features near schools - Increased prices due to the proximity to the city center, 68.93 % **Affordability** Not effective 71 making it difficult for low- and moderate-income groups to Effective 32 31.07 % afford housing **Urban density** - More mixed-use buildings creating greater vibrancy and Not effective 51 49.51 % enhancing the public realm Effective 52 50.49 % **Residential density** - Conversion of SFHs into MFHs and ABs, increasing Not effective 50 48.54 % residential density Effective 53 51.46 % Distance and - Decline in privacy after KDR and increasing neighborly Not effective 74 71.84 % overlooking (vis-à-vis) conflicts 29 Effective 28.16 % Open spaces - Less open space, sun exposure and more overlooking Not effective 81 78.64 % 21.36 % Effective 22 Vegetation - Less vegetation cover and access to green spaces after Not effective 57 55.33 % 44.67 % Effective 46 Cleanliness and waste - Increasing waste due to the mismanagement of cleaning Effective 51 49.51 % management contractors, not to the population increase Not effective 52 50.49 % - Increased interpersonal interactions but decreased Social conditions & 36.89 % Effective 38 networking communal support networks after KDR - The garden provides a meeting place, playground, benches for sitting, and shelter from the weather - Shade and shelter are provided by the garden trees and Not effective 65 63.11 % surrounding coffee shops

Table 3. Indicators of urban environment and neighborhood attractiveness

apartment buildings, resulting in 52 new units. The total number of units now equals 98, equivalent to 656.6 residents, with a 35 % increase from 20 to 27 persons per hectare.

Without ancillary mechanisms, the local environment is experiencing adverse environmental effects, such as decayed and congested streets with poor air quality and pollution, accumulated trash, declining greenery, lack of parking spaces, and, consequently, straining infrastructure (Fig. 4).

The change in the urban form also increases energy and water use in the neighborhood, according to the residents' responses. It should be noted that 64.1 % of the respondents cited sun exposure and ventilation, while 57.6 % added the decline of garden surfaces, trees, and vegetation cover.

Concerns about the declining housing situation, social conditions, and the rebuilding process, often characterized by extremely high costs and longer timelines, push many residents to oppose large-scale KDR.

#### From an urban design perspective

A highly connected grid-pattern road network is beneficial for densification and enhances communication between urban spaces and buildings. With numerous access points, it ensures a transitional and bridging role. However, the increasing scale of monolithic development leads to a decline in the permeability of grid patterns (Fig. 5).

The implementation of housing densification focuses on upgrading physical and demographic conditions rather than improving living conditions. KDR is more common in 40–70-year-old housing due to outdated built forms or inefficient renovations. KDR is more prevalent in areas parallel to tramways and gardens, with no redevelopment plan, but opportunistic logic. The survey revealed that 80.4 % of respondents confirmed that overlooking, the distance between newly built buildings, negatively impacts privacy. The (re)built environment is not always shaped according to densification capacity; the extreme BCR at ground level is chosen

automatically. Horizontal extensions and vertical uplifts often violate regulations, increasing the height and street aspect ratio (Fig. 6).

The study found that although ABs in high-density environments offer amenities, transportation, and walkability, discrepancies in physical characteristics and architectural treatment led to a loss of positive morphological qualities.

#### From an economic perspective

The demographic demand for affordable housing is increasing; however, the impact of densification on affordability is complex. Limited land availability and unbalanced density-based housing supply barely ensure housing affordability.

The house price-to-income ratio in Algeria is a reliable indicator of housing affordability (Bellal, 2009), with 71 % of the respondents stating ownership as the dominant tenure (Centre for Affordable Housing Finance in Africa, 2021). Middle-income families need to save their annual income for over nine years to purchase an average housing unit (Deniz et al., 2008). According to the interviewed private real estate agency, the private real estate market in Algeria has seen a 26.1-fold increase in 2022 due to such factors as location and reputation. However, the gap between the National Minimum Wage (NMW), approximately \$145 per month (\$1 = 137.55 DA), which amounted to \$1,740 per year in 2023, and real estate developer prices ranging between \$8,725 and \$11,632 per square meter, is significant. Moreover, 38 % of respondents believe that neighborhood house prices are controlled by real estate developers, making private market houses unaffordable for most residents of Setif. Likewise, higher prices for newly built houses also contribute to inefficiencies in the housing sector in the RWN.

According to the interviewed single respondents and young couples, the SNR resulting supply has exacerbated affordability challenges for lower- and moderate-income groups. This has created new opportunities for high-income individuals, especially

those who have faced income shocks or job losses due to the COVID-19 pandemic.

#### From a social perspective

Social stress, often seen as a direct result of density, seems to have been reduced by the presence of urban voids. This gender-inclusive urban space element is associated with numerous positive outcomes for urban liveability, such as physical and mental health benefits (Sugiyama et al., 2018). It allows neighbors of different age groups from different blocks to sit together, which is particularly valuable during summer and during Ramadan after evening prayers. Such a creative strategy is equally valuable for densification, serving as a buffer zone for social and cultural activity. It represents a dialectical amalgam that connects public and private interests, thereby increasing the economic and social benefits for the community of residents. From a garden to a playground, and a meeting place after rehabilitation, this urban void is crucial to address smaller dwelling units and apartment living resulting from densification (Nebbad et al., 2023). During Covid-19, these voids were valuable assets for hosting isolated neighbors.

The co-ownership status (property of La Société Coopérative des Chemins de Fer de Sétif) and non-transferability have been key to preserving these voids against infill development. Indeed, the residents' associations opposed attempts to build the garden, as they considered the high cost of social connectivity, public realm restoration, and the recovery of place memory. A total of 19.7 % of the respondents experienced financial, social, and emotional costs due to displacement, resulting in the loss of proximity to parents, friends, and relatives, leading to community dissolution and gentrification.

Young and elderly respondents expressed confusion about KDR demolitions, resulting in displacement, and dissatisfaction with environmental alterations leading to high costs, inconvenience, and unpopularity (Power, 2009), negatively impacting surrounding neighborhoods.

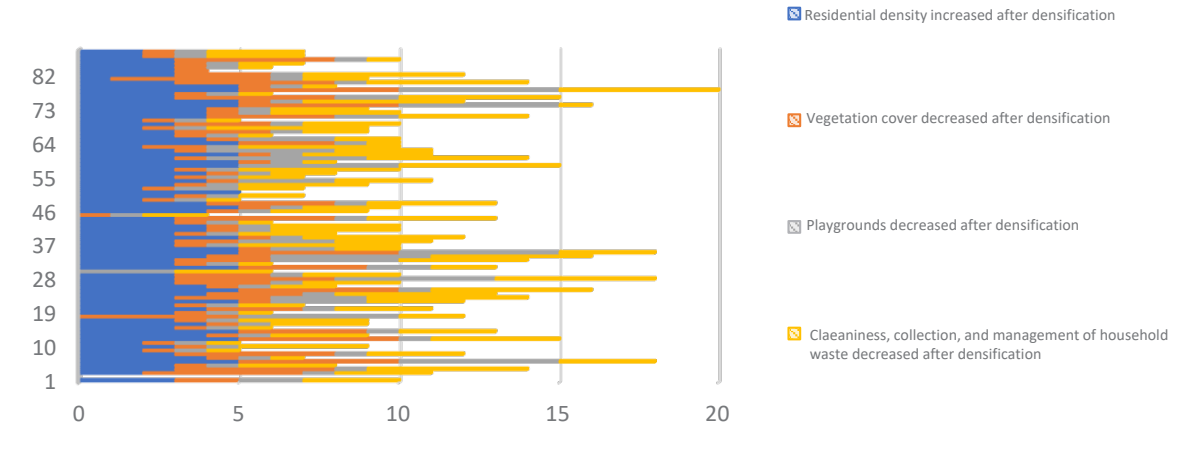


Fig. 4. Increasing residential density / vegetation cover, playgrounds, and cleanliness. Source: survey results

#### From a governance perspective

The public administration's disengagement in managing these renewal operations is disturbing and has a negative impact on the quality of the urban environment.

Conversely, the residents acknowledged that private development is not favorable to shared governance. Many respondents opposed a topdown structure because it primarily concerns their own built environment and quality of life. Although the survey did not mention governance questions, concerns regarding control and responsibilities surfaced during the interviews. The residents are recognizing the limitations of a resident-centered approach, and there is a noticeable divergence in opinions about governance when it comes to openended questions. There is a 50-50 split between those who demand top-down regulations and those who advocate for dependent residents within a corporate environment, along with a complaint system and a client satisfaction approach. Such disagreements affect the performance of local management in the neighborhood.

SNR lacks resident involvement in decision-making, yet their position is critical. Early consultation and inclusion of residents with diverse backgrounds are crucial for the success of urban renewal schemes. Moreover, top-down regulations or voluntary standards are not the only mechanisms to achieve sustainability in urban development. There are also co-regulation and self-regulation.

#### Discussion

In the late 1980s, public spending cuts led to a shift in housing policy funding, resulting in the withdrawal of costly housing and refurbishment programs, and prioritizing new housing units over preserving existing dwellings. As a result, housing renewal initiatives are being transferred to new entities because existing institutions are unable to deliver new housing at a local level (Djafri et al., 2021).

When the public administration becomes increasingly disengaged from urban renewal, the private sector's growing involvement in KDR is seen as a gentrification driver favoring speculative markets and real estate development. Indeed, with building from scratch becoming a legitimized tool,

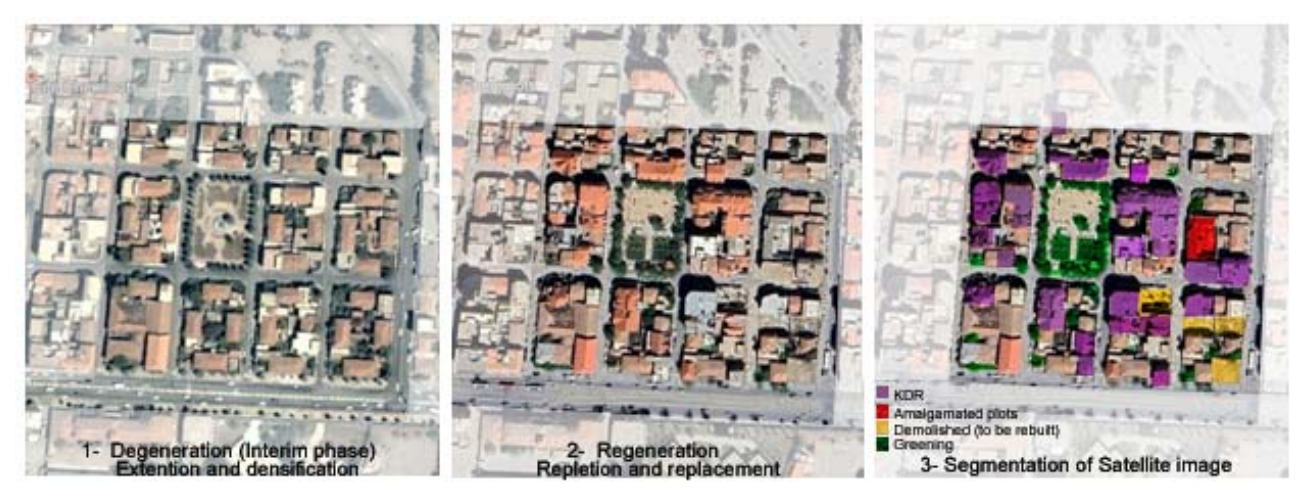


Fig. 5. Building footprint segmentation related to the RWN. Source: Google Earth 2004–2023, adapted by the authors



Fig. 6. Apartment buildings with increasing FAR in the RWN. Source: authors (2023)

69 % of respondents viewed the trickle-down public strategy and laissez-faire attitude as abandonment, with concerns that local authorities may relocate residents far from their social networks.

The study found that inadequate inherited housing stock, unbalanced supply and demand, and delays in public rental housing programs exacerbate space shortages for growing families. Real estate developers capitalize on this opportunity to increase housing density and, thereby, their profitability. Speculators often purchase older, centrally-located properties with low-income and middle-class tenants who may be vulnerable to tempting offers. However, certain types of housing stock and locations are more vulnerable, such as blocks surrounding the garden, which are undergoing extensive regeneration due to access to green spaces and recreational opportunities (Fig. 7).

Multimodal transportation networks, including buses, taxis, trains, and trams, are being developed as thoroughfares with mixed uses and commercial functions. Road networks, especially tramway routes, provide services that are accessible by car and within walking distance. Location, housing ownership, and distance from the city center are important factors in shaping identity and social status. The key drivers of SNR include the growing household needs for accommodation, identity creation, and income generation.

31 % of the respondents approved the shift to multi-family housing (not necessarily in ABs), but 63 % confirmed the emergence of a new pattern of apartment buildings in the RWN (Fig. 8). With over 26 with KDR out of 72 houses (37 %) (Fig. 5), we recognize this shift in housing pattern and typology, leading to a 35 % increase in population density, which is even higher around the garden and multimodal transportation axis (Fig. 7). Both the surrounding neighborhoods

city center experience spillover effects. The interviewed developers confirmed that they prioritized maximizing FAR over plot and block structures. In doing so, they ignored the integration of buildings with other morphological elements. They neglected other elements, such as the size, proportion, and style of the openings. This led to increased building coverage, heterogeneous urban patterns, and vertical roughness, thereby creating a patchwork landscape. Renewal was limited to replacing semi-detached villas with pitched roofs with higher flat-roofed blocks, affecting housing stock consistency and negatively impacting infrastructure, facilities, and satisfaction, particularly in historic urban areas. This disregard for part-to-whole relationships in the urban form has significant implications for housing infrastructure and satisfaction.

The involvement of building professionals in neighborhood renewal led to increased speculation and a surge in prices due to the focus on redevelopment potential and densification capacity. This urban dynamic resulted in significant price increases in the first and second rings of the city over the past three decades. This intensified speculation caused land prices to soar, resulting in the condemnation of traditional urban fabrics and the proposal of functional solutions to transform architectural and urban morphology, evolving from single plots of SFH units to large-scale MFH blocks and ABs (Fig. 8). In addition, large-scale neighborhood renewal has accelerated.

However, the change in the urban form is not necessarily an adverse effect, but when coupled with overlooking (vis-à-vis) and the decline in garden surfaces, trees, and vegetation cover, it can have negative consequences. By 2023, some demolished properties with high potential were still vacant despite the decline in prices following bans on apartment building permits.



Fig. 7. Redevelopment magnets. Source: authors

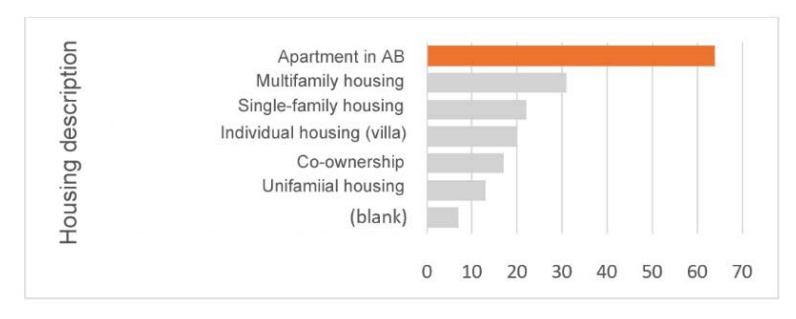


Fig. 8. Shift in housing type and typology from SFHs to ABs. Source: survey results

A part-to-whole renewal program can provide energy and time savings, economic advantages, and community benefits, thereby contributing to a sustainable environment. Furthermore, a participatory approach and local management are crucial for mitigating residents' reactions.

#### Conclusion

This study examines the urban landscape of the RWN from a morphological process perspective to understand how individual plot changes impact the urban environment.

Studying the relationships between socioeconomic changes and housing densification will enhance the theoretical framework for a better understanding of the developmental cycle with morphological periods and the conceptualization of the gradual transformation of the urban landscape from adjustment and repletion to climax. The development of the case study goes through three main phases: generation, degeneration, and regeneration. Generation begins with the cooperative society of railway workers in Setif, followed by the transformation and densification of single-family houses. Degeneration is the interim phase, followed by regeneration, which involves the proliferation of multi-family houses and apartment buildings.

The study found that partnerships between landowners, contractors, and developers have accelerated the process of SNR, with building from scratch becoming the new modus operandi. Densification alters cityscapes, neighborhood character, and residents' redeployment, with quantity issues and profits becoming more important than the hierarchical arrangement of morphological elements.

The complex process of urban renewal is a social and technical partnership that requires a multifaceted approach involving politicians, designers, and the community. Factors such as a lack of corporate mechanisms, communication issues, unequal public participation, misguided regulations, and an immature

legal framework hinder the renewal process. Urban renewal aims to improve transparency, fairness, and community involvement. Intrinsically sociological, it is not just about physical and financial aspects, but also about cultural, economic, and political aspects. To create a better society, the living space must be reconstructed according to the inherent values of housing in the neighborhood and changing socioeconomic contexts, as well as residents' expectations, promoting sustainability and inclusion.

Aposteriori, on the one hand, prioritizing FAR over building heights, types, setbacks, and street widths limited the necessary latitude and flexibility in the relationship between the plan and (re)development to provide more coherence to the renewal process in a responsive planning approach. On the other hand, under-prioritizing sustainability goals leads to speculation, gentrification, unbalanced affordability, and difficulty in accessing decent housing for lowand moderate-income households.

Although this study only covers the RWN, the findings apply to other surrounding neighborhoods and monocentric Algerian cities. It offers a nuanced vision to provide decision-makers with insights that can enable more affordable housing and guide socially sustainable strategies, prompting them to reconsider applied housing densification and SNR processes.

An additional thorough investigation would logically follow this study. The first step involves a comparison with another pericentral neighborhood undergoing significant transformation to determine if the processes have similar drivers and outcomes. The second step involves a morphological investigation before and after new planning decisions regarding restrictions on apartment buildings in subdivisions. A more holistic approach is needed to understand correlations and make evidence-based attempts to assess post-occupancy performance in a way that targets the core obstacles to sustainability.

#### References

Amer, M., Mustafa, A., Teller, J., Attia, S., and Reiter, S., (2017). A methodology to determine the potential of urban densification through roof stacking. *Sustainable Cities and Society*, Vol. 35, pp. 677–691. DOI: 10.1016/j.scs.2017.09.021.

Armstrong, G., Wilkinson, S., and Cilliers, E. J. (2023). A framework for sustainable adaptive reuse: Understanding vacancy and underuse in existing urban buildings. *Frontiers in Sustainable Cities*, Vol. 5. DOI: 10.3389/frsc.2023.985656.

Bellal, T. (2009). Housing supply in Algeria: affordability matters rather than availability. *Theoretical and Empirical Researches in Urban Management*, Vol. 4, No. 3 (12), pp. 97–114.

Belmahdi, H. S. and Djemili, A. (2022). Urban landscape structure anatomy: Structure patterns and typology identification in the space-time of Setif City, Algeria. Frontiers of Architectural Research, Vol. 11, No. 3, pp. 421–439. DOI: 10.1016/j.foar.2021.12.004.

Bennedjai, R. and Bencherif, M. (2022). Local urban management for improving the quality of life in Algerian collective housing estates. *Journal of Urban Planning and Development*, Vol. 148, Issue 2. DOI: 10.1061/(ASCE)UP.1943-5444.0000820.

Bibri, S. E., Krogstie, J., and Kärrholm, M. (2020). Compact city planning and development: Emerging practices and strategies for achieving the goals of sustainability. *Developments in the Built Environment*, Vol. 4, 100021. DOI: 10.1016/j.dibe.2020.100021.

Boudjabi, N. H., Bouzahzah, F., and Bouchareb, A. (2018). Urban strategies for a renewal of Algerian Cities: Constantine of tomorrow. *Civil Engineering and Architecture*, Vol. 6, No. 1, pp. 18–24. DOI: 10.13189/cea.2018.060102.

Bounoua, L., Bachir, N., Souidi, H., Bahi, H., Lagmiri, S., Khebiza, M. Y., and Nigro, J. (2023). Sustainable development in Algeria's urban areas: population growth and land consumption. *Urban Science*, Vol. 7, Issue 1, 29. DOI: 10.3390/urbansci7010029.

Cavicchia, R. (2023). Urban densification and exclusionary pressure: emerging patterns of gentrification in Oslo. *Urban Geography*, Vol. 44, Issue 7, pp. 1474–1496. DOI: 10.1080/02723638.2022.2100174.

Centre for Affordable Housing Finance in Africa (2021). 2021 Housing Finance in Africa Yearbook. Johannesburg: Centre for Affordable Housing Finance in Africa, 258 p.

Colonna, F. (1988). Marc Côte, L'Algérie ou l'espace retourné. *Annales. Histoire, Sciences Sociales*, Vol. 43, Issue 6, pp. 1406–1409. DOI: 10.1017/S0395264900073807.

Conzen, M. R. G. (1969) Alnwick, Northumberland: a study in town-plan analysis Institute of British Geographers Publication 27, 2<sup>nd</sup> edt. London: Institute of British Geographers, 131 p.

Dessouky, N., Wheeler, S., and Salama, A. M. (2023). The five controversies of market-driven sustainable neighborhoods: an alternative approach to post-occupancy evaluation. *Social Sciences*, Vol. 12, Issue 7, 367. DOI: 10.3390/socsci12070367.

Deniz, B., Peltier, N., Buckley, R., De Brular, L., and Larbi, H. (2005). The Macroeconomic and Sectoral Performance of Housing Supply Policies in Selected MENA Countries: A Comparative analysis. [online] Available at: http://documents.worldbank.org/curated/en/724091468248086869/The-Macroeconomic-and-sectoral-performance-of-housing-supply-policies-in-selected-MENA-countries-a-comparative-analysis [Date accessed August 4, 2023].

Djafri, R. and Osman, M. M. (2021). Housing crisis in Algeria: challenges and perspectives. *Planning Malaysia*, Vol. 19, Issue 5, pp. 220–232. DOI: 10.21837/pm.v19i19.1073.

Diafat, A. and Madani, S. (2016). Urban changes in the city of Setif, Algeria: Colonial and postcolonial periods. In *Urban Planning in North Africa* (1st ed.). Routledge. DOI: 10.4324/9781315548753.

Giddings, B. and Rogers, R. (2021). Compacting the city centre: densification in two Newcastles. *Buildings and Cities*, Vol. 2, No. 1, pp. 185–202. DOI: 10.5334/bc.74.

Guedoudj, W., Ghenouchi, A., and Toussaint, J. Y. (2020). Urban attractiveness in public squares: the mutual influence of the urban environment and the social activities in Batna. *urbe. Revista Brasileira de Gestão Urbana*, Vol. 12, e20190162. DOI: 10.1590/2175-3369.012.e20190162.

National report on housing for the Conference on Housing (2014). [online] Available at: https://habitat3.org/wp-content/uploads/National-Report-Africa-Algeria-Final-in-English.pdf [Date accessed August 4, 2023].

Harris, L. R., Watts, M. E., Nel, R., Schoeman, D. S., and Possingham, H. P. (2014). Using multivariate statistics to explore trade offs among spatial planning scenarios. Journal of applied ecology, Vol. 51, Issue 6, pp. 1504-1514. DOI: 10.1111/1365-2664.12345.

Lacheheb, D., Madani, S., and Ballout, A. (2017). Housing densification: Transformation or urban renewal (Case study for subdivision in Setif, Algeria). International conference on working class districts 2017 (Vienna, Austria), University of Applied Sciences FH Campus Wien, WienerWissens-Welt, pp. 99–105.

Lees, L. (2008). Gentrification and Social Mixing: Towards an Inclusive Urban Renaissance? *Urban Studies*, Vol. 45, Issue 12, pp. 2449–2470. DOI: 10.1177/0042098008097099.

Mouaziz-Bouchentouf, N. (2022). De la villa à l'appartement. Analyse des parcours résidentiels dans les quartiers périphériques d'Oran (Algérie). *Territoire en mouvement Revue de géographie et aménagement*, Vol. 52. DOI : 10.4000/tem.9038.

Nebbad, T., Diafat, A., and Madani, S. (2023). Sustainable renewal of an empty block to public urban space: gentrification of the railway workers' housing estate and its garden's urban interface, Sétif, Algeria. *Green Building & Construction Economics*, Vol. 4, Issue 1, pp. 199–213. DOI: 10.37256/gbce.4120232241.

Neuman, M. (2005). The compact city fallacy. *Journal of Planning Education and Research*, Vol. 25, Issue 1, pp. 11–26. DOI: 10.1177/0739456X04270466.

Pinnegar, S., Randolph, B., and Freestone, R. (2015). Incremental urbanism: characteristics and implications of residential renewal through owner-driven demolition and rebuilding. *Town Planning Review*, Vol. 86, No. 3, pp. 279–301. DOI: 10.3828/tpr.2015.18.

Power, A. (2009). Housing and sustainability: demolition or refurbishment? *Urban Design and Planning*, Vol. 163, Issue 4, pp. 205–216. DOI: 10.1680/udap.2010.163.4.205.

Prenant, A. (1953). Facteurs du peuplement d'une ville de l'Algérie intérieure : Sétif. *Annales de Géographie*, Vol. 62, No. 334, pp. 434–451. DOI: 10.3406/geo.1953.13052.

Sharifi, A. and Yamagata, Y. (2016). Resilient urban planning: major principles and criteria. *Energy Procedia*, Vol. 61, pp. 1491–1495. DOI: 10.1016/j.egypro.2014.12.154.

Sugiyama, T., Carver, A., Koohsari, M. J., and Veitch, J. (2018). Advantages of public green spaces in enhancing population health. *Landscape and Urban Planning*, Vol. 178, pp. 12–17. DOI: 10.1016/j.landurbplan.2018.05.019.

# РЕКОНСТРУКЦИЯ РАЙОНА: О ВЕНЧУРНОМ СТРОИТЕЛЬСТВЕ В СЕТИФЕ, АЛЖИР

Дхиа Эддин Закария Лачехеб<sup>1,2\*</sup>, Саид Мадани<sup>2,3</sup>

<sup>1</sup>Институт архитектуры и урбанизма, Университет Батна 1, Батна, Алжир

<sup>2</sup>Лаборатория PUViT, Университет Сетиф 1, Сетиф, Алжир

<sup>3</sup>Институт архитектуры и наук о земле, Университет Сетиф 1, Сетиф, Алжир

\*E-mail: zakaria.lacheheb@univ.batna.dz

#### Аннотация

Введение: В статье рассматривается один из типов спекуляции недвижимостью, который играет ключевую роль в переустройстве городской среды и характеризуется уплотнением застройки и недоступными ценами. Цель исследования: проанализировать, как жилье, расположенное вокруг центра, в форме города-сада претерпевает постепенное обновление в историческом центре Сетифа, Алжир. Исследование отражает цель ООН в области устойчивого развития № 11 (устойчивые города и населенные пункты) с точки зрения взаимосвязи между уплотнением застройки, сокращением зеленых насаждений и социально-экономическими последствиями. Методы: В качестве количественных источников мы использовали опрос, основанный на наблюдении, и анкету по показателям устойчивого развития, а в качестве качественных источников — полуструктурированные интервью и фокус-группы. Результаты: Исследование показало, что типологический сдвиг от жилых домов, предназначенных для проживания одной семьи, к многоквартирным домам обусловлен не изменением предпочтений в выборе жилья, а ориентированной на прибыль стратегией землепользования. Этот сдвиг привел к проблемам доступности жилья и джентрификации, которые, в свою очередь, нарушают социально-экономическую сплоченность. Процесс уплотнения и перехода к проживанию в квартирах приводит к разрушению архитектурного облика зданий и физических характеристик района. В исследовании подчеркивается важность проактивных, коллективных и инклюзивных методов в городском планировании и управлении в целях реализации восходящего подхода, направленного на противодействие спекулятивному обновлению кварталов, вызванному либеральной политикой. Предлагается набор инструментов, связанных с уплотнением застройки, для продвижения принципов, отраженных в целях устойчивого развития.

**Ключевые слова:** реконструкция района, спекуляция недвижимостью, уплотнение, социальный капитал, джентрификация.

#### BUFFER ZONE POLICY AND ITS IMPACT ON THE LAND VALUE AND THE QUALITY OF THE BUILT ENVIRONMENT IN WORLD HERITAGE SITES: THE CASE OF KAMPUNG JAWA, MELAKA, MALAYSIA

Seyed Mohammad Mousavi<sup>1</sup>, Shariyeh Hosseininasab<sup>2</sup>, Wagas Ahmed Mahar<sup>3,4\*</sup>

- <sup>1</sup> Department of Architectural Engineering, Faculty of Art and Architecture, Persian Gulf University, Bushehr, Iran
- <sup>2</sup> Department of Architecture, COMSATS University Islamabad (CUI), Lahore Campus, Lahore, Pakistan
- <sup>3</sup> Department of Architecture, Faculty of Architecture and Town Planning, Aror University of Art, Architecture, Design and Heritage, Sukkur, Pakistan
- <sup>4</sup> Sustainable Building Design (SBD) Lab, Department of Urban and Environmental Engineering (UEE), Faculty of Applied Sciences, Université de Liège, Liège, Belgium

#### **Abstract**

Introduction: Buffer zones in the context of World Heritage sites play an important role in protecting historic monuments and buildings, as well as their adjacent conservation areas, from disruptions caused by urban development. However, properties within the boundaries of buffer zones may be subject to legislative limitations and restricted construction regulations. This may affect the market value of these properties and make them unfavorable for public and private investors. Purpose of the study: The study aims to critically analyze the impact of buffer zone policy on urban development, specifically on the land value and the quality of the built environment in the context of World Heritage sites. The case study for this research is Kampung Jawa (KJ) in the World Heritage City of Melaka, Malaysia. Methods: A combination of qualitative and quantitative methods was used to conduct this research. The required data was gathered through direct observations, semi-structured and informal interviews with stakeholders and local authorities, as well as a review of available statistical data and maps. A site observation and a questionnaire survey were conducted to examine all the structures in KJ. Results: The research findings revealed that the low land value of buffer zones might be caused by several context-specific conditions, eventually turning them into greyfields. The research recommends a design solution for the area. The research also suggests that certain decisions at the policy-making level, including the involvement of all stakeholders, can be the key to improving the land value and property market within buffer zones.

Keywords: buffer zone; World Heritage sites; land value; grey field; Malaysia.

#### Introduction

A buffer zone is an impartial area located between two states, serving to separate them in order to protect each other from the other's opposing forces (Martin and Piatti, 2008; Pendlebury et al., 2009; thefreedictionary.com, 2014). In general, the main function of buffer zones is to protect the core zone from external disturbances. This protection should be in line with the improvement of the area, as well as the benefits for the local population (Münch et al., 2016). The purpose of a buffer zone is both normative and technical (Martin and Piatti, 2008). The protection of buffer zones not only takes into account the "structural and technical" issues of historic environments but also protects their "functional" and "visual" aspects (Habibi et al., 2015; Martin and Piatti, 2008; Moradi et al., 2014).

In controlling the transition between the heightened protection of World Heritage sites and the surrounding territories, a buffer zone may set limits to

protect views, settings, land uses, and other aspects, but may also positively encourage developments that would be beneficial to the site and the community (Daneshmandian et al., 2020; National Trust and English Heritage, 2011). Neumann (1997) mentions some examples in various locations where the creation of buffer zones leads to new state limitations and interventions in land use. These legislative limitations may reduce property demand and make buffer zones unattractive for investors, as they would prefer to invest in surrounding modern areas with fewer building restrictions and higher profits. This may cause buffer zones to remain underdeveloped and fail to respond to market demands, while redevelopments are quickly taking place in the surrounding areas. These underdeveloped areas lead to the emergence of grey fields, which decrease the potential land value of buffer zones. The grey fields located in the buffer zones of World Heritage sites have more specific potential compared to the

<sup>\*</sup>Corresponding author's e-mail: architectwagas@hotmail.com

physical properties that other grey fields may have. This research takes KJ in Melaka, Malaysia, as a case study to investigate the potential impacts of buffer zone policy on the land value in the context of World Heritage sites. It attempts to address the consequences of changes in the land value for the condition of the built environment in this area.

#### Literature Review

In the context of World Heritage sites, a buffer zone generally acts as a support area around the heritage properties by providing an additional layer of protection. The primary objective is twofold: first, to ensure the conservation of the protected area by regulating undesirable or damaging influences; second, to support necessary protective measures while maintaining the progressive interface of the core zone with the adjacent zone. It is therefore anticipated that a buffer zone provides a context for heritage governance by incorporating the surrounding landscape with the core zone (Palaiologou and Griffiths, 2019; Schlee, 2017).

Therefore, a buffer zone is an area surrounding the nominated property that has complementary legal and/or customary restrictions placed on its use and development in order to give an added layer of protection to the property (UNESCO, 2019). The definition of a buffer zone in the context of World Heritage sites has evolved from its original form in 1977 to the most recent one outlined in the 2019 version of the Operational Guidelines for the Implementation of the World Heritage Convention (UNESCO, 2008). Before 1990, buffer zones were only considered as the inner strips of a protected core zone situated next to the boundaries that might result in disconnecting the property from its surroundings. Peripheral zones encompassing areas located immediately outside the boundaries were the redefinition of such zones in 1993 (Gilmour and Van San, 1999).

In policy and practice, however, implementing the buffer zone theory has several impacts on area development and the life of the local community. According to Wells and Brandon (1993), the main function of buffer zones is to protect core zones, while generating profits for local people is of secondary importance. Furthermore, many researchers have noted the failure of buffer zones in numerous projects, as they did not plan to buffer the core zone in order to enhance local livelihoods (Martino, 2001). Based on various definitions of buffer zones, they suggest constraints on the land use distribution of such areas (Neumann, 1997). Additionally, some implications of buffer zone policy represent restrictions on certain human activities within the area (Meffe and Carroll, 1994). Numerous studies have tested the efficacy of buffer zones; however, most of them focus on the ecological buffering functions in comparison with the socioeconomic ones (Heinen and Mehta, 2000).

Nonetheless, the best description for a buffer zone suggests that the area should create mutual support between the conservation area and benefits for the local community (Habibi et al., 2015; Short, 2012; Tavernor, 2007).

In the context of World Heritage properties, buffer zones are delineated areas at the periphery of the core zone that contribute to the preservation, management, integrity, and sustainability of the World Heritage area with regard to its Outstanding Universal Value (OUV) (Martin and Piatti, 2008). Buffer zones are intended to simultaneously reduce individual impacts on conservation areas and address the socioeconomic demands of the affected people (Ahmad et al., 2012). However, buffer zones can help establish a significant system that contributes to the benefits of World Heritage sites for stakeholders and local communities, in order to develop a sustainable network (UNESCO, 2011). Buffer zones should be considered as integral parts of the state party's commitment to the protection and management of the World Heritage sites, as effective management and protection are essential requirements for World Heritage properties. Nonetheless, buffer zone policy is only one of the tools to ensure the management and protection of heritage sites. While the fundamental features of buffer zones are common for cultural, natural, and mixed properties, the implementation of buffer zones would be different for each specific property (Martin and Piatti, 2008). A buffer zone is not just a secondary zone meant to support a primary zone, but rather an equal, complementary, and inseparable part of the core zone. This statement reinforces the idea that planning the conditions and boundaries of inscribed zones, buffer zones, and even tertiary zones must be designed in tandem. In addition to visual and physical characteristics, buffer zones also interact with the natural environment, traditions, local knowledge, moral or social aspects from both the past and present, informal activities, and other intangible attributes of cultural heritage environments (Martin and Piatti, 2008).

KJ as the Most Significant Part of the Buffer Zone in Melaka

Malaysia has many heritage sites, most of which have buffer zones around them. Melaka, located in southwest Malaysia, was recognized as a World Heritage city by UNESCO in 2008 due to its OUV (Mohd-Isa et al., 2011). For this research, Kampung Jawa (KJ) in Melaka was considered as a case study after shortlisting six other heritage sites in Malaysia. The purpose of this study was to review the impact of the buffer zone policy on the land value and, consequently, the quality of the built environment in the area. All the shortlisted cases were selected based on specific criteria, including being a significant heritage site, the implementation of buffer zone policy on the site, and being affected

by buffer zone policy over time (Fig. 1a). After reviewing the shortlisted cases and conducting initial field surveys, it was determined that KJ best met the specified criteria. Furthermore, the team found it more convenient to gather data in the KJ case due to the easy accessibility of the site.

KJ is located in the buffer zone of the historic city of Melaka, encompassing an area of 6.5 acres on the northern bank of the Melaka River, known as the origin of urban development for Melaka city (Wahid et al., 2011). It is bounded by Kee Ann and Pasar Baru streets. Bunga Raya Street is a significant local trading area located in the eastern part of KJ. The history of KJ can be traced back to the beginning of the Melaka Sultanate around the 15th century. In fact, it was a settlement site for fishermen, particularly traders from Java (Liang, 1983). Before 1988, KJ was a dynamic area with a variety of activities, including a traditional bazaar, a municipal market, and various types of informal activities. However, KJ's condition deteriorated after the collapse of the municipal market in 1988. Similarly, local traditional businesses, especially bazaars and vendor activities, were affected and consequently declined. Furthermore, the role of the Melaka River as the main transportation hub and river activities have decreased over the years. In addition, a few setbacks, including the relocation of taxi and bus stations far away from the new site, deteriorated KJ's status. The depopulation of the area increased when the local inhabitants left KJ after two fire disasters, one in the 1960s and the other in the 1990s (Wahid et al., 2011). As a result, KJ was transformed into a residential slum area (Fig. 1b). Meanwhile, the construction of large new commercial buildings outside of KJ significantly decreased the site's economy. While there are some lively activities within the site, their unfavorable condition cannot compete with the new commercial developments in nearby areas. Therefore, despite being in a strategic area, KJ is now underdeveloped and suffering from a low-density built environment compared to its neighboring districts. The combination of the abovementioned facts turned KJ into a grey field.

Given the historical and socioeconomic significance of this area, there is a need to restore the site's importance and develop its potential by identifying significant factors that can enhance the land value of this historic area of the city through sustainable urban approaches.

#### Methods

In order to create a successful revitalization approach in grey fields within buffer zones, it is important to determine the significant contributing factors that affect the growth and decline of the land value in the context of the urban fabric, which ultimately affects the spatial quality of the environment. After reviewing the available literature and considering the situation and context requirements, five factors were identified for this study: built and unbuilt area ratio, density, land use distribution, quality of existing buildings and structures, social vitality, and active frontage of buildings. The data was collected through available documents and statistics, GIS maps, field surveys, site observation, and interviews. The observation was conducted by going door to door, recording events on-site, and documenting building properties that were significant in contributing to the land value and spatial quality of the area. After mapping the collected data, the next step was to interview local residents and members of the community who worked and lived on the site. The goal was to identify the strengths, opportunities, weaknesses, and threats of the site from the stakeholders' points of view. Furthermore, a survey of individual buildings was conducted based on identified factors and plot ratio, and data was collected from local authorities. This data was used to triangulate a synthesized map showing land values. Later, local authorities

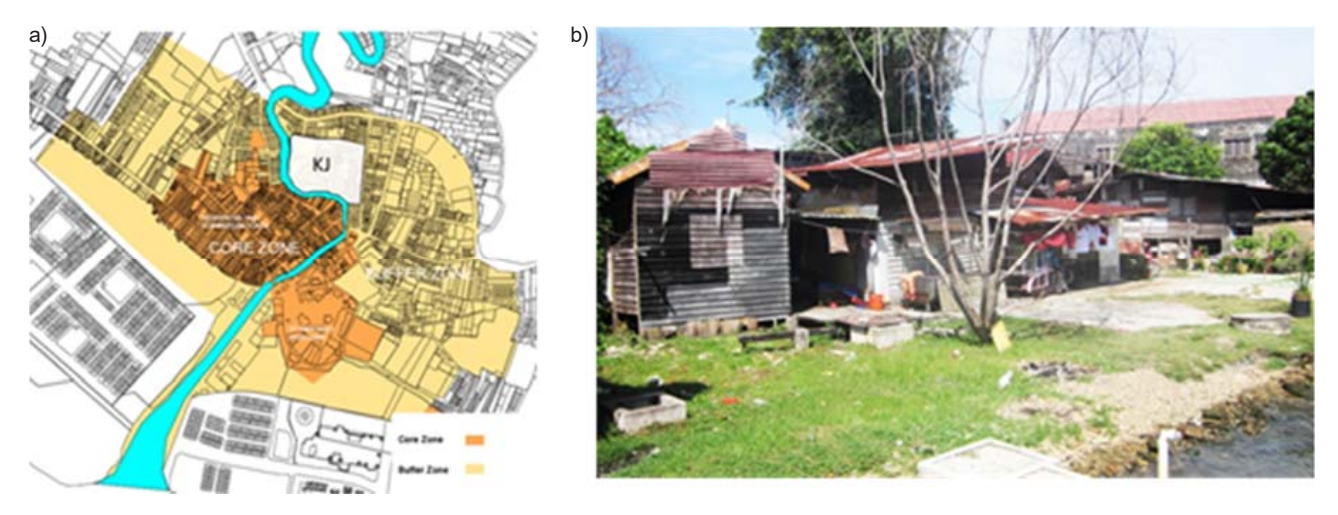


Fig. 1: a) location of KJ in Melaka, b) KJ as a residential slum area

were interviewed about the land value of plots, and the area was mapped once more to validate the previous findings. The analysis and processing of the data resulted in the development of a final map of the area, which divided the available buildings and structures on the site into two categories: retainable and non-retainable buildings. This provided insight into the spatial quality of the area and helped to formulate a proposal for future development of the area. Fig. 2 depicts the methodological framework of this study.

#### Results

The first factor that was surveyed was the 'built and unbuilt area ratio' in KJ. Fig. 3a shows a solid and void map of KJ. According to these maps, there are numerous disorganized vacant lots, open spaces with undefined functions, and unused parking lots on the site. These neglected lands have tarnished the image of this important district, turning it into a dormant, quiet, and unsafe area. As can be seen from the number of building stories (density map) (Fig. 3b), most of the structures in KJ are singlestory buildings. However, throughout its periphery, especially in the new surrounding developments, there is a wide range of building heights, all of which have a higher density.

Fig. 4a demonstrates the land use distribution. Almost all commercial buildings are located on

Bunga Raya (eastern part) and Kee Ann streets. The percentage of vacant buildings and storage areas in KJ is higher compared to its neighboring areas. In addition, residential houses (detached or bungalows) are the main types of properties in KJ. According to the building quality map, the majority of the residential buildings on the site are in a deteriorated condition. The building quality was assessed based on the structure's quality, the current condition of the facades, and the architectural style of the existing buildings, which could to some extent indicate the durability and timeline of the buildings. The building quality map illustrates the quality of the existing buildings on the site. Based on the map, building quality was categorized into three groups: good, medium, and poor. Generally, most of the buildings in KJ have poor structural conditions, and the rundown condition of their facades and appearance has reduced some of them to abandoned houses (Fig. 4b).

Fig. 5a reveals the building styles in terms of architecture. As mentioned, this factor was used as a supporting criterion to evaluate the building quality, as it would indicate the durability and material quality of the existing buildings. Three building styles were chosen for the site: vernacular/traditional, modern, and buildings with no architectural significance. The latter indicates buildings with temporary materials,

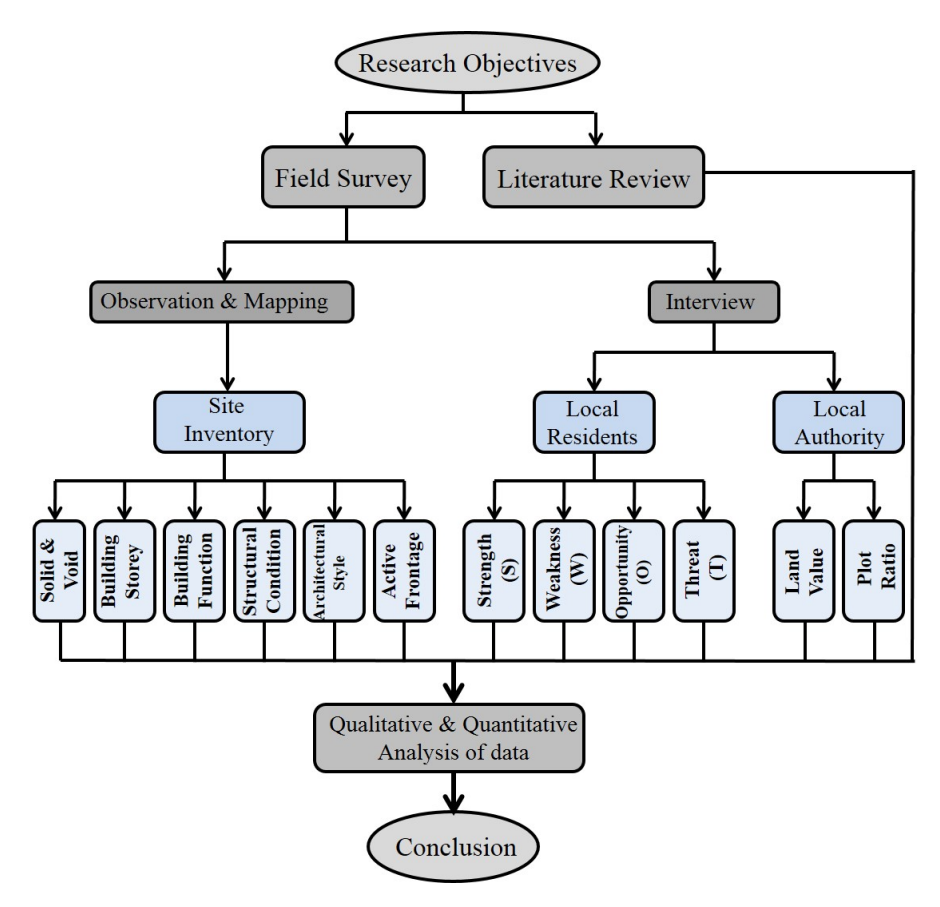


Fig. 2. Methodological framework

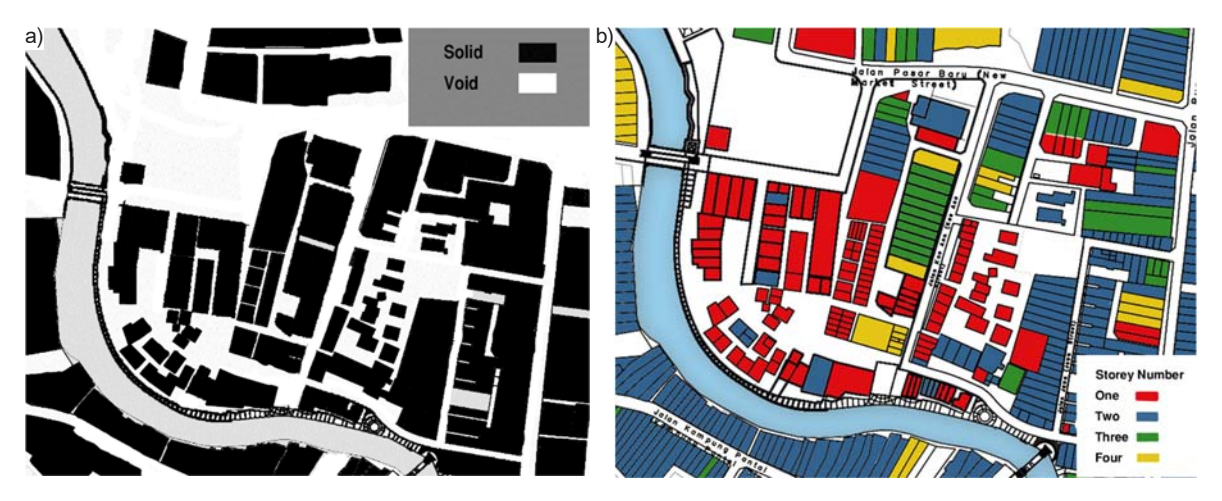


Fig. 3: a) solid & void map, b) density map

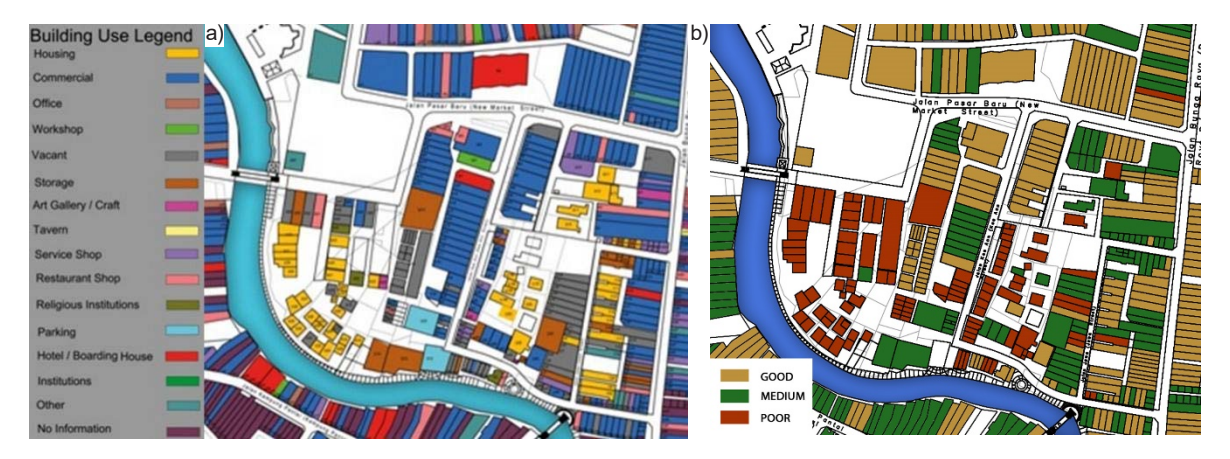


Fig. 4: a) land use distribution map, b) building quality map

such as wood and bamboo, which are not long-lasting structures. Buildings with active frontage have transparent and interactive facades that can create interaction between passersby and activities taking place within the buildings. In contrast, buildings with inactive frontage lack this quality and, therefore, do not contribute to creating vitality and social life in the area. This will have an impact on the retail business and, eventually, the economic prosperity of the area. While most buildings on Keep Ann and Bunga Raya streets benefit from active frontage due to their location in a popular commercial area, the concentration of storage areas, vacant buildings, and parking lots create many inactive building frontages in KJ (Fig. 5b).

#### Triangulation by Local Residents

An interview including open-ended questions was conducted with members of the local community who live, work, and visit KJ. They were asked questions about the strengths, opportunities, weaknesses, and threats of KJ based on five points, as well as the plot ratio. Most respondents declared that they preferred KJ due to its friendly shopping atmosphere. There is a wide range of affordable and unique merchandise, such as bridal accessories, school uniforms, medicine, and various kinds of clothes, as well as

general comfort for daily shopping. Therefore, more than half of the respondents shared the same opinion that shopping was their top priority when visiting this district. As a result, river activities also attracted the highest number of respondents (about 18 %). In conclusion, it is easy to understand that retail shopping activity was the greatest strength of this underdeveloped site (Fig. 6a). Additionally, nearly all respondents declared that five common weaknesses of the site include a lack of urban amenities within the site, an unsafe walking environment, especially at night, run-down structures, a lack of public transportation (relocation of the bus station to another site), and the migration of locals to other districts leading to the depopulation of KJ. Among the main weaknesses of KJ, run-down structures received the most attention from the participants. In second place were the inadequate and unsatisfactory urban amenities (Fig. 6b).

The informal interview with the locals of KJ demonstrated that they identified five main opportunities at the site. These opportunities include the Melaka River as a significant element within the site, a traditional bazaar offering a wide range of affordable products, existing hawkers and

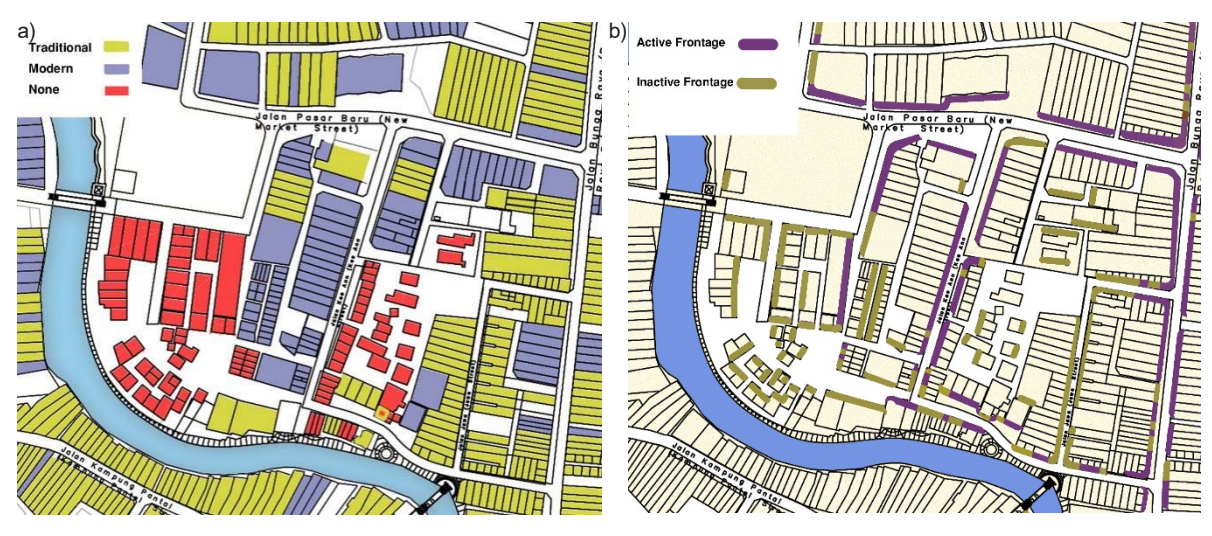


Fig. 5: a) architectural style of the buildings, b) active frontage of the buildings

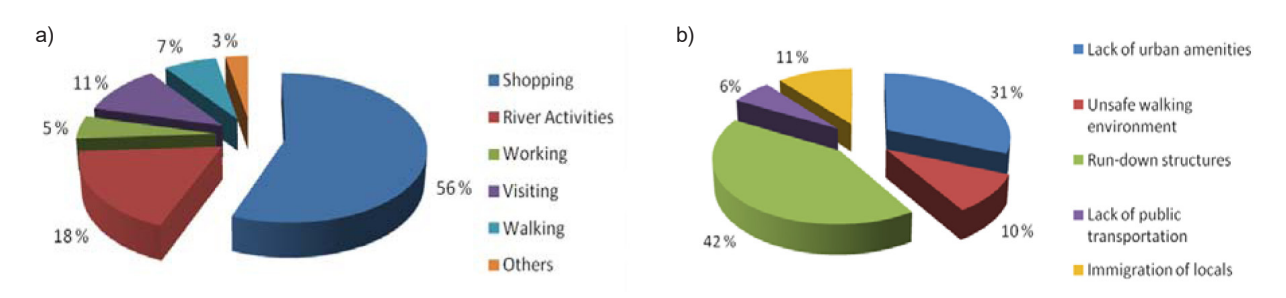


Fig. 6: a) strengths of KJ, b) weaknesses of KJ

vendors engaging in informal activities throughout the site, rows of shophouses, and the proximity of KJ to the World Heritage site (core zone). According to Fig. 7a, a traditional bazaar is considered the primary opportunity. Nevertheless, the majority of respondents chose commercial activities as an essential opportunity. These commercial services included bazaar lanes, hawker and vendor activities, and shophouses, which together accounted for 64 % of responses. The final part pertained to those participants who were residents of KJ. They explained the major factors that endangered the site. Most of them (about 52 %) expressed concerns about the local community migrating to other parts of the city, which was seen as the most serious threat. This resulted in the reduction of residential houses on the site and its transformation into a primarily commercial area. The other notable threat was shopping activities, both formal (bazaar) and informal (hawkers and vendors), which accounted for 26 % and 19 % of responses, respectively (Fig. 7b). Such activities typically have their disadvantages on the site, including pollution, an increase in traffic, and a lack of safety for the residents.

#### Validations by Local Authorities

Permissible land use, plot ratio, and building density are significant factors that should be considered in land-use planning. These main issues

may set limits for how much can be built and what can be built (Christensen, 2014). In particular, within the World Heritage buffer zones, certain legislative restrictions, such as limited plot ratio and compatible land use, must be adhered to. Through interviews (using open-ended questions) with local authorities, the permissible plot ratio for the lots was identified. According to the municipal authority's plans, the core zone of Melaka has a plot ratio (PR) of 2.5:1 and the buffer zone has a PR of 3.5:1. Thus, it can be concluded that the optimal plot ratio in the core zone is PR  $\leq$  2.5, while in the buffer zone it is 1 < PR  $\leq$  3.5. Consequently, the non-optimal plot ratio in the core zone is PR > 2.5, while in the buffer zone, it is PR > 3.5 or PR  $\leq$  1 (Fig. 8a).

To validate the previous data obtained from direct observation and site inventory in terms of five factors and plot ratio, the land value of the lots in KJ was obtained through interviews with local authorities. The approximate land value in KJ was revealed to be between RM 500 (USD 120.9) and RM 1,500 (USD 362.8) per square meter, and RM 2,719 (USD 657.6) per square meter for Kee Ann Street. Moreover, Bunga Raya Street (the main commercial road that borders the eastern part of KJ) had the highest land value, ranging from RM 3,130 (USD 756.9) to RM 4,023 (USD 972.9) per square meter, in comparison with the other commercial streets. In other words,

the land value was 68.8 % higher compared to the inner part of KJ (Fig. 8b).

#### **Discussion**

After validating and cross-analyzing the obtained data, the following facts were revealed:

- A high percentage of the area is covered with vacant land, abandoned lots, undefined open spaces, large on-street parking lots, and single-story buildings. This results in the low massing of the main part of KJ, which hinders the connectivity of the buffer zone to the core zone. Moreover, it disrupts the image of the district and transforms it into a dormant, quiet, and unsafe area.
- Despite the high potential of the land in this strategic location, the land use distribution is not compatible. This results in an unsafe area with the lowest level of vibrancy.
- There are many inactive spaces, that decrease the liveliness and vitality of the area, with numerous vacant buildings and warehouse areas in KJ. However, there is a high concentration of pedestrians on its adjacent streets (Bunga Raya and Kee Ann).
- The presence of temporary and run-down structures, along with a lack of lively activities, has turned the residential area facing the Melaka River into a slum area. In addition, these residential houses do not have the optimal plot ratio.

By overlaying the aforementioned maps (land use distribution, density, building condition, vitality, active frontage, solid and void, and plot ratio), and triangulating with local residents' opinions, the buildings were categorized into two groups: retainable and non-retainable buildings. Retainable buildings are those with acceptable structural conditions, functional activity, and high architectural and heritage value. Non-retainable buildings consist of structures in poor condition that are functionally inactive and lack architectural and heritage value. In addition, buildings with acceptable structural conditions that were vacant or used for commercial purposes have also been included in this group (Fig. 9a). After validating and synthesizing the data with local authorities, it was concluded that nearly all non-retainable buildings in KJ had the lowest land value.

It can be stated that the buildings in this part of the buffer zone have run-down structures and incompatible building functions, despite being in a valuable part of the buffer zone, lacking any architectural significance. Most of the buildings in KJ should be demolished due to the high potential for redevelopment as a key part of the buffer zone. Fig. 9b illustrates the site after the removal of inadequate structures.

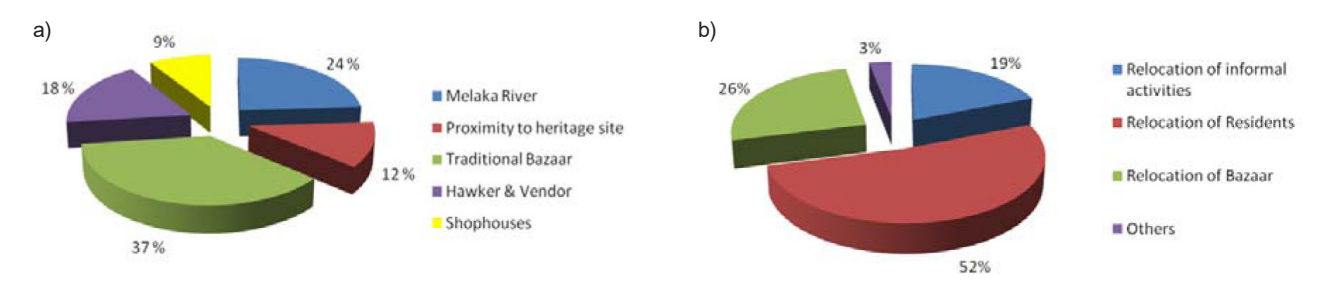


Fig. 7: a) opportunities in KJ, b) threats in KJ

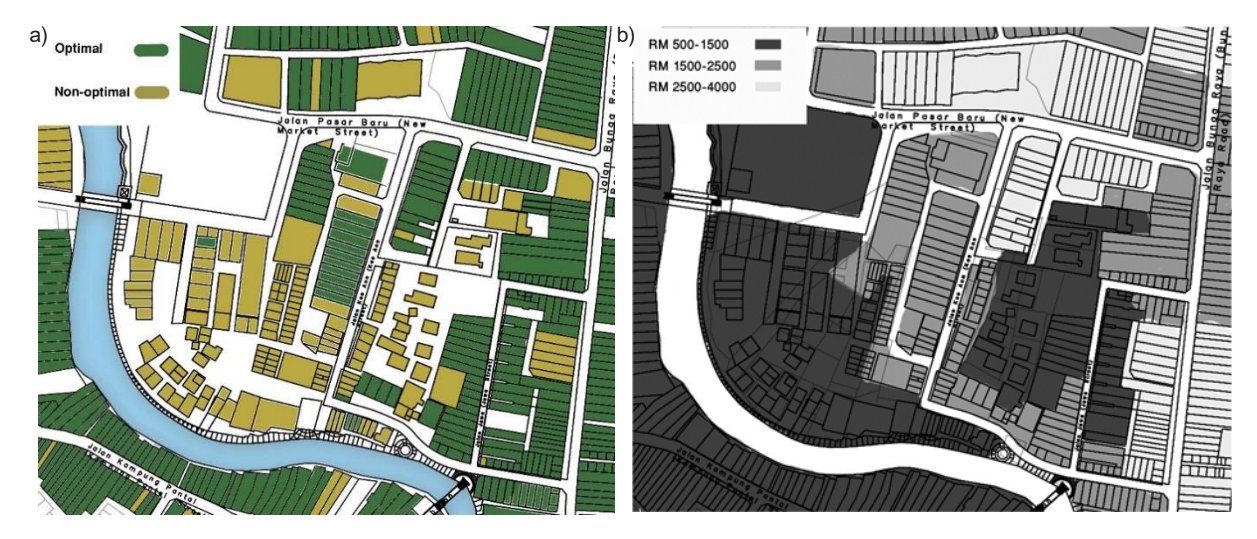


Fig. 8: a) plot ratio map, b) land value map

Potential Design Proposals for Redevelopment

At this stage, proposals to increase the land value can be directly based on the aforementioned five factors and the plot ratio. There are endless possibilities for combining these factors to develop various methods of increasing land value. One conceptual diagram is shown below (Fig. 10).

The following shows some of these combinations: Compatible building function: Improving the imbalanced status of KJ by introducing mixed-use development, including residential, social activities, and commercial uses within the site.

Active frontage: Relocating and replacing buildings such as warehouses and wholesale outlets with various vibrant land uses that have more transparent frontage in order to enliven the site.

Optimal building height and plot ratio: Introducing mid-rise buildings on the site instead of the existing single-story buildings to achieve the optimal plot ratio and high density on the site.

Adequate solid and void ratio: Creating enough open spaces with specific functions (such as parks, greenery, plazas, and parking) instead of having large vacant lands. It also includes connecting

these spaces to enhance visual and physical accessibility.

The proposed master plan includes various social activities in public open spaces, pedestrian connections. commercial or mixed-use developments. entertainment. handicraft local displays, and street vendors or hawkers in a critical attempt to revive the local spirit of the place as well as the historical identity of this site (Fig. 11a). While all the new developments have been focused on the existing Melaka historical riverfront, architectural character, skyline, visual qualities, and cultural traditions, they have also provided significant benefits for the local population. Fig. 11b depicts the status of KJ before and after the revitalization development. As can be seen, KJ has low density, vast and empty lands, dilapidated and slum structures, unappealing views, mono-functional and single-story buildings, disorganized linkages, and weak connections with other parts of Melaka. Undoubtedly, after development, it will have high density, defined open spaces with various functions, multi-functional buildings, mixed-use structures, pleasant visual and physical permeability, walkable and vibrant public

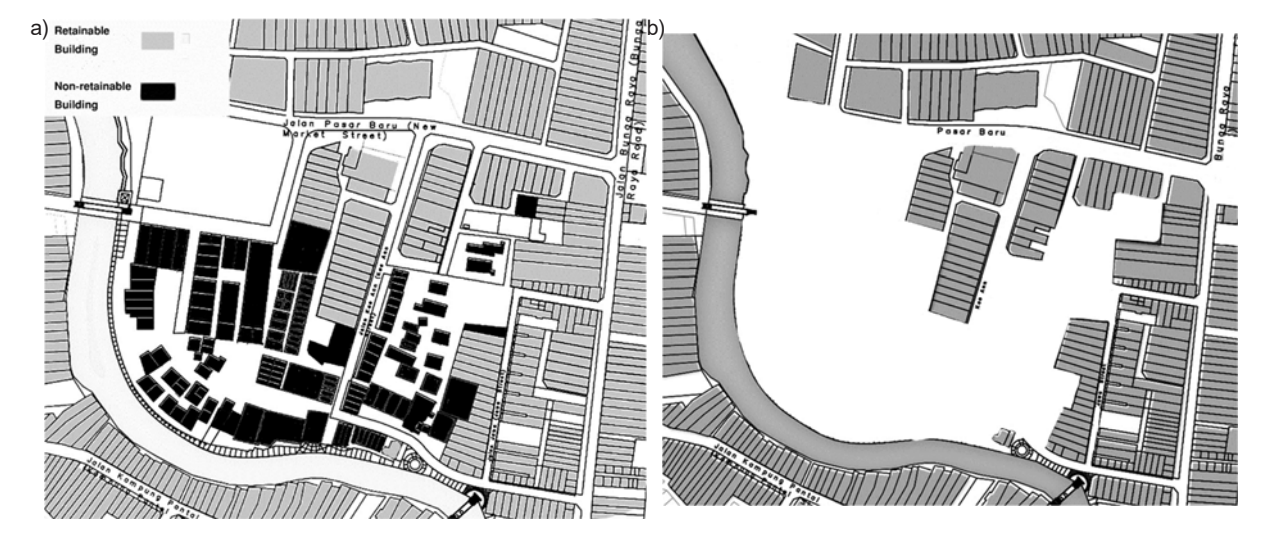


Fig. 9: a) status of structures after analysis, b) KJ after removal of dilapidated structures

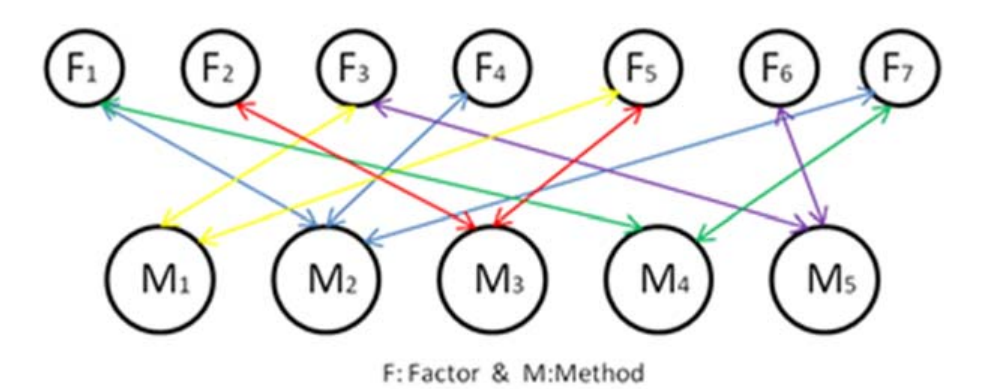


Fig. 10. Conceptual diagram illustrating the interaction between factors and methods

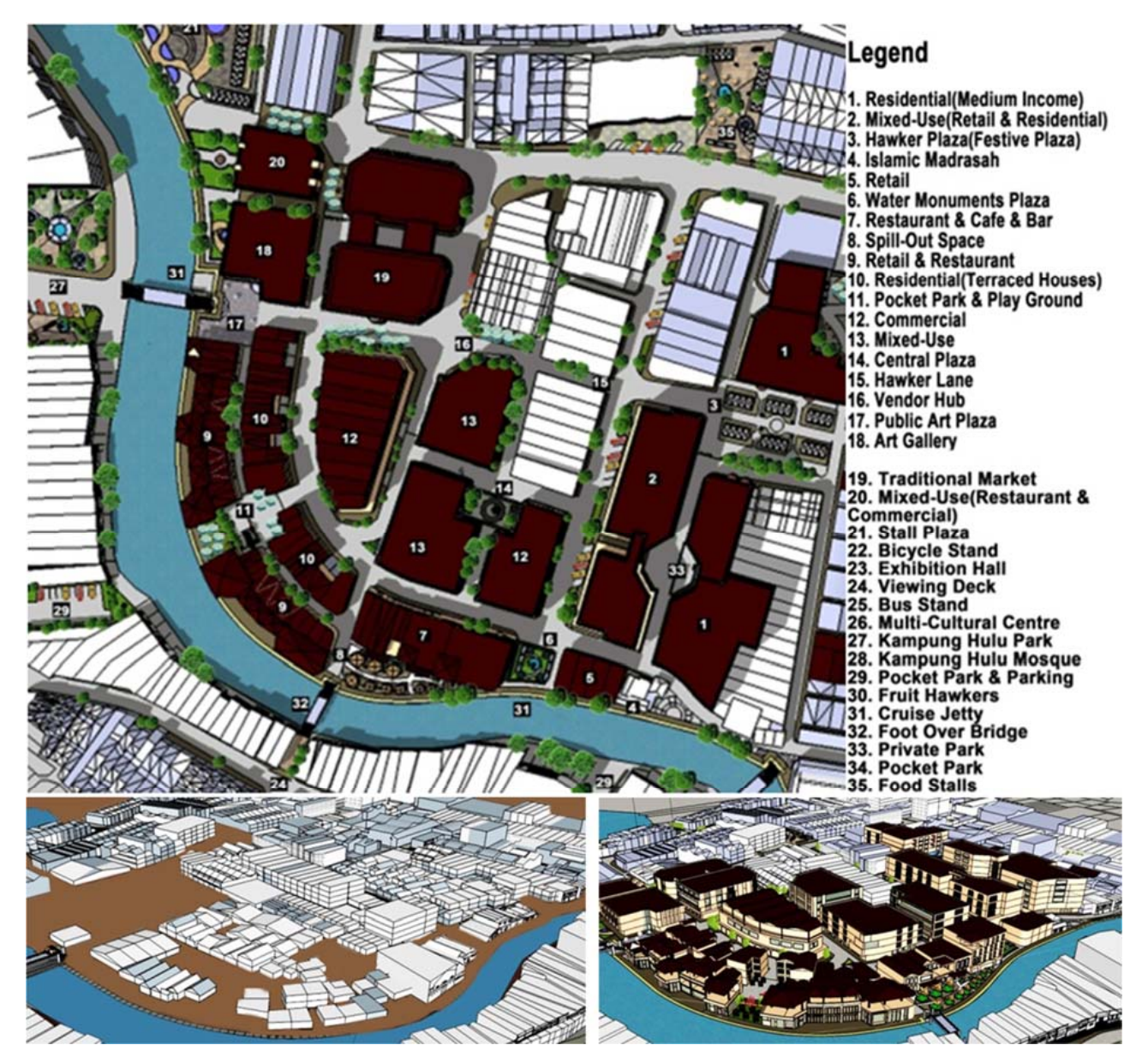


Fig. 11: a) master plan, b) before and after revitalization

areas full of social activities, optimum plot ratio, diversity, legibility, and robustness.

#### **Conclusions and Recommendations**

KJ is an underdeveloped area due to the regulatory restrictions of the buffer zone policy, and, as a result, it has the lowest land value compared to its adjacent districts. This has led to the existence of undeveloped vacant lands, incompatible land use, slum areas, dilapidated buildings, and inadequate provision of urban amenities on the site. The revitalization approach in this study was conducted based on the participation of three stakeholders: the local community, visitors, and the government (local authorities). The participation of local authorities and residents, in addition to the perspective of visitors, is key to revitalizing the land value of high-potential districts within historical buffer zones (Fig. 12).

Low land value is considered a serious threat because it implies a low willingness of people to invest in buffer zones. This results in a decrease in market demand, as they are interested in investing in the new areas of the city. Sustainable development should be based on a harmonious relationship between the existing built forms in the historic core zone and new proposals for the buffer zone. Finally, the urban revitalization approaches in this study can increase the current land value, improve the locals' living standards, and generate profits for the local authorities, developers, and residents.

#### **Acknowledgments**

We would like to express our gratitude to Universiti Teknologi Malaysia (UTM) for providing supervision and guidance for this project.

# People (Strength, Weakness, Opportunity, Threat) Designer (solid and void, building function, storey, condition, style, active frontage) Government (Plot ratio, Land value)

Fig. 12. Revitalization approach based on triple participation

#### References

Ahmad, C. B., Hashim, I. H. M., Abdullah, J., and Jaafar, J. (2012). Stakeholders' perception on buffer zone potential implementation: a preliminary study of Tasek Bera, M'sia. *Procedia - Social and Behavioral Sciences*, Vol. 50, pp. 582–590. DOI: 10.1016/j. sbspro.2012.08.061.

Christensen, F. K. (2014). Understanding value changes in the urban development process and the impact of municipal planning. *Land Use Policy*, Vol. 36, pp. 113–121. DOI: 10.1016/j.landusepol.2013.07.005.

Coleman, A. (1982). Dead space in the dying inner city. *International Journal of Environmental Studies*, Vol. 19, Issue 2, pp. 103–107. DOI: 10.1080/00207238208709976.

Daneshmandian, M. C., Behzadfar, M., and Jalilisadrabad, S. (2020). The efficiency of visual buffer zone to preserve historical open spaces in Iran. *Sustainable Cities and Society*, Vol. 52, 101856. DOI: 10.1016/j.scs.2019.101856.

Feronti, S. M. (2003). *Greyfield redevelopment for community revitalization: An exploration of applications*. PhD Thesis. University of Florida, Gainesville, FL, USA.

Gilmour, D. A. and Van San, N. (1999). Buffer zone management in Vietnam. Hanoi: IUCN Vietnam, 86 p.

Habibi, K., Pourahmad, A., and Meshkini, A. (2015). *Urban rehabilitation and renovation in the old textures*. Tehran: Entekhab Press, 101 p.

Heinen, J. T. and Mehta, J. N. (2000). Emerging issues in legal and procedural aspects of buffer zone management with case studies from Nepal. *The Journal of Environment & Development*, Vol. 9, No. 1, pp. 45–67.

Liang, C. S. (1983). The Central District of Melaka Town. In: Sandhu, K. S. and Wheatley, P. (eds.). *Melaka: the transformation of a Malay capital c. 1400-1980*. Kuala Lumpur: Oxford University Press, pp. 652–707.

Martin, O. and Piatti, G. (eds.) (2008). World heritage and buffer zones. *International Expert Meeting on World Heritage and Buffer Zones*, March 11–14, 2008, Davos, Switzerland, 201 p.

Martino, D. (2001). Buffer zones around protected areas: a brief literature review. *Electronic Green Journal*, 1 (15). DOI: 10.5070/G311510434.

Meffe, G. K. and Carroll, C. R. (1994). Principles of conservation biology. Sunderland: Sinauer Associates Inc., 600 p.

Mohd-Isa, A. F., Zainal-Abidin, Z., and Hashim, A. E. (2011). Built heritage maintenance: a Malaysian perspective. *Procedia Engineering*, Vol. 20, pp. 213–221. DOI: 10.1016/j.proeng.2011.11.158.

Moradi, A., Mohob Ali, M. H., and Amirkabirian, A. (2014). *Twelve restoration studies*. Tehran: Center for Urban and Architecture Studies and Research, 142 p.

Münch, A., Nielsen, S. P. P., Racz, V. J., and Hjalager, A.-M. (2016). Towards multifunctionality of rural natural environments? An economic valuation of the extended buffer zones along Danish rivers, streams and lakes. *Land Use Policy*, Vol. 50, pp. 1–16. DOI: 10.1016/j.landusepol.2015.08.024.

National Trust and English Heritage (2011). Proposal for a buffer zone for the world heritage site of Studley Royal Park including the ruins of Fountains Abbey. [online] Available at: https://nt.global.ssl.fastly.net/binaries/content/assets/website/national/regions/yorkshire/places/fountains-abbey-and-studley-royal-water-garden/pdf/world-heritage-site-management-plan/fasr-buffer-zone-submission-to-who-feb-2012.pdf [Date accessed: March 15, 2023].

Neumann, R. (1997). Primitive ideas: protected area buffer zones and the politics of land in Africa. *Development and Change*, Vol. 28, Issue 3, pp. 559–582. DOI: 10.1111/1467-7660.00054.

Palaiologou, G. and Griffiths, S. (2019). The uses of space syntax historical research for policy development in heritage urbanism. In: Šćitaroci, M. O., Šćitaroci, B. B. O., and Mrđa, A. (eds.). *Cultural Urban Heritage: Development, Learning and Landscape Strategies*. Cham: Springer, pp. 19–34.

Peirce, N. (1995). Vacant urban land—hidden treasure. National Journal, No. 9, 3053.

Pendlebury, J., Short, M., and While, A. (2009). Urban World Heritage Sites and the problem of authenticity. *Cities*, Vol. 26, Issue 6, pp. 349-358. DOI: 10.1016/j.cities.2009.09.003.

Prins, H. H. T. and Wind, J. (1993). Research for nature conservation in south-east Asia. *Biological Conservation*, Vol. 63, Issue 1, pp. 43–46. DOI: 10.1016/0006-3207(93)90071-8.

Robinson, E. J. Z., Albers, H. J., and Busby, G. M. (2013). The impact of buffer zone size and management on illegal extraction, park protection, and enforcement. *Ecological Economics*, Vol. 92, pp. 96–103. DOI: 10.1016/j.ecolecon.2012.06.019.

Sayer, J. (1991). Rainforest buffer zones: guidelines for protected area managers. Gland: UICN, 94 p.

Schlee, M. B. (2017). The role of buffer zones in Rio de Janeiro urban landscape protection. *Journal of Cultural Heritage Management and Sustainable Development*, Vol. 7, No. 4, pp. 381–406. DOI: 10.1108/JCHMSD-10-2015-0040.

Shafer, C. L. (1999). US national park buffer zones: historical, scientific, social, and legal aspects. *Environmental Management*, Vol. 23, pp. 49–73. DOI: 10.1007/s002679900167.

Short, M. J. (2012). Planning for tall buildings. London: Routledge, 240 p.

Tavernor, R. (2007). Visual and cultural sustainability: the impact of tall buildings on London. *Landscape and Urban Planning*, Vol 83, Issue 1, pp. 2–12. DOI: 10.1016/j.landurbplan.2007.05.010.

thefreedictionary.com (2014). *Buffer zone*. [online] Available at: http://www.thefreedictionary.com/buffer+zone [Date accessed April 29, 2014].

UNESCO (2008). Operational guidelines for the implementation of the World Heritage Convention. Paris: UNESCO World Heritage Centre, 163 p.

UNESCO (2011). Convention concerning the protection of the world cultural and natural heritage. Paris: United Nations Educational, Scientific and Cultural Organization, 48 p.

UNESCO (2019). Operational guidelines for the implementation of the World Heritage Convention. Paris: UNESCO World Heritage Centre, 177 p.

Wahid, N. A., Lee, Y. L., Kamaluddin, N. A., Saleh, F. A., Abdullah, A. A., Zarebidaki, E., Aliyas, Z., Nahad, N. F., Anjomshoaa, E., and Idid, S. Z. A. (2011). Restoring "genus loci" in Kampung Jawa, historic city of Melaka buffer zone. In: 11<sup>th</sup> International Congress of Asian Planning Schools Association (APSA) Conference, September 19–21, 2011, Tokyo, Japan, pp. 1526–1537.

Wells, M. P. and Brandon, K. E. (1993). The principles and practice of buffer zones and local participation in biodiversity conservation. *Ambio*, Vol. 22, No. 2/3, pp. 157–162.

# ПОЛИТИКА СОЗДАНИЯ БУФЕРНЫХ ЗОН И ЕЕ ВЛИЯНИЕ НА СТОИМОСТЬ ЗЕМЛИ И КАЧЕСТВО ЗАСТРОЙКИ ПРИМЕНИТЕЛЬНО К ОБЪЕКТАМ ВСЕМИРНОГО НАСЛЕДИЯ НА ПРИМЕРЕ КАМПУНГ-ДЖАВЫ, МАЛАККА, МАЛАЙЗИЯ

Сейед Мохаммад Мусави<sup>1</sup>, Шарийе Хоссейнинасаб<sup>2</sup>, Вакас Ахмед Махар<sup>3,4\*</sup>

- <sup>1</sup> Кафедра архитектурного проектирования, факультет искусства и архитектуры, Университет Персидского залива, Бушер, Иран
- <sup>2</sup> Факультет архитектуры, Исламабадский университет COMSATS (CUI), кампус в Лахоре, Лахор, Пакистан
- <sup>3</sup> Кафедра архитектуры, факультет архитектуры и градостроительства, Университет искусства, архитектуры, дизайна и наследия Арор, Суккур, Пакистан
- <sup>4</sup> Лаборатория устойчивого проектирования зданий (SBD), кафедра градостроительства и экологической инженерии (UEE), факультет прикладных наук, Льежский университет, Льеж, Бельгия

#### Аннотация

Введение: Буферные зоны в контексте объектов всемирного наследия играют важную роль в том, что касается защиты исторических памятников и зданий, а также прилегающих к ним охранных зон, от городской застройки. Однако здания, располагающиеся в границах буферных зон, могут страдать от законодательных ограничений, в том числе ограничений, касающихся строительства. Такие ограничения могут повлиять на рыночную стоимость и сделать такую недвижимость непривлекательной для государственных и частных инвесторов. Целью исследования является критический анализ влияния политики создания буферных зон на градостроительство, в частности, на стоимость земли и качество застройки в контексте объектов всемирного наследия. В качестве объекта исследования выбран район Кампунг-Джава в городе Малакка (Малайзия), внесенном в список всемирного наследия ЮНЕСКО. Методы: В рамках исследования применялись качественные и количественные методы. Требуемые данные были получены путем непосредственных наблюдений, полуструктурированных и неформальных интервью с заинтересованными сторонами и местными органами власти, а также анализа имеющихся статистических данных и карт. В целях тщательного изучения сооружений в Кампунг-Джаве проведены наблюдения на месте и анкетный опрос. Результаты: Низкая стоимость земли в буферных зонах может быть обусловлена рядом специфических условий, трансформирующих эти зоны в заброшенные. Предлагается проектное решение для рассматриваемого района. Показано, что определенные решения на уровне формирования политики, включая вовлечение всех заинтересованных сторон, могут стать определяющими в повышении стоимости земли и улучшении рынка недвижимости в буферных зонах.

**Ключевые слова:** буферная зона; объекты всемирного наследия; стоимость земли; заброшенная территория; Малайзия.

<sup>\*</sup>E-mail: architectwaqas@hotmail.com

# Guide for Authors for submitting a manuscript for publication in the «Architecture and Engineering»

The journal is an electronic media and accepts the manuscripts via the online submission. Please register on the website of the journal http://aej.spbgasu.ru/, log in and press "Submit article" button or send it via email aejeditorialoffice@gmail.com.

Please ensure that the submitted work has neither been previously published nor has been currently submitted for publication in another journal.

#### Main topics of the journal:

- 1. Architecture
- 2. Civil Engineering
- 3. Geotechnical Engineering and Engineering Geology
- 4. Urban Planning
- 5. Technique and Technology of Land Transport in Construction

#### Title page

The title page should include:

The title of the article in bold (max. 90 characters with spaces, only conventional abbreviations should be used); The name(s) of the author(s); Author's(s') affiliation(s); The name of the corresponding author.

#### Abstract and keywords

Please provide an abstract of 100 to 250 words. The abstract should not contain any undefined abbreviations or unspecified references. Use the IMRAD structure in the abstract (introduction, methods, results, discussion).

Please provide 4 to 6 keywords which can be used for indexing purposes. The keywords should be mentioned in order of relevance.

#### Main text

It should have the following structure:

- 1) Introduction,
- 2) Scope, Objectives and Methodology (with subparagraphs),
- 3) Results and Discussion (may also include subparagraphs, but should not repeat the previous section or numerical data already presented),
- 4) Conclusions,
- 5) Acknowledgements (the section is not obligatory, but should be included in case of participation of people, grants, funds, etc. in preparation of the article. The names of funding organizations should be written in full).

#### General comments on formatting:

- Subtitles should be printed in Bold,
- Use MathType for equations,
- Tables should be inserted in separate paragraphs. The consecutive number and title of the table should be placed before it in separate paragraphs. The references to the tables should be placed in parentheses (Table 1),
- Use "Top and Bottom" wrapping for figures. Figure captions should be placed in the main text after the image. Figures should be referred to as (Fig. 1) in the text.

#### References

The journal uses Harvard (author, date) style for references:

- The recent research (Kent and Park, 1990)...
- V. Zhukov (1999) stated that...

#### Reference list

The list of references should only include works that are cited in the text and that have been published or accepted for publication. Personal communications and unpublished works should only be mentioned in the text. Do not use footnotes or endnotes as a substitute for a proper reference list. All references must be listed in full at the end of the paper in alphabetical order, irrespective of where they are cited in the text. Reference made to sources published in languages other than English or Russian should contain English translation of the original title together with a note of the used language.

#### **Peer Review Process**

Articles submitted to the journal undergo a double blind peer-review procedure, which means that the reviewer is not informed about the identity of the author of the article, and the author is not given information about the reviewer.

On average, the review process takes from one to five months.